Université d'Ottawa - University of Ottawa

I dedicate this thesis to my mother, my wife, Su, and my niece, Fiona, for their love.

Abstract

The electro-deposition of thiol and sulfide monolayers has been studied with Electrochemical Quartz Crystal Microbalance (EQCM), chronoamperometry, FTIR, and cyclic voltammetry. The surface concentrations of alkanethiols/alkanethiolates calculated from the oxidative charge and from the EQCM signal using the Sauerbrey equation are in excellent agreement for depositions done in alkaline and pH neutral aqueous solutions. This allowed the measurement of the kinetics of the oxidative deposition of alkanethiols and alkanethiolates on gold. These experiments show that the oxidative depositions of alkanethiols and alkylthiolates occur in two steps. The oxidative deposition can be described by a combination of a potential dependent instantaneous nucleation-growth process and a potential independent Langmuir process. These results show that the rate of deposition of these compounds as well as their coverage can be controlled by an applied electric field. The effects of temperature and concentration on the oxidative deposition process are also reported. The electro-deposition of sulfide was found to be complex. In a pH neutral solution, sulfides go through a slow dissociative adsorption process and form a monolayer of thiolates. In alkaline solution, the oxidative adsorption of sulfide is faster. This observation is compatible with an S_{N2} reaction between physisorbed sulfides and hydroxyl ions.

Acknowledgments

I would like to thank Dr. Mario Morin, my supervisor, for his guidance and teaching me how to conduct research independently. I sincerely appreciate his patience and encouragement, without which I could not finish this thesis.

I wish to thank all my colleagues, Dr. Dongfang Yang, Dr. Nadereh Mothat, Dr. Hassan Al-Maznai, Martin Byloos, Mark Soucy, Daniel Picard, Sandra Rifai, Marie Laferriere, Marc Simard and Marie-Christine Nolet. I thank them for their support, useful discussions, and for the great fun that we had working together.

A very special thanks to my mother, my father, my brother, Deyang, my sister-in-law, Qiang, my wife, Su and my niece, Fiona for their love, support and encouragement.

Finally, I would like to thank the University of Ottawa for a scholarship.

Table of contents

List of Tables

List of Figures

electron transfer, (3) detachment of the reductive thiolates. Active sites for the nucleation may come from (a) local conformational disorder of the alkyl-chains, (b) metal surface defects. Copy from ref. 1-66.

Figure 2-1: Potential-time behavior at the working electrode in cyclic voltammetry, where v is the scan rate. E_t^a: Anodic potential limit, E_t^C: Cathodic potential limit.

Figure 2-2: A three-electrode system.

Figure 2-3: Model of the double layer region at the electrode/solution interface. σ^i is the ionic charge density in the inner Helmholtz plane (IHP), σ^d is the ionic charge density in the outer Helmholtz plane (OHP). Copy from ref. 2-2.

Figure 2-4: Potential-time curve in chronoamperometry.

Figure 2-5: Current-time response for a chronoamperometry experiment. Curves a, b, c represent different final potentials E_2: a) the reaction is diffusion controlled, b) the reaction is kinetic controlled and c) there is mixed control.

Figure 2-6: s-polarized and p-polarized light of incident and reflected beams on a metal surface. $E_{p,i}$ and $E_{p,r}$ are the electric field of incident and reflected p-polarized radiation. $E_{s,i}$ and $E_{s,r}$ are the electric field of incident and reflected s-polarized radiation.

Figure 2-7: Schematic diagram of IRAS (Infrared Reflection-Adsorption Spectroscopy) experiment. (ν_a: asymmetric -CH stretching mode transition dipole moment; ν_s: symmetric -CH stretching mode transition dipole moment).

Figure 2-8: Dependence of the resonance frequency on temperature for an AT-cut quartz crystal and crystals cut with small deviation. Copy from ref. 2-12.

Figure 2-9: Electrochemical cell used for cyclic voltammetry.

scan rate 5 mV s^{-1}, 20 Hz, 5 mV RMS; EQCM measurements: Potential scan rate: 10 mV s^{-1}.

Figure 3-7: Potential step curves (average of five trials of experiments) for the oxidative deposition of a) 1 mM octanethiolate; b) 1 mM butanethiolate on gold in 0.1 M KOH. The potential is stepped from -1.25 V for octanethiolate and -1.10 V for butanethiolate to the potentials indicate on the curves.

Figure 3-8: Mass change (dotted line, average of five trials of experiments) fitted with eq. 3-4 (solid line) for the oxidative adsorption of a) octanethiolate b) first five seconds for octanethiolate and c) butanethiolate on gold in 0.1 M KOH solution. For clarity only every 10^{th} (Fig.3-8a and c) and 20^{th} (Fig. 3-8b) data point is shown.

Figure 3-9: Fitted rate constants k_1 (---▲---) and k_2 (---▼---) for the oxidative deposition of octanethiolate in 0.1 M KOH at different deposition potentials done using eq. 3-4.

Figure 3-10: Chronoamperograms of the butanethiolate oxidative deposition on gold in 0.1 M KOH. The potential is stepped from –1.10 V to the potential shown on each chronoamperogram.

Figure 3-11: Plot of the moles of butanethiolate deposited which were calculated from the integrated charge of chronoamperograms in Fig. 3-10 (---▲---) and from the EQCM measurements (---▼---).

Figure 3-12: Chronoamperograms of the butanethiolate oxidative deposition on gold in 0.1 M KOH solution. The empty circles are data points. The solid line is the fit with the instantaneous nucleation and growth model (eq. 3-2). The dashed line is the fit with eq. 3-7. The potential is stepped from –1.10 V to the potential a) –0.90 V; b)-0.86 V; c)-0.82 V.

potential is stepped from –1.10 V to the peak potential of the cyclic voltammograms at each temperature. For clarity only every 20th data points are shown.

Figure 4-5: Mass change for potential steps causing the oxidative deposition of butanethiol on gold in 0.1 M $KClO_4$ for the first 5 sec of deposition at O: 5^0C , Δ: 15^0C , ∇: 25^0C , □: 35^0C. The potential is stepped from –1.10V to the peak potential of the cyclic voltammograms of each temperature. For clarity only every 20th data point is shown.

Figure 4-6: Arrhenius plots of the rate of oxidative deposition of butanethiol on gold in 0.1 M $KClO_4$ at different overpotential O: 0.2 V vs. Ep; Δ: 0.04 V vs. Ep; ∇: Ep; □: -0.04 V vs. Ep. Ep is the peak potential in the cyclic voltammogram recorded at each temperature. The dashed lines are linear fits.

Figure 4-7: Cyclic voltammograms and EQCM signals for the oxidative adsorption/reductive desorption of octanethiol on gold recorded in 0.1 M KOH at (a) 35^0C, (b) 25^0C, (c) 15^0C, (d) 5^0C. Potential scan rate: 10 mV s^{-1}.

Figure 4-8: Mole of electron (calculated from 5 cyclic voltammograms such as those in Figure 4-7, dashed line) and the mole of octanethiol deposited (calculated from 5 EQCM measurements such as those in Figure 4-7, solid line) at different temperatures.

Figure 4-9: Mass change for potential steps causing the oxidative deposition of octanethiol on gold in 0.1 M KOH at (a) 5^0C, (b) 15^0C, (c) 25^0C, (d) 35^0C. The potential is stepped from –1.10 V to □: 0.04 V vs Peak potential (Ep); O: Ep; Δ: -0.04 V vs Ep. For clarity only every 20th data point is shown.

Figure 4-10: Mass change for potential steps causing the oxidative deposition of octanethiolate on gold in 0.1 M KOH at the temperatures shown on the figure. The

Chapter 1

Introduction

1.1. Self-assembled monolayers of sulfur compounds and their applications

In 1983, Nuzzo and Allara [1-1] showed that self-assembled monolayers (SAMs) of alkanethiolates on gold can be obtained by the adsorption of dialkyl disulfides from solution. Since then SAMs of organo-sulfur compounds on different metallic surfaces have been studied extensively [1-2 - 1-4]. Applications of these materials as chemical and biochemical sensors [1-5 - 1-12], corrosion inhibitors [1-13 - 1-15], in electroplating [1-16, 1-17], optics [1-18] and electro-catalysis [1-19] have been reported.

An advanced field of applications is that of chemical sensors. Densely packed SAMs of thiols are well suited for the design of chemically modified electrodes. The alkanethiolate monolayer on gold prevents solvent and ions from approaching the electrode surface, therefore decreasing the double layer capacitance. This results in the reduction of non-faradaic and faradaic currents. Electron transfer at the interface occurs either by electron tunneling across the monolayer, or at defect sites in the monolayer. This allows the creation of a selective molecular "trap", which is shown in Figure 1-1.

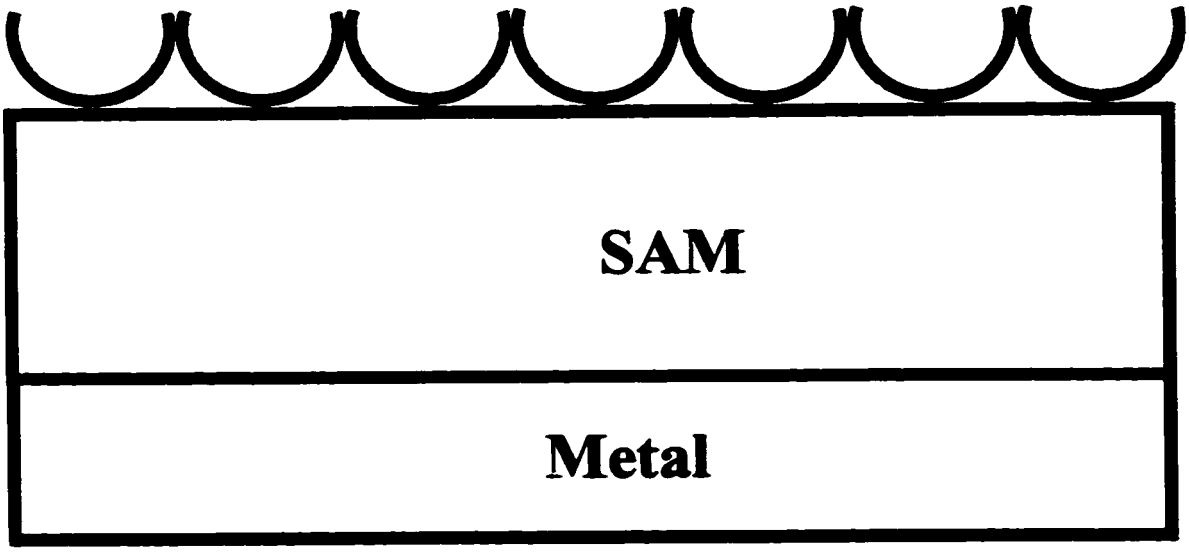

Figure 1-1: Diagram of a SAM used as a chemical sensor. ∪: functional groups.

A thiol with a functional group, which has specific interactions with an analyte, is first adsorbed on the gold surface. The resulting modified electrode becomes a selective molecular "gate". For example, a 3-mercaptopropionic acid ($COOH(CH_2)_2SH$, MPA) SAM has been used as a sensor [1-10 – 1-12]. It selectively interact with the lysine groups ($H_2N(CH_2)_4CHNH_2COOH$) of Cytochrome *c*. This immobilizes the protein onto the electrode, and aligns the redox center of the protein (i.e. the heme group) towards the electrode surface for fast electron transfer [1-10, 1-11]. The MPA monolayer was also used [1-12] for the electrochemical detection of dopamine;

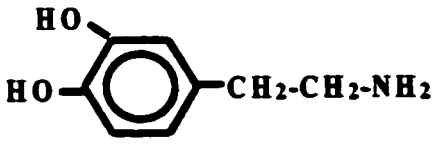

which is a neurotransmitter involved in Parkinson's disease.

For these types of applications, the SAMs must be stable, and their structures and coverages must be reproducible. It is therefore important to understand how such SAMs can be formed.

1.2. Formation of organo-sulfur SAMs on gold

1.2.1. Preparation of SAMs on gold by incubation

The first and most widely used method for preparing thiolate SAMs on gold involves the incubation of a gold substrate in a dilute alkanethiol ethanolic solution. This spontaneous adsorption of thiols takes a relatively long time (hours to days) to form an ordered monolayer. Several other metallic substrates allow for the formation of organo-sulfur SAMs, but most of the work reported has been done on the thiolate/gold system. This is due to the inertness of gold, and the ease of formation of SAMs on gold (see below).

The structure and stability of the thiolate SAMs are determined by the combination of three types of forces, shown in Figure 1-2.

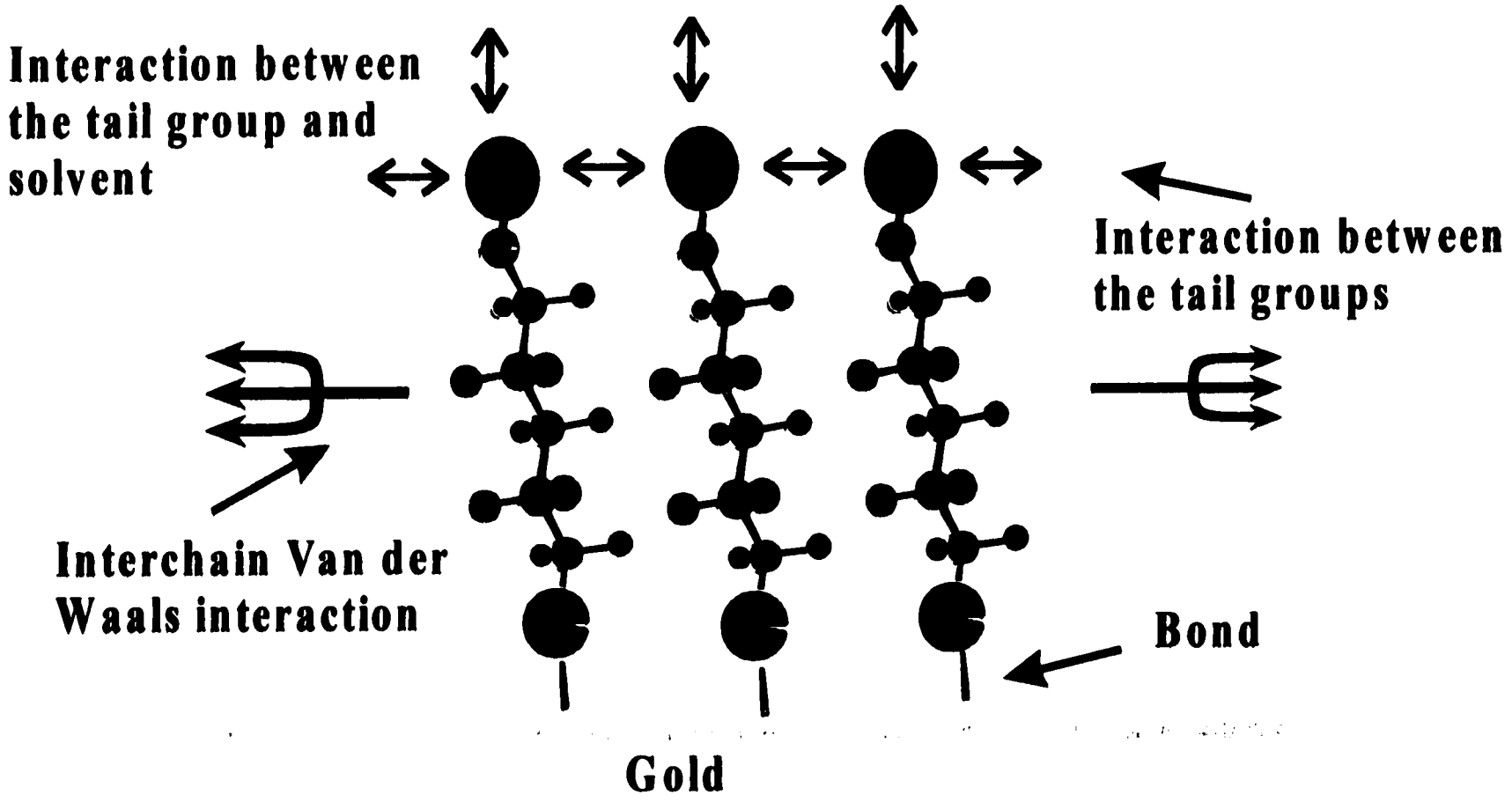

Figure 1-2: A schematic view of interactions in a SAM on gold.

They are (a) the interaction between the sulfur and gold surface (i.e. the gold-sulfur bond), (b) the interactions between adsorbates and (c) the interactions between the adsorbates and the solvent. The sulfur-gold bond is believed to be covalent with partial ionic character and the bond strength is estimated to be 170 KJ mol^{-1} [1-2, 1-3, 1-20]. The intermolecular interactions between the adsorbed alkanethiols are weak Van der Waals forces. It was estimated that this interaction is -2 KJ mol^{-1} per methylene group [1-2, 1-3, 1-7]. Interadsorbate interactions, such as hydrogen bonding, were shown to help order carboxylate terminated thiols (see below).

1.2.2. Structure of thiolate SAMs on gold (111)

High Energy Electron Diffraction (HEED) [1-21, 1-22] and Low Energy Electron Diffraction (LEED) [1-23] studies of monolayers of alkanethiolates on a Au (111) surface show that the sulfur atoms form an hexagonal lattice with a sulfur-sulfur spacing of 4.97 Å, and a calculated area per molecule of 21.4 $Å^2$. Helium diffraction [1-24] and atomic force microscopy (AFM) [1-25] confirmed that the structure of alkanethiolate SAMs on Au (111) is commensurate with the gold lattice and corresponds to a $\sqrt{3}$ X $\sqrt{3}$ R 30^0 overlayer. This structure is shown in Figure 1-3. The sulfur-sulfur distance of 4.97 Å corresponds to the second-nearest-neighbor distance on Au (111). STM (scanning tunneling microscopy) [1-26 – 1-30] studies also suggested the same structure. This structure is in agreement with theoretical calculations [1-31], which suggest that the thiol head groups are adsorbed in the three-fold hollow sites on Au (111). Alkanethiolates have two binding modes at the Au (111) hollow site, one with a (Au-S-C) angle of 180^0 (sp) and

the other of 104^0 (sp^3), the latter one is calculated to be more stable by 0.41 kcal mol^{-1} [1-31].

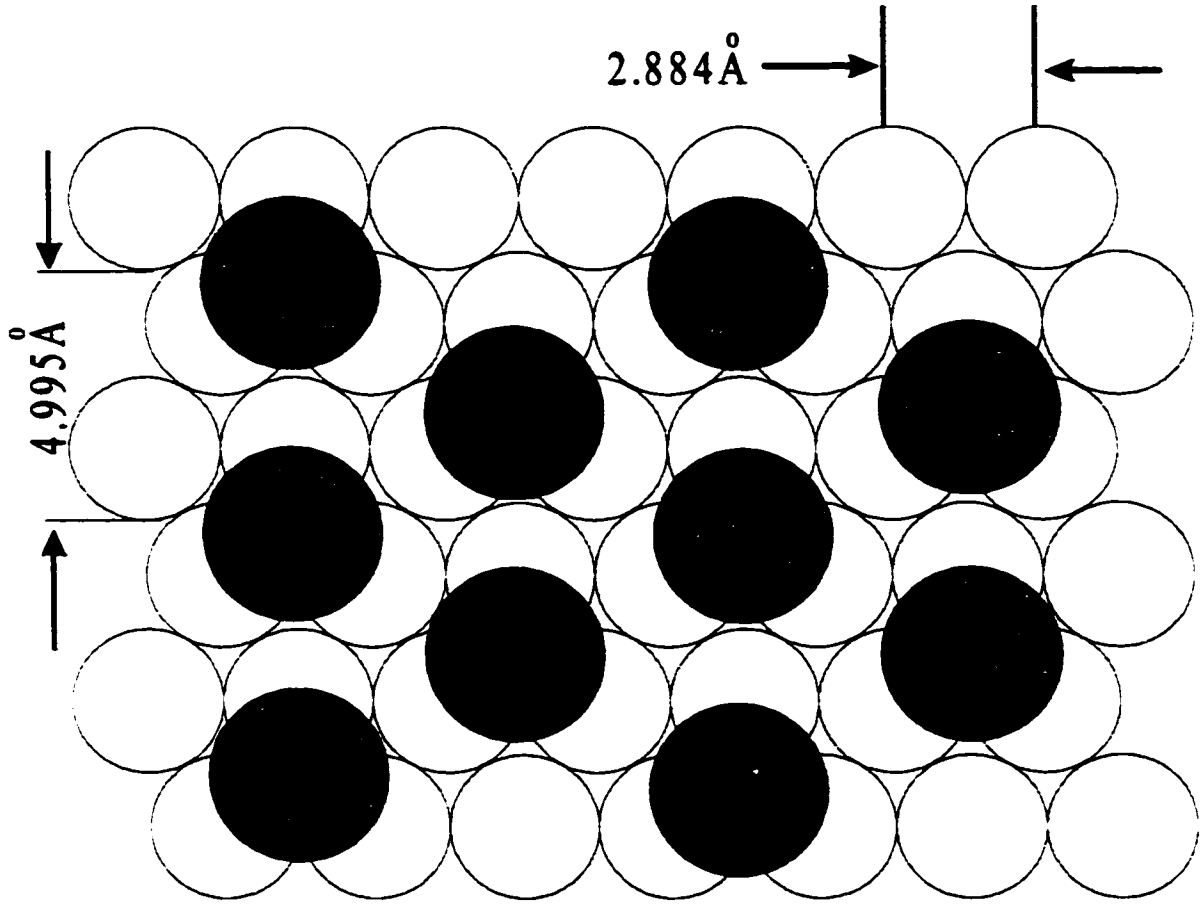

Figure 1-3: Top view of a $\sqrt{3}$ X $\sqrt{3}$ R 30^0 alkanethiolate overlayer (black circle) and the hexagonal Au (111) surface atoms (open circles).

IR spectroscopy revealed that the long alkyl chains (R ≥ 10 carbons) are mostly in an all-trans configuration and in a crystalline-like state [1-20, 1-32]. Moreover, FTIR studies show that the alkyl chains in thiolate SAMs on Au (111) are usually titled by about 30^0 [1-20, 1-33, 1-34] from the surface normal (see figure 1.4). The rotation of the C-C-C plane about the plane formed by the molecular-axis and the surface normal is between 52^0 ~

55^0 [1-20, 1-21, 1-34, 1-35]. The tilt of the alkyl chain, maximizes the chain-chain Van der Waals interactions, and results in an assembly with an ~5 Å sulfur-sulfur distance. This spacing is larger than the separation of 4.6 Å between alkyl chains in a close packed unit cell.

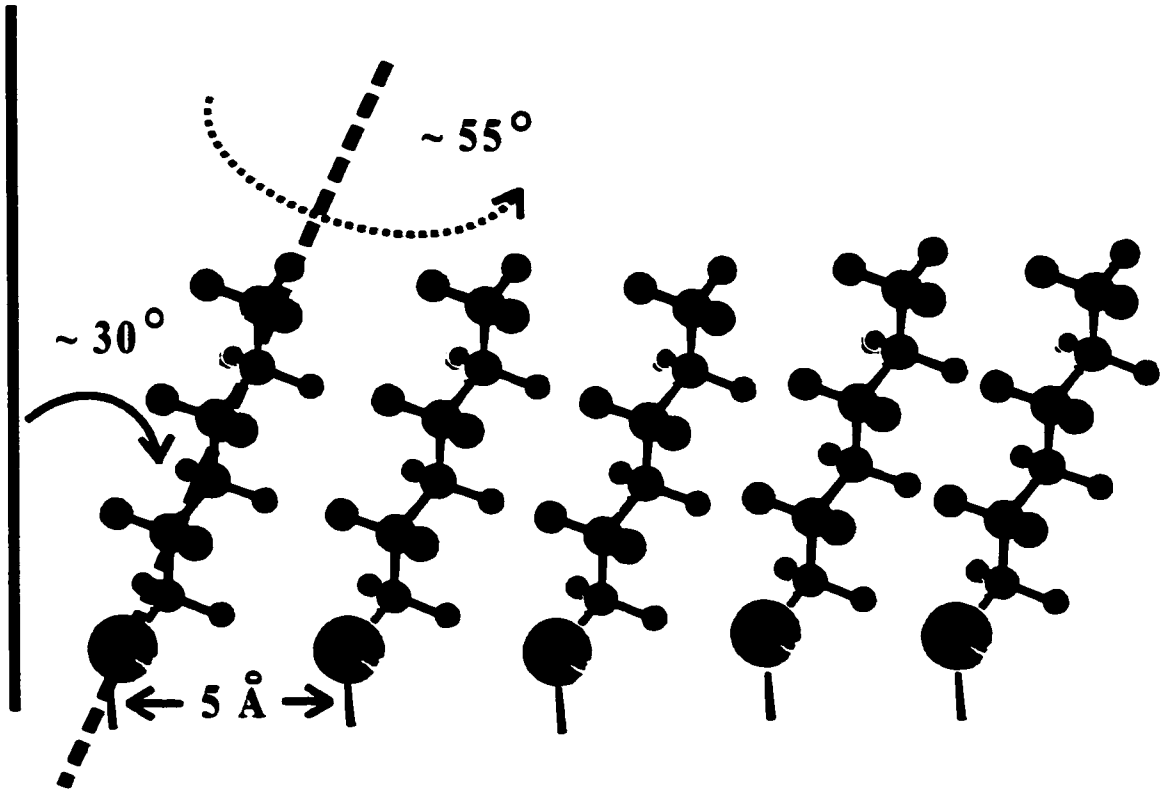

Figure 1-4: Orientation of the all-trans alkyl chains of alkanethiolate SAM on gold (111).

An orthorhombic unit cell comprising four thiols was suggested by Helium diffraction measurements [1-36]. This orthorhombic unit cell has dimensions of 3a x $2\sqrt{3}$a (a = 2.884 Å is the Au nearest neighbor distance). It corresponds to a c (4x2) superlattice of a $\sqrt{3}$ X $\sqrt{3}$ R 30^0 hexagonal lattice. This structure was subsequently confirmed by

Grazing Incidence X-Ray Diffraction (GIXD) [1-37] and STM [1-28, 1-30]. Other structures have also been reported.

1.2.3. Factors influencing the formation of thiolate SAMs on Au (111)

The $\sqrt{3}$ X $\sqrt{3}$ R 30^0 structure of thiolate SAMs on Au (111) mentioned above is the most common one. The factors that were found to influence the final structure of thiolate SAM are now discussed.

1.2.3.1. Solvent

Ethanol is the most commonly used solvent. Many other organic solvents have been used as incubation media. There are two forces involved in the solvent effect. They are the interactions between the alkanethiol end group and the solvent, and the solubility of the thiols. For alkanethiols, polar solvents increase the driving force for adsorption, however the decrease of the solubility of the thiols in such solvent often lead to disordered monolayers.

Bain et al [1-38] found that using hexadecane as a solvent to prepare hexadecanethiol SAMs, leads to abnormally low contact angles. They assigned this observation to the incorporation of solvent into the monolayer. Schneider and Buttry [1-39] found that in acetonitrile, multilayers of thiols are formed.

1.2.3.2. Concentration

Although the thiol concentrations that have been used range from micromolar to pure liquid thiols, millimolar concentrations are typically used. At lower thiol concentrations (in the micromolar range), a longer incubation time is required to form a complete monolayer because thiol adsorption is limited by mass transport [1-38, 1-40, 1-41].

Rowntree et al [1-42] found that at low concentrations (~ 5 X 10^{-6} M), SAM formation proceeds by island growth. The orientation of the alkyl chains was monitored by FTIR spectroscopy for incubation in thiol solutions of different concentrations. At low concentrations, a disordered thiolate layer is formed.

1.2.3.3. Incubation time and temperature (thermal annealing)

Gold substrates are usually incubated in a thiol solution for 30 min to 24 hours. Adsorption of 80% of a monolayer is fast (a few minutes), but the ordering of the monolayer and the adsorption of the remaining 20% is slow. However, longer incubation times do not always generate a more ordered monolayer.

Kim et al [1-43], using STM (Scanning Tunneling Microscopy) and QCM (Quartz Crystal Microbalance), reported the formation of multilayers when a gold substrate is exposed to an alkanethiol ethanolic solution for 4 to 6 days.

The adsorbed alkanethiolates are mobile [1-44]. It has been suggested that the slow organization involves displacement of both the adsorbed thiolates and surface gold atoms. Increasing the temperature causes the monolayer to rearrange into a more ordered structure. An STM study of dodecanethiolate SAMs on Au (111) [1-37] showed that deposition of the SAMs at 50 ^{0}C doubled the size of the highly ordered domains as compared with SAM deposited at 20 ^{0}C. An X-ray diffraction study [1-28] showed that thermal annealing of a dodecanethiolate SAMs at 90 ^{0}C in vacuum also resulted in the domain size increasing from about 90 Å to around 1000 Å.

1.2.3.4. Alkyl chain length and terminal group

The Van der Waals interactions between the alkyl chains is a driving force for thiol adsorption. Alkanethiols with long chain-lengths form more ordered SAMs.

The IR measurements of Porter et al [1-45] suggested that SAMs of short alkanethiols ($C_nH_{2n+1}SH$, $n \leq 9$) are disordered and liquid like. More ordered SAMs are formed by thiols with alkyl chains of 10 to 18 methylene units [1-4]. There is evidence that even longer chain lengths lead to disorder under the same deposition conditions [1-46].

The addition of one methylene group to the alkanethiols causes a change of orientation of the terminal methyl group of alkanethiol SAMs on gold [1-2, 1-20, 1-47]. Alkyl chains with odd and even number of methylene groups, shown in Figure 1-5, illustrate the

variation of the orientation of the terminal methyl group. This is the result of the Au-S-C bond angle of about 110^0 for all alkanethiols.

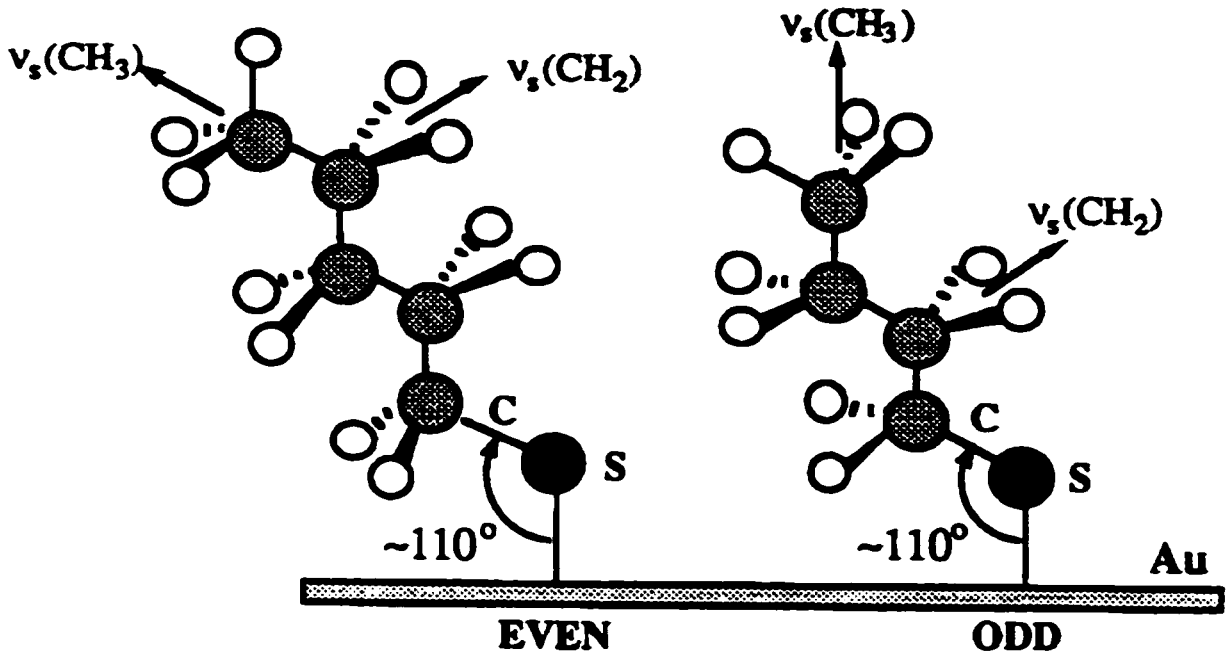

Figure 1-5: Orientation of the methyl group of alkanethiolates with odd and even number of methylene groups. Copy from ref.1-2.

For thiolate SAMs with functional groups, there are other interactions such as hydrogen bonding, which stabilize the SAMs. For example, Mizutani et al [1-48, 1-49] revealed the existence of intermolecular hydrogen bonding in a MPA (3-mercaptopropionic acid) monolayer using *in-situ* STM. Bilewicz et al [1-50] also found an hydrogen bonding network cross-linking amide groups. They also examined the effect of hydrogen bonding networks on electron transfer through the SAMs.

The size of the functional group influences the SAM structure. Obviously, the larger adsorbate will form a lower coverage, disordered layer. For example, the study of SAMs of 6-[4-(phenylazo)phenoxy]hexane-1-thiol revealed an incommensurate lattice with a primitive unit cell that encompassed an area of 48 $Å^2$ [1-51, 1-52, 1-53]. If we assume that the unit cell has two molecules, the molecular area is 24 $Å^2$, which is larger than the 21.5 $Å^2$/ molecule in $\sqrt{3}$ X $\sqrt{3}$ R 30^0 packing of alkanethiols.

The above discussion shows that the formation of thiol SAMs on gold by incubation is influenced by many factors. This method has several limitations:

(1) The time required to form the ordered layer is relatively long.

(2) It is difficult to control the thiol coverage on gold.

(3) There is limited selectivity in the compounds that adsorb. Thus, the formation of monolayers with multiple components is difficult.

(4) It is sensitive to the presence of contaminants.

1.3. Formation of organo-sulfur SAMs on gold by electro-deposition

1.3.1. Preparation of SAMs on gold by electro-deposition

To better control SAM formation and remove the limitations of the incubation method, the electro-deposition of thiols on gold has been used [1-39, 1-54 – 1-58]. This method involves the immersion of the gold substrate in an alkaline solution containing thiolates. A sufficiently positive potential is applied to the gold electrode to oxidatively deposit

thiolates onto gold. Compared to the incubation method, the deposition of a full monolayer only takes a few seconds. The rapidity of this deposition method does not compromise the quality of the self-assembled monolayers. The electrodeposited monolayers have the same surface coverage, structure, and electrochemical properties as the monolayers obtained via the incubation method. The electrochemical deposition method also allows *in situ* cleaning of the substrate prior to the deposition of a monolayer. This cleaning of the substrate is important since it improves the quality and stability of the monolayer.

The electrochemical deposition method provides more control over the formation of self-assembled monolayers of thiols. For example, by controlling the number of moles of electrons transferred (i.e. the charge), we can control the coverage of SAMs. By controlling the oxidative deposition potential, we can selectively adsorb different molecules and thus form multi-component monolayers.

1.3.2. Reductive desorption/ oxidative deposition of alkanethiols on gold

The cyclic voltammogram of oxidative deposition/ reductive desorption of butanethiolates in 1 mM butanethiolate / 0.1 M KOH solution is shown in Figure 1-6.

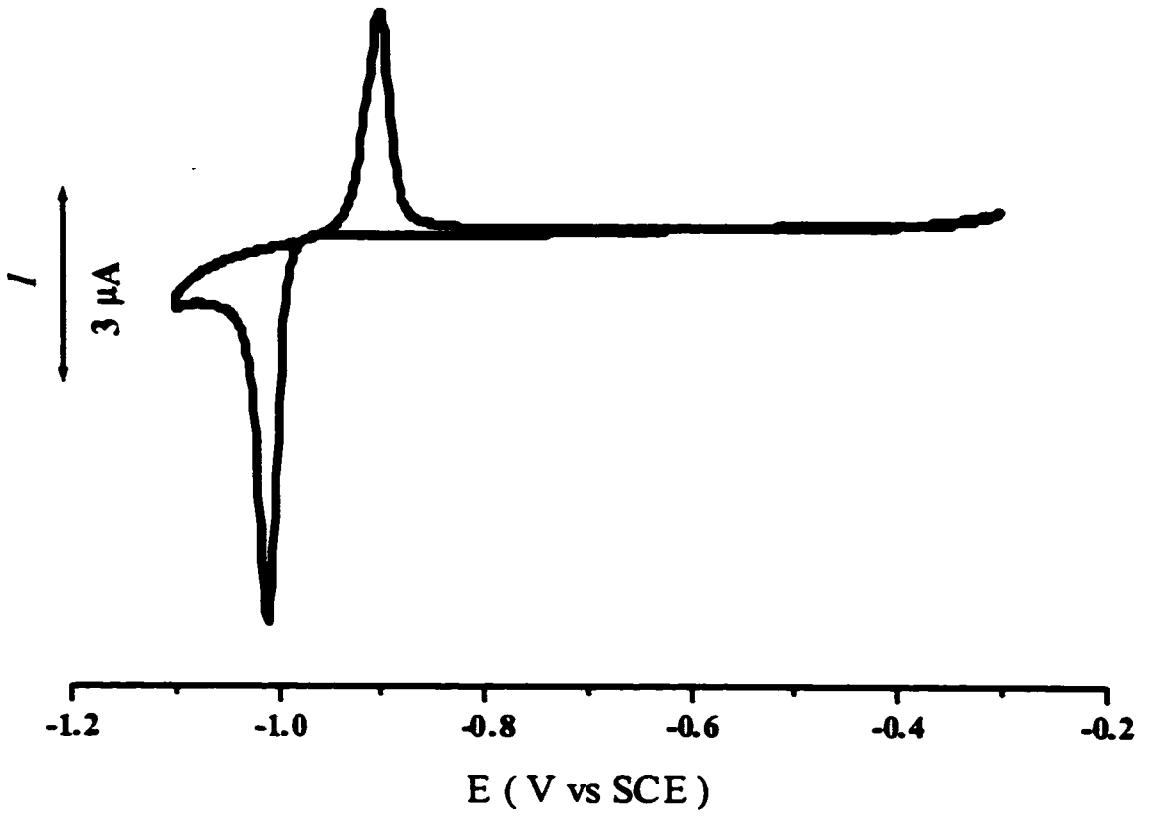

Figure 1-6: Cyclic voltammogram of oxidative deposition/ reductive desorption of butanethiolate. Solution: 1 mM butanethiolate in a 0.1 M KOH solution, scan rate: 10 mV s^{-1}.

We see that the oxidative and reductive current peaks are sharp and symmetric. The absolute value of the integrated charge of the oxidative peak and reductive peak in the cyclic voltammogram are equal. The oxidative and reductive peak potentials are –0.87 V and –1.02 V vs SCE, respectively. The difference between the peak potentials of

these two processes are constant for different scan rates [1-57]. This intrinsic hysterisis indicates that the oxidative deposition is not the reverse process of the reductive desorption of thiols.

The reductive desorption of thiolate SAMs can be prompted by applying a sufficiently negative potential [1-39, 1-58, 1-59, 1-60]. It is believed to be a one-electron process [1-61, 1-62].

$$R\text{-}S\text{-}Au + e^- \rightarrow RS^- + Au \qquad (1\text{-}1)$$

The mechanism of this process has been the subject of several chronoamperometric studies [1-59, 1-60, 1-63, 1-64]. Two models of the reductive desorption process have been suggested [1-59, 1-60, 1-65, 1-66]. One of them is the nucleation and growth model [1-59, 1-60, 1-65]. This mechanism is shown in Figure 1-7. In this model, the desorption starts at etching centers. Those etching centers are generated where cation permeation occurs when a sufficiently negative potential is applied. Then the thiolates desorb from the holes. In these studies [1-59, 1-60, 1-65], the transient current in the chronoamperograms becomes asymmetric (i.e. a fast initial increase followed by a slow decay of the current) at higher values of the reductive overpotential. This slowing down of the rate of nucleation and growth was suggested to be caused by the diffusion of the reduced thiolate away from the edge of the etching center as shown in Figure 1-7.

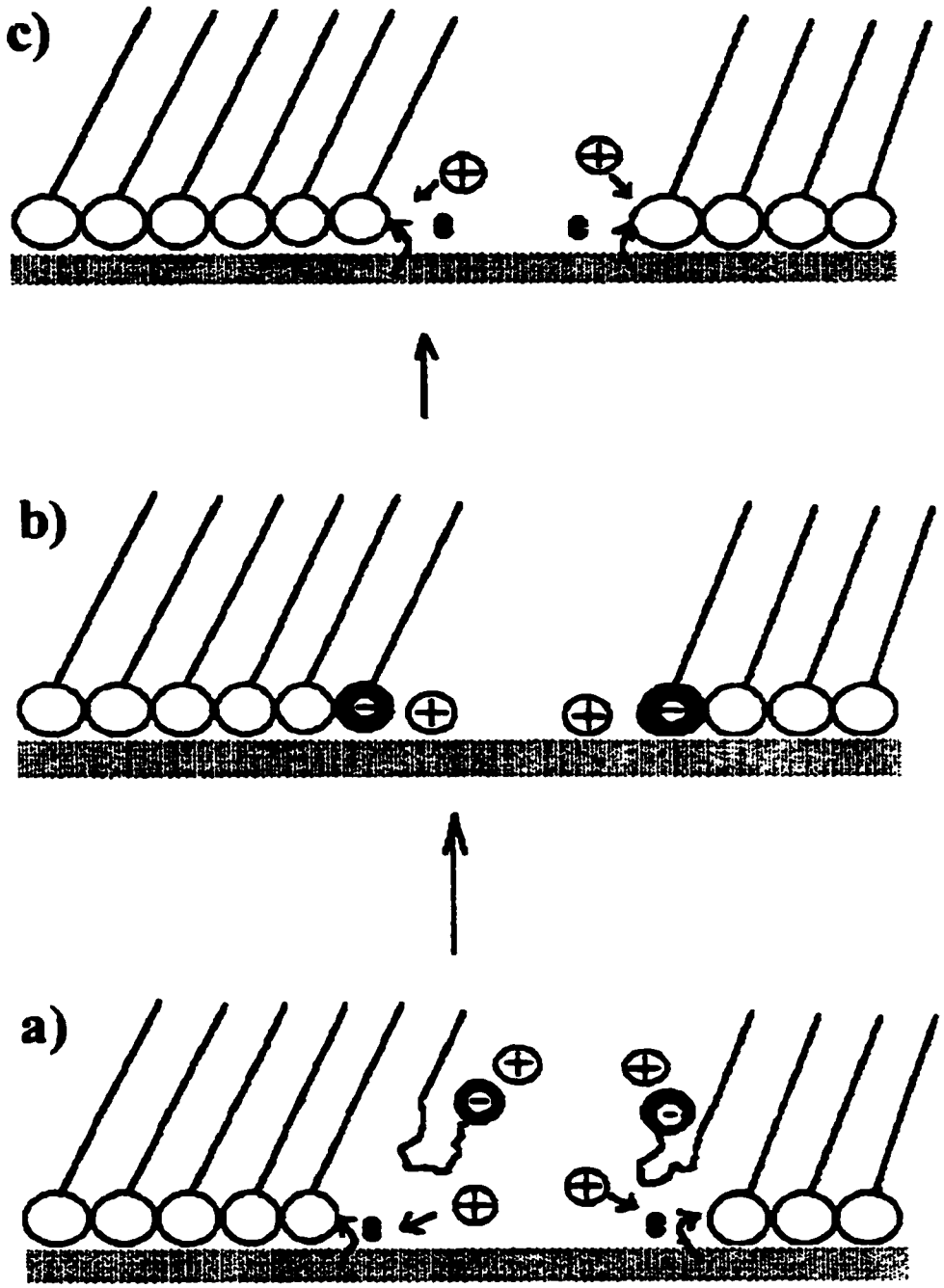

Figure 1-7: Mechanism of an etching center for a nucleation and growth model. (a) The reduced thiol has to overcome the chain-chain attraction to diffuse away from the surface. (b) once the reduced thiol is removed from the electrode surface, the reduction of the next thiol can occur. (c) A thiol at the edge of an etching center is reduced. Copy from ref. 1-60.

The other reductive desorption model [1-66] involves two desorption routes, which occur simultaneously in a given experimental situation. They are shown in Figure 1-8. One of them is the shrinkage of the thiol domains. It was described to follow three steps: (1) electrolyte and solvent redistribution next to thiol domains, (2) reduction of the sulfur heads under the influence of the strong electric field, (3) detachment of the reduced thiolates from their neighbors in the monolayers. The other route is the nucleation and growth process described above. In this model and the previous one, it has been suggested that the step of detachment of the reduced thiolate from the surface causes the asymmetric chronoamperograms.

It is generally accepted that the thiolate formation on gold is initiated by a fast one-electron oxidative step, which results in the covalent attachment of the sulfur to the gold surface. Next, the intermolecular interactions between the alkyl chains drive a slow reorganization process that yields the final structure. However, the mechanism of the monolayer formation is unknown. The goal of this study is to elucidate the mechanism of the oxidative deposition of organo-sulfur compounds on gold from aqueous solution.

Short ($n \leq 12$) alkane sulfur compounds are used in this study. This choice is motivated by their relatively high solubility in the aqueous solution which allows measurements at different concentrations. For the longer chain thiols, it was found [1-67] that after their reductive desorption they formed aggregates or micelles that remained at the surface, due to their low solubility in aqueous solutions.

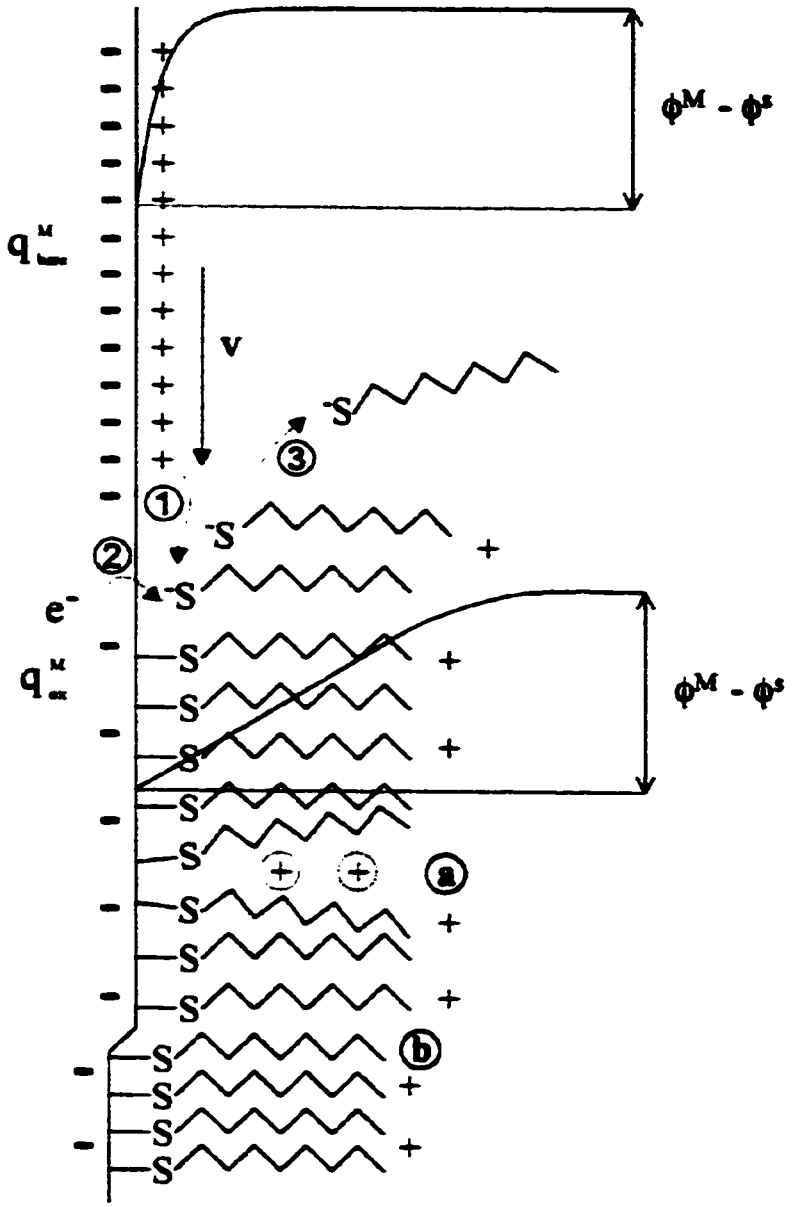

Figure 1-8: Schematic representation of the reductive desorption of a thiol monolayer at a fixed potential drop $\phi^M - \phi^S$. The upper potential profile is the bare surface and the lower is a surface coated thiol SAM. The desorption potential is assumed to be negative to the PZC of bare and coated electrode surface. Desorption from the film edge is assumed to consist of three steps: (1) surface redistribution of electrolyte ions, (2) electron transfer, (3) detachment of the reductive thiolates. Active sites for the nucleation may come from (a) local conformational disorder of the alkyl-chains, (b) metal surface defects. Copy from ref. 1-66.

This thesis is a study of the electro-formation of SAMs of sulfur compounds on gold. The structure of the thesis is as follow. In Chapter 2, we describe the experimental methods and set-ups used in this study. In Chapter 3, EQCM, cyclic voltammetry, chronoamperometry and potential-step experiments are used to study the kinetics of the oxidative adsorption of alkanethiolates and alkanethiols on gold from aqueous solutions. Mechanisms for the oxidative adsorption of these two species are presented. In Chapter 4, we examine the effect of the temperature and concentration on this process and estimate the activation energy for the oxidative deposition of thiols. Finally, the electro-adsorption of another organic sulfur compound, dialkyl sulfide, is described in Chapter 5. A brief conclusion is presented in Chapter 6.

References:

[1-1]: Nuzzo, R.G.; Allara, D.L. *J. Am. Chem. Soc.* **1983,** 105, 4481.

[1-2]: Ulman, A., *An Introduction to Ultra-Thin Organic Films* Academic press, San Diego, **1991.**

[1-3]: Ulman, A. *Chem. Rev* **1996,** 96, 1533.

[1-4]: Finklea, H.O., *Electroanalytical Chemistry* Vol.19, P109 Bard, A.J; Rubinstein, I Eds; Marcel Dekker, New York, **1990.**

[1-5]: Murray, R.W., *Molecular Design of Electrode Surface* Wiley, J. (Ed.) New York, **1992.**

[1-6]: Thoden Van Velzen, E.U.; Engbersen, J.F.J.; de Lange, P.J.; Mahy, J.W.G.; Reinhoudt, D.N. *J. Am. Chem. Soc.* **1995,** 117, 6853.

[1-7]: Chailapakul, O.; Sun, L.; Xu,C.; Crooks, R.M. *J. Am. Chem. Soc.* **1993,** 115, 12459.

[1-8]: Malem,F.; Mandler, D. *Anal. Chem.* **1993,** 65, 37.

[1-9]: Gooding, J.J.; Praig, V.G.; Hall, E.A.H. *Anal. Chem.* **1998,** 70, 2396.

[1-10]: Amador, S.M.; Pachence, J.M.; Fischetti, R.; McCauley, J.P.; Smith A.B.; Blasie, J.K. *Langmuir* **1993,** 9, 812.

[1-11]: Clark, R.A.; Bowden, E.F. *Langmuir* **1997,** 13, 559.

[1-12]: Giz, M.J.; Duong, B.; Tao, J. *J. Electroanal. Chem.* **1999,** 465,72.

[1-13]: Laibinis, P.E.; Whitesides, G.M. *J. Am. Chem. Soc.* **1992,** 114, 9022.

[1-14]: Scherer, J.; Vogt, M.R.; Magnussen, O.M.; Behm, R.J. *Langmuir* **1997,** 13, 7045.

[1-15]: Stratmann, M. *Adv. Mater.* **1990,** 2, 191.

[1-16]: Eliadis, E.D.; Nuzzo, R.G.; Gewirth, A.A.; Alkire, R.C. *J. Electrochem. Soc.* **1997**, 144,96.

[1-17]: kelly, J.J.; Tian, C.; West, A.C. *J. Electrochem. Soc.* **1999**, 146, 2540.

[1-18]: Katz, H.E.; Wilson, W.L.; Schller, G. *J. Am. Chem. Soc.* **1994**, 116, 6636.

[1-19]: Zagal, J. *Coord. Chem. Rev.* **1992**,119,89.

[1-20]: Nuzzo, R.G.; Zegarski, B.R.; Dubois, L.H. *J. Am. Chem. Soc.* **1987**, 109, 733.

[1-21]: Strong, L.; Whitesides, G.M. *Langmuir* **1988**, 4, 546.

[1-22]: Chidsey, C.E.D.; Loiacono, D.N. *Langmuir* **1990**, 6, 682.

[1-23]: Dubois, L.H.; Zegarski, B.R.; Nuzzo, R.G. *J. Chem. Phys.* **1993**, 98, 678.

[1-24]: Chidsey, C.E.D.; Liu, G.Y.; Rowntree, Y.P.; Scoles, G. *J. Chem. Phys.* **1989**, 91, 4421.

[1-25]: Alves, C.A.; Smith, E.L.; Porter, M.D. *J. Am. Chem. Soc.* **1992**, 114, 1222.

[1-26]: Widrig, C.A.; Alves, C.A.; Porter, M.D. *J. Am. Chem. Soc.* **1991**, 113, 2805.

[1-27]: Kim, Y.-T; McCarley, R. L; Bard, A. J. *J. Phys. Chem.* **1992**, 96, 7416.

[1-28]: Fenter, P.; Eisenberger, P.; Liang, K.S. *Phys. Rev. Lett.* **1993**, 70, 2447.

[1-29]: CamilloneIII, N.; Chidsey, C.E.D.; Liu, G.Y.; Scoles, G.J. *J. Phys. Chem.* **1993**, 98, 3503.

[1-30]: Poirier, G.E.; Tarlov, M.J. *Langmuir* **1994**, 10, 2853.

[1-31]: Sellers, H.; Ulman, A.; Shnidman, Y.; Eiler, J.E. *J. Am. Chem. Soc.* **1993**, 115, 9389.

[1-32]: Snyder, R.G. *J. Chem. Phys.* **1967**, 47, 1316.

[1-33]: Parikh, A.N.; Allara, D.L. *J. Chem. Phys.* **1992**, 96, 927.

[1-34]: Nuzzo, R.G.; Korenic, E.M.; Dubois, L.H. *J. Chem. Phys.* **1990**, 93, 767.

[1-35]: Butt, H-J.; Seifert, K.; Bamberg, E. *J. Phys. Chem.* **1993**, 97, 7316.

[1-36]: CamilloneIII, N.; Chidsey, C.E.D.; Liu, G.Y.; Scoles, G.J. *J. Chem. Phys.* **1993**, 98, 3503.

[1-37]: Delamarche, E.; Michel, B.; Gerber, Ch.; Anselmetti, D.; Guntherodt,H-J.; Wolf, H.; Ringsdorf, H. *Langmuir* **1994**, 10, 2869.

[1-38]: Bain, C.D.; Troughton, E. B.; Tao, Y-T.; Evall, J.; Whitesides, G. M; Nuzzo, R. G. *J. Am. Chem. Soc.* **1989**, 111, 321.

[1-39]: Schneider, T.W.; Buttry, D.A. *J. Am. Chem. Soc.* **1993**, 115, 12391.

[1-40]: Whitesides, G.M.; Laibinis, P.E. *Langmuir* **1990**, 6, 87.

[1-41]: Biebuyck, H.A.; Bain, C.D.; Whitesides, G.M. *Langmuir* **1994**, 10, 1825.

[1-42]: Truong, K.D.; Rowntree, P.A. *J. Phys. Chem .B* **1996**, 100, 19917.

[1-43]: Kim, Y.-T.; McCarley, R. L.; Bard, A. J. *Langmuir* **1993**, 9, 1941.

[1-44]: McCarley, R.L.; Dunaway, D.J.; Willicut, R.J. *Langmuir* **1993**, 9, 2775.

[1-45]: Porter, M.D.; Bright, T.B.; Allara, D.L.; Chidsey, C.E.D. *J. Am. Chem. Soc.* **1987**, 109, 3559.

[1-46]: Becka, A.M.; Miller, C.J. *J. Phys. Chem.* **1992**, 96, 2657.

[1-47]: Laibinis, P.E.; Whitesides, G.M.; Allara, D.L.; Tao, Y-T.; Parikh, A.N.; Nuzzo, R.G. *J. Am. Chem. Soc.* **1991**, 113, 7152.

[1-48]: Sawaguchi, T.; Sato, Y.; Mizutani, F. *Phys. Chem. Chem. Phys.* **2001**, 3, 3399.

[1-49]: Sawaguchi, T.; Sato, Y.; Mizutani, F. The 200th Meeting of The Electrochemical Society, Inc. and the 52nd Meeting of The International Society of Electrochemistry, San Francisco, California, **2001**.

[1-50]: Sek, S.; Misicka, A.; Bilewicz, R. *J. Phys. Chem. B* **2000**, 104, 5399.

[1-51]: Wolf, H.; Ringsdorf, H.; Delamarche, E.; Takami, T.; Michel, B.; Gerber, Ch.; Jaschke, M.; Butt, H-J.; Bamberg, E. *J. Phys. Chem.* **1995**, 99, 7102.

[1-52]: Delamarche, E.; Michel, B. *Thin Solid Films* **1996**, 273, 54.

[1-53]: Delamarche, E.; Michel, B.; Biebuyck, H.A.; Gerber, C. *Adv. Mater.* **1996**, 8, 719.

[1-54]: Kawaguchi, T.; Yasuda, H.; Shimazu, K.; Porter, M. D. *Langmuir* **2000**, 16, 9830.

[1-55]: Frubose, C.; Doblhofer, K. *J. Chem. Soc. Farad. Trans.* **1995**, 91(13), 1949.

[1-56]: Ma, F.; Lennox, R. B. *Langmuir* **2000**, 16, 6188.

[1-57]: Qu, D.; Morin, M. *J. Electroanal. Chem.* **2001**, 517,45.

[1-58]: Weisshaar, D.E.; Lamp, B.D.; Porter, M.D. *J. Am. Chem. Soc.* **1992**, 114, 5860.

[1-59]: Yang, D-F; Morin, M *J. Electroanal. Chem.* **1997**, 429, 1.

[1-60]: Yang, D-F; Morin, M *J. Electroanal. Chem.* **1998**, 441, 173.

[1-61]: Widrig, C.A.; Chung, C.; Porter, M.D. *J. Electroanal. Chem.* **1991**, 310, 335.

[1-62]: Walczak, M.W.; Alves, C.A.; Lamp, B.D.; Porter, M.D. *J. Electroanal. Chem.* **1996**, 395, 103.

[1-63]: Calvente, J.J.; Kovacova, Z.; Sanchez, M.D.; Andreu, R; Fawcett, W.R. *Langmuir* **1996**, 12, 5696.

[1-64]: Calvente, J.J.; Kovacova, Z.; Andreu, R; Fawcett, W.R. *J. Chem. Soc. Farad. Trans.* **1996**, 92, 3701.

[1-65]: Vinokurov, I.A.; Morin, M.; Kankare, J. *J. Phys. Chem. B* **2000**, 104, 5790.

[1-66]: Mulder, W.H.; Calvente, J.J.; Andreu, R. *Langmuir* **2001**, 17, 3273.

[1-67]: Byloos, M.; Al-Maznai, H.; Morin, M. *J. Phys. Chem. B* **1999**, 103, 6554.

Chapter 2

Experimental

We used various electrochemical and spectroscopic techniques for the study of the electrodeposition of organo-sulfur compounds on gold. Here, these techniques are described. They are cyclic voltammetry (CV), differential capacitance, chronoamperometry, ex-situ IR spectroscopy, in-situ IR spectroscopy, and Electrochemical Quartz Crystal Microbalance (EQCM). In this chapter, we also describe sample preparations and experimental setups. In the last section, the data analysis is detailed.

2.1. Theoretical concepts of the experimental methods

2.1.1. Cyclic Voltammetry (CV)

Cyclic voltammetry involves applying a linear variation of the potential to an electrode and measuring the resulting current generated at this electrode. The potential applied to the electrode varies between two values as shown in Figure 2-1. The potential is normally generated with a function generator and applied to the working electrode through a potentiostat. The curve of the resulting current vs applied potential can be recorded with an X-Y recorder, oscilloscope or stored in a computer. The current is

displayed on the vertical axis and the horizontal axis is the potential axis (actually it is also a time axis).

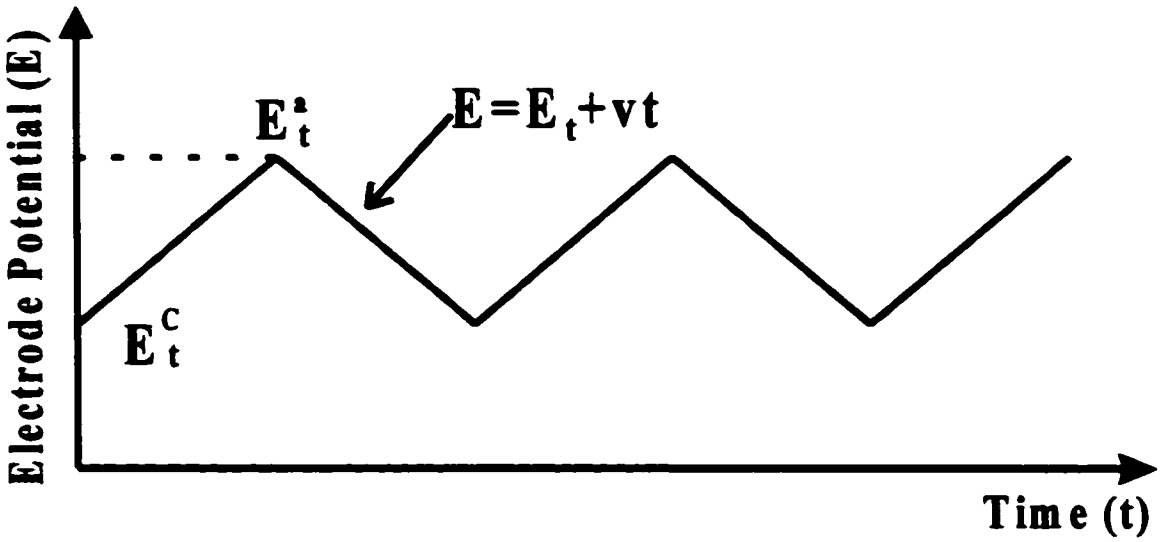

Figure 2-1: Potential-time behavior at the working electrode in cyclic voltammetry, where v is the scan rate. E_t^a: Anodic potential limit, E_t^c: Cathodic potential limit.

We use a three-electrode system shown in Figure 2-2 to record cyclic voltammograms. This is due to a small but non-negligible potential drop (iR_s) in the solution [2-1] as shown in Figure 2-2. When the potential of the working electrode is measured against a reference electrode, a voltage drop equal to iR_s will be included in the measured potential. R_s is the solution resistance between these two electrodes and i is the current. When iR_s is very small, a two-electrode system [2-2] is used because the iR_s drop can be neglected and the potential of the reference electrode remains constant. But when the iR_s potential drop gets larger, a three-electrode system must be used. A counter (also called auxiliary) electrode is introduced to the system. The current i then flows between the

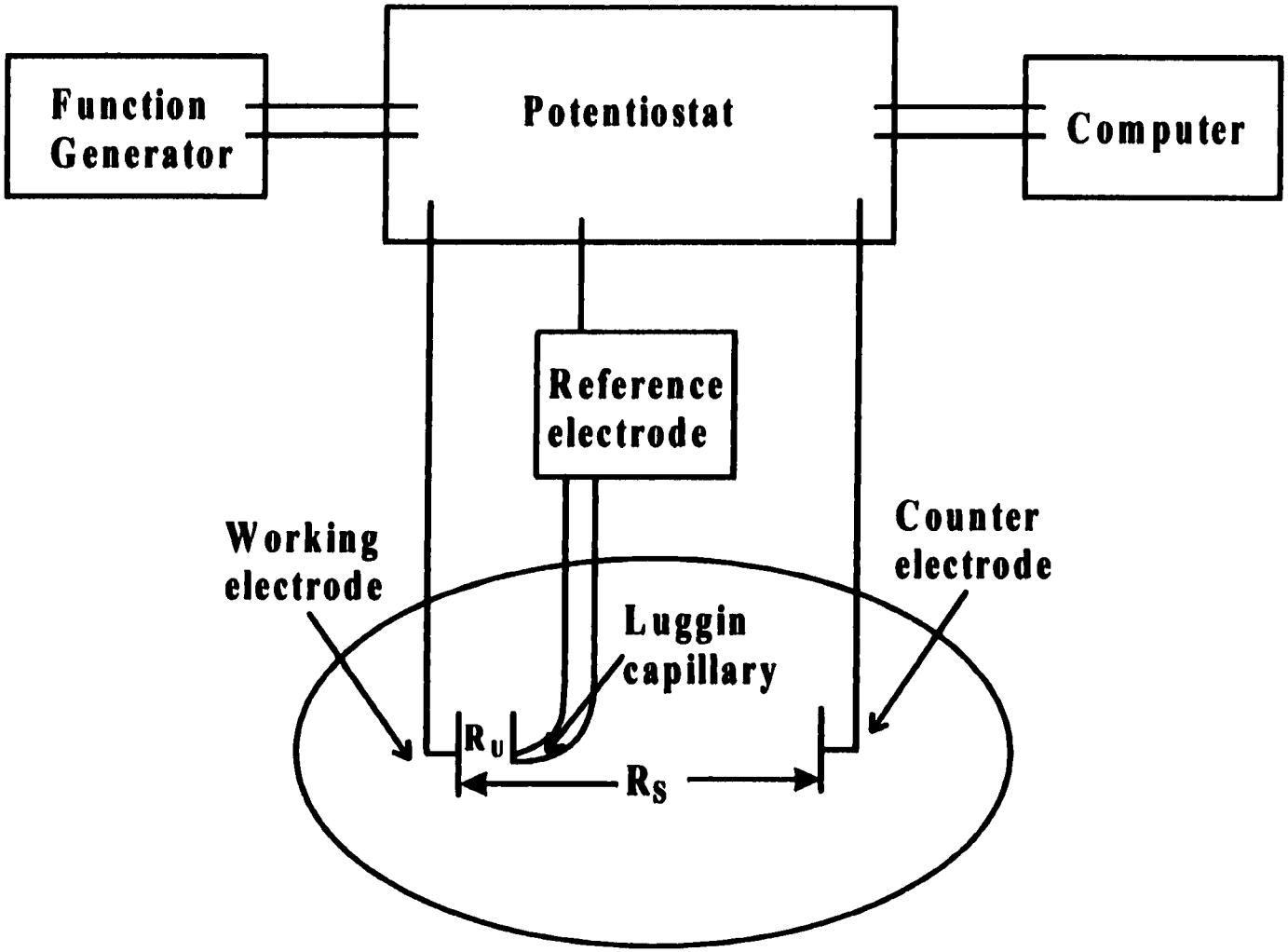

Figure 2-2: A three-electrode system.

counter and the working electrode. A separate reference electrode is used to monitor the potential (E) of the working electrode. In this configuration, i is the current passing between the working electrode and the counter electrode, and E is the potential applied to the working electrode relative the reference electrode potential. The absence of a significant current flowing into or out of the reference electrode ensures a stable reference potential. This is achieved by having a very high input impedance for the reference electrode connection to the potentiostat. Hence, the current only flows between the working and counter electrode. Even in this arrangement, a potential drop called iR_u, where R_u is the uncompensated solution resistance, still occurs and cannot be neglected. The uncompensated resistance is reduced by using a Luggin capillary located near the working electrode. Unfortunately, this error cannot be totally corrected. It is limited by the distance between the working electrode and Luggin capillary. The current distribution will become inhomogeneous if the tip of the Luggin capillary is placed too close to the working electrode. The best distance between the tip of the Luggin capillary and working electrode is dependent on the size of the tip of the Luggin capillary. Normally it is twice the tip's diameter [2-2].

In cyclic voltammetry, the current is separated into two components. The Faradaic current comes from the electron transfer process across the electrode/solution interface. The non-Faradaic current (capacitive current) is due to the depletion/accumulation of charged species at the electrode/solution interface when the potential is varied. This causes a transient current. This

process does not involve electron transfer. These two kinds of current are normally coupled and are difficult to separate (see below).

Cyclic voltammetry was used for two purposes. One of them is to check the quality and cleanliness of the surface of the gold electrode. The other is to obtain information about the electrochemical properties of organic monolayers and their oxidative adsorption/reductive desorption processes. From the shape of the reductive and oxidative current peaks, peak potentials, integrated charges and double-layer capacities, quantitative information about the coverage of molecules on the gold electrode and qualitative information on the strength of their bonds with the surface and the adsorption kinetics is obtained.

2.1.2 Differential Capacitance

The formation of an electrical double layer at the electrode/solution interface is shown in Figure 2-3.

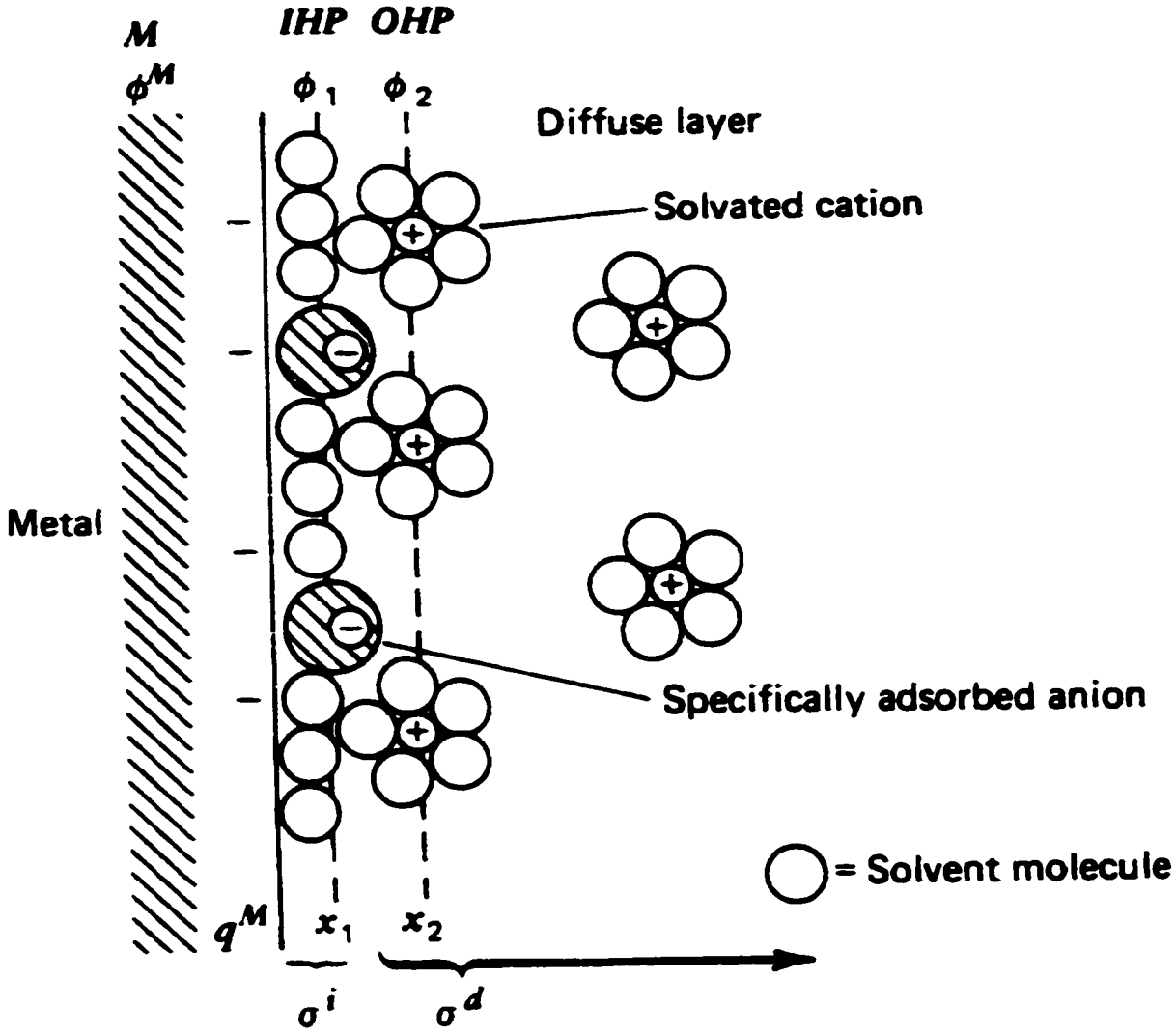

Figure 2-3: Model of the double layer region at the electrode/solution interface. σ^i is the ionic charge density in the inner Helmholtz plane (IHP), σ^d is the ionic charge density in the outer Helmholtz plane (OHP). Copy from ref. 2-2.

This double layer can be considered as a parallel plate capacitor. The capacitance, C, is thus define as

$$C = Q / E \qquad (2\text{-}1)$$

Q is the charge on a plate and E is the potential difference between the plates.

When we cause a small alternation of potential, δ E, to the electrode, it will be accompanied by a small change, δ Q, of the charge. d Q/ d E is a better description of the process of double layer change, than the value of the capacitance itself. Since d Q/ d E has the dimensions of capacitance, it is usually called differential capacitance, C_d.

$$C_d = d Q / d E \qquad (2\text{-}2)$$

The variation of C_d with the potential gives information on the structure of the double layer at the electrode/solution interface.

To measure how the differential capacitance changes with the potential, we cycle the electrode potential in the region of interest. The potential scan rate will be typically of 5 mV s^{-1}. A small sinusoidal perturbation (AC amplitude 5 mV, frequency 20 Hz) is superposed on this potential ramp. The output from the potentiostat, which is in the form of an AC current, is fed into an impedance analyzer where the current is separated into its in-phase components (the phase angle is zero compared with the initial AC signal), and quadrature components (the phase angle shift 90^0 relative to the initial AC signal). The two outputs from the impedance analyzer are fed into the computer. The differential capacitance of the double layer was determined using the following analysis:

The equivalent circuit for the electrode/solution interface was assumed to be a simple series RC circuit:

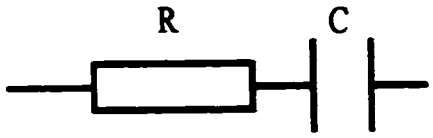

The impedance of this circuit is given by

$$Z = R + (1 / i\omega C) \qquad (2\text{-}3)$$

Where R is the solution resistance between the working electrode and the tip of the Luggin capillary and C is the capacitance of the electrode/solution interface. ω is the circular frequency which is equal to $2\pi f$, where f is the frequency of the AC potential. If an alternating current is flowing through this circuit, the total current is given by

$$I = V_{ac} / Z = V_{ac} / (R + 1 / i\omega C) \qquad (2\text{-}4)$$

The real and imaginary components of the current are

$$I_{re} = V_{ac}\omega^2 RC^2 / 1+\omega^2 R^2 C^2 \qquad (2\text{-}5)$$

$$I_{im} = V_{ac}\omega C / 1+\omega^2 R^2 C^2 \qquad (2\text{-}6)$$

where V_{ac} is the root mean square value of the AC potential.

From equations 2-5 and 2-6, the following expression for the capacitance C can be derived:

$$C = (I_{re}^2 + I_{im}^2) / V_{ac}\omega I_{im} \qquad (2\text{-}7)$$

The purpose of using the differential capacitance measurement here is to obtain information on the double layer change, especially when alkanethiolate adsorption/desorption occurs. This will help us in the analysis of our EQCM result (see below).

2.1.3. Chronoamperometry

Chronoamperometry is a potential-step experiment. In this experiment, the potential of the working electrode is changed instantaneously, and the current-time response is recorded. A potential - time profile (as shown in Figure 2-4) is applied to the working electrode. In our case, the initial potential E_1 is chosen such that there are no Faradaic processes occurring. Then at time t = 0, the potential is instantaneously changed to a new value E_2. The final potential E_2 is chosen in a region where a Faradaic reaction occurs. The typical current - time curves for a chronoamperometry experiment are shown in Figure 2-5 for a system where no chemisorption occurs.

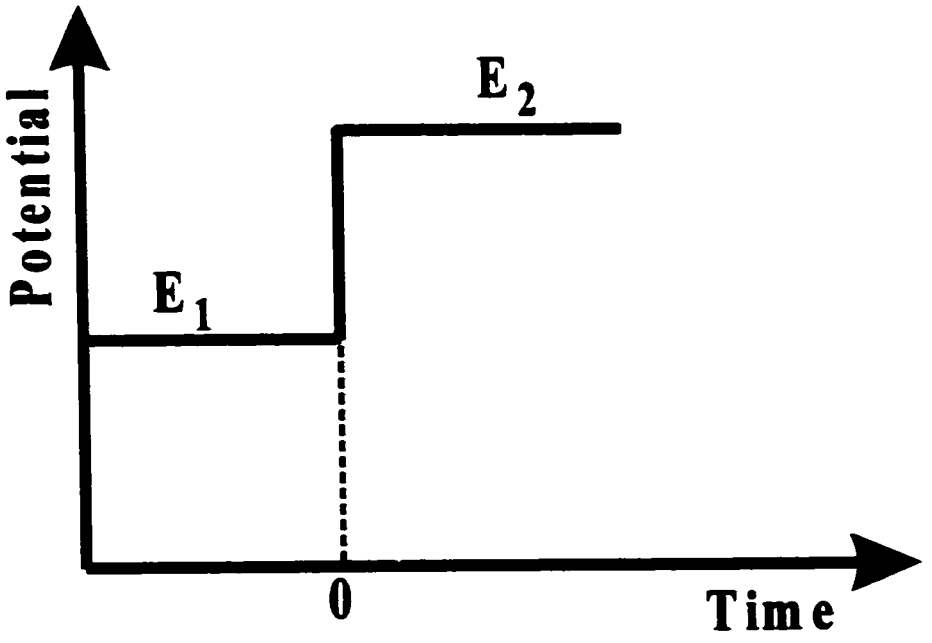

Figure 2-4: Potential-time curve in chronoamperometry.

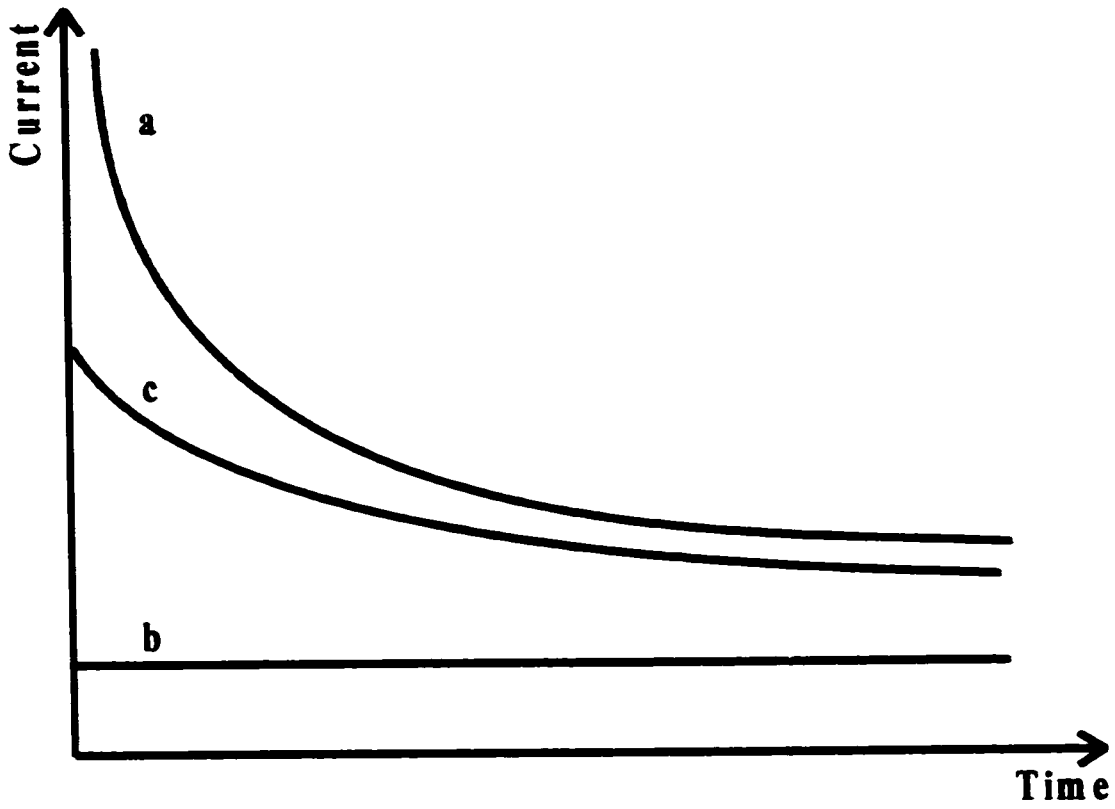

Figure 2-5: Current-time response for a chronoamperometry experiment. Curves a, b, c represent different final potentials E_2: a) the reaction is diffusion controlled, b) the reaction is kinetic controlled and c) there is mixed control.

Chronoamperometry is used to study the kinetics of electrochemical reactions. The current transient is a measure of the process by which the electrochemical system reaches a new equilibrium state. As shown in Figure 2-5, at different values of final potential, different current-time responses are obtained. From the shape of the current-time responses and the corresponding final potentials, we can obtain kinetics information on the reaction under study.

We have used chronoamperometry experiments to study alkanethiol electrodeposition processes on gold. As mentioned previously, the Faradaic current and capacitive current are normally coupled. These two kinds of currents occur simultaneously. So, we cannot separate the capacitive and Faradaic charges from the total charge in the chronoamperometry experiment, except if they occur on a different time scale. This is not the case in our experiments.

2.1.4. Ex-situ FTIR reflectance spectroscopy

IR spectroscopy allows the identification of functional groups in organic compounds. It is a useful tool in the study of the structure and orientation of organic monolayers [2-3]. From the IR spectra, we can obtain information about the average direction of transition dipoles in adsorbates relative to the surface.

In grazing incidence IR spectroscopy, an incident beam of infrared radiation is reflected from a monolayer covered metal surface and into a detector. At a metal surface, the IR adsorption phenomenon follows a selection rule [2-4, 2-5, 2-6]. This selection rule is that only transition dipoles with components perpendicular to the metal surface can be excited.

The selection rule is based on the coupling of the electric dipoles of molecules on a surface and the electric field of IR light. When the infrared light is reflected from a metal surface, as shown in Figure 2-6, s-polarized radiation

(which has an electric field polarized perpendicular to the plane of incidence and parallel to the plane of the metal surface) will undergo a phase shift of 180° at all angles of incidence. Therefore, the electric field of the incident light and its electric image cancel each other at the metal surface. However, p-polarized radiation (the electric field is polarized parallel to the plane of incidence), whose electric field is mostly perpendicular to the plane of a metal surface, generates an electric image in the metal surface. This electric image will have the inverse vectorial orientation as that of the p-polarized radiation. A reinforcement (doubling) of the electric field occurs as a result of the combination of the p-polarized radiation with its electric image. Thus, vibrational excitations can occur using p-polarized IR light. A grazing angle maximizes the electric field perpendicular to the surface.

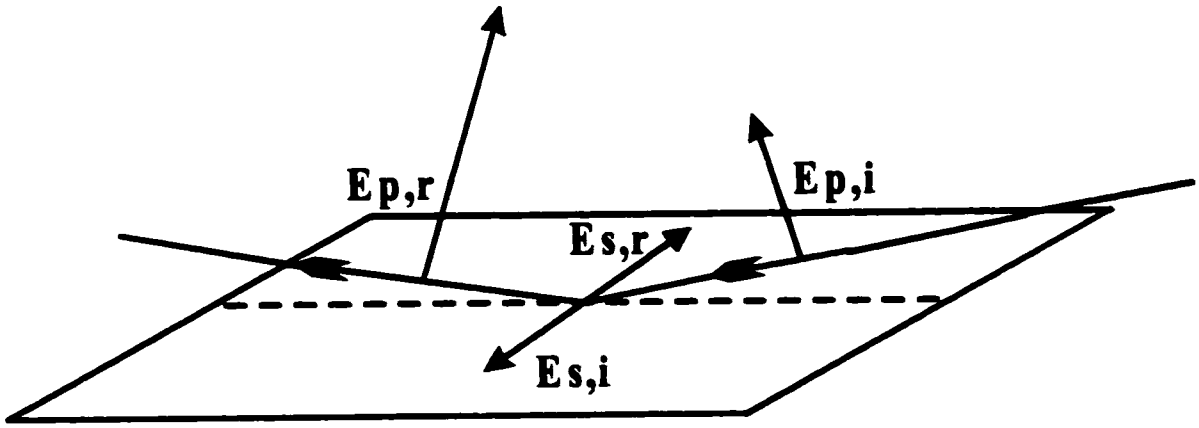

Figure 2-6: s-polarized and p-polarized light of incident and reflected beams on a metal surface. $E_{p,i}$ and $E_{p,r}$ are the electric field of incident and reflected p-polarized radiation. $E_{s,i}$ and $E_{s,r}$ are the electric field of incident and reflected s-polarized radiation.

This selection rule gives us the possibility of obtaining information on the orientation of molecular species at the interface. For example, the intensity of the methylene vibrational modes in the spectra is a function of the tilt angle of the alkyl chain relative to the metal surface, as shown in Figure 2-7.

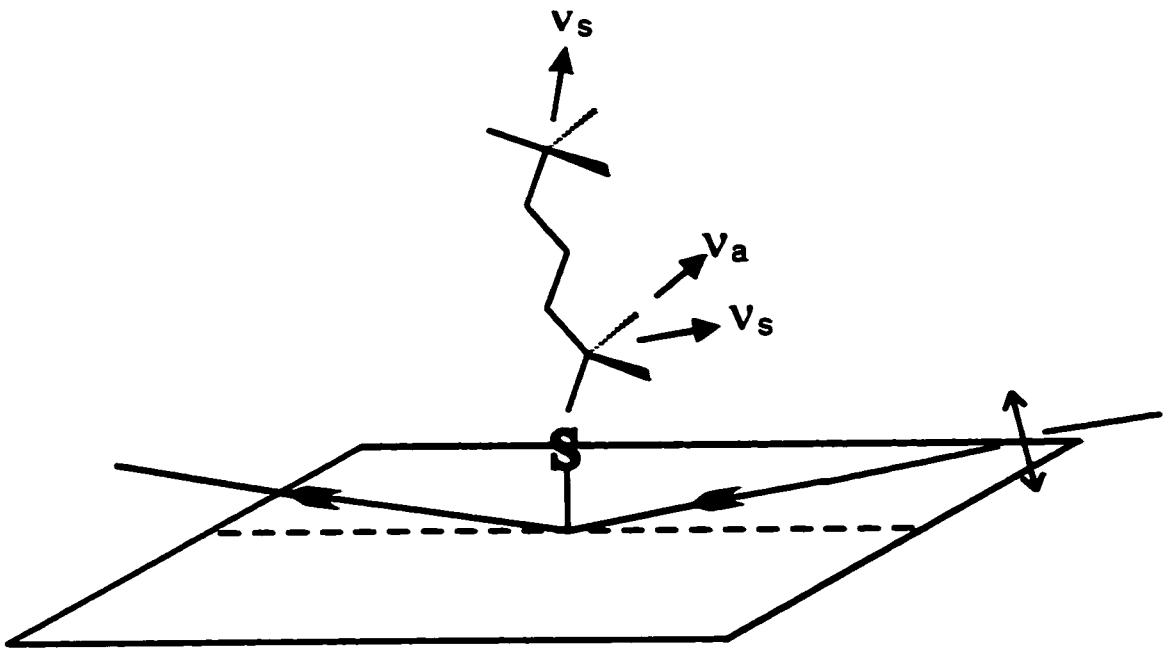

Figure 2-7: Schematic diagram of IRAS (Infrared Reflection-Adsorption Spectroscopy) experiment. (ν_a: asymmetric -CH stretching mode transition dipole moment; ν_s: symmetric -CH stretching mode transition dipole moment).

In our ex-situ IR spectroscopy experiments, an infrared beam was reflected from a monolayer covered Au (111) surface and the reflectance spectrum was recorded. A second spectrum was taken under the same conditions except that there was no monolayer on the Au (111). The absorbance spectrum is then

calculated using: $A = - \log (I / I_0)$, where I and I_0 are the reflected intensities of the monolayer coated and clean Au (111) surfaces respectively.

2.1.5. In-situ FTIR reflectance spectroscopy

In-situ grazing incidence IR spectroscopy is used to monitor the variations of the IR spectra at a metal surface when it is subjected to different electrochemical conditions, which cause adsorption or desorption of molecules. To change the electrochemical conditions on the metal substrate, the potential-step method described above is used. The variations of the IR spectra recorded while following a potential step are caused by many factors. These include adsorption, desorption and chemical transformations of IR active species at the metal surface.

Due to the fact that the transition dipoles of the species in the solution are randomly oriented, the species in the solution can adsorb both s- and p-polarized light equally well. So if the variations are observed only with p-polarized incident IR light, the species that caused this variation are at the metal surface.

2.1.6. Electrochemical Quartz Crystal Microbalance (EQCM)

QCM (Quartz Crystal Microbalance) is used to measure the mass change at a surface. This is achieved by monitoring the change of the resonant frequency of a quartz

crystal, which is caused by a mass change. A decrease in mass will correspond to an increase in frequency and vice versa. When QCM is used in electrochemical experiments, it allows simultaneous monitoring of the electrochemical parameters of the system (i.e. potential and current) and the effective mass of the electrode. In this case, the expression electrochemical quartz crystal microbalance (EQCM) is used. EQCM has become a useful tool in electrochemistry.

The EQCM measures the resonant frequency of a quartz crystal when one of the electrodes is exposed to an electrolyte solution and maintained under potential control. The other electrode is exposed to air. Many phenomena can give rise to a frequency change. Viscoelastic changes at the electrode surface, loss or addition of mass at the electrode surface, and mechanical stress are the most common factors causing changes of the resonant frequency [2-7, 2-8, 2-9]. In the simplest case, the frequency shift is only caused by mass changes at the surface of the quartz crystal. In this case, in the approximation that the adsorbates form a rigid layer, a linear equation called the Sauerbrey equation [2-10] describes the relationship between the frequency and mass:

$$\Delta f = - 2f_0^2 \Delta m / A(\mu_q \rho_q)^{1/2} \qquad (2\text{-}8)$$

where Δf, and Δm are the frequency and mass change respectively, f_0 is the frequency of the quartz crystal before mass change, A is the piezoelectric active area, μ_q is the shear modulus, and ρ_q is the quartz density. Other than Δf and Δm, all the other terms are

constants. Thus equation 2-8 can be rewritten as: $\Delta m = -\Delta f \times S$. In our case [2-11], S is 5.608 ng cm^{-2} Hz^{-1}.

The quartz crystal we used in the EQCM experiments is an AT-cut quartz crystal. The AT-cut quartz crystal is prepared by slicing through a quartz crystal at an angle of 35^0 15' with respect to the X-crystallographic axis. There are other cuts made from quartz, such as X-cut, Y-cut, BT-cut and so on. The AT-cut quartz crystal is most often used because:

1) It has a relatively high frequency.

2) It exhibits excellent frequency vs temperature stability.

3) Its a low cost.

The excellent frequency vs temperature stability is very important in our kinetics studies. The frequency vs temperature characteristics of the AT-cut crystal are shown in Figure 2-8 [2-12]. From the graph, we find that around room temperature, the frequency changes little with the temperature change.

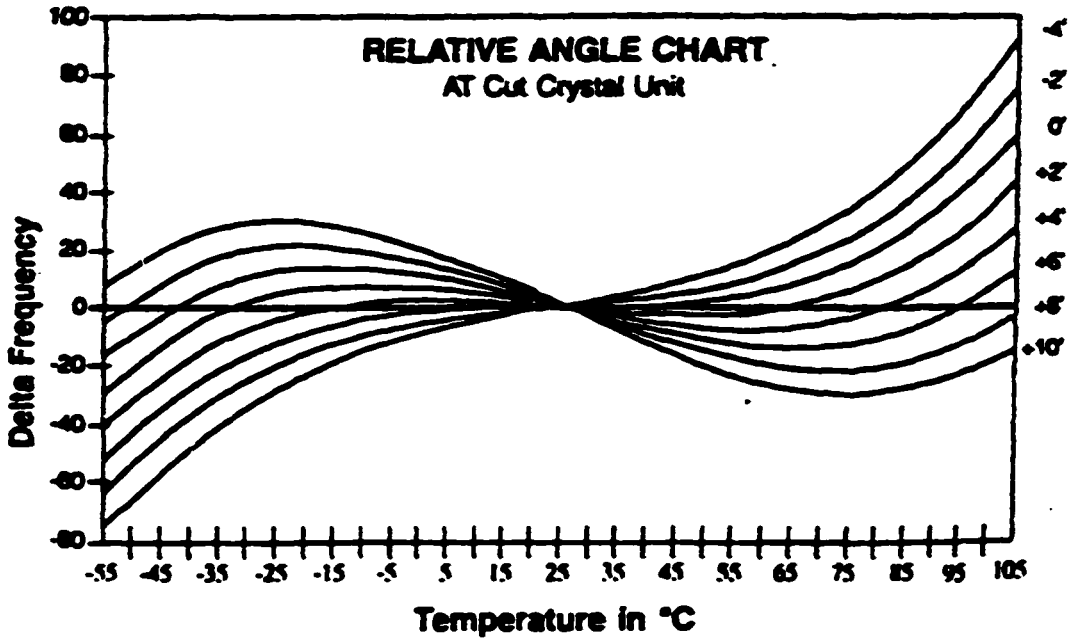

Figure 2-8: Dependence of the resonance frequency on temperature for an AT-cut quartz crystal and crystals cut with small deviation. Copy from ref. 2-12.

We use EQCM to study the process of adsorption on a gold surface. In our case, the mass change on the electrode surface is directly proportional to the EQCM response (see Chapter 3).

2.2. Experimental Setups

2.2.1. Cyclic Voltammetry

Cyclic voltammetry was carried out in a three-electrode cell [2-2], shown in Figure 2-9. The working electrode was an Au (111) single crystal (99.999%,

Johnson Matthey), the counter electrode was a gold wire and the reference electrode was a saturated calomel electrode (SCE) (Fisher Scientific). The reference electrode was immersed in a container filled with a saturated solution of KCl. The solution was in electrical contact with the electrolyte in the main electrochemical cell through a salt bridge. The salt bridge was terminated by a Luggin capillary, which was close to the working electrode in order to decrease the iR_u drop. The other end of this bridge was a tube, which was dipped into the saturated KCl solution in a bottle containing the reference electrode. A three way stopcock was positioned in the middle of the salt bridge. This prevented the KCl solution from flowing from the bottle to the electrochemical cell and therefore contaminating the electrolyte solution with Cl^-. There were two inlets on the top of the electrochemical cell. One was used for degassing the solution and the other to keep a positive argon pressure. Another port on the side of the cell let the argon gas out through a bubbler. The electrochemical cell was placed inside a Faraday cage to diminish electrical and magnetic interferences.

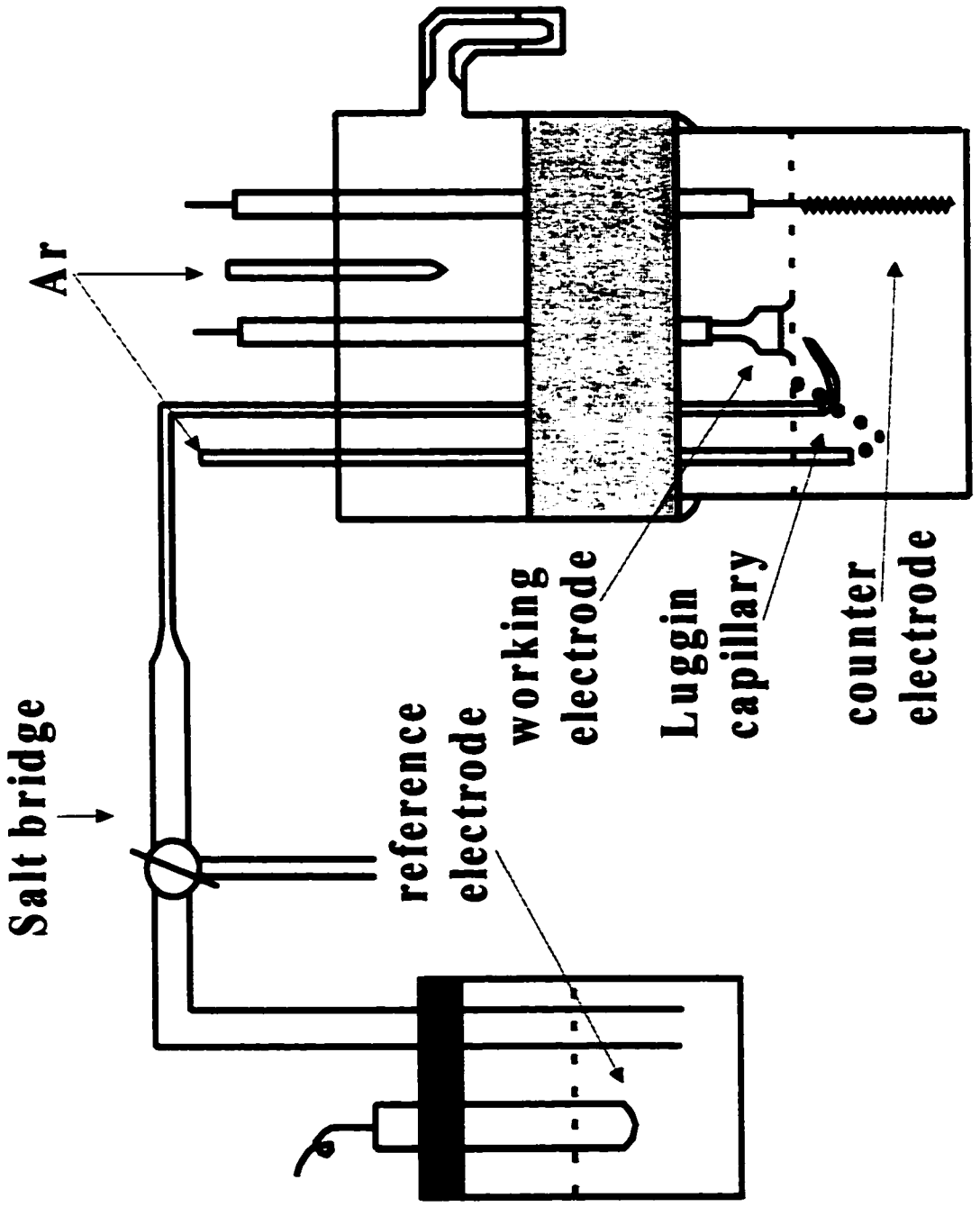

Figure 2-9: Electrochemical cell used for cyclic voltammetry.

Two modifications of this three-electrode cell will be presented for the cyclic voltammetry measurements simultaneous with either EQCM or *in-situ* FTIR. All the potentials given in this thesis are relative to a saturated calomel electrode (SCE).

The cyclic voltammetry measurements were usually done with a Solartron (Solartron Group Inc., England) electrochemical interface (Model 1287). It was connected to a computer for digital acquisition of cyclic voltammograms, and controlled by a software called Corrware© (Scribner Associates, Charlottesville, VA). The cyclic voltammograms were plotted by the software called Corrview© (Scribner Associates, Charlottesville, VA). When cyclic voltammetry was combined with other methods, different potentiostats and software were used (see below).

2.2.2. FTIR spectroscopy

2.2.2.1. Ex-situ experiment

The ex-situ IR spectroscopy experiments were carried out in a nitrogen-purged Nicolet Magna-IR 550 spectrometer. An angle of 80^{O} between the surface normal and the beam direction was used as shown in Figure 2-10. The IR radiation of the incident beam was p-polarized by a ZnSe wire grid polarizer.

Because the amount of light absorbed by a monolayer of organic molecules is very small (10^{-3} to 10^{-4} in absorbance units),1000 scans (at a resolution of 2 cm^{-1}) are averaged to increase the signal/noise ratio in the spectra.

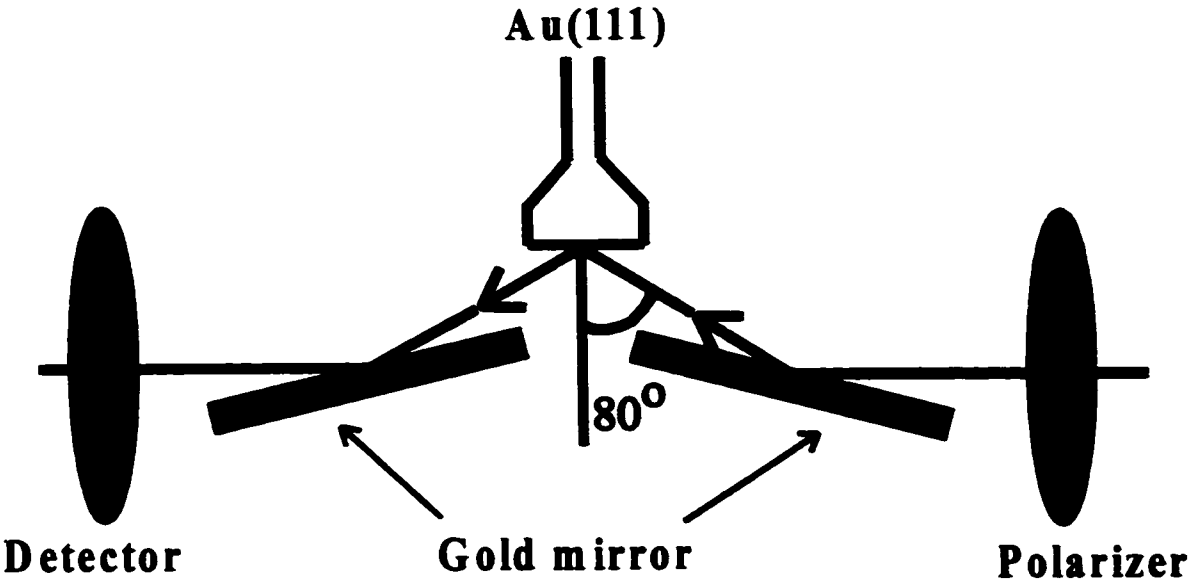

Figure 2-10: Ex-situ IR experimental set-up.

2.2.2.2. In-situ experiment

The in-situ experiments were carried out with the same instrument used for the ex-situ IR spectroscopy experiment. A potentiostat (Omni 90, Cypress System, Inc.) was used to control the potential applied to the gold electrode. The electrochemical cell used for the in-situ IR spectroscopy experiments and the optical setup are described in Figure 2-11 [2-13]. A 60° CaF_2 trapezoidal prism was used as the optical window mounted at the bottom of the cell. The angle of incidence of the IR light at the electrode surface was 85 ± 3°. In this cell, the Au (111) is pressed onto

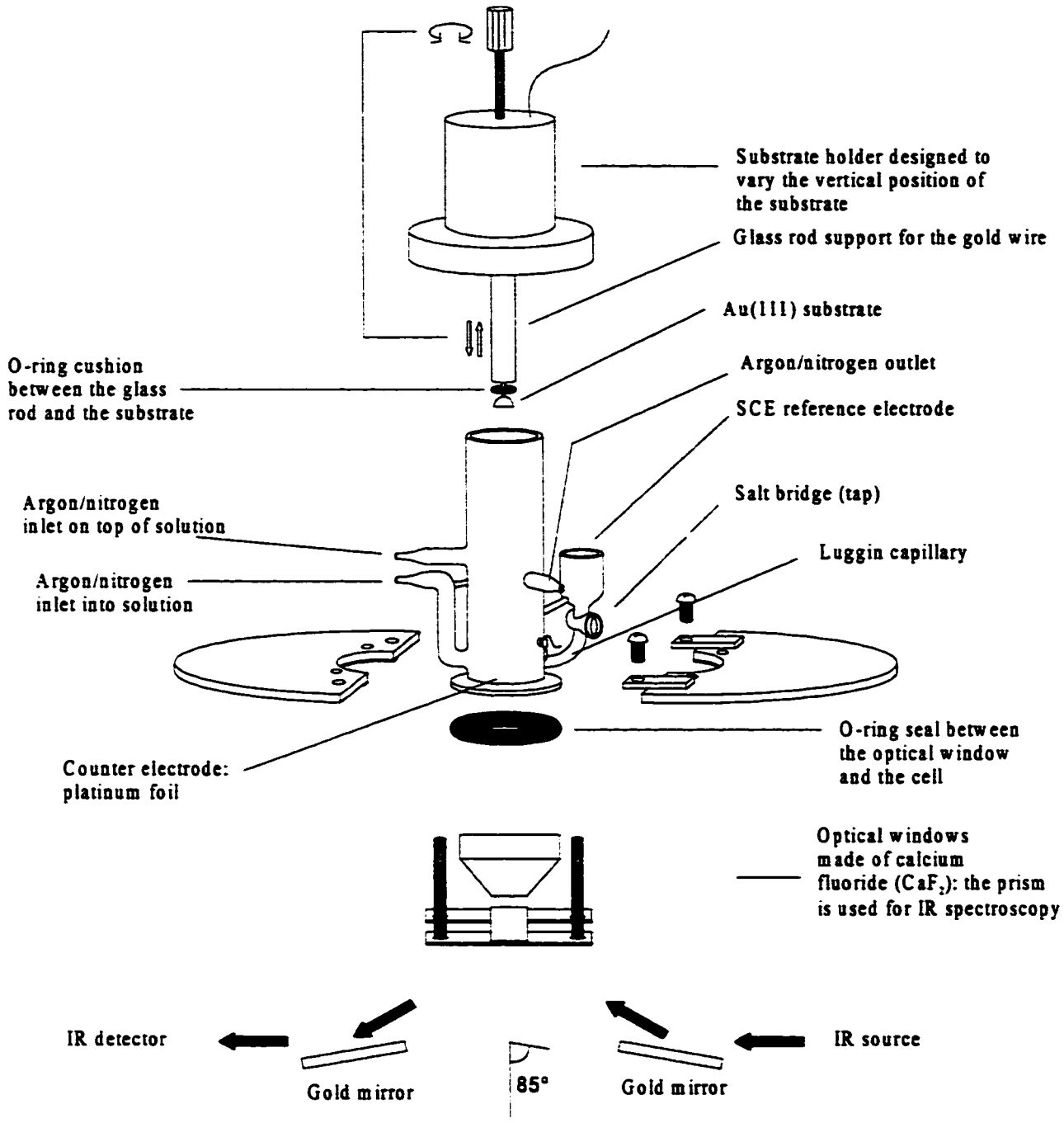

Figure 2-11: Electrochemical cell for the in-situ IR spectroscopy experiment. Copy from ref. 2-13.

the CaF_2 window to form a thin electrolyte layer of a few micrometers. This decreases the contributions of IR adsorption from the electrolyte (i.e. water molecules). Therefore, the small variation of IR adsorption due to the electro-deposition of sulfur compounds on the gold surface can be observed more easily. The cyclic voltammograms taken in these experiments were measured with the potentiostat mentioned above and recorded on a X-Y recorder (Yokogawa, model 3023).

2.2.3. Electrochemical Quartz Crystal Microbalance (EQCM)

2.2.3.1. EQCM measurements at room temperature

All the EQCM experiments were carried out with an EG&G QCA-917 quartz crystal analyzer and an EG&G 263A potentiostat (Perkin Elmer Instrument Inc.) controlled with the Power Suite software (Princeton Applied Research, Perkin Elmer Instrument Inc.). The cyclic voltammetry and potential-step experiments, carried out during EQCM measurements, are performed with the same potentiostat and software.

The electrochemical cell used for EQCM measurements is shown in Figure 2-12 [2-14]. The dashed line in the Figure 2-12 is a water jacket added to the cell (see below). On the right side of the cell, there is a quartz crystal holder. An assembly diagram of this holder is shown in Figure 2-13 [2-11, 2-14]. The holder was made of Telfon© and stainless-steel. Two Viton© O-rings were used to reduce the mechanical stress on the quartz crystal.

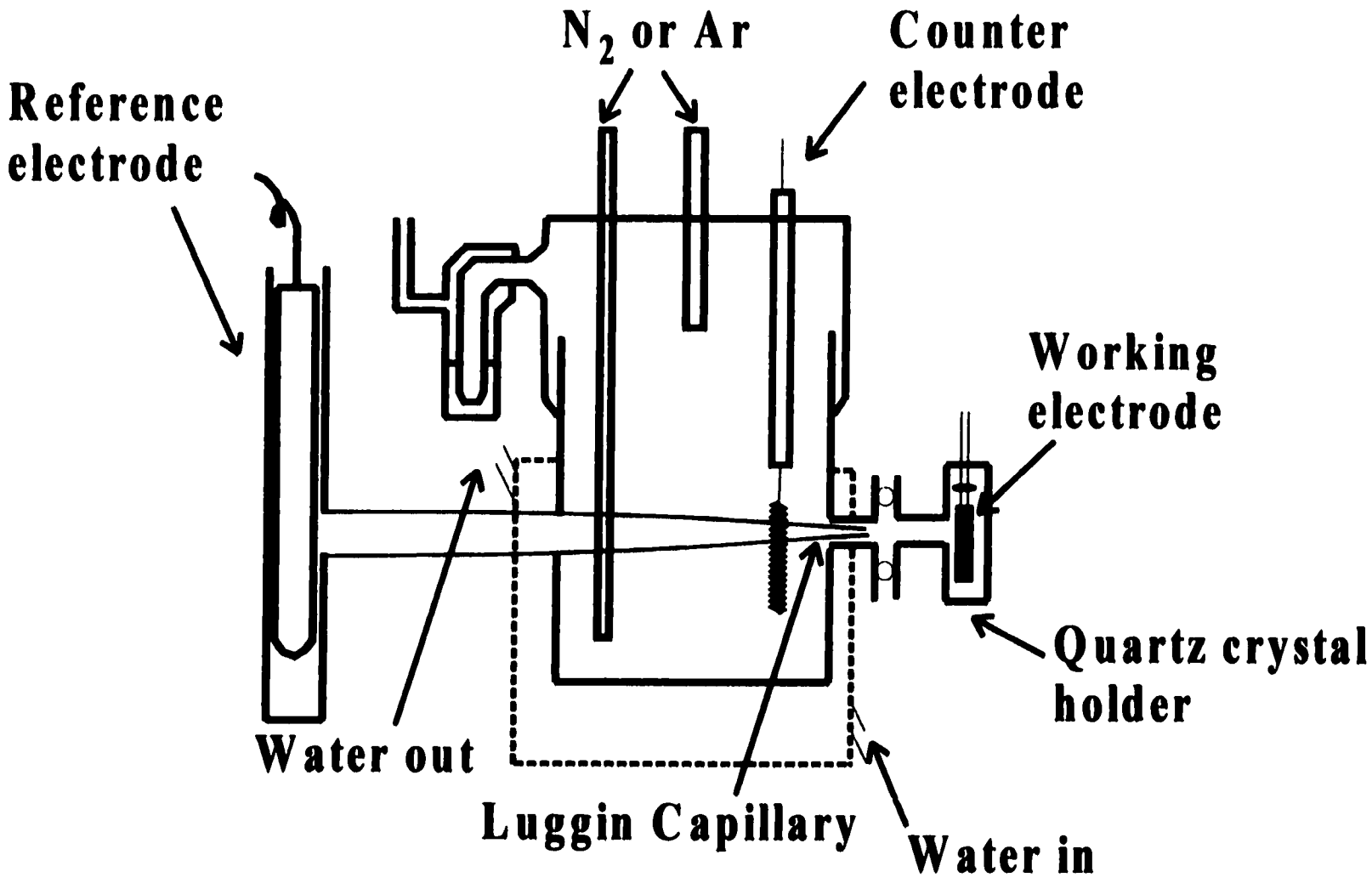

Figure 2-12: Electrochemical cell for EQCM experiments (modified from ref. 2-14).

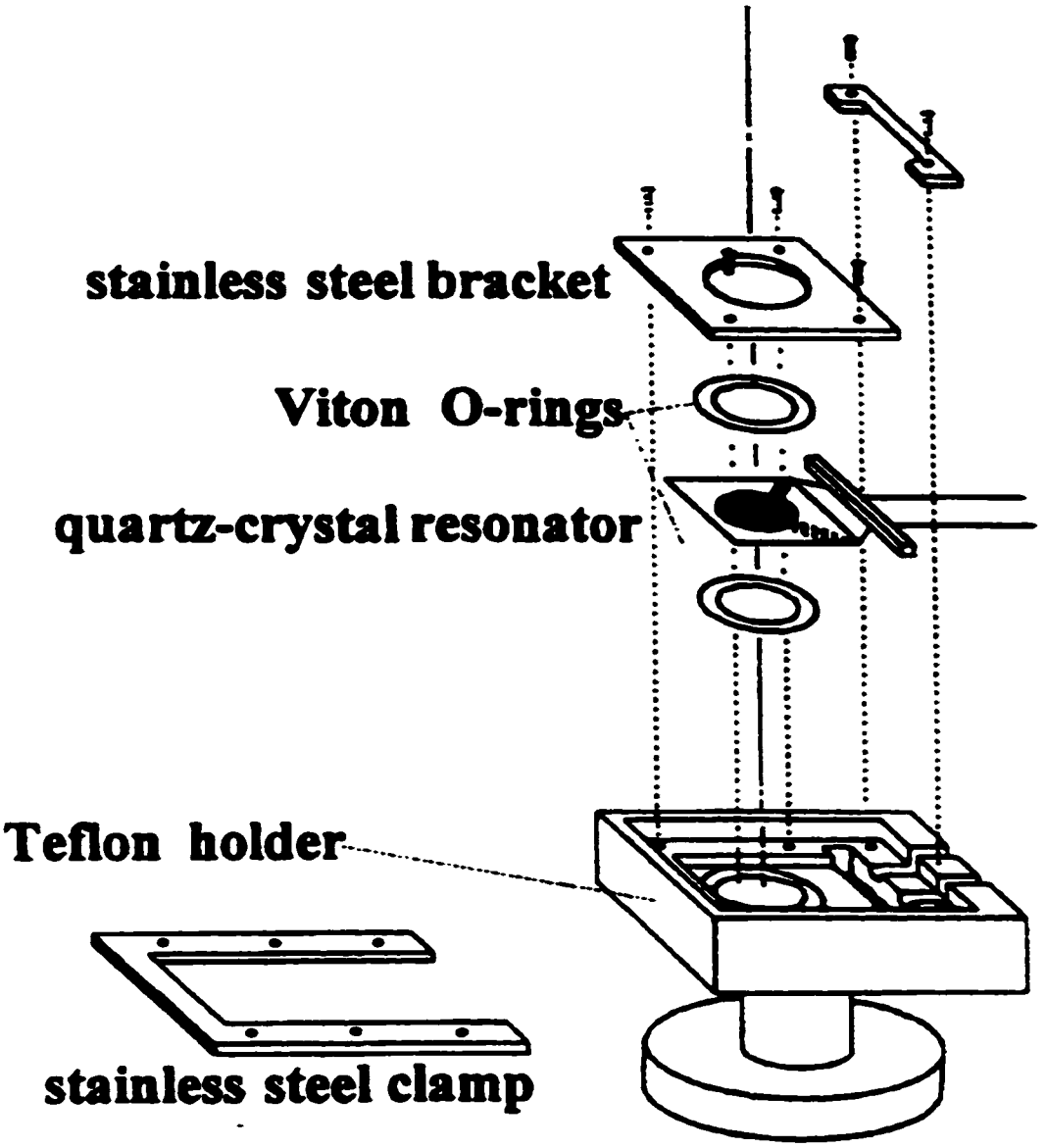

Figure 2-13: Telfon© holder of the quartz crystal resonator. Copy from ref. 2-14.

2.2.3.2. Temperature control of the EQCM cell

The temperature of the EQCM cell is adjusted with a thermostatted water bath (model 1180A VWR Scientific). A digital thermometer (Fluke model 51K/J, John Fluke MFG. Co., Inc.) was used to measure the temperature of the solution in the cell next to the quartz crystal surface. The electrochemical cell is the same except a water jacket is added.

The temperature vs time are given in Table 2-1. From Table 2-1, we see that the temperature of the electrolyte solution is controlled within $\pm$ 0.2 ^{0}C

2.2.4. Differential capacitance

The differential capacitance measurements were done with a Solartron impedance analyzer (model 1260, Solartron Group Inc., England) and potentiostat (model 1287). The electrochemical cell used is the one described in Figure 2-12.

2.3. Chemicals and cleaning of the electrochemical cell

2.3.1. Chemicals

KOH and LiOH were from Aldrich (99.99%, semiconductor grade and 99.95%, respectively). $KClO_4$ was from BDH, and it was recrystallized twice

Table 2-1: Variation of the temperature vs time in the temperature controlled EQCM experiment.

Time (min)	Temperature (°C)			
0	6.0	15.4	24.6	34.0
2	5.9	15.5	24.7	34.0
4	5.9	15.6	24.7	34.4
6	5.8	15.6	24.9	34.5
8	6.0	15.6	24.9	34.4
14	6.0	15.6	25.0	34.5
20	5.9	15.6	24.7	34.5
24	5.9	15.5	24.8	34.5
28	6.0	15.5	25.0	34.4
30	5.9	15.6	25.0	34.4
Average (°C)	5.9	15.6	24.8	34.4
Standard deviation (°C min^{-1})	0.1	0.1	0.1	0.1

Butanethiol and octanethiol were purchased from Aldrich (99+% purity). Butanesulfide, octanesulfide and pentamethylene sulfide were purchased from Aldrich. Octanesulfide was recrystallized twice in ethanol (Omnisolv, BDH) before use. Butanesulfide and pentamethylene sulfide were purified by liquid chromatography (LC). A silicon gel (70 – 230 mesh) was used, with a mobile phase of hexane (Omnisolv, BDH). High Pressure Liquid Chromatography (HPLC) was also used to purify butanesulfide and pentamethylene sulfide. In this case, 80% methanol (Omnisolv, BDH) in de-ionized water was the mobile phase. The purity of the sulfide compounds was checked with Gas Chromatography/Mass Spectrometry (GC/MS). All the solutions were prepared with deionized distilled water (Milli-Q system).

2.3.2. Cleaning of the electrochemical cell and quartz crystal

In order to prevent contaminants from affecting the results of the electrochemical experiment, maintaining the cleanliness of the electrochemical system is of utmost importance.

The working electrode is a 9 MHz AT-cut quartz crystal covered with gold sputtered on a Ti layer. Prior to use, the electrodes were cleaned by the following procedure: First, the gold electrode was covered with concentrated sulfuric acid for 5 min. Then it was rinsed with de-ionized water and put in ethanol for 10 min. It was rinsed with Milli-Q water (i.e. de-ionized and distilled water) prior to assembly.

The glass parts of all types of electrochemical cells were immersed into hot sulfuric acid for several hours in order to destroy organic impurities. The parts of the cell were then rinsed with Milli-Q water. The Teflon© quartz crystal holder and Viton© o-rings were cleaned by the same procedure as the quartz crystal. All the parts were stored in de-ionized water until they were used.

2.4. Characterization of the gold surface

2.4.1. Gold (111) single crystal

The gold single crystal was made from pure gold (99.999%, Johnson Matthey). An induction furnace was used to make the single crystal. X-ray back-scattering was used to align the single crystal within 0.5^0 of the (111) plane. The crystal was then polished with diamond paste until a smooth surface is obtained. The mechanical polishing was followed by an electrochemical polishing to get rid of microscopic defects [2-15, 2-16]. This was done via the galvanostatically controlled oxidation of the Au (111) surface in 1 M $HClO_4$. The initial preparation of the Au (111) single crystal consists in repetitively flame annealing it in a natural gas flame and quenching it with Milli-Q water until the desired cyclic voltamogram is obtained (see below) [2-17].

Once the Au (111) single crystal was prepared, a cyclic voltammogram in a 0.1M $HClO_4$ solution between -0.2 V and 1.4 V was recorded and is shown in

Figure 2-14. This cyclic voltammogram is used as a fingerprint to verify the quality of the surface of the Au (111) single crystal. This is because the current peaks related to the formation of the surface oxide (between 1.40 V and 0.60 V) are characteristic of the crystallographic orientation of the gold electrode [2-2, 2-18]. Cyclic voltammetry was also used to check that the supporting electrolyte was free of oxygen and of trace impurities. It should be noted that gold in KOH solutions is very sensitive to the presence of oxygen and organic impurities [2-19]. Alkaline conditions were chosen to push the H_2 evolution to more negative potentials. This is necessary to study the reductive desorption/oxidative deposition of thiolates. A typical cyclic voltammogram of a clean Au (111) electrode in a 0.1 M KOH solution is shown in Figure 2-15 and it is similar to the literature [2-19].

2.4.2. Gold quartz crystal

The cyclic voltammogram of the gold covered quartz crystal in 0.1M $HClO_4$ is shown in Figure 2-16. The cyclic voltammogram in Figure 2-16 is not typical of a Au (111) surface. From the cyclic voltammogram, we know that the surface of the gold coated quartz crystal is made of domains of different crystallographic orientations.

To characterize the surface of the gold-coated quartz crystal, lead underpotential deposition (upd) was used. The cyclic voltammogram of the reductive deposition of a

monolayer of lead on gold is well understood [2-20, 2-21]. The coverage and electrosorption valency for the deposition of a monolayer of lead are known [2-21, 2-22]. This system is thus used to verify if the frequency response to the lead reductive deposition and oxidative desorption follows the Sauerbrey equation. It also gives a qualitative indication of the crystallinity of the gold film since the shape of the voltammogram of the lead upd is sensitive to the crystallographic orientation of the gold surface [2-20]. Figure 2-17 shows a typical voltammogram for lead upd on the Au coated quartz crystal. The reductive deposition consists of a broad current peak at 0.02 V followed by a sharp current peak at –0.25 V. The oxidative desorption is almost a mirror image of the reductive voltammogram. There is a sharp current peak at –0.23 V and a smaller, very sharp current peak at –0.19 V. There is then a broad current peak centered at 0.03 V. A comparison with cyclic voltammograms of lead upd recorded on a Au (111) single crystal electrode indicates that the gold film has a large component of (111) domains [2-20]. On Figure 2-17, the frequency prior to the reductive deposition is almost constant between 0.20 V and 0.10 V. There is then a frequency decrease, which starts at the onset of the first reductive current peak. The rate of decrease of the frequency tracks the shape of the voltammogram. There are two regions of faster frequency decrease separated by a region of slower frequency decrease. The frequency decreases by approximately 67 Hz from 0.20 V to –0.40 V. The positive going potential scan shows that the oxidative removal of the Pb causes a frequency increase back to its initial value. The variation of the frequency once again tracks the shape of the voltammogram. The validity of the Sauerbrey equation for this system was verified by converting the frequency change of 67 Hz to the number of moles of lead deposited using this equation. We then plotted the

moles of electron (i.e. the charge calculated from the cyclic voltammogram) as a function of the moles of lead deposited in Figure 2-18. The slope of this graph is the electrosorption valency. We obtained an average electrosorption valency of 2.11(±0.01). This agrees with previous measurements, which gave values between 2.08 and 2.18 [2-22]. We estimated from the measurements of the charge and the mass, roughness factors (RF) ranging from 1.3 to 1.5 for the gold-coated quartz crystals used in this study. The lead upd measurements show that the gold electrodes are relatively crystalline, with a (111) texture and with low RF values.

2.5. Concentration of alkanethiolates in aqueous alkaline solutions

In this study, cyclic voltammetry, EQCM, and potential step experiments are carried out in different concentrations of alkanethiolates in aqueous alkaline solution. The concentration of each solution is determined as follows.

1.1 μL of butanethiol was injected into 100 mL of 0.1 M KOH solution. We waited for 15 hours to let the butanethiols dissolve into the solution. 10 mL of this sample was taken and mixed with a known quantity of a silver nitrate solution (2.08×10^{-3} M) to precipitate mercaptan as silver mercaptide. The excess silver ions were titrated with ammonium thiocyanate using ferric ammonium sulfate as the indicator. The preparation and titration were carried out at room temperature. After the concentration of this sample was determined, it was diluted to make butanethiolate solutions of lower concentration.

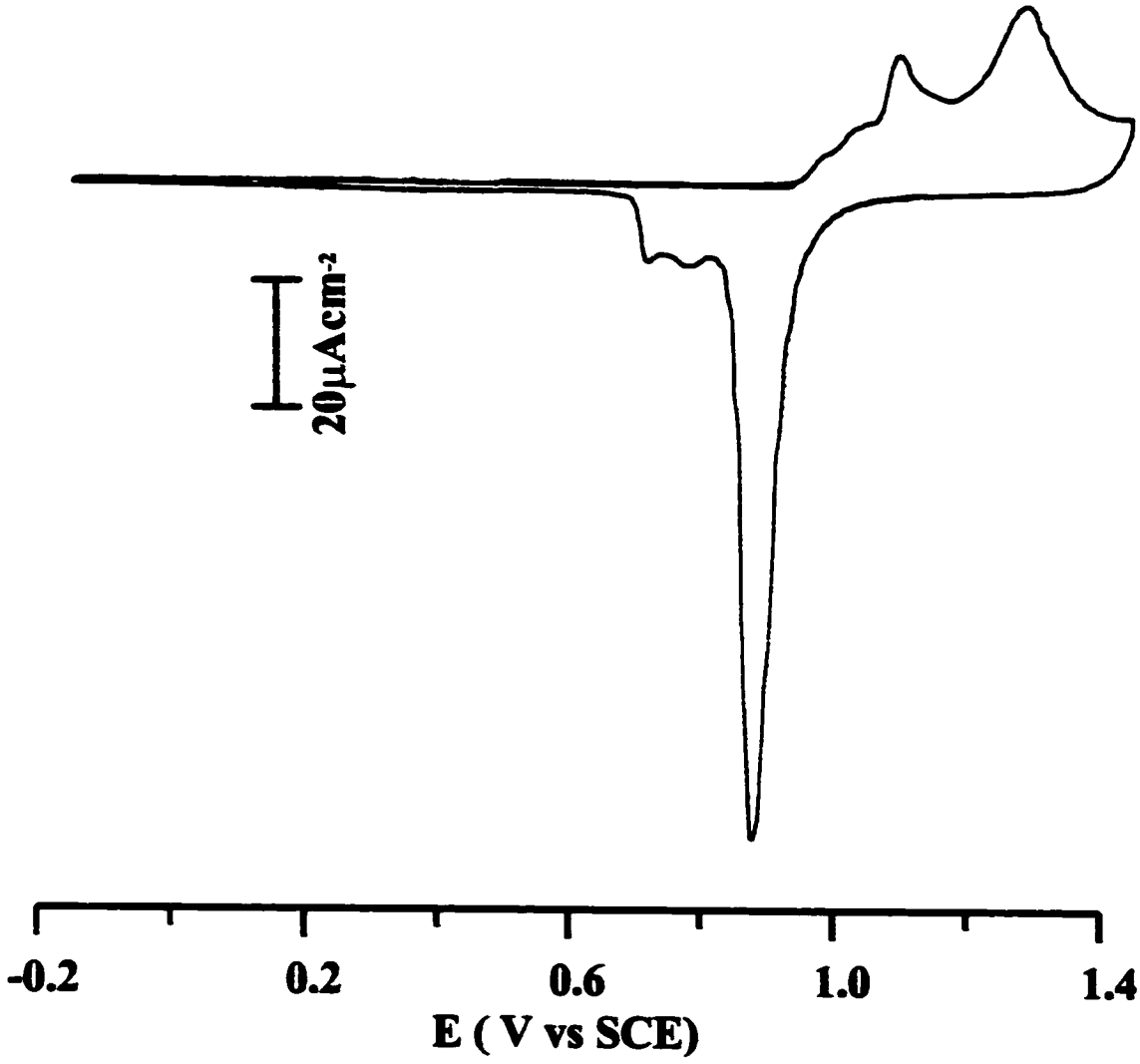

Figure 2-14: Cyclic voltammogram of Au (111) in 0.1 M $HClO_4$ recorded at a potential scan rate of 20 mV S^{-1}.

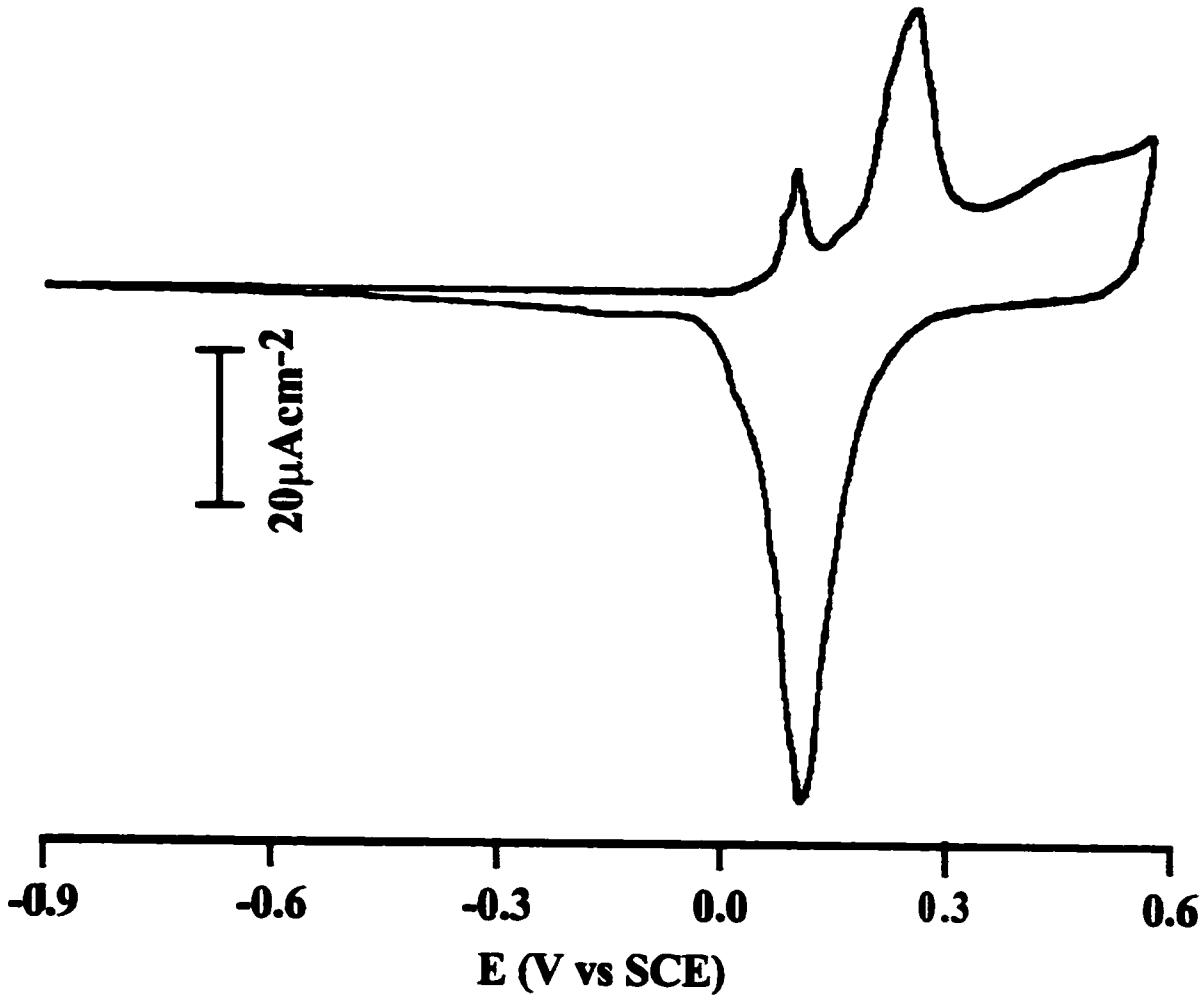

Figure 2-15: Cyclic voltammogram of Au (111) in 0.1 M KOH recorded at a potential scan rate of 20 mV S^{-1}.

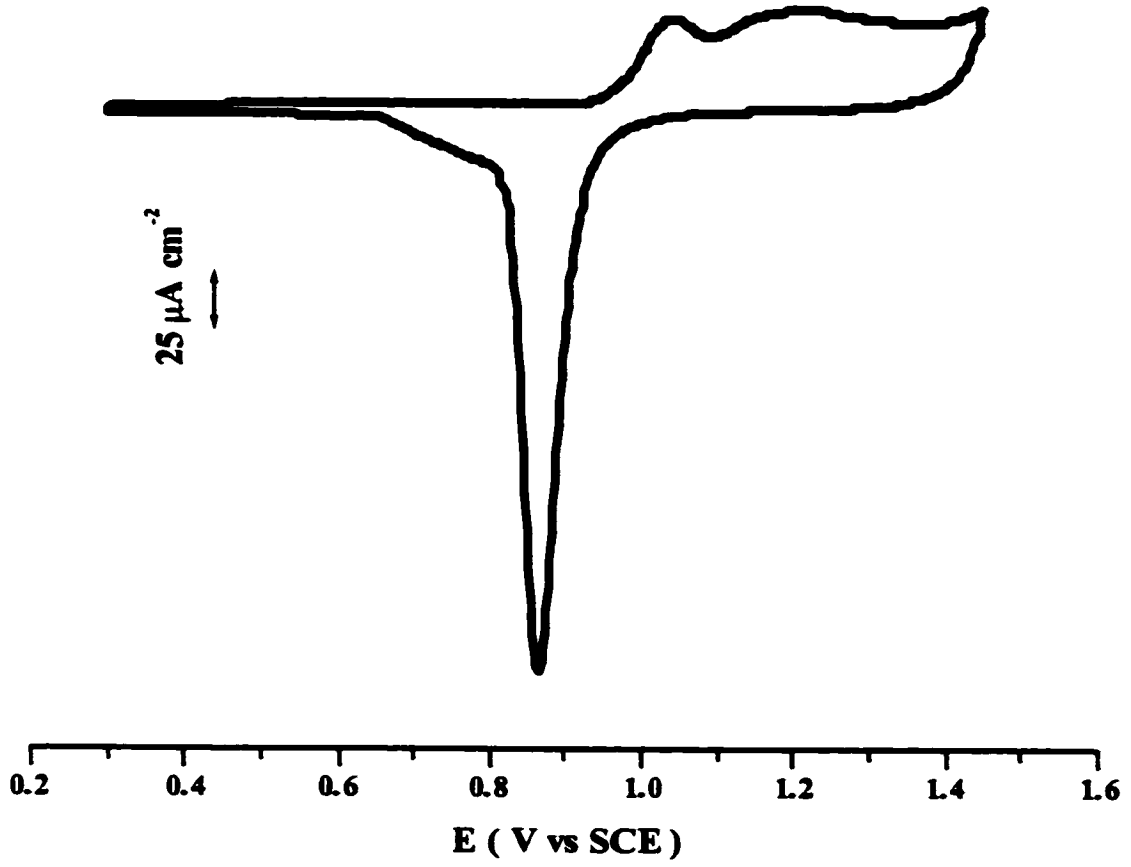

Figure 2-16: Cyclic voltammogram of a gold coated quartz crystal in 0.1 M $HClO_4$ recorded at a potential scan rate of 20 mV s^{-1}.

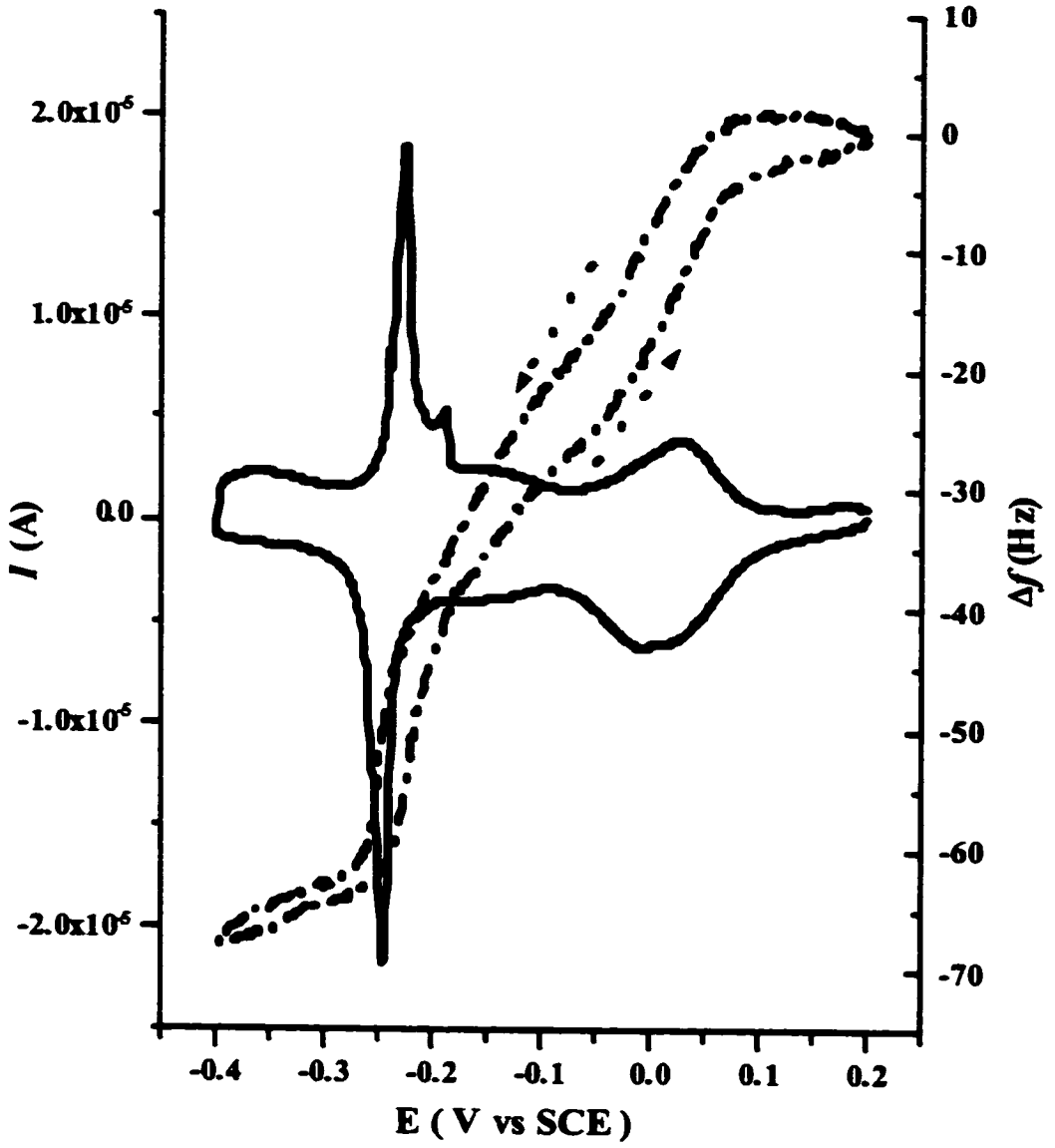

Figure 2-17: Current (solid line) and EQCM frequency (dashed line) for the lead underpotential deposition on a gold electrode from a 5mM $Pb(ClO_4)_2$, 10mM $HClO_4$, 0.1M $KClO_4$ solution. Potential scan rate: 20 mV s^{-1}.

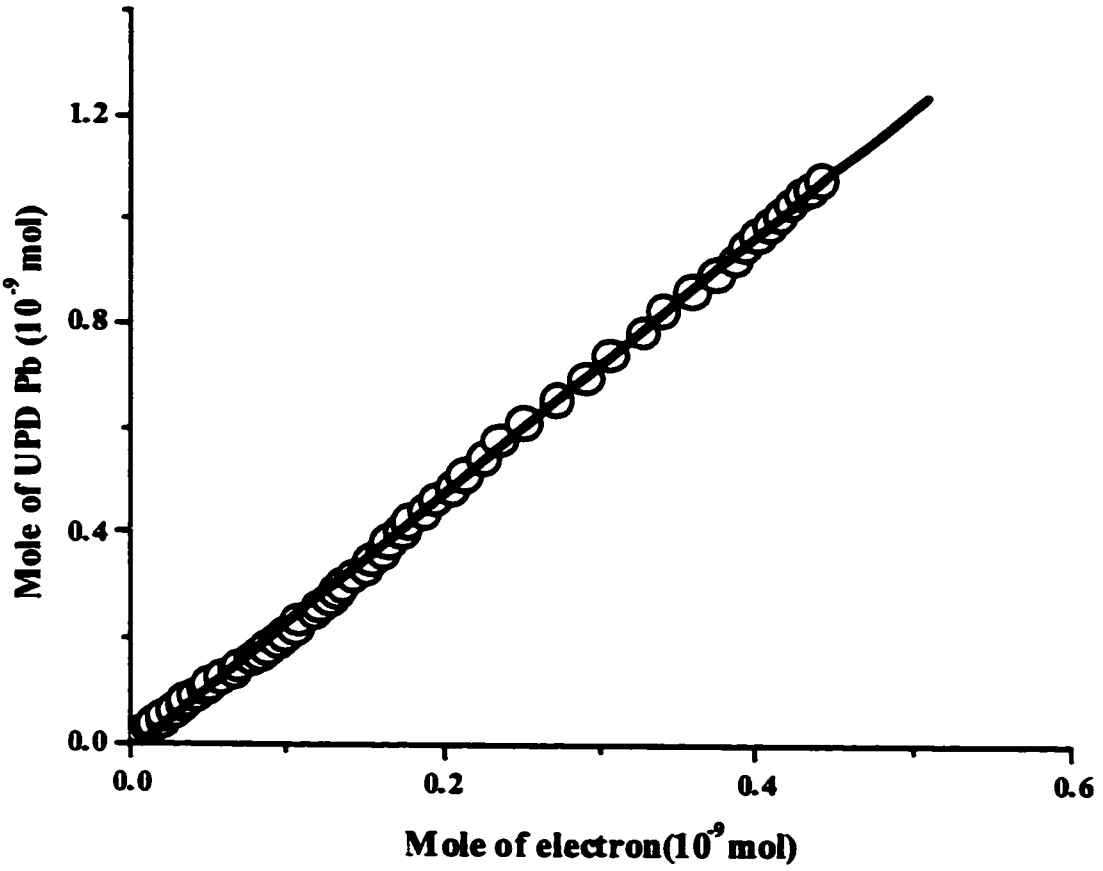

Figure 2-18: Graph of the moles of electrons calculated from the cyclic voltammogram in Figure. 2-17 vs the moles of lead deposited calculated from the EQCM signal in Figure 2-17. The lines are linear fits. For clarity, only every 5th data point is shown.

2.6. Data Analysis

The following will be presented in this section:

1. The integration of current peaks in cyclic voltammograms

2. The calculation of signal to noise and drift of the frequency in the EQCM experiment

3. The fitting procedure for the mass vs time curves in the EQCM / potential step experiments.

2.6.1. Integration of current peaks.

In this thesis, we studied the oxidative deposition of organo-sulfur compounds on gold. The charge integration will focus on the oxidative current peak in the cyclic voltammogram. As mentioned before, there are two kinds of charge, Faradaic charge and capacitive charge. Only Faradaic charge comes from the electron transfer process. So we must remove the capacitive charge in order to get the Faradaic charge which is used for the estimation of the surface coverage. This is done by doing a "baseline correction". The initial and final points of the baseline are chosen before and after the current peak. A polynomial fit is used to link the two regions. The charge is obtained by integrating the current peak above the baseline.

For cyclic voltammograms, such as the butanethiolate oxidative deposition in alkaline solution, the current peak is narrow, sharp and symmetric (as shown in Figure 2-

19a). The baseline correction process is simple and accurate. The region for choosing the initial and final points of the baseline is very narrow. So the error in this integration is estimated to be about 1%. However, in other cyclic voltammograms, such as butanethiol oxidative deposition in 0.1 M $KClO_4$ at low temperatures, the current peak is broad and asymmetric (as shown in Figure 2-19b) and at the edge of hydrogen evolution. It is more difficult to determine the initial and final points of the baseline. So in these cases, the error in the integration could be up to 10%.

2.6.2. Signal to noise and drift in the EQCM experiment

The signal to noise (S/N) and drift of the frequency affect the reliability of our EQCM results. The following experiment was done to determine the S/N and drift.

We hold the potential at a value in the double layer region (-0.35 V) for a butanethiolate coated gold electrode and record the frequency for 30 minutes. The drift is determined by measuring the average value of the frequency in the first minute (f_1) and last minute (f_2). Then the drift is defined as $|(f_2 - f_1)/30|$ Hz min^{-1}. Its value is 0.3 Hz min^{-1}. For the S/N calculation, we average the frequency over 5 minutes in a region in which the drift is lower than 0.01 Hz min^{-1}. The S/N is defined as the standard deviation of the frequency in this region, which is 0.16 Hz.

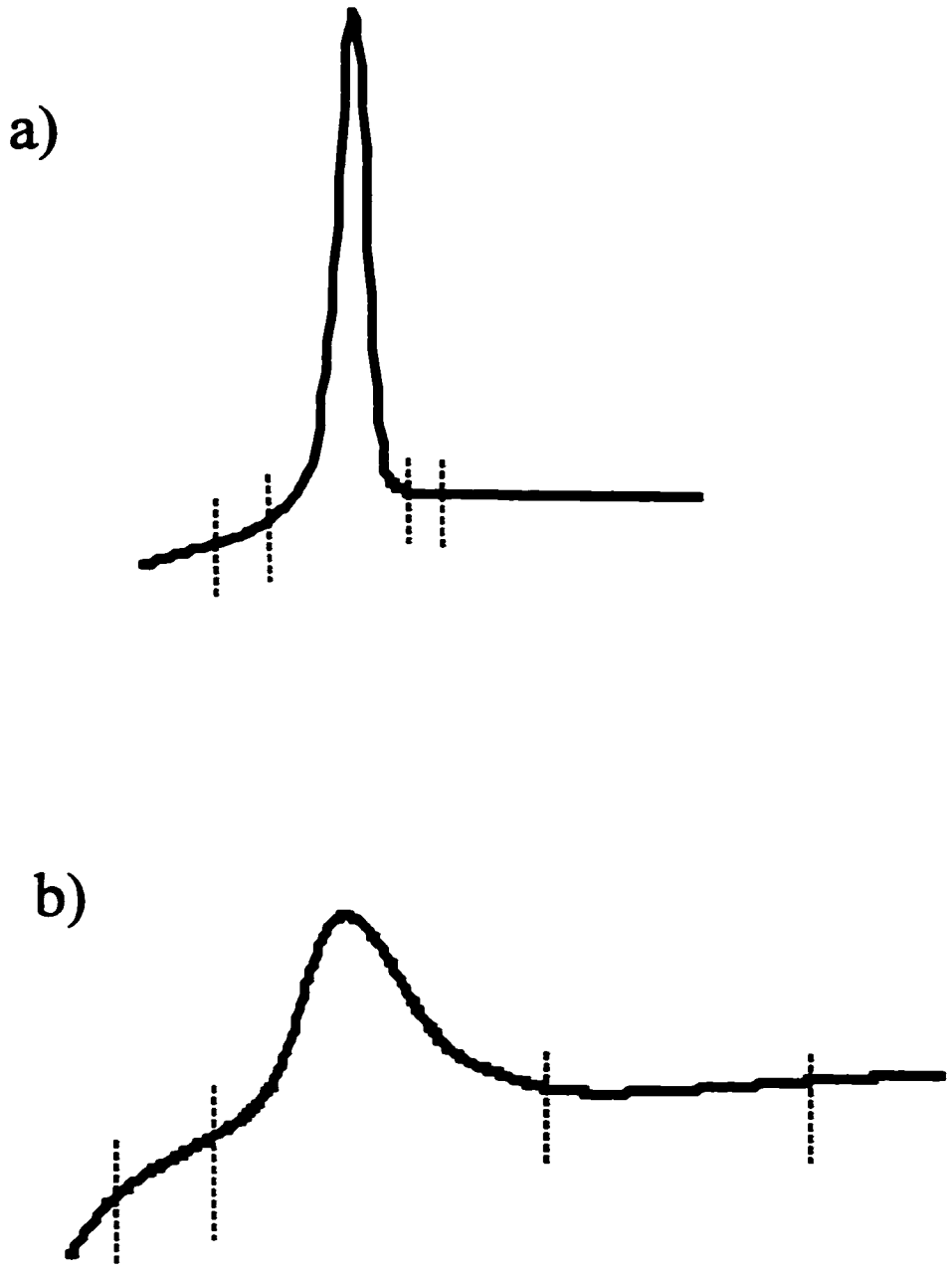

Figure 2-19: The scheme of charge integration. a) butanethiolate oxidative deposition in 0.1 M KOH. b) butanethiol oxidative deposition in 0.1 M $KClO_4$. The dashed vertical line in the graph show the region for choosing the initial and final points of the baseline.

2.6.3. Fitting procedure

To study the kinetics of the electro-deposition of sulfur compounds onto the gold surface, mass-time curves were obtained from the EQCM combined with potential-step experiments. A two-step model was used to describe the adsorption process. The rate constants for these two steps are obtained from fitting the mass-time curves with a bi-exponential equation (see chapter 3). The fitting was carried out using a software called Origin© (Microcal Software Inc.)

A nonlinear least squares fitting (NLSF) procedure was used. The nonlinear regression method is based on the Levenberg-Marquardt (LM) algorithm [2-23]. The fitting procedure is as follows. There are two types of variables in the data, which represent the results of our measurements. One is the independent (input) variable, which in our case is the time, t. The other is the dependent (output) variable, which in our case is the mass change, Δm. A mathematical expression in the form of eq. 2.9 is used.

$$\Delta m = f(t\,;\, P_1, P_2, P_3, \ldots) \qquad (2\text{-}9)$$

The f in equation 2-9 represents the theoretical model that fits the data. The model usually depends on one or more parameters P_1, P_2, P_3, ... The aim of the fitting procedure is to find the values of the parameters which best describe the data. The standard way of defining the best fit is to choose the parameters so that the sum of the

squares of the deviations (χ^2) of the theoretical curve(s) from the experimental points for a range of independent variables is at its minimum. χ^2 is given by:

$$\chi^2 (P_1, P_2, P_3, ...) = 1 / (n^{eff} - P) \sum_i w_i [\Delta m_i - f(t_i ; P_1, P_2, P_3, ...)]^2 \qquad (2\text{-}10)$$

Here, Δm_i is the experimental point at time t_i , n^{eff} is the total number of experimental points used in the fitting, P is the total number of adjustable parameters used in the fitting, and $(n^{eff} - P)$ is usually referred to the number of degrees of freedom. w_i represents the weight of each experimental point.

As it will be discussed later, 80% to 90% of the alkanethiol deposition occurs in a few seconds. Therefore, the rate constant for the first-step, k_1, is much larger than that of the second step, k_2. In order to get a more accurate rate constant k_1 from the fitting, the data at short time have bigger weighting factor than the data at longer time.

References:

[2-1]: Greef, R.; Peat, R.; Peter, L.M.; Pletcher, D.; Robinson *Instrumental Methods in Electrochemistry* Ellis Horwood Limited, **1985.**

[2-2]: Bard, A.J.; Faulkner, L.R. *Electrochemical Methods- Fundamentals and Applications* John Wiley & Sons, Inc. **1980.**

[2-3]: Nuzzo, R.G.; Allara, D.L. *J. Am. Chem. Soc.* **1983,** 105, 4481.

[2-4]: Ashley, K.; Pons, S. *Chem. Rev.* **1988**, 88, 673.

[2-5]: Greenler, R.G. *J. Chem. Phys.* **1966**, 44, 310.

[2-6]: Woodruff, D. P.; Delchar T. A. *Modern Techniques of Surface Science* Cambridge University Press: Great Britain, **1992.**

[2-7]: Buttry, D.A. ; Ward, M.D. *Chem. Rev.* **1992,** 92,1355.

[2-8]: Ward, M.D. *Physical Electrochemistry-Principles Methods and Applications* P293, Rubinstein, I (Eds) Marcel Dekker, New York, Basel, Hong Kong **1995.**

[2-9]: Hapel, M *Interfacial Electrochemistry- Theory, Experiment and Applications* P599, Wieckowski, A (Eds) Marcel Dekker, New York, Basel **1999.**

[2-10]: Sauerbrey, G. *Z .Phys.* **1959**, 155, 206.

[2-11]: Model QCA917 Quartz Crystal Analyzer Instruction Manual SEIKO EG&G.

[2-12]: Lu, C. *Applications of Piezoelectric Quartz Crystal Microbalance.* Vol. 7, P19 Lu, C, Czanderna, A.W., eds . Amsterdam: Elsevier, **1984.**

[2-13]: Byloos, M. M. Sc. Thesis, University of Ottawa **2001.**

[2-14]: Jerkiewicz G.; Vatankhah G.; Zolfaghari A.; Lessard J. *Electrochemistry Communications* **1999**, 1, 419.

[2-15]: Yang, D.-F.; Wilde, C.P.; Morin, M. *Langmuir* **1996**, 12, 6570.

[2-16]: Al-Maznai, H.M. Ph.D. Thesis, University of Ottawa **1999.**

[2-17]: Qu, D. M. Sc. Thesis, University of Ottawa **1998.**

[2-18]: Angerstein-Kozlowska, H.; Conway, B.E.; Hamelin, A.; Stoicoviciu, L. *J. Electroanal. Chem.* **1987**, 228, 429.

[2-19]: Hamelin, A.; Sottomayor, M.J.; Silva, F.; Chang, S-C; Weaver, M.J. *J. Electroanal. Chem.* **1990**, 295, 291.

[2-20]: Hamelin, A. *J. Electroanal. Chem.* **1984**, 165, 167.

[2-21]: Hamelin, A.; Lipkowski, J. *J. Electroanal. Chem.* **1984**, 171, 317.

[2-22]: Melroy, O.; Kanazawa, K.; Gordon, J.G.; Buttry, D.A. *Langmuir* **1987**, 2, 697.

[2-23]: Press, et. al. *Numerical Recipes in C, The Art of Scientific Computing* Cambridge University Press, New York , **1988.**

Chapter 3

The oxidative adsorption of alkanethiols and alkanethiolates on gold from aqueous solutions

3.1. Introduction

There is a wealth of information about thiolate SAM's on gold once they are formed (see Chapter 1). However, there are unsolved issues related to the adsorption process of the organo-sulfur compounds on gold. Recently, more attention has been paid to the kinetics of SAM formation [3-1 - 3-35]. Most studies [3-1 - 3-33] of the adsorption of alkanethiols on gold surfaces are carried out under open circuit conditions (i.e. without an applied potential). In the case of the kinetics of thiolate SAM formation on gold, different mechanisms have been suggested [3-1 - 3-16, 3-18 - 3-25]. A bi-phasic kinetics model was initially proposed to describe SAM formation [3-1]. After that, most of studies supported this two-step process [3-1 - 3-4, 3-9, 3-10, 3-12, 3-16, 3-19]. One-step and three-step processes were also found in a limited number of studies [3-5, 3-8, 3-20 - 3-23]. Only Langmuir adsorption models were used in these studies. The time scale for the formation of a SAM varied from seconds [3-2 - 3-4, 3-12, 3-16, 3-20 - 3-22] to hours or days [3-1, 3-5, 3-8 - 3-10, 3-23, 3-24], but always followed a two-step Langmuir process.

A variety of techniques were used in kinetics studies, such as FTIR spectroscopy [3-3], ellipsometry , contact angle measurements [3-1, 3-2], surface plasmon resonance (SPR)

spectroscopy [3-4, 3-5], surface second harmonic generation study (SHG) [3-6], atomic force microscopy (AFM) [3-7, 3-8], scanning tunneling microscopy (STM) [3-10], impedance analysis [3-11, 3-12], chronoamperometry [3-13, 3-14], X-ray photoelectron spectroscopy (XPS) [3-15] and Electrochemical Quartz Crystal Microbalance (EQCM) [3-16 – 3-30].

EQCM and Scanning probe microscopy measurements provided the most direct information on the adsorption/desorption of thiols from a gold surface. We will use EQCM to measure the kinetics of the oxidative adsorption of alkanethiols and alkanethiolates because of its better time resolution.

Past QCM measurements were mostly done in the absence of potential control in organic media [3-2 - 3-23], gas phase [3-27 - 3-29] and in air [3-24, 3-25]. A series of papers written by D.S. Karpovich, H.M. Schessler and G.J. Blanchard [3-20 - 3-22], on the adsorption kinetics of alkanethiolate SAMs on gold reported that the formation of the monolayer occurs in one step. It was described by a Langmuir adsorption isotherm. From their studies, they extracted the thermodynamic quantities ΔG, ΔH and ΔS for monolayer formation. They found that ΔG and ΔH are –5.5 Kcal mol^{-1} and –19.9 Kcal mol^{-1}, respectively. The formation of an alkylthiol SAMs on gold is a spontaneous and exothermic process. ΔS was found to be –48 cal mol^{-1}. The organized thiol SAMs form from a disordered state (in the air or solution). This decreases the entropy. Increasing the temperature will make ΔG more positive. Therefore, the SAMs formation is more difficult at higher temperature.

K.Shimaxu, I.Yagi, Y.Sato and K.Uosaki [3-16] used EQCM to measure the self-assembling process of ferrocenylundecanethiol on a gold surface. A two-step process was found. It was described by a fast adsorption step followed by a slower adsorption step whose rate was 2 orders of magnitude smaller. The total frequency change in this study matches the expected mass corresponding to a full monolayer. They concluded that the observed frequency change represents the real mass change on the surface. In a recent paper [3-17], T. Kawaguchi, H. Yasuda, K. Shimazu and M.D. Porter studied the reductive desorption process of self-assembled monolayers of alkylthiols using EQCM. They drew the same conclusions as before, but the observed frequency change in this case did not match the integrated charge of desorption very well. They assign this discrepancy to cation adsorption (i.e. double layer effect).

T.W. Schneider and D.A. Buttry [3-18] used EQCM to monitor the adsorption and desorption of several long chain alkanethiolates on gold in organic solvents. They found that SAM formation is solvent dependent. After ruling out visco-elastic effects, they found that the discrepancy between the surface coverages calculated from the charge and from the mass change was due to the fact that the charge they used did not account for the capacitive charge [3-12, 3-17, 3-18, 3-36, 3-37].

C. Frubose and K. Doblhofor [3-19] used EQCM along with impedance spectroscopy to study the kinetics of the self-assembly process of octadecanethiol on gold in ethanolic electrolyte solutions. Two-step kinetics was found. The formation process in this study was done with an applied potential. The kinetics of the film formation are

found to be the same when the applied potential was set in the range of – 0.6V to 0.2V vs SCE.

The goal of this chapter is to measure the kinetics of alkanethiolate and alkanethiol oxidative deposition on gold in aqueous solution and establish the mechanism of electroformation of self-assembled monolayers of alkylthiolates.

3.2. Oxidative deposition of alkanethiolates on gold from an alkaline solution

We used EQCM to study the oxidative deposition of alkanethiolates. The charges involved in the reductive desorption or oxidative deposition of alkanethiolates can be taken as a measure of the surface coverage [3-38]. This allows a verification of the validity of the Sauerbrey equation [3-39] for the low molar mass alkanethiolates (butanethiolate and octanethiolate) used in this study. This verification was done by examining the oxidative deposition and subsequent reductive desorption of butanethiolate and octanethiolate on a gold-coated quartz crystal from alkaline aqueous solutions.

Figure 3-1 shows two cyclic voltammograms. These two voltammograms correspond to 1 mM butanethiolate in a 0.1 M LiOH (Figure 3-1a) and in a 0.1 M KOH (Figure 3-1b). In those alkaline solutions, narrow and symmetric oxidative and reductive current peaks are observed. The narrowness is related to the fact that the thiols are deprotonated [3-40]. The initial negative-going potential scan shows that, between –0.2 V and –0.8 V, the current and the frequency are almost constant until the onset of the

reductive current. As the reductive current increases, the frequency increases. The frequency increase tracks the reductive current peak. After the reductive current peak, the frequency is relatively constant. On the positive going potential scan, the frequency first rises slowly, then at the onset of the oxidative current peak the frequency decreases. It returns to its original value at –0.60 V and remains constant up to –0.20 V. The current peak in a 0.1 M LiOH (Figure 3-1a) is broader than that in the 0.1 M KOH (Figure 3-1b). This may due to the current peak in the 0.1 M LiOH is at the edge of the hydrogen evolution. The hydrogen evolution current also cause the data points in Figure 3-2 not go through the zero (see below).

The EQCM response follows closely the current response. However, the assignment of the frequency response to a change of the mass of the alkanethiolate at the surface is complicated by the fact that the capacitive (double layer reorganization) and faradaic (oxidative adsorption of thiolate) processes are occurring simultaneously [3-41]. To estimate the contribution of the capacitive process to the charge and frequency we did the following measurements. First, the capacitive charge was estimated from chronoamperometric measurements [3-41] to be 26 (±2) $\mu C\ cm^{-2}$ for octanethiols. This is approximately 25% of the total oxidative charge. EQCM measurements in 0.1 M KOH and 0.1 M LiOH background electrolytes showed a frequency change of +0.4 Hz or less in the range of potential where the oxidative deposition of butanethiolates occurs. This value is much smaller than the 8 to10 Hz observed for the deposition of a monolayer of alkylthiolates. We then assume that the capacitive and faradaic processes are additive and correct the total current for the capacitive process. We do not correct the frequency

for the capacitive process since the error on the frequency is as large as this correction (typically ±0.4 Hz). Finally plots of the moles of electrons (obtained from the oxidative charge corrected for the capacitive charge) as a function of the moles of butanethiolates deposited (obtained from the frequency change and the Sauerbrey equation) in 0.1 M KOH and 0.1 M LiOH are obtained and shown in Figure 3-2. The slopes are 1.09 ± 0.05 (in KOH) and 1.04 ± 0.06 (in LiOH) mole of electron per mole of butanethiolate. The slope is obtained from the average of five plots of the moles of electrons as a function of the mole of butanethiolate deposited. This corresponds to the deposition of 83 (±4) g (in 0.1 M KOH) and 86 (±5) g (in 0.1 M LiOH) of butanethiolate deposited per mole of electron. The molar mass of butanethiolate is 89 g. Thus, these results agree with the one-electron process of alkanethiol desorption or deposition on gold [3-42]. This shows that the frequency change is mainly caused by the mass increase due to the oxidative deposition of butanethiolates and that the approximations that we made are reasonable. They also agree with the previous studies of the oxidative adsorption of alkylthiols on gold in organic media [3-16 - 3-18]. No large frequency changes due to solvent and ion displacement are observed in contrast to previous studies of the electroadsorption of other organic molecules, such as pyridine adsorbed on gold [3-43, 3-44]. However, pyridine is weakly adsorbed, where the alkanethiolates are chemisorbed.

Figure 3-3 shows the cyclic voltammograms of the oxidative adsorption and reductive desorption of octanethiolate in 0.1 M LiOH (Figure 3-3a) and 0.1M KOH (Figure 3-3b). The reductive current peaks are at more negative potentials (-1.08 V in KOH and –1.13 V in LiOH) than those of butanethiolate shown in Figure 3-1a and 3-1b.

It is also the case for the narrow oxidative current peak observed at –0.94 V in both alkaline solutions. These potential shifts were previously discussed [3-40, 3-41]. The thicker layers are more difficult to reduce, and thus, are reduced at more negative potentials. The more important interadsorbate interactions facilitate the oxidative adsorption and thus octanethiolates are oxidatively deposited at more negative potentials. On the initial negative-going potential scan, the frequency is almost constant from –0.20 V to –1.02 V. It increases over the range of potential corresponding to the reductive current peak. On the subsequent positive-going potential scan, the frequency decreases slowly up to -1.00 V, which corresponds to the onset of the oxidative current peak. The frequency decreases sharply over the narrow potential range of the oxidative current peak. Then from –0.91 V to –0.20 V it has a constant value close to the initial one. A plot of the moles of electron (obtained from the oxidative charge corrected for the capacitive charge) as a function of the moles of octanethiolate deposited (obtained from the frequency change and the Sauerbrey equation) in 0.1 M KOH and 0.1 M LiOH is obtained and shown in Figure 3-4. Electrons per adsorbed octanethiolates of 1.08 ± 0.03 in 0.1 M KOH and 1.05 ± 0.02 in 0.1M LiOH were obtained from the slopes in Figure 3-4. These correspond to 134 (±4) g and 138 (±3) g of octanethiolates per mole of electrons, respectively, and these values are close to the molar mass of octanethiolate of 145 g. These measurements give a ratio of (g of octanethiolate/g of butanethiolate) deposited per mole of electron of 1.6 (±0.1). This is within error equal to the ratio of the molecular weight of octanethiolate to butanethiolate (1.63).

The EQCM results for the butanethiolate and octanethiolate reductive desorption/ oxidative deposition in the aqueous 0.1 M LiOH and 0.1 M KOH are similar. These results support the suggestion that double layer effects (solvent and ion displacements) are not very important in these EQCM results. Li and K have molar masses of 7 g mol^{-1} and 40 g mol^{-1}, respectively. The frequency change would be different in the two electrolytes if adsorption (desorption) of cations occurred during our experiments and contributed to the frequency change. Our results differ from the important cation effect observed by Shimazu et al. [3-17] for the reduction of adsorbed octanethiol in a 0.1 M KOH and 0.1 M NaOH ethanolic solution. This is probably related to the different interactions of ions and alkanethiolate with these solvents (water and ethanol).

The absence of double layer effects related to the reorganization of the electrical double layer at the alkylthiol coated gold electrode in the EQCM data is surprising. Differential capacitance (DC) measurements done prior to the EQCM measurements provide some insights into this observation. The DC and EQCM measurements were recorded at 5 mV s^{-1} and 10 mV s^{-1} respectively and are shown in Figure 3-5 and Figure 3-6 for butanethiolate and octanethiolate respectively. As shown in Figure 3-5, in KOH and LiOH, the capacity of a butanethiol coated gold electrode is constant from –0.30 V to –1.00 V, as is the frequency. However, the capacity starts to increase just after the frequency has started to increase. This small lag of the capacity relative to the frequency suggests that ion migration to the surface starts after the reductive desorption of the butanethiol. A similar effect is observed for the oxidative deposition of the butanethiolate where the capacity decreases prior to the frequency decrease. The

capacity and frequency of an octanethiolate coated gold electrode is constant from –0.30 V to –1.07 V in the 0.1 M KOH and LiOH solutions. The difference between the capacity and frequency, when the reductive desorption/oxidative deposition occurs on the gold surface, are similar to that of butanethiol, as shown in Figure 3-6. We also note that the separation between the capacity and frequency changes is larger in KOH. This cation effect is observed for oxidative deposition of both butanethiolate and octanethiolate. We do not know the origin of the effect of the cation on the capacity during the oxidative deposition. Further studies are needed. Notwithstanding this uncertainty on the origin of the cation effect, the capacity measurements are compatible with the formation (destruction) of a double layer at the gold surface after (before) desorption (adsorption) of the alkanethiolate suggested previously [3-40]. We can rule out that this observation is related to the different potential scan rates used for the EQCM and DC measurements since the reverse effect would be expected. The capacitive change should precede (follow) the mass changes for the reduction (oxidation).

The results described above show that the Sauerbrey equation can be applied to the oxidative deposition and reductive desorption of these two alkanethiolates. Thus the surface concentration of alkanethiolate can be obtained from EQCM measurements. The measure of the frequency change caused by a potential step thus provides a direct measure of the electrodeposition kinetics of alkanethiolates.

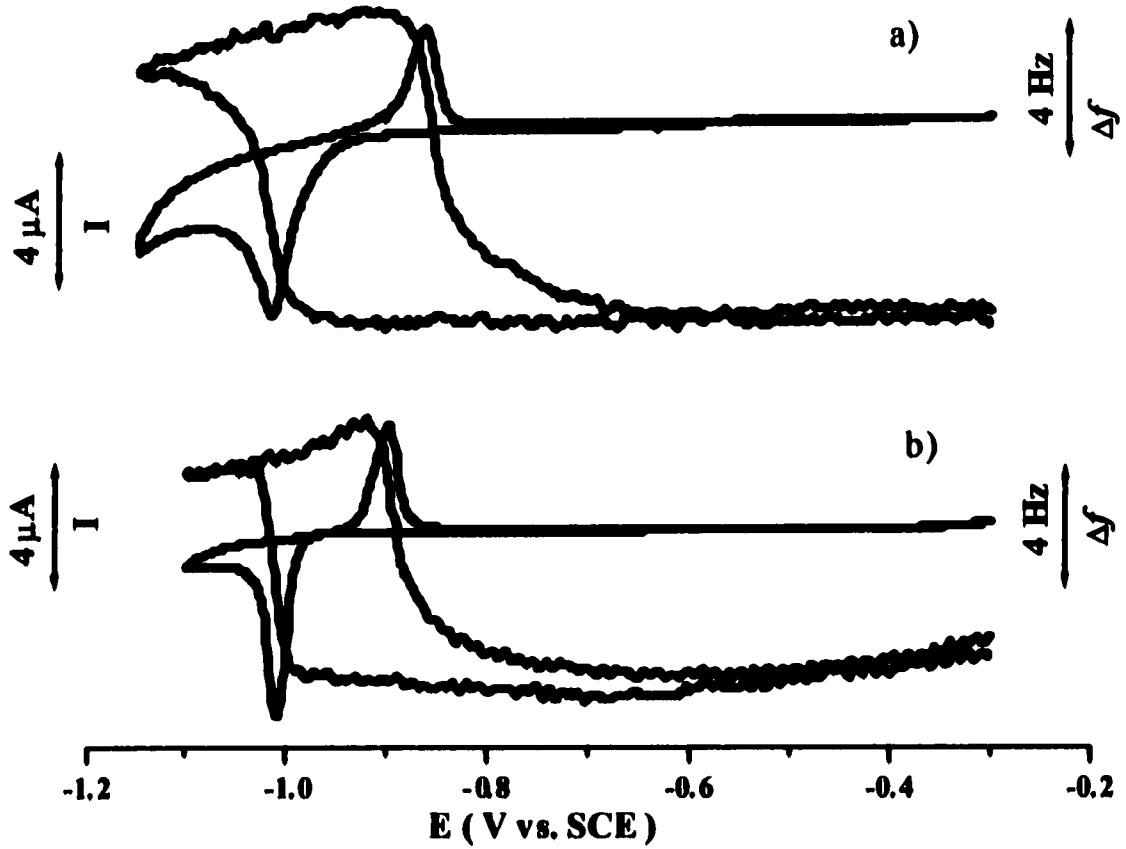

Figure 3-1: Cyclic voltammograms and EQCM signals for the oxidative adsorption/reductive desorption of butanethiolates on gold recorded in a) 1 mM butanethiol, 0.1 M LiOH; b) 1 mM butanethiol, 0.1 M KOH, Potential scan rate: 20 mV s^{-1}.

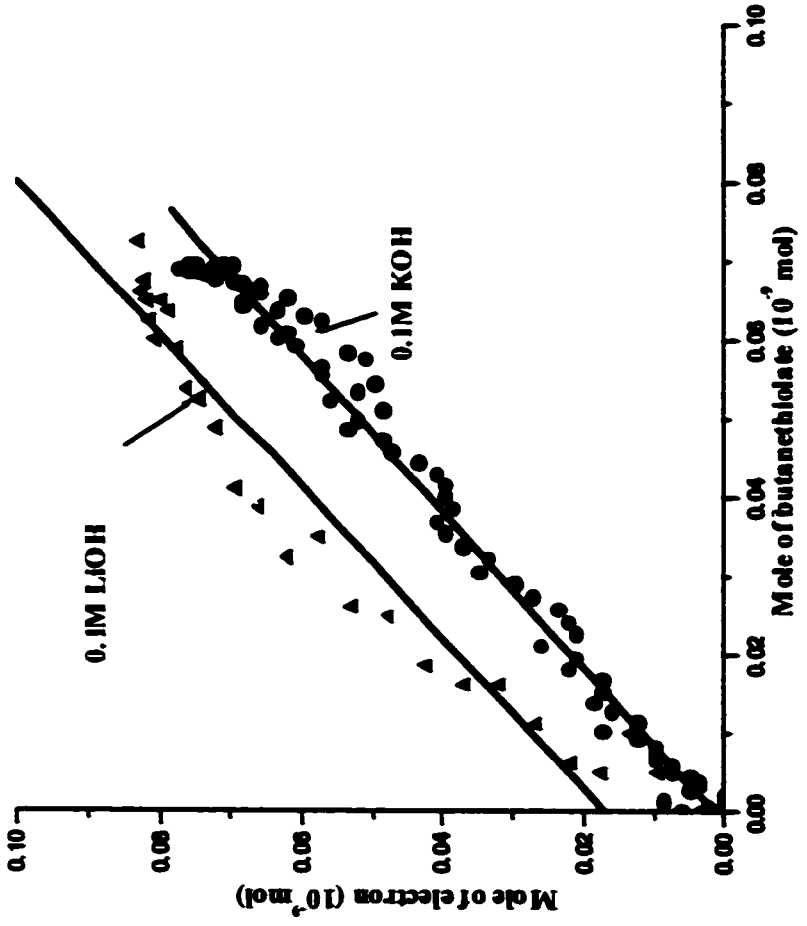

Figure 3-2: Graph of the mole of electron calculated from the cyclic voltammograms in Figs. 3-1a) and 3-1b) (corrected for the capacitive change) vs the mole of butanethiolate deposited calculated from the frequency change in Figs. 3-1a) and 3-1b). The lines are linear fits.

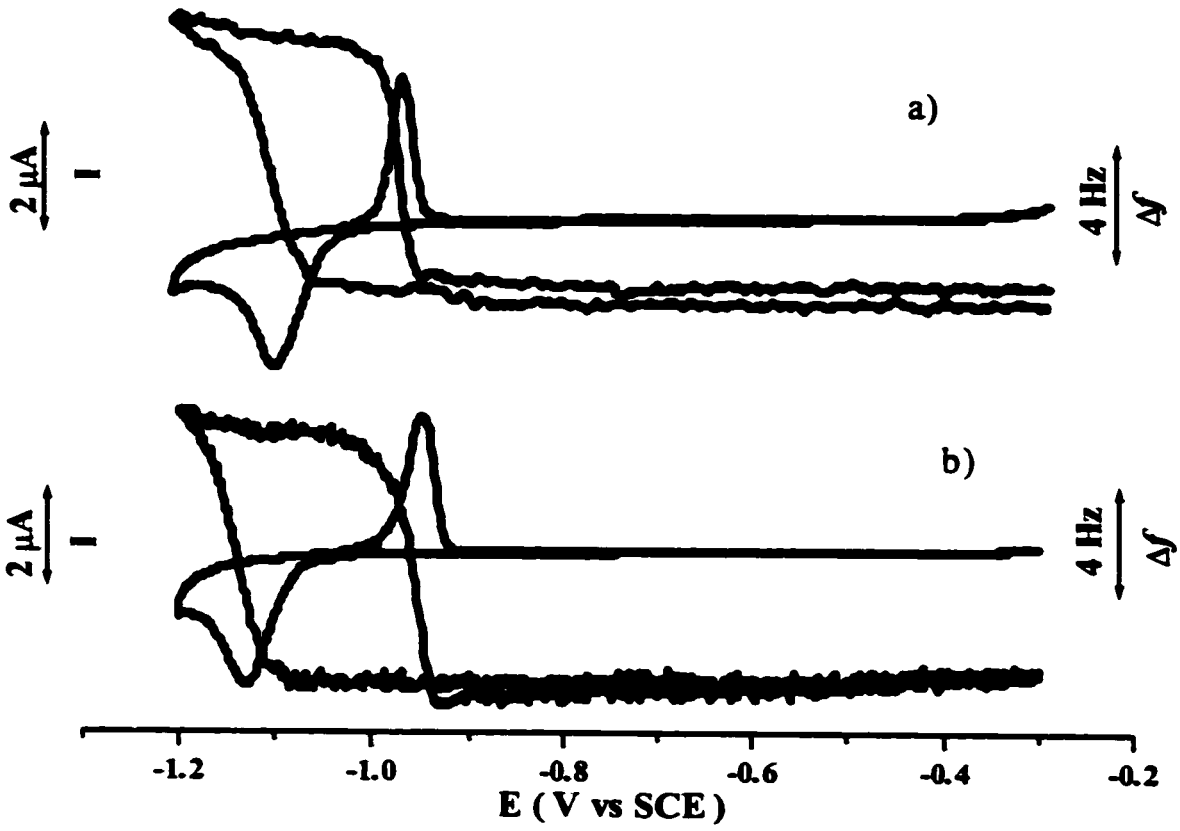

Figure 3-3: Cyclic voltammograms and EQCM frequencies for the oxidative adsorption/reductive desorption of octanethiolate on gold recorded in a) 1 mM octanethiol, 0.1 M LiOH solution; b) 1 mM octanethiol, 0.1 M KOH solution. Potential scan rate: 20 mV s^{-1}.

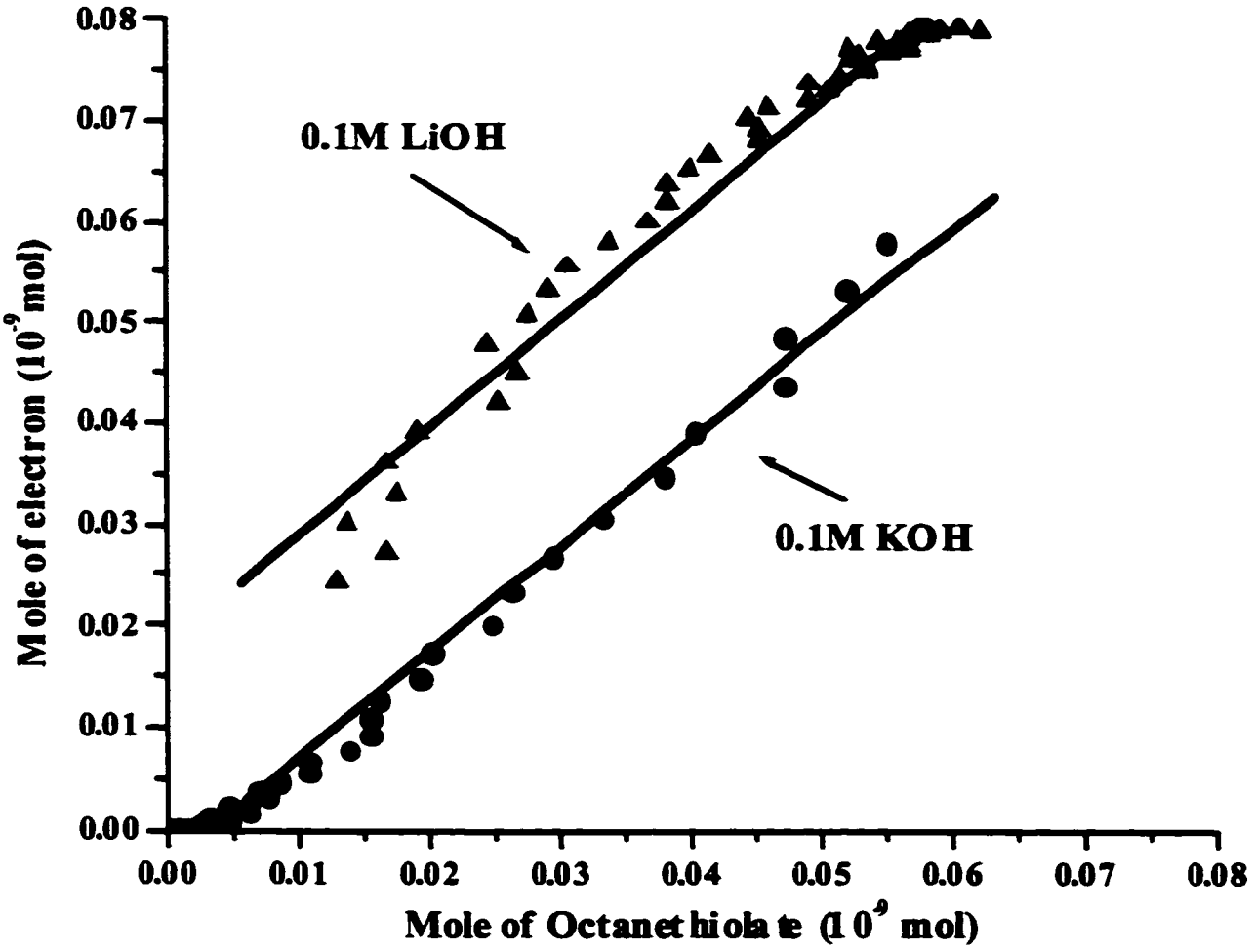

Figure 3-4: Graph of the mole of electron calculated from the cyclic voltammograms in Figs. 3-3a) and 3-3b) (corrected for the capacitive change) vs the mole of octanethiolates deposited calculated from the EQCM signals in Figs. 3-3a) and 3-3b). The lines are linear fits.

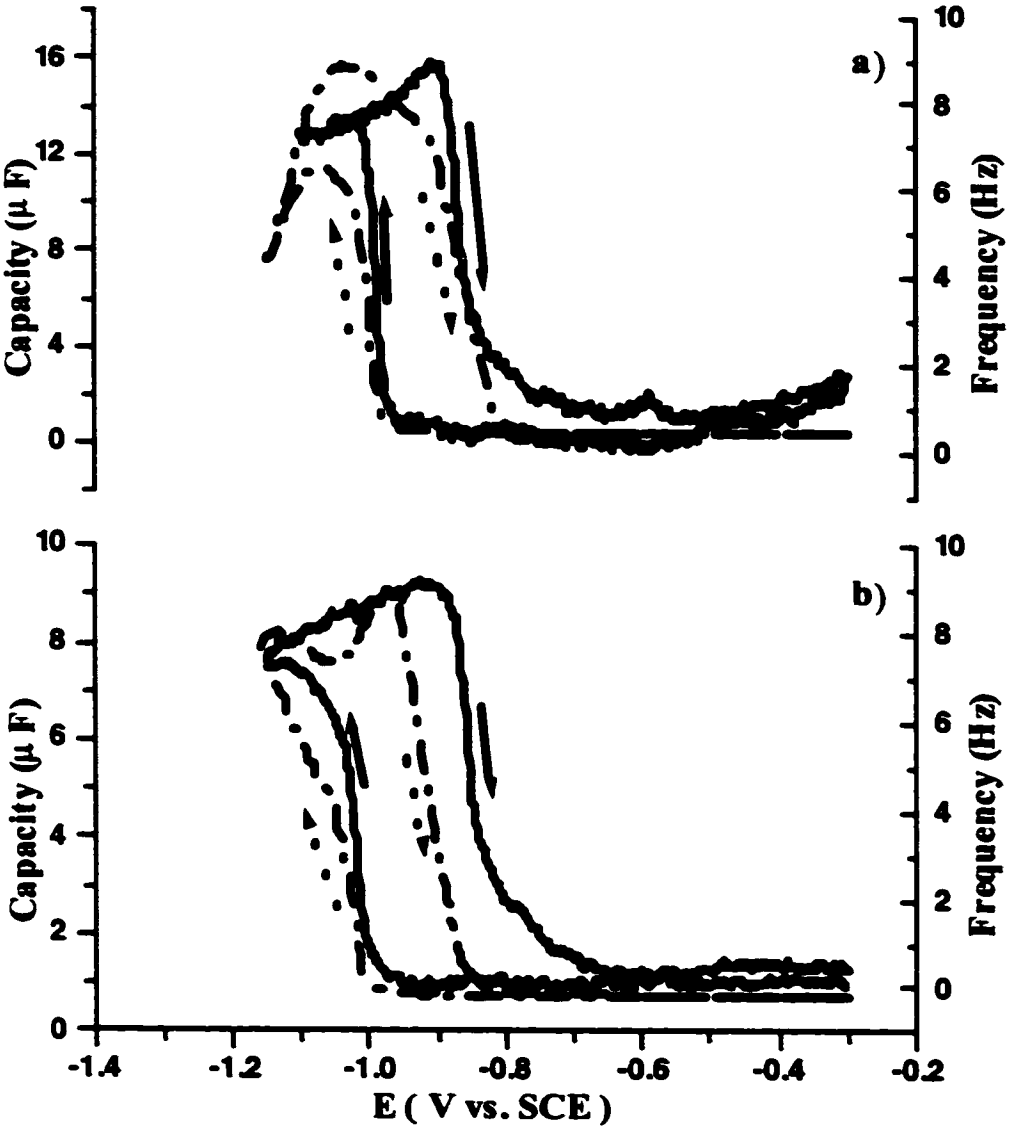

Figure 3-5: Capacity (empty circle) and EQCM signal (solid line) for the oxidative deposition and reductive desorption of butanethiolate on gold from 1mM butanethiolate in a) 0.1 M LiOH and b) 0.1 M KOH. Differential Capacitance measurement: Potential scan rate 5 mV s^{-1}, 20 Hz, 5 mV RMS; EQCM measurements: Potential scan rate: 10 mV s^{-1}.

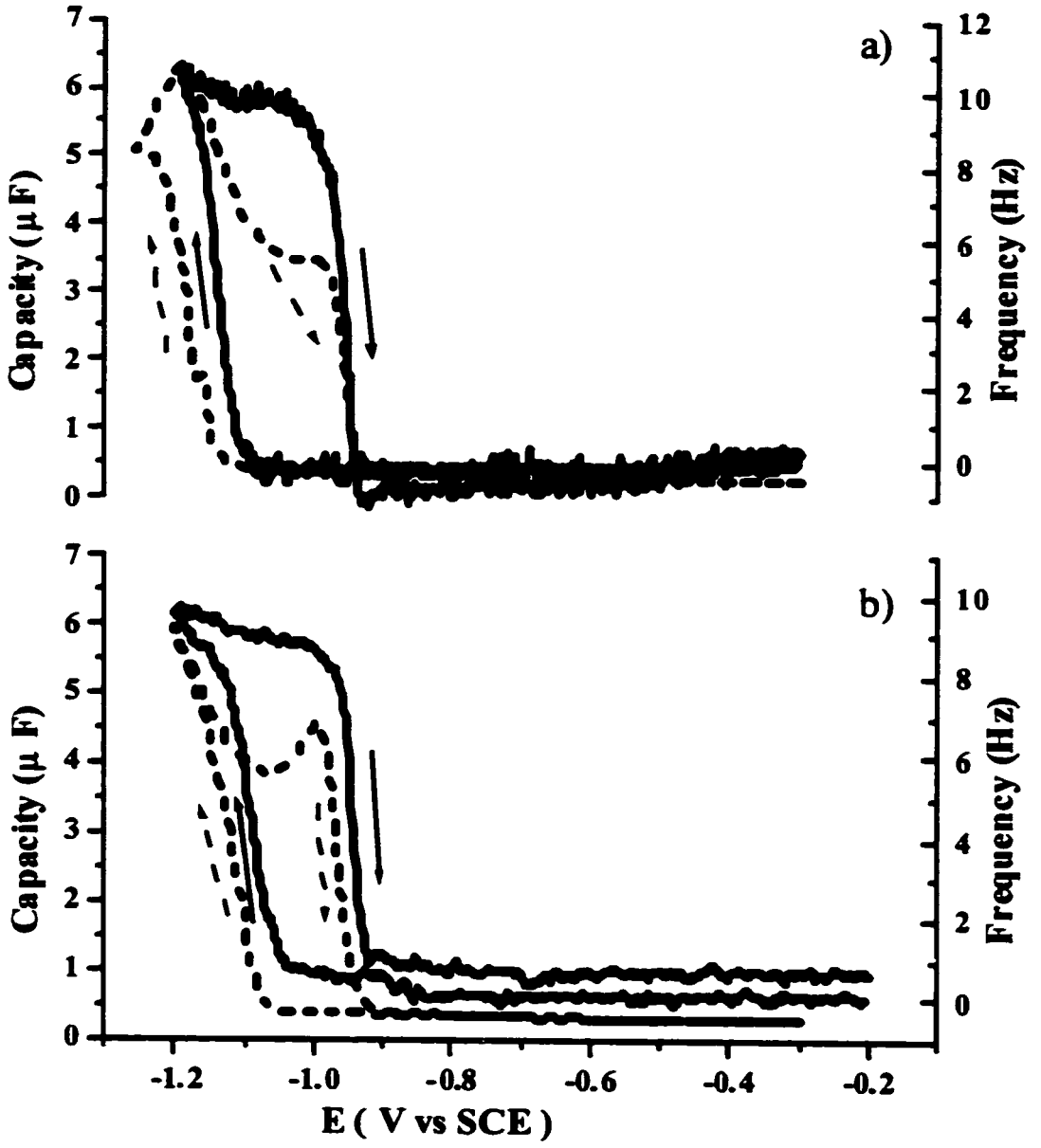

Figure 3-6: Capacity (empty circle) and EQCM signal (solid line) for the oxidative deposition and reductive desorption of octanethiolate on gold from 1mM octanethiolate in a) 0.1 M LiOH and b) 0.1 M KOH. Differential Capacitance measurement: Potential scan rate 5 mV s^{-1}, 20 Hz, 5 mV RMS; EQCM measurements: Potential scan rate: 10 mV s^{-1}.

3.3. Kinetics study of the oxidative adsorption of alkanethiolates on gold

The Δm vs time curves corresponding to different potential steps for butanethiolate and octanethiolate in 0.1 M KOH are shown in Figure 3-7. The potential steps start from –1.10 V for butanethiolate and from –1.25 V for octanethiolate. These potentials are more negative than their potentials of reduction. The gold surface is uncoated at these potentials and this is where we measure the frequency prior to the oxidative adsorption of the alkanethiolate (at time t<0). The potential is then stepped to values ranging from –0.82 V to –0.86 V for butanethiolate and –0.93 V to –0.97 V for octanethiolate. These potentials are positive enough to form a full monolayer.

As shown in Figure 3-7, the Δm vs time curves depend on the value of the deposition potential. However, the total mass (frequency) changes are the same (within experimental error) for all potential steps. The Δm's agree with the masses calculated from the oxidative charges. For both alkanethiolates, a bi-exponential increase of the mass is observed. Immediately after the potential step, there is a fast mass increase. Also, the more positive the applied potential, the faster the initial increase of mass. There is a second rate of mass increase, which seems to be less dependent on the applied potential since for both alkanethiolates we see that the slopes of the mass change vs time are similar at long time. However, the magnitude of this slow component decreases as the potential is made more positive to the point that it is completely absent for the oxidative deposition of octanethiolate at the most positive (faster) deposition potential. There are others differences between the two compounds. The oxidative adsorption of

butanethiolate for the most negative deposition potential (-0.86 V) starts slowly then almost stops after about 5% of the mass has been deposited. This small change could be due to adsorption on defect sites. The adsorption then restarts after a few seconds and continues uninterrupted until a full monolayer is formed. The oxidative formation of a monolayer of butanethiolate is also slower than the formation of a monolayer of octanethiolate. The slow component accounts for the deposition of a larger fraction of the butanethiolate than the octanethiolate. This chain-length dependent kinetics is similar to the one reported for open circuit conditions [3-1, 3-4, 3-5].

The observed two-step electrodeposition is similar to previous reports on the adsorption of alkanethiols under open-circuit conditions [3-3, 3-4, 3-9, 3-10, 3-12, 3-16, 3-25], except that the oxidative deposition is more than 2 orders of magnitude faster. This agrees with the study of I. Rubinstein et al. [3-2], who found that the rate of the adsorption is a function of the applied potential. However, it differs from the results of Doblhofer et al. [3-19] who reported a potential independent rate of oxidative deposition of octadecanethiol on gold. However, in that study, the applied potentials were more positive (-0.6 V to 0.2 V vs. SCE) than those we used here to form a monolayer. At such positive deposition potentials, diffusion limited, potential independent rates are expected, or they might not be visible due to the limited time resolution of EQCM. This observed potential independent oxidative deposition of alkanethiols may also be due to the pH-neutral ethanolic solution used in their study (see below).

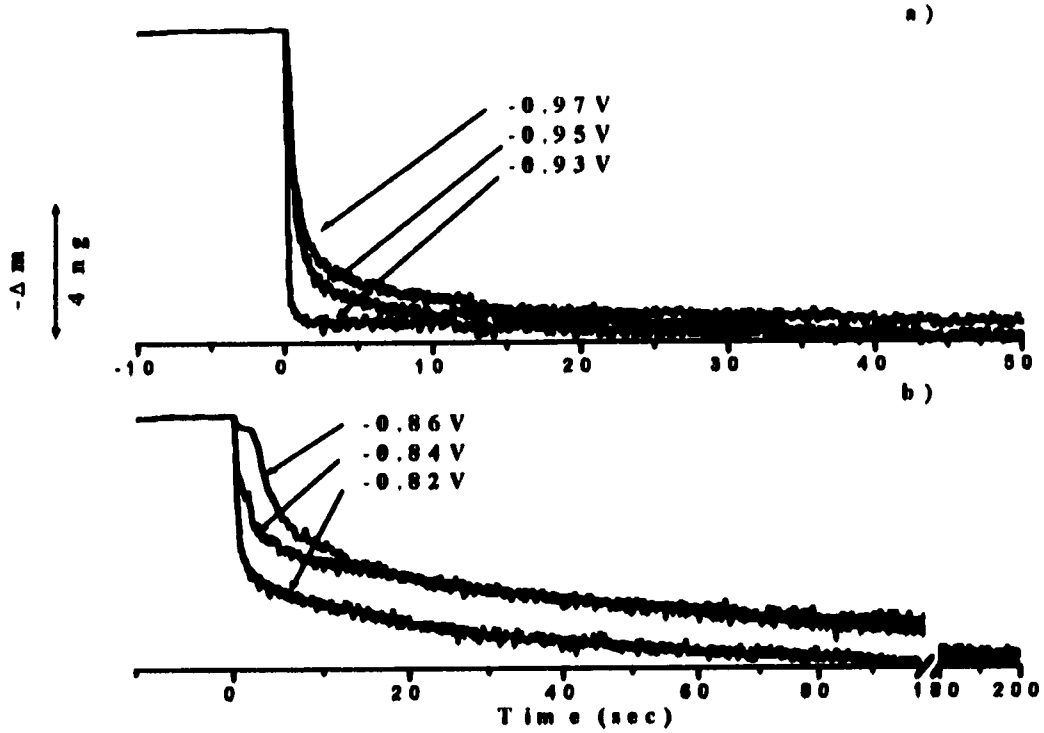

Figure 3-7: Potential step curves (average of five measurements) for the oxidative deposition of a) 1 mM octanethiolate; b) 1 mM butanethiolate on gold in 0.1 M KOH. The potential is stepped from -1.25 V for octanethiolate and -1.10 V for butanethiolate to the potentials indicate on the curves.

We used a two-step model to describe the oxidative deposition of butanethiolate and octanethiolate. In this model, one of the steps is described by a nucleation and growth model [3-45]. This model has been previously used to analyze chronoamperometric data obtained for the reduction of self-assembled alkanethiolate monolayers [3-14, 3-15].

The nucleation and growth model has been shown to successfully describe electrodeposition and electrodesorption processes, which involve adsorbates having significant attractive interactions between them. In the nucleation and growth model, the oxidative deposition begins at some defect sites on the gold surface called nucleation centers. The activation energy, ΔG_a, for the creation of these nucleation centers and the subsequent growth are dependent on several factors. The applied overpotential, η, is one of them. The more positive η is, the faster is the oxidative adsorption. It can be shown [3-14, 3-45] that the rate of growth K_{N-G} in the nucleation and growth model follows this simple equation:

$$K_1 = K_{N-G} = A_{N-G} \exp(-\Delta G_a/RT). \quad (3\text{-}1)$$

There are two limiting cases in the nucleation and growth model. In one case the rate of growth of the nucleation centers is fast. This is called instantaneous nucleation. In this case, all nuclei will be formed at the beginning and growth will occur only from these sites. The current transient is described by the following equation:

$$I/I_m = t/t_m \exp\left(-\left(t^2 - t_m^2\right)/2t_m^2\right), \quad (3\text{-}2)$$

where I is the current at time t after the potential step, and I_m is the maximum current which occurs at time t_m. The other limiting case is called progressive nucleation, which corresponds to similar rates of creation of nucleation center and rate of growth.

The current transient for progressive nucleation and growth is represented by the following equation:

$$I/I_m = t^2/t_m^2 \exp(-(t^3 - t_m^3)/3t_m^3) \qquad (3\text{-}3)$$

When the coverage of the thiolate on the gold surface reaches around 80-90% of a full monolayer, the interactions between the alkane chains will significantly influence the expansion of the nucleation center. These adsorbates are quite large and are likely to block more than the size given by an all-trans configuration. This would decrease the rate of nucleation. In this range of coverage, the deposition is likely to follow a Langmuir model where the adsorption is occurring randomly.

The observed rate constants for these two processes are calculated from fitting the plot of mass change against time with the following bi-exponential equation, which is a nucleation and growth model and a Langmuir model. In our case, due to the large interaction between the deprotonated sulfur and the gold surface, the instantaneous nucleation will be used in our fitting. Therefore, the model is:

$$m(t) = m_{max} A \exp(-k_1 t^2) + m_{max}(1-A) \exp(-k_2 t), \quad (3\text{-}4)$$

where m(t) is the mass of alkanethiolates oxidatively adsorbed at a time t after the potential step. m_{max} is the total mass change for a full monolayer. A is the percentage of total mass change in the first step. k_1 and k_2 are the rate constants for the first (nucleation and growth) and second (Langmuir) step in the electro-formation of a thiolate SAM.

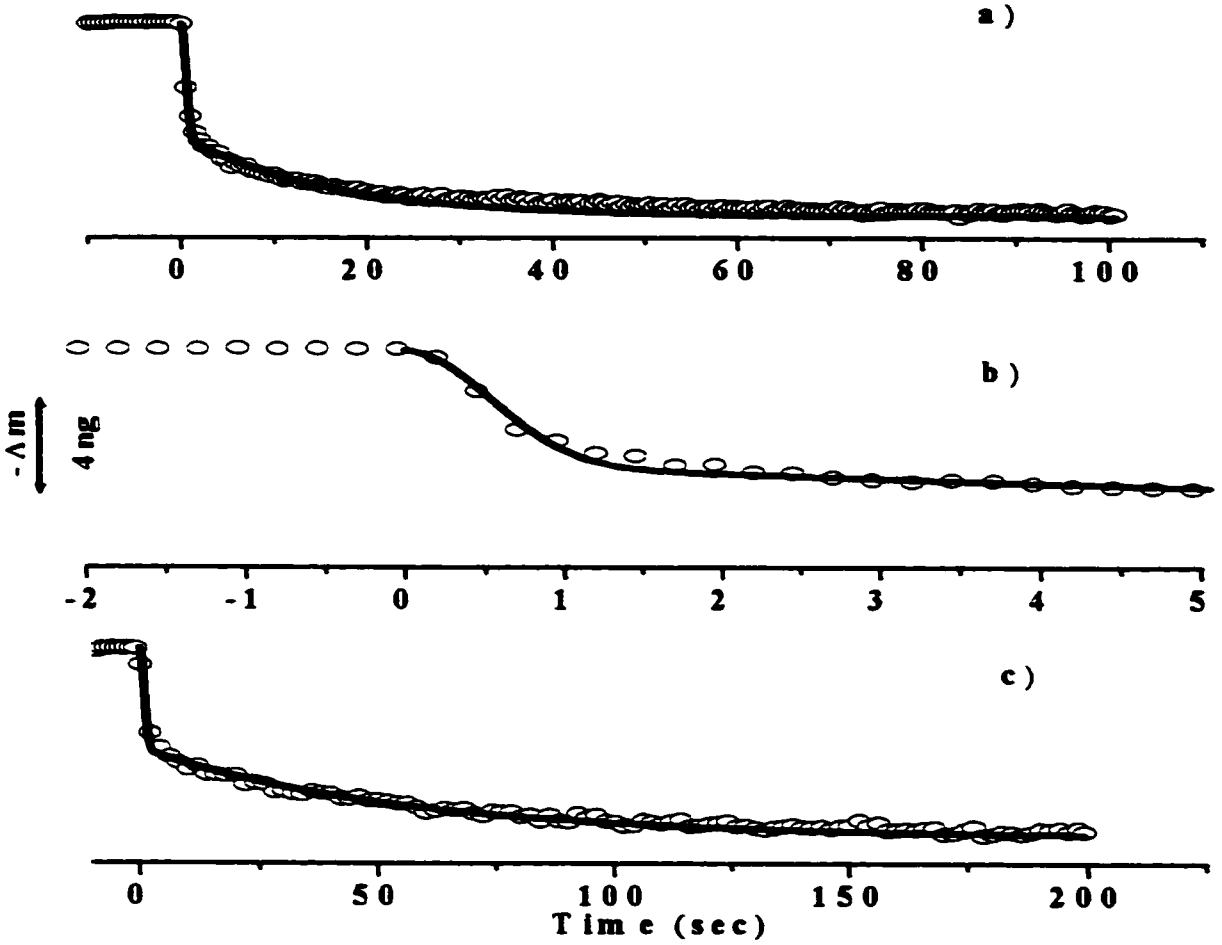

Figure 3-8: Mass change (dotted line, average of five trials of experiments) fitted with eq. 3-4 (solid line) for the oxidative adsorption of a) octanethiolate b) first five seconds for octanethiolate and c) butanethiolate on gold in 0.1 M KOH solution. For clarity only every 10^{th} (Fig.3-8a and c) and 20^{th} (Fig. 3-8b) data point are shown.

We see in Figure 3-8 that the fits (solid lines) done using equation 3-4 describe the oxidative deposition of butanethiolate (Figure 3-8c) and octanethiolate (Figure 3-8a) adequately in 0.1 M KOH. Figure 3-8b shows the first five seconds for the deposition of octanethiolate in KOH. We see that the initial deposition of octanethiolate is adequately described by a nucleation and growth model. The deposition starts slowly and then accelerates as is typical of a nucleation and growth process. After approximately two seconds, the deposition is much slower.

In Figure 3-9, the rate constants, k_1 and k_2 obtained from these fittings are plotted against the applied potential for the octanethiolate in 0.1 M KOH. The rate constant of the first step, k_1, varies exponentially with the applied potential. An exponential fit shows that k_1 varies by one order of magnitude with a change of potential of 28 (±2) mV. Assuming that k_1 has a Nernstian behavior:

$$k_1 = A\exp(-\alpha nFE/RT) \qquad (3\text{-}5)$$

where k_1 is the rate constant, α is the transfer coefficient, E is the applied potential relative to the reversible potential E°, n is the number of the electrons transferred, F is the Faraday constant, T is the temperature, R is the gas constant and A is a pre-exponential, we obtain a transfer coefficient, α, of 0.5. This suggests that the rate-limiting step for the oxidative adsorption occurs close to the electrode surface. The rate constant of the second step, k_2, is independent of the applied potential. As the potential becomes more positive, a smaller fraction of the thiolates is deposited via this Langmuir mechanism to the point that at potentials more positive than –0.94 V no octanethiolates are deposited via this mechanism.

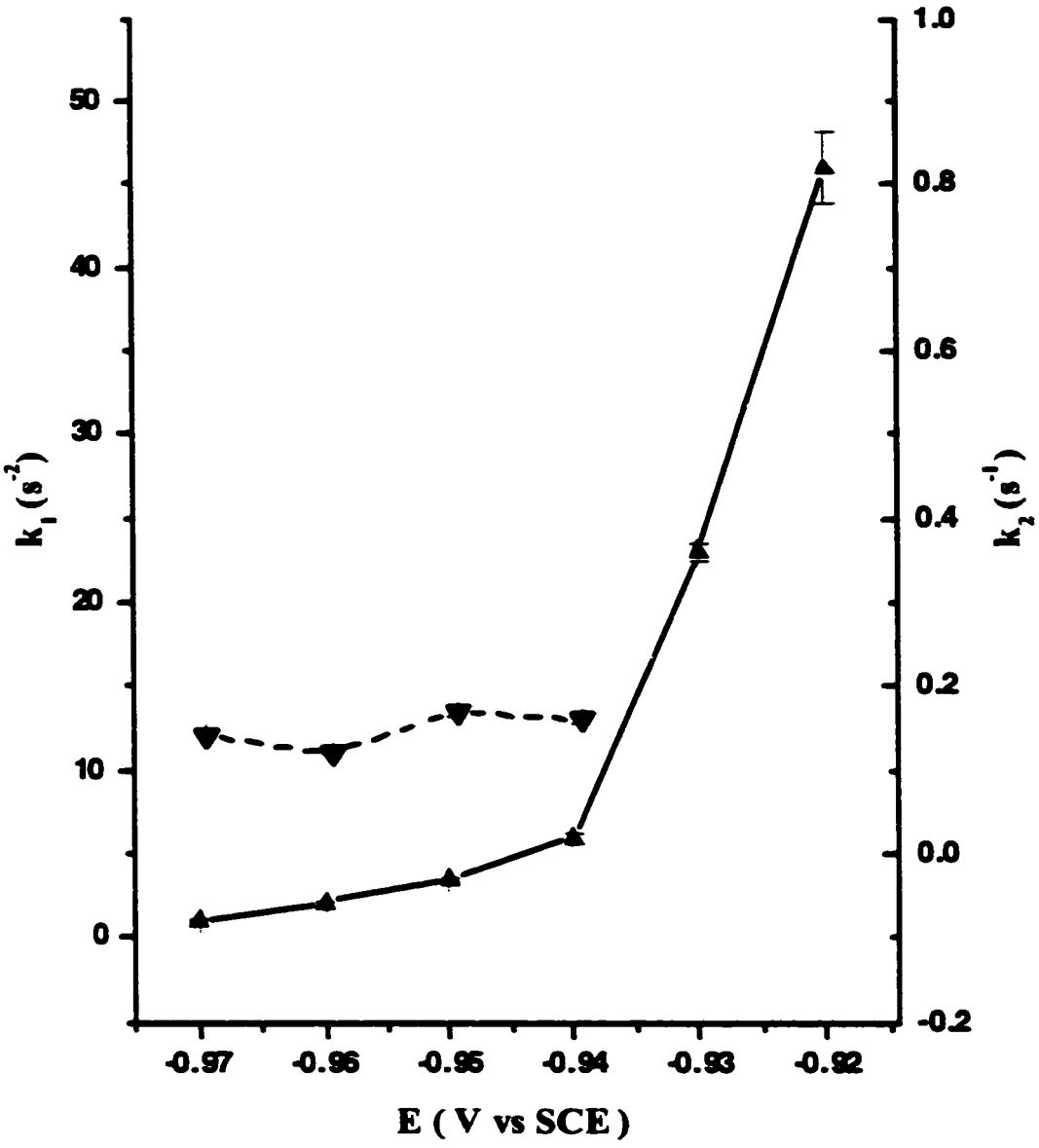

Figure 3-9: Fitted rate constants k_1 (---▲---) and k_2 (---▼---) for the oxidative deposition of octanethiolate in 0.1 M KOH at different deposition potentials obtained using eq. 3-4.

The analysis of the oxidative deposition of butanethiolate yields similar conclusions. However, the narrowness of the deposition current peak (see Figure 3-1) limits the number of potential steps that can be taken and thus reduces the accuracy of the analysis. Nevertheless, we found that k_1 increases by one order of magnitude for a change of the potential of 20 (±4) mV. The value of k_2 (0.03 s^{-1}) is independent of the applied potential and is about one order of magnitude slower than the one measured for octanethiolate (0.17 s^{-1}). This analysis shows that the deposition via a nucleation and growth mechanism displays a similar potential dependence for both butanethiolate and octanethiolate. However, rates for the potential independent Langmuir processes vary greatly.

Although the fits show that the deposition is occurring in two-step, the nature of each step is not very clear, especially the second Langmuir step. In this step, the frequency decreases exponentially with time. There are two possibilities that could cause an exponential decrease. One is the reorganization of the thiolate SAMs described above. This possibility was supported by many studies [3-1, 3-8 to 3-11, 3-16, 3-19, 3-31 to 3-33, 3-46]. However, most of these studies were carried out under open circuit conditions [3-1, 3-9 to 3-11, 3-16, 3-19, 3-32] or in the gas phase [3-8, 3-31, 3-33, 3-46]. In our case, we found that the decrease of the amount of thiolate deposited via the Langmuir process seems to be related to the rate of the nucleation and growth deposition process, k_1. We suggest the following interpretation of k_2. When the coverage is high, the deposition becomes difficult and follows Langmuir kinetics since it occurs at the boundary between islands of thiolates. The decrease of the magnitude of the Langmuir process, as the potential becomes more

positive, could be related to the size of the islands. The amount of boundaries created when islands of thiolates collide will depend on the size of the islands. We can expect the average size of the islands of thiolates to increase, as the deposition potential is made more positive. This would decrease the amount of domain boundaries and thus decrease the magnitude of the Langmuir component.

The observation that the Langmuir process is slower for shorter thiolates (i. e. butanethiolate) could also be related to the size of the islands of butanethiolate. The weaker interadsorbate interactions would certainly decrease the size of the islands of butanethiolate and therefore increase the number of domain boundaries. This effect, combined with the increased disorder inside the islands of short chain thiolates, are likely to make the deposition of butanethiolates at high coverages more difficult and thus slower. The variation of the oxidative adsorption process with the rate of deposition could also be related to the formation of different phases as was observed in some studies [3-5, 3-8, 3-31, 3-33, 3-46]. Under open-circuit conditions and for a low coverage, octadecanethiol adsorbs flat on gold. As the coverage increases, there is a phase transition from a horizontal to a vertical orientation of the alkyl chains. It is possible that for slow deposition rates (i. e. at more negative deposition potentials) that this phase transition is the source of the two-step mechanism that we observed. At more positive potentials, the faster deposition rate could force the alkanethiolate to adsorb vertically. Both suggestions are compatible with our data.

The other possibility is that the diffusion of alkanethiolates to the surface slows down the nucleation and growth process. Such a model was described by Buess-Herman and co-workers [3-47, 3-48]. The diffusion-limited process also decays exponentially with time, and is described by the following equation [3-48]:

$$i = q_{mon}\pi A^2 D \exp(-\pi A^2 D N_0 t), \qquad (3\text{-}6)$$

where A is a constant, D is the diffusion coefficient , N_0 is the number of nuclei, and q_{mon} is the charge corresponding to the formation of a full monolayer.

In order to clarify the nature of the second step, we did chronoamperometric measurements. The chronoamperograms of the deposition of butanethiolate are shown in Figure 3-10. The potential step starts from –1.10 V in 0.1 M KOH. After the potential step, there is a smooth current transient, which corresponds to the oxidative deposition of alkanethiolates. The maximum current (I_m), occurs at time t_m, which changes with the final potential. I_m increases when the potential becomes more positive and t_m decreases. The current transients last less than 0.4 s and t_m is at time less than 30 ms. After 0.4 s, the current became too small to be detected (less than 5 nA). In the KOH solution (Figure 3-10), the current transients become more symmetric when the final potential is set to more negative values. They become more asymmetric when the final potential is set to more positive values. After the potential step, the integrated charge in the short time scale (~ 0.4 s) decreases when the final potential becomes more negative and only a partial monolayer is formed in this time range.

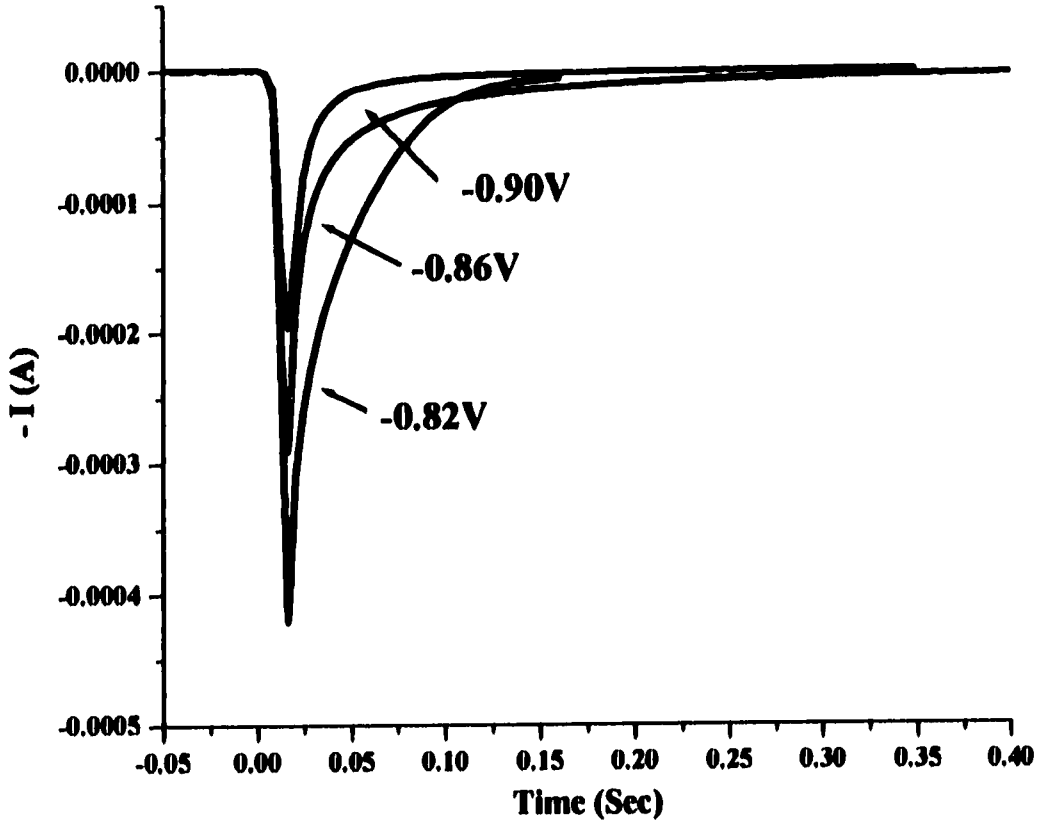

Figure 3-10: Chronoamperograms of the butanethiolate oxidative deposition on gold in 0.1 M KOH. The potential is stepped from –1.10 V to the potential shown on each chronoamperogram.

A comparison of the results of the chronoamperometric and EQCM measurements in 0.1M KOH is shown in Figure 3-11. The moles of butanethiolates deposited on gold at the different final potentials are drawn in this graph. One curve is from the integrated charge. The other is from the frequency change during the first two seconds after the potential step. The EQCM results show that during the first two seconds after the potential step, the mass change decreases as the final potential becomes more negative. The offset of two curves in the graph comes from the integrated charge in the chronoamperometric measurement, which is not corrected for the capacitive charge [3-13]. As mentioned before, we cannot separate the capacitive charge from the total integrated charge, since the Faradic current and capacitive current occur simultaneously in the chronoamperometric measurements. This suggests that the oxidative current in the chronoamperometric study, which is caused by the oxidative deposition of the alkanethiolates, cannot be directly compared with the mass change. The large difference between them in the KOH may be due to the partial coverage of alkanethiolates formed on that time scale.

The mechanism of the oxidative deposition of alkanethiolates on gold can be obtained from the chronoamperograms. To fit the chronoamperograms, we used an instantaneous nucleation and growth model, which was discussed in the previous section.

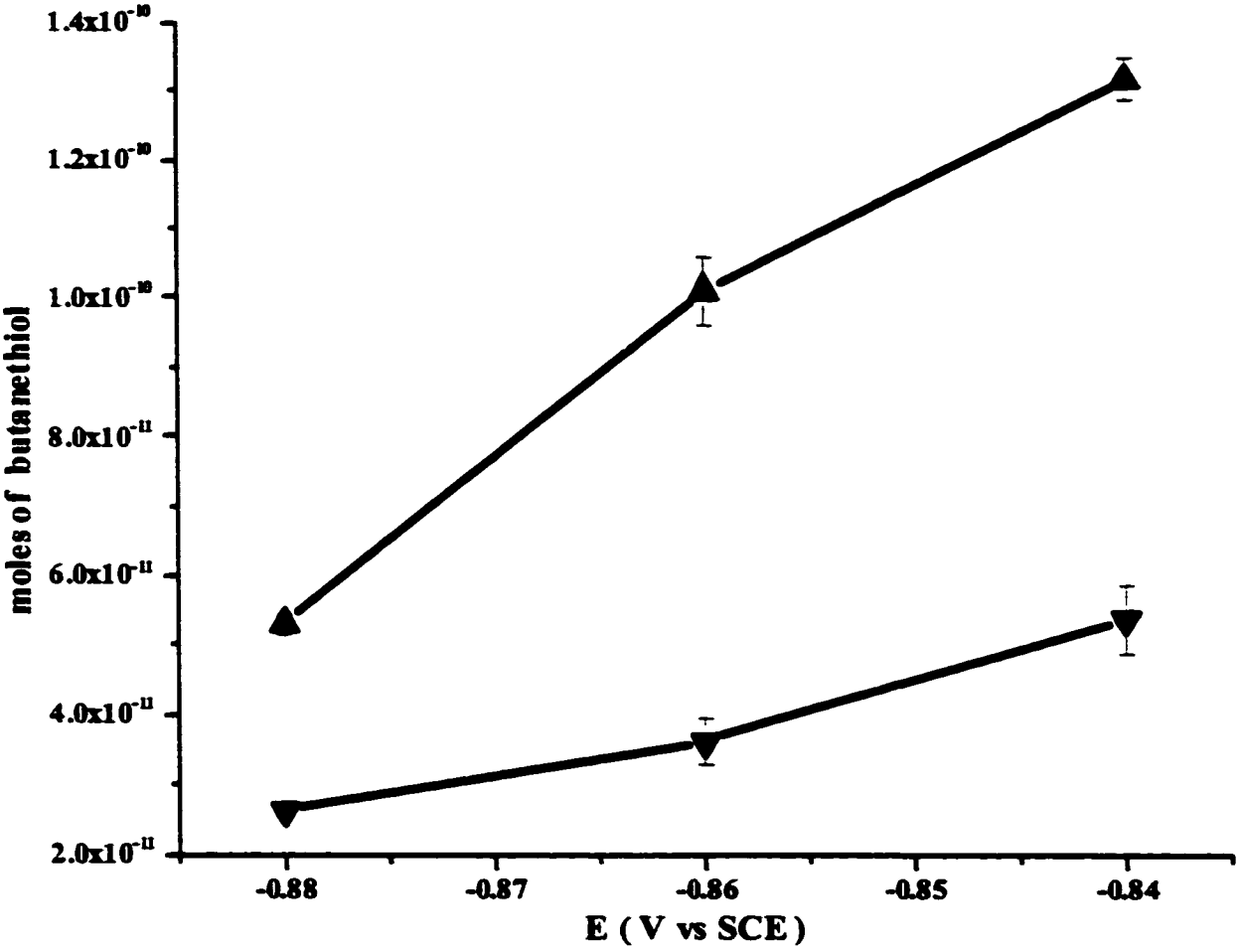

Figure 3-11: Plot of the moles of butanethiolate deposited which were calculated from the integrated charge of chronoamperograms in Fig. 3-10 (---▲---) and from the EQCM measurements (---▼---).

Due to the short-time scale in the chronoamperometry experiment, only the nucleation and growth model was used. On this short time scale, only the first step in EQCM is measured.

The fits of the chronoamperograms of the oxidatively deposited butanethiolates on gold are shown in Figure 3-12. As shown in Figure 3-12a, when stepping to –0.90 V (a small overpotential applied), the chronoamperogram (empty circle) is fitted by an instantaneous nucleation and growth model (solid line). There is no diffusion limitation in this case. Since a small overpotential is applied, the rate of the growth of the islands is relatively slow. This rate is slower than that of the diffusion. The conditions in this case are similar to those of open circuit conditions. Thus we suggest that the two-step adsorption model can be described as an instantaneous nucleation and growth model followed by a reorganization or annealing process when a small overpotential is applied.

When the deposition potential is –0.82 V (i.e. large overpotential), the chronoamperograms become asymmetric, as shown in Figure 3-12c. This may be caused by the fact that the nuclei can only grow to a certain size [3-45]. There are two possibilities that could cause this limiting growth. One is the gold surface. Even though we found that the gold surface of the EQCM quartz crystal has a large component of (111) domains (see Chapter 2), it is not homogenous. It contains different terraces. Therefore, on one terrace, the growth of the nucleation center will stop at the step, because the nuclei cannot jump to the next terrace and continue to grow on the other terrace. The other one is the diffusion of thiolates to the surface. Once the nucleation centers are generated and grow

to a relatively large size, the rate of growth slows down and becomes smaller. This happens at large overpotentials. In such a case, a large number of nucleation centers are generated. There is a depletion of the thiolates next to the surface due to the high rate of oxidative deposition. The rate thus becomes limited by the diffusion of thiolates from the solution. Therefore, oxidative deposition in the chronoamperograms occurs at two rates: The nuclei grow to a certain size and slow down at time t', then the thiolates are deposited through the diffusion-limited process (Langmuir process). Normally $t' \leq t_m$ [3-45], but if we assume that $t' = t_m$, then it gives:

$$I(t)/I_m = t/t_m \exp(-(t^2 - t_m^2)/2t_m^2) \qquad (t < t') \qquad (3\text{-}7a)$$

$$I(t) = -A \exp(-k^*(t-t_m)) \qquad (t \geq t'), \qquad (3\text{-}7b)$$

where A is a pre-exponential and k^* is the rate constant of the diffusion process.

The fits done using Equations 3-7a and 3-7b are shown in Figure 3-12c as a dashed line.

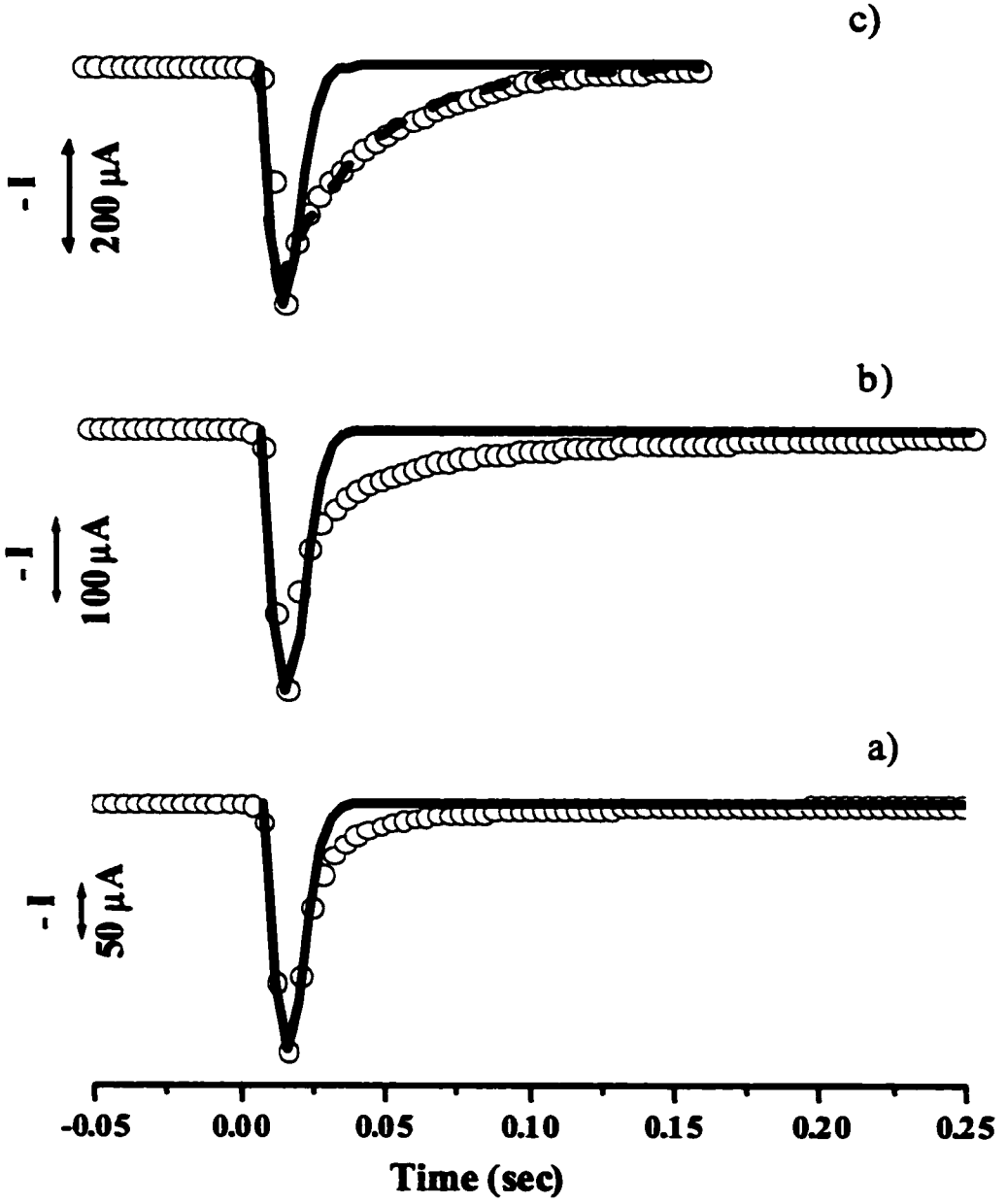

Figure 3-12: Chronoamperograms of the butanethiolate oxidative deposition on gold in 0.1 M KOH solution. The empty circles are data points. The solid line is the fit with the instantaneous nucleation and growth model (eq. 3-2). The dashed line is the fit with eq. 3-7. The potential is stepped from –1.10 V to the potential a) –0.90 V; b)-0.86 V; c)-0.82 V.

We can see that the instantaneous nucleation and growth model, followed by a diffusion-limited process describes the chronoamperogram of the oxidative deposition of butanethiolate well (Figure 3-12c). We noticed that this only happens when a large overpotential is applied (at more positive potential). This differs from the open circuit experiments. So we suggest that the two-step adsorption model can be described by an instantaneous nucleation and growth model followed by a diffusion-limited process. For the octanethiolate, we find that the Langmuir adsorption process, which was suggested to be a reorganization process, almost disappears at more positive deposition potentials. The instantaneous nucleation and growth model, followed by a diffusion-limited process described this case very well. For butanethiolate, the second step in the adsorption process is always assigned to a reorganization.

In summary, the oxidative deposition of alkanethiolates on gold consists of two steps: A fast, potential dependent step followed by a slow, potential independent step. The fast deposition follows an instantaneous nucleation and growth mechanism, and the slow deposition occurs via a Langmuir process. At slow deposition rates, the Langmuir process is described as a reorganization process. At higher deposition rates, for octanethiolate, the Langmuir process is described as a diffusion-limited process. For the butanethiolate, the Langmuir process seems to be related to a reorganization of the monolayer.

3.4. Kinetic study of the oxidative adsorption of alkanethiols on gold from a 0.1 M $KClO_4$ solution

3.4.1 Validity of Sauerbrey equation

As mentioned before, in order to use EQCM to study the oxidative deposition of alkanethiols, we must first verify the validity of the Sauerbrey equation. Due to the very low solubility of octanethiol, we only used butanethiol in this study.

The EQCM signal and cyclic voltammogram of butanethiol in 0.1 M $KClO_4$ are shown in Figure 3-13. The potential is scanned between –0.3 V and –1.0 V vs SCE. On the initial negative going potential scan, the current and frequency are almost constant until –0.75 V. Then, as the current due to the reductive desorption of butanethiol appears, the frequency increases. The frequency does not change much for potentials more negative than –0.94 V, even though there is a relatively significant reductive current after the reductive desorption current peak. On the following positive going potential scan, the onset of the frequency decrease corresponds to the broad oxidative current peak. After the oxidative current peak, the frequency decrease is much slower and smaller. At -0.3 V the frequency is almost the same as the initial one.

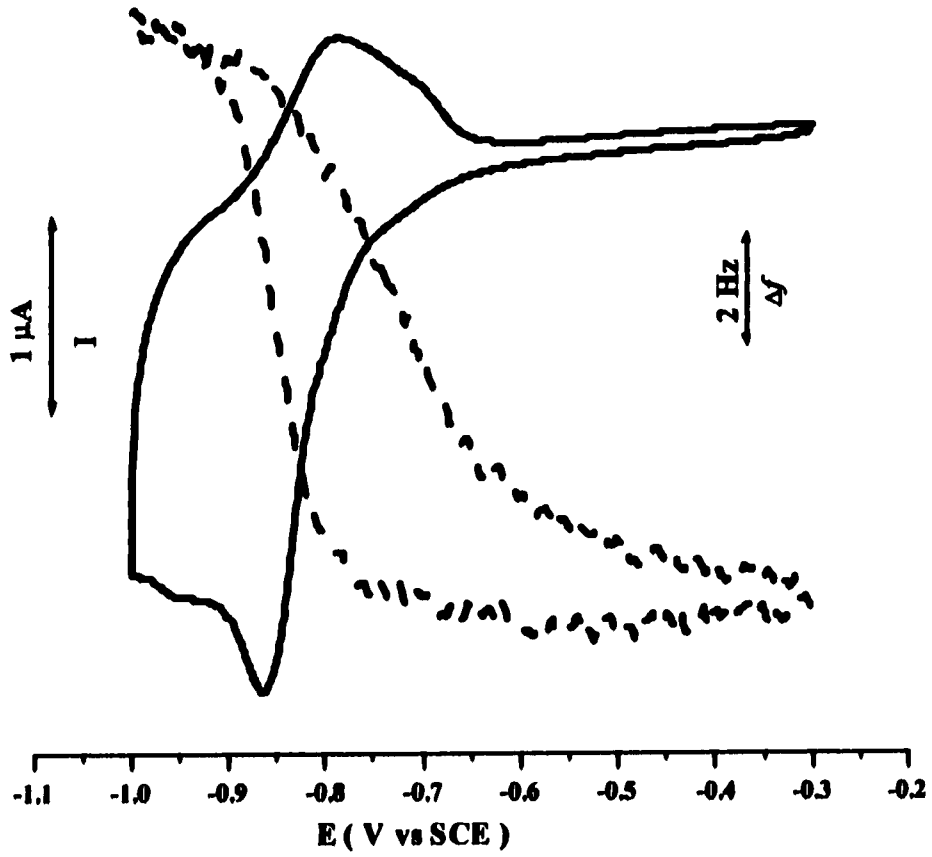

Figure 3-13: Cyclic voltammogram and EQCM frequency for the oxidative adsorption/reductive desorption of butanethiol on gold recorded in 0.1 M $KClO_4$. Potential scan rate: 20 mV s^{-1}.

The frequency change (Hz mV^{-1}) in 0.1 M $KClO_4$ is slower than in an alkaline solution (see Figure 3-1) for the same potential scan rate. This matches the cyclic voltammograms in these solutions. There is a broad oxidative current peak in the $KClO_4$ solution and a sharp oxidative current peak in the KOH solution. The narrowing of the current peak in the alkaline solution may be due to the fact that the thiols are deprotonated [3-40].

A plot of the moles of electron (obtained from the oxidative charge corrected for the capacitive current) as a function of the moles of butanethiol deposited (obtained from the frequency change and the Sauerbrey equation) in 0.1 M $KClO_4$ solution is shown in Figure 3-14. The slope (mole of electron per mole of butanethiol) of this graph is 1.15 ± 0.09 (an average of five measurements). This corresponds to the deposition of 79 (±8) g of butanethiol per mole of electrons. The molar mass of butanethiol is 90 g. Thus the EQCM data agrees with a one-electron process for the alkanethiol desorption or deposition on gold [3-42]. This result shows that the Sauerbrey equation is also valid in 0.1 M $KClO_4$. This supports the suggestion that we made in the previous section, that the double layer effects are not very important in our EQCM studies. This also agrees with the fact that the OH^- and ClO_4^- ions are not chemically adsorbed on the gold surface in the range of potential we used.

The validity of the Sauerbrey equation in the $KClO_4$ solution allows us to combine EQCM with potential step experiments to study the kinetics of the oxidative deposition of alkanethiols on gold.

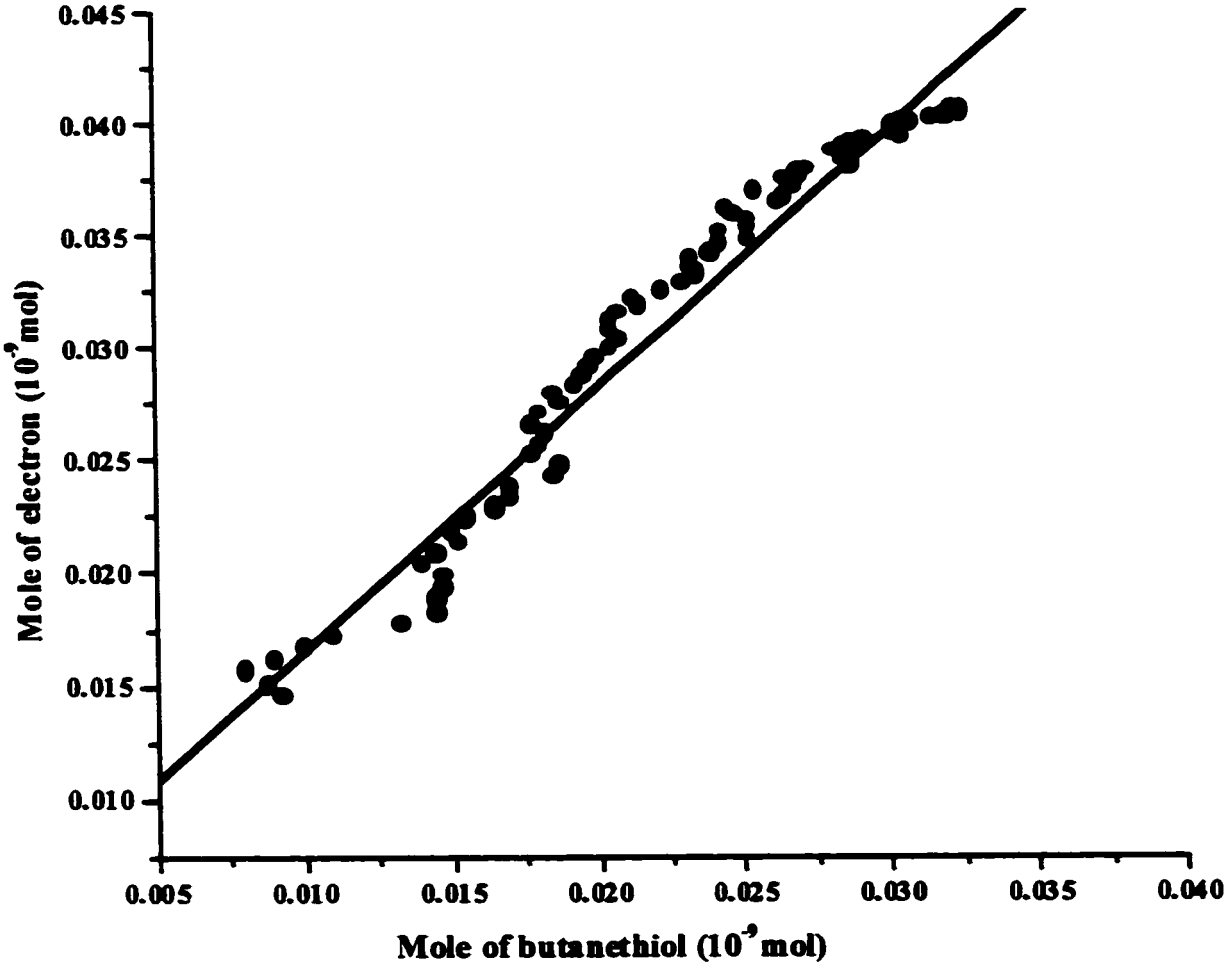

Figure 3-14: Graph of the mole of electrons calculated from the cyclic voltammogram in Fig. 3-13 vs the mole of butanethiol deposited calculated from EQCM signal in Fig. 3-13. The line is a linear fit.

3.4.2 Kinetic study of the oxidative deposition of alkanethiols on gold

The mass changes corresponding to different potential steps for butanethiol in 0.1 M $KClO_4$ are shown in Figure 3-15. In these experiments, the potential is initially set at –1.00 V. This potential is more negative than the potential of the reduction of the butanethiol and thus the gold surface is uncoated. The frequency prior to the oxidative adsorption of the alkylthiols (at time $t<0$) is constant. The potential is then stepped to values ranging from –0.40 V to –0.76 V to cause the formation of a monolayer. In this study, the range of the final potentials is larger than that in the previous study done in alkaline solutions, which was only from –0.82 V to –0.86 V. This is due to the broad oxidative current peak in $KClO_4$. The mass change vs time curves in Figure 3-15 depend on the deposition potential. However, the total mass (frequency) changes are almost the same for all potential steps and they also agree with the mass calculated from the oxidative charges shown in Figure 3-13.

Similarly to the deposition of alkanethiolates, a bi-exponential increase of the mass is observed. This two-step electro-deposition of alkanethiols in $KClO_4$ solution is analyzed with the same model used for the deposition of alkanethiolates. This model consists of a nucleation and growth process and a Langmuir process. The observed rate constants for these two steps are calculated from the fitting of the plot of mass change against time with equation 3-4.

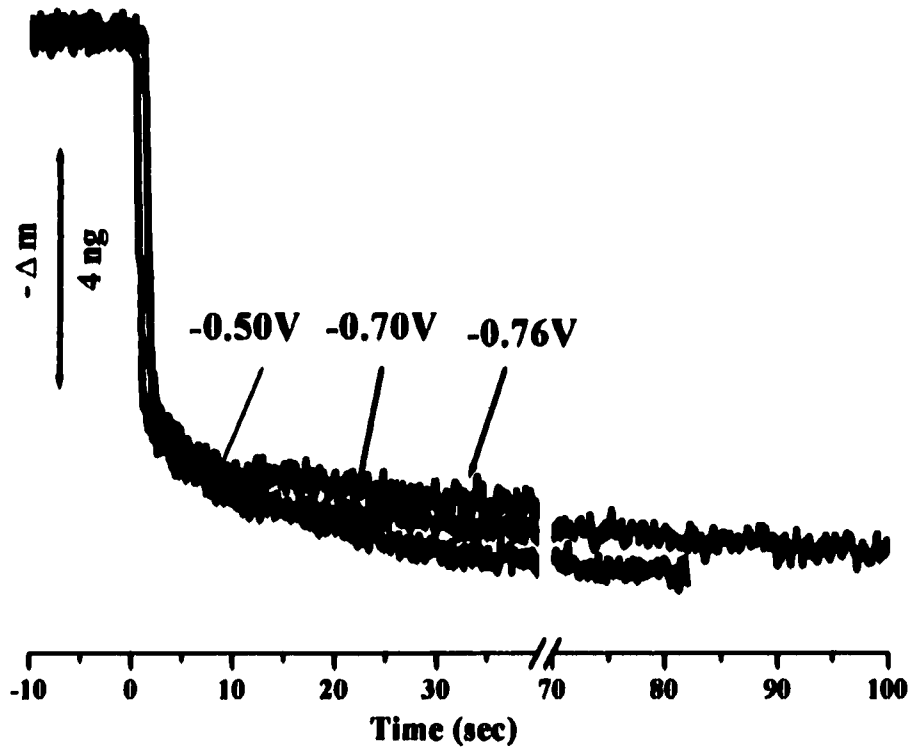

Figure 3-15: Potential steps for the oxidative deposition of butanethiol on gold from 1 mM butanethiol/ 0.1 M $KClO_4$ aqueous solution (the curves are averages from five measurements). The potential is stepped from -1.00V to the potentials shown on each curve.

In Figure 3-16, we see a fit (solid line), done using the bi-exponential equation 3-4. This model describes the oxidative deposition of alkanethiols adequately in the range of potentials used in this study.

In Figure 3-17, the rate constants k_1 and k_2 are plotted against the applied potential. k_1 varies slightly with the applied potential. An exponential fit shows that k_1 increases by one order of magnitude with a change of potential of 224 (±30) mV. Assuming that k_1 as a Nernstian behavior, we would obtain a transfer coefficient, α, of 0.06. Such a small transfer coefficient suggests that the rate-limiting step for the oxidative adsorption is at the electrode surface. The rate constant of the second step, k_2, is independent of the applied potential and is one order of the magnitude smaller (slower) than the value of k_2 in 0.1 M KOH.

Chronoamperometric measurements of the oxidative deposition of butanethiol were carried out in a 0.1 M $KClO_4$ solution, in order to identify the origin of the last step. Chronoamperograms of the deposition of butanethiol are shown in Figure 3-18. The potential step starts from –1.00 V in 0.1 M $KClO_4$. After the potential step, there is a smooth current transient, which corresponds to the oxidative deposition of butanethiol. The maximum current (I_m) occurs at time t_m, which changes with the final potential. I_m increases when the potential becomes more positive and t_m decreases. The current transients last less than 0.4s and t_m is less than 30 ms. After 0.4 s, the current became too small to be detected. As shown in Figure 3-18, the oxidative current transients are relatively symmetric at more positive deposition potentials. They become asymmetric,

when the deposition potentials are more negative. The integrated charge in the short time scale (~ 0.4 s) is constant for the potentials shown in Figure 3-18. These results agree with the EQCM measurements.

A comparison of the chronoamperometric and EQCM measurements in the 0.1 M $KClO_4$ solution is shown in Figure 3-19. The EQCM measurements in the $KClO_4$ solution show that the mass changes in the first two seconds, after stepping to different final potentials, is almost constant and accounts for 80% to 90% of the total mass change. The reason for the offset of the two curves in the graph was described in the last section. In $KClO_4$, a full monolayer is deposited and the mass obtained for the EQCM measurements is about 75% of the one calculated from the charge. This is expected, since the capacitive charge is about 25% of the total charge.

A nucleation and growth model (equation 3-2) was used to fit the chronoamperograms in Figure 3-18. The fits are shown in Figure 3-20. We see in Figure 3-20, that at more positive potential (-0.40 V), the chronoamperogram is fitted by an instantaneous nucleation and growth model relatively well. There is no significant diffusion limitation in this case. So the second step in the adsorption process is described as a reorganization process, which is similar to the process under open circuit conditions. The oxidative deposition of alkanethiols on gold in 0.1 M $KClO_4$ solution is not strongly dependent on the applied electric field (see below). Therefore, the adsorption process should be similar to the one observed under open circuit conditions.

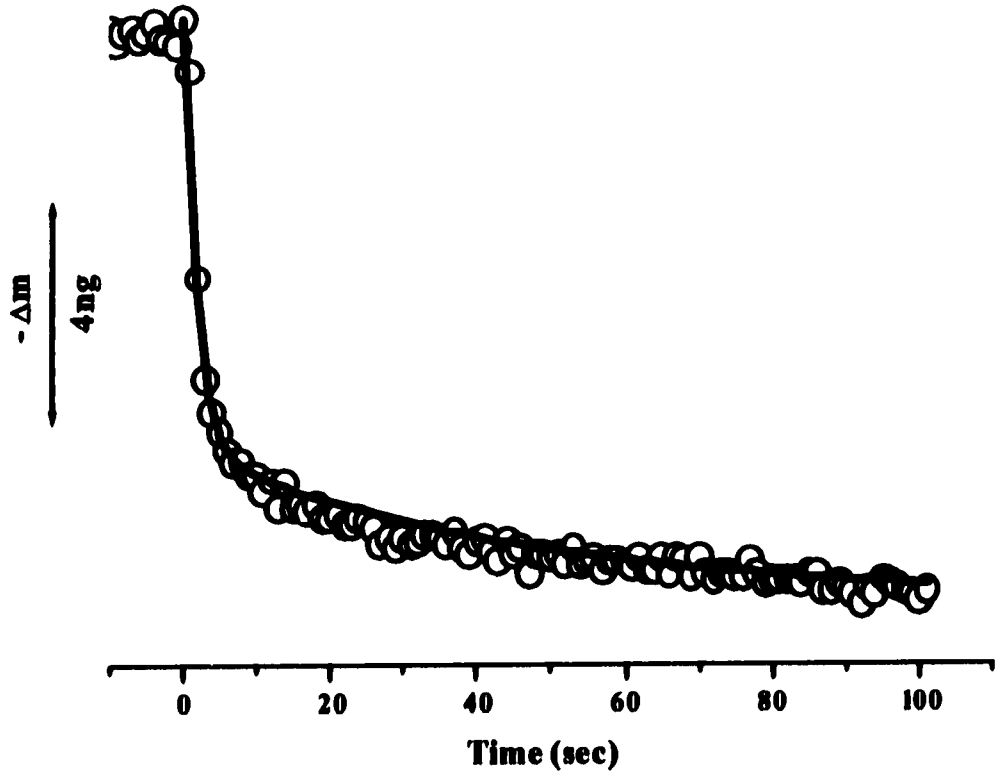

Figure 3-16: Mass change (dotted line, average of five measurments) fitted with eq. 3-4 (solid line) for the oxidative deposition of butanethiol on gold in 0.1 M $KClO_4$ solution. The deposition potential is –0.76 V. For clarity only every 50th data point is shown.

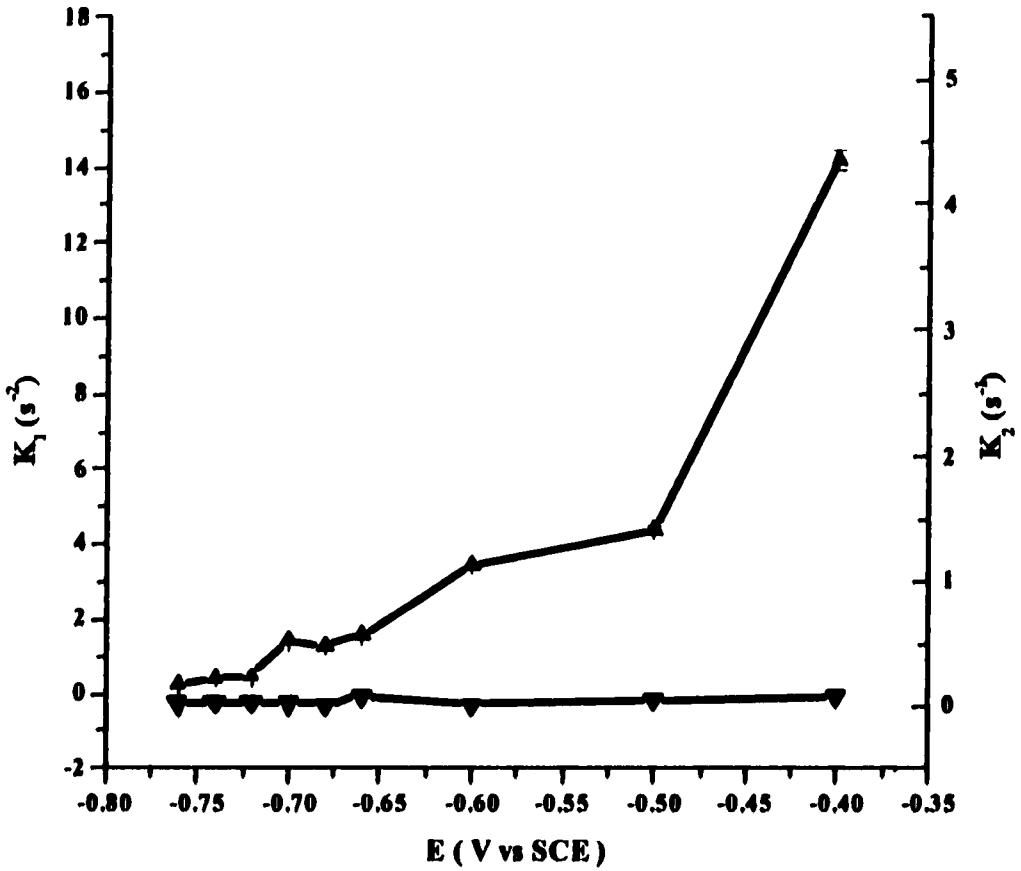

Figure 3-17: Fitted rate constants k_1 (---▲---) and k_2 (---▼---), using eq. 3-4, for the oxidative deposition of butanethiol at different applied potentials in 0.1 M $KClO_4$.

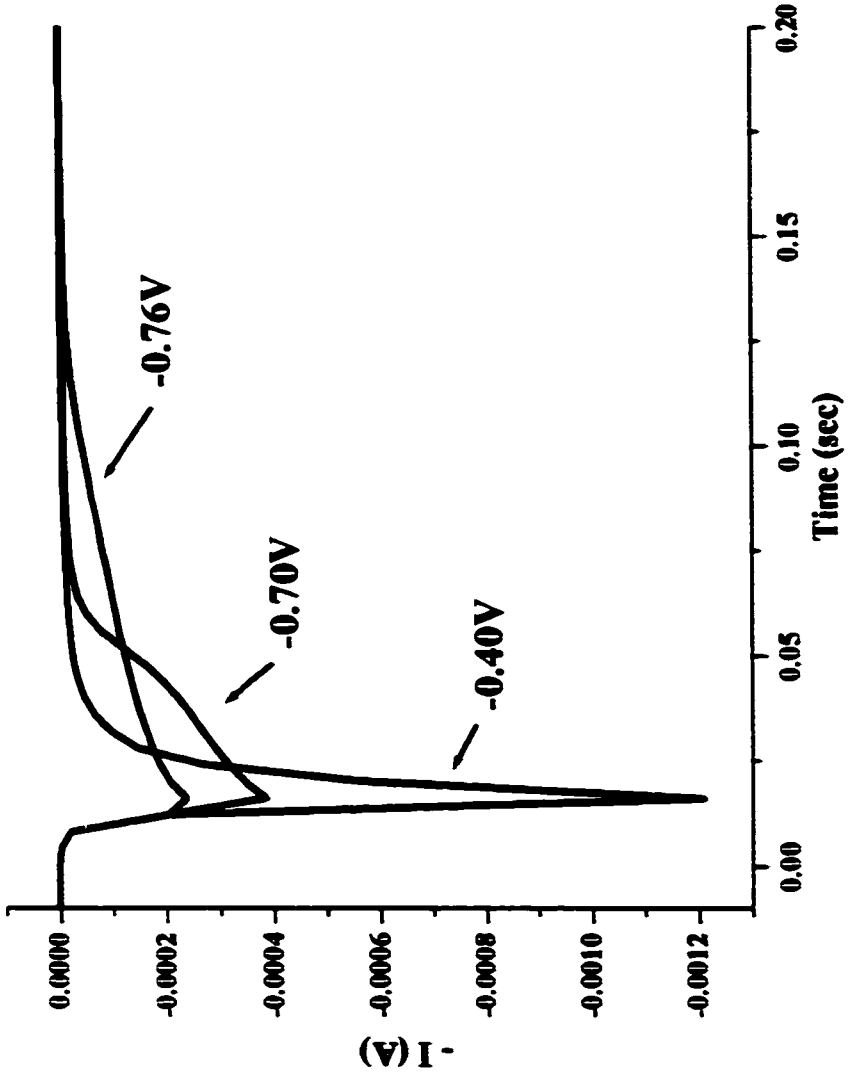

Figure 3-18: Chronoamperograms of the oxidative deposition of butanethiol on gold in 0.1 M $KClO_4$ solution. The potential is stepped from –1.00V to the potentials indicated on the chronoamperograms.

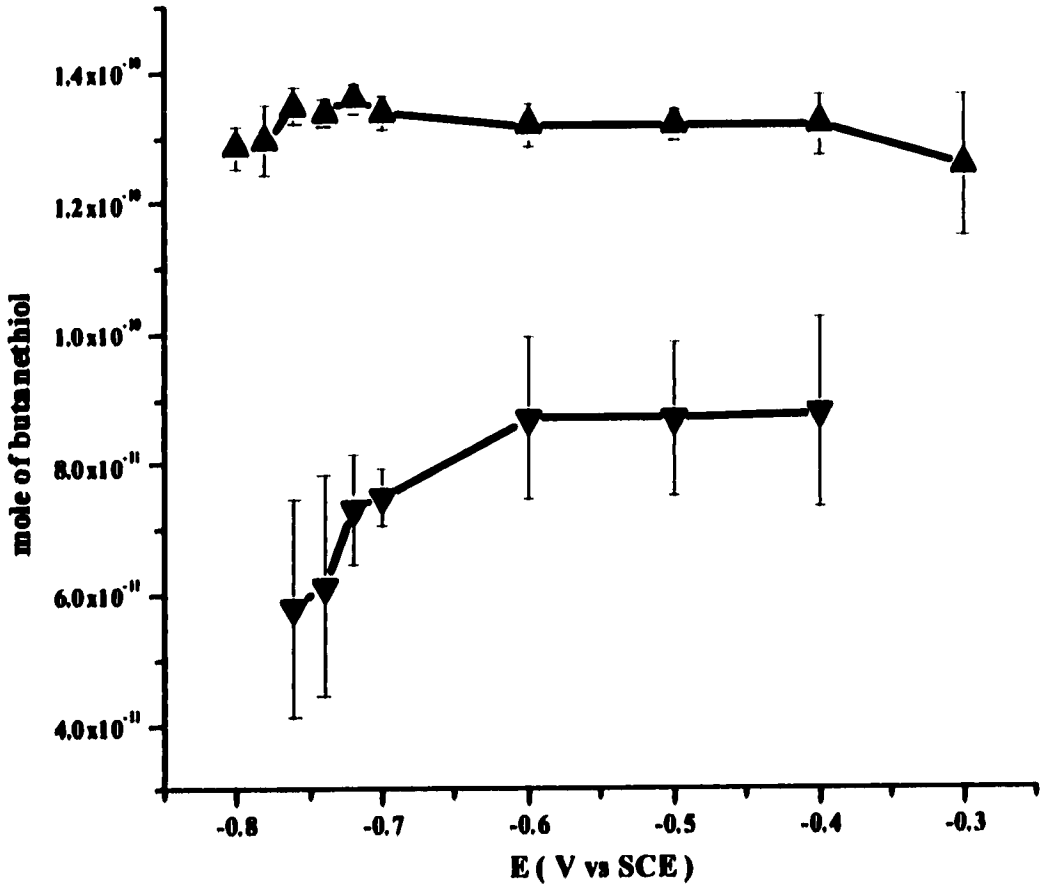

Figure 3-19: Plot of the mole of the butanethiol deposited, which were calculated from the integrated charge of the chronoamperograms such as those in Fig. 3-18 (---▲---) and from the EQCM measurements such as those in Fig. 3-15 (---▼---).

When the final potential becomes more negative, the chronoamperograms become asymmetric. Obviously, since it happens at small overpotentials, this will not be due to a diffusion-limited process (see above). We also notice that the shape of the chronoamperograms in 0.1 M $KClO_4$ solution is potential-dependent, even though the total charges are potential independent. This asymmetric chronoamperogram indicates that there is a process, which is slower than the rate of nuclei generation. Since a very small transfer coefficient, α, was observed, we suggest this process takes place at the electrode surface. We assign this surface process to the dissociation of the S-H bond. Losing one proton cannot be detected by the EQCM measurement. The energy of dissociation of the S-H bond is not expected to be strongly dependent on the applied potential. The activation energy of the dissociation of the S-H bond on gold is thus a weak function of the overpotential ($\Delta G_{diss}(\eta)$). k_{diss}, the rate constant of the dissociation of S-H bond at the surface is given as:

$$k_{diss} = A_{diss} \exp(-\Delta G_{diss}(\eta)/RT), \qquad (3\text{-}8)$$

where A_{diss} is a pre-exponential, R is the gas constant and T is the temperature.

Similarly to the nucleation and growth model discussed elsewhere [3-13, 3-14, 3-45], the dissociation of the S-H bond could begin at some defects on the surface. The rate of the creation of the nucleation center, k_c, is given by

$$k_c = A_c \exp(-\Delta G_c(\eta)/RT), \qquad (3\text{-}9)$$

where ΔG_c is the activation energy for the creation of the nucleation center, which depends on the applied overpotential. The number of etching centers, M, varies with time and is represented as

$$M(t) = M_0 (1 - \exp(-k_c t)), \qquad (3\text{-}10)$$

where M_0 is the maximum number of nuclei having a critical size such that they can grow [3-45].

When a more positive potential (large overpotential) is applied, the rate of dissociation of the S-H bond increases and k_{diss} increases more than k_c. The deposition then follows an instantaneous nucleation and growth process as shown in Figure 3-20a. When the potential becomes more negative (small overpotential), the rate of the dissociation of S-H bond decreases and it becomes the rate-limiting step. Under these conditions, the current is given by

$$I(t) = nFM(t)\exp(-k_{diss}\, t). \qquad (3\text{-}11)$$

As shown in Figure 3-20b and Figure 3-20c, fits using equation 3-11 adequately represent the deposition for low overpotential.

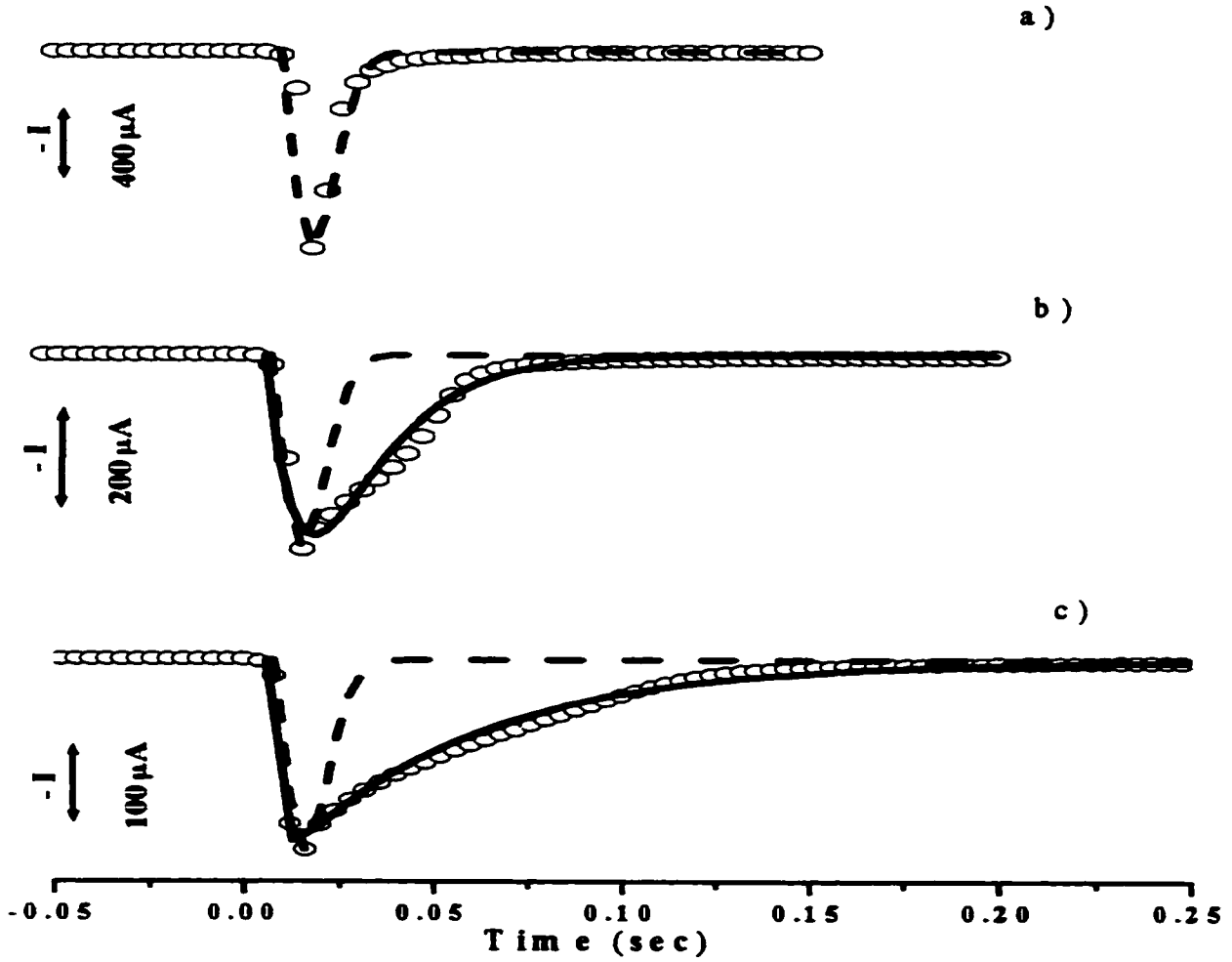

Figure 3-20: Chronoamperograms of the butanethiol oxidative deposition on gold in 0.1 M $KClO_4$. The empty circles are data points. The dashed line is the fit with the instantaneous nucleation and growth model (eq. 3-2). The solid line in b) and c) is the fit with eq. 3-11. The potential is stepped from –1.00 V to a)-0.40 V; b)-0.70 V; c)-0.76 V.

3.5. Mechanisms for the oxidative deposition of alkanethiolates and alkanethiols on gold from aqueous solutions

The observed transfer coefficient, α, in KOH solution (0.5) is almost one order of magnitude larger than in $KClO_4$ solution (0.06). This indicates that even though the oxidative deposition of alkanethiols and alkanethiolates both follow a two-step process, the first steps are different. There are several differences in the first (fast) step of the alkanethiol and alkanethiolate oxidative deposition on gold. In summary

1. In the alkaline solution, the shape of Δm vs. t curves and the chronoamperograms show a stronger dependence on the deposition potential than those in 0.1 M $KClO_4$.

2. The mass change in the first step (80% to 90% of the total mass change) in 0.1 M $KClO_4$ occurs in a few seconds after the potential step and is almost independent of the final potential. But in the alkaline solution, it changes significantly with the final potential.

3. Even though the instantaneous nucleation and growth model can be used to fit both of the chronoamperograms, we assign the origin of the asymmetric chronoamperograms at slow deposition rates to different processes.

These are obvious kinetic differences and they should originate from the fact that one compound is protonated (alkanethiols in 0.1 M $KClO_4$ aqueous solution) and the other one is not (alkanethiolates in the aqueous alkaline solution). The solvation energies [3-49, 3-50, 3-51] of the two compounds differ greatly. This is one energy barrier, which the

species in the bulk solution must overcome to adsorb onto the surface. For ethanethiol in pH neutral aqueous solution, it is around –5.5 kJ mol^{-1} [3-49, 3-50]. For ethanethiolate, since it is deprotonated, the solvation energy in an alkaline aqueous solution is between –293 to –335 kJ mol^{-1} [3-51]. Another important factor is the activation energy for the dissociation of the S-H bond of alkanethiol. This is not the case for the alkanethiolate, since it is already deprotonated. The breaking of the S-H bond is probably the energy barrier for the oxidative deposition of alkanethiol.

Based on these results and the discussion presented above, we suggest the following mechanisms for the oxidative deposition of the alkanethiolate (Figure 3-21) and alkanethiol (Figure 3-22) on gold from aqueous solution.

The mechanism of oxidative deposition of alkanethiolate from an aqueous alkaline solution is shown in Figure 3-21. The activation energy in the first step of this process comes from the desolvation of the thiolate. When we apply a small overpotential, the Fermi-level of the gold electrode decreases. Therefore the number of the alkanethiolates that diffuse to the surface is small and a small mass change is measured. This is compatible with the relatively slow rate of nuclei generation. When a large (more positive) overpotential is applied, more desolvated alkanethiolates diffuse to the surface and become adsorbed. This agrees with the mass increasing with the potential becoming more positive. This corresponds, in the nucleation and growth model, to the creation of a large number of nucleation centers when a large overpotential is applied. This also agrees with the observed diffusion-limited rate observed for the most positive deposition

potentials. We note that the transfer coefficient of 0.5 calculated from the EQCM data is compatible with desolvation being the rate-limiting step in the oxidative deposition of butanethiolate.

The mechanism of oxidative deposition of alkanethiols in 0.1 M $KClO_4$ aqueous solution is shown in Figure 3-22. Instead of the solvation energy, the energy of the dissociation of the S-H bond is the largest energy barrier in the first step of the mechanism. The barrier of the desolvation still exists, but it is relatively small. Therefore, alkanethiols should adsorb easily onto the surface once an overpotential is applied. This agrees with the EQCM results, which show a large mass change (around 80% to 90% of the total mass change) in the first few seconds of deposition.

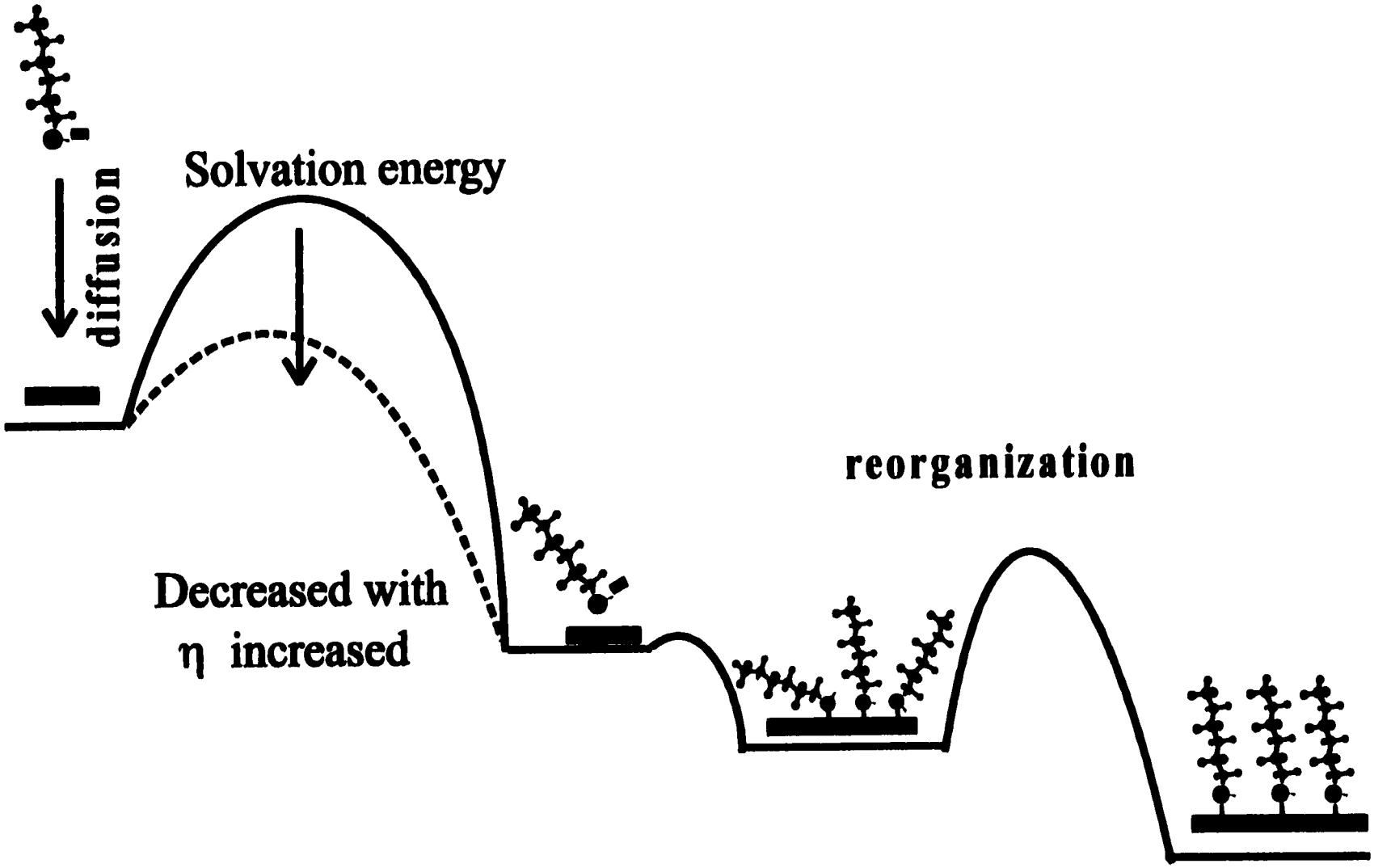

Figure 3-21: Mechanism of the oxidative deposition of alkanethiolate on gold from aqueous alkaline solution.

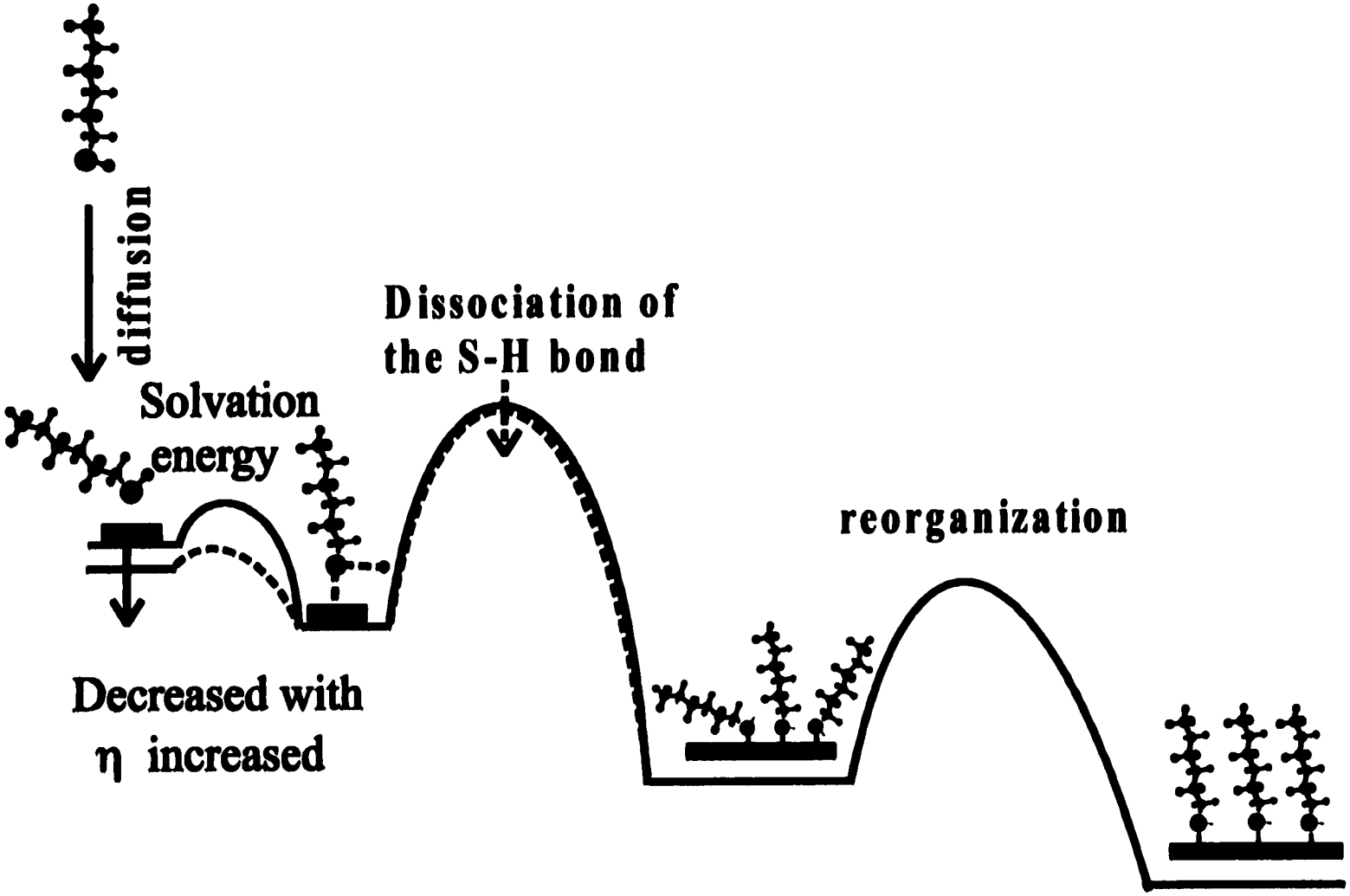

Figure 3-22: Mechanism of the oxidative deposition of alkanethiol on gold in the aqueous pH-neutral solution.

It is surprising that the oxidative deposition of butanethiol is faster than that of the butanethiolate in the first few seconds, since the concentration of butanethiol in 0.1 M $KClO_4$ is only 3 x 10^{-4} M (saturated solution). This is almost 10 times smaller than in the KOH. The low solubility of the butanethiol in the 0.1 M $KClO_4$ aqueous solution could cause the butanethiol to aggregate and stay in the vicinity of the surface. The existence of alkanethiol aggregates remaining at the surface was shown by electrochemical methods [3-40, 3-41], in-situ FTIR [3-52, 3-53] and in-situ STM [3-54] measurements. This phenomenon is also found in our EQCM measurements. Figure 3-23 is a plot of the mass change in the reductive desorption of butanethiol in the 0.1 M $KClO_4$ solution at different scan rates. We noticed that the mass change decreased with increasing scan rate. For high scan rates, the time between the butanethiol reductive desorption and its oxidative redeposition is short. So most of the butanethiols stay close to the electrode surface instead of diffusing to the bulk solution. EQCM only detects molecules leaving the surface. Therefore, the decrease in the mass change is due to the butanethiol aggregates that stay on the surface.

After adsorption of the alkanethiols, the dissociation of the S-H bond takes place. This process is not expected to display a strong dependence on the applied electric field. The small transfer coefficient observed in the $KClO_4$ solution is compatible with a surface process (i.e. the breaking of the S-H bond) being the rate-limiting step. The slower step is assigned to the adsorption at domain boundaries. An EQCM study done by Frubose and Doblhofer [3-19] showed that the deposition of alkanethiol from a pH-neutral ethanolic solution does not depend on the potential. This result supports our mechanism.

The interactions between the solvent (ethanol) and the alkylthiol are not very large. Hence, the breaking of the S-H bond should be the rate-limiting step under these conditions and the rate of deposition is potential independent.

In summary, the rate of oxidative adsorption of butanethiol on gold is a two-step process that is weakly dependent on the deposition potential. We suggest that the weak effect of the electric field is due to the fact that the rate-limiting step in the adsorption of butanethiol is the surface dissociation of the S-H bond. The mechanism of oxidative adsorption of butanethiol contrasts with the one of butanethiolate where desolvation was found to be the rate-limiting step. Finally, control of the deposition rate with an applied potential is difficult for the thiol but is easier in the case of the thiolate.

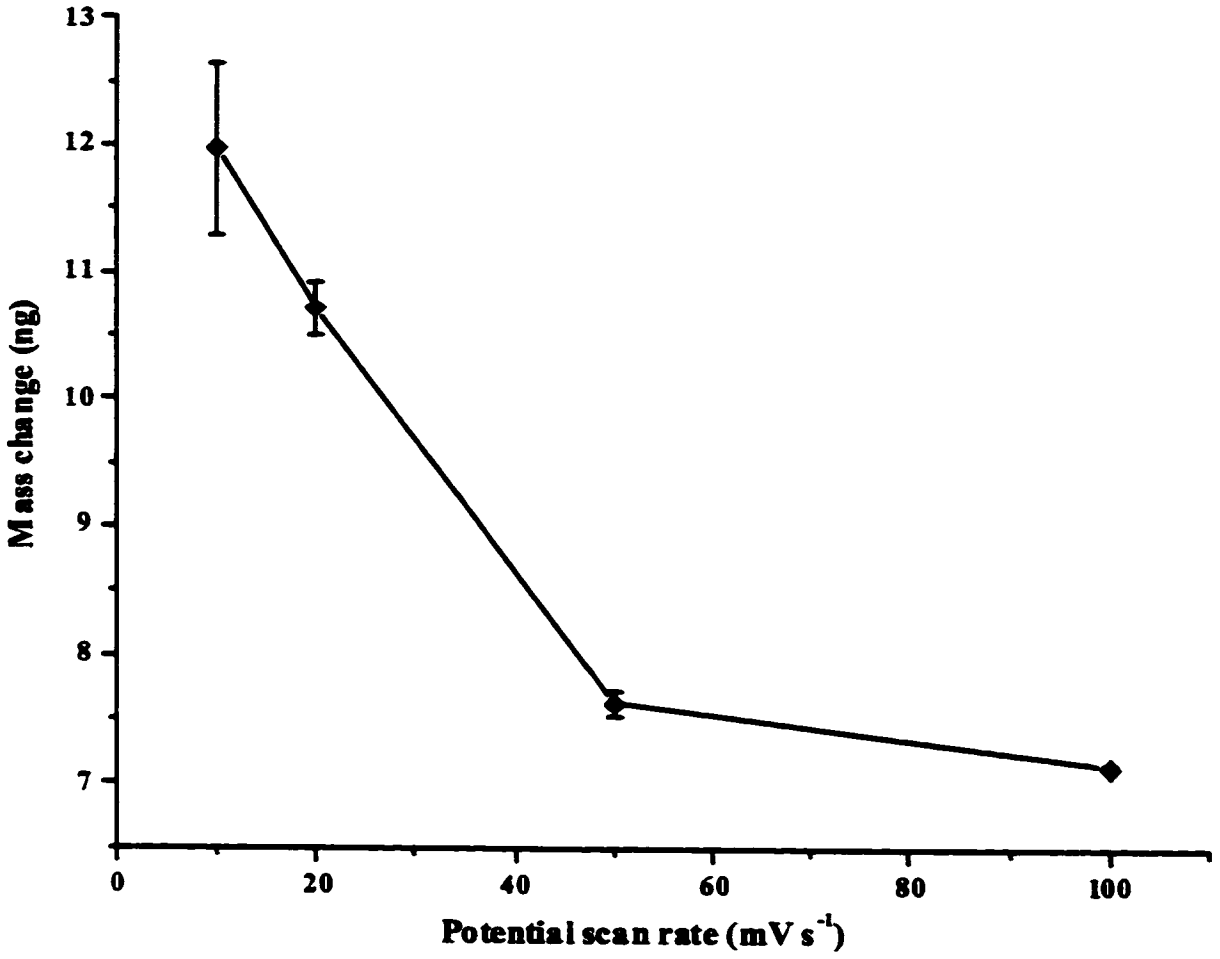

Figure 3-23: Plot of the mass change for the reductive desorption of butanethiol in 0.1 M $KClO_4$ at different potential scan rates.

References:

[3-1]: Bain, C.D; Troughton, E. B; Tao, Y.-T; Evall, J; Whitesides, G. M; Nuzzo, R. G *J. Am. Chem. Soc.* **1989**, 111, 321.

[3-2]: Hannoch, R. ; Rubinstein, I. *J. Am. Chem. Soc.* **1998**, 120, 13444.

[3-3]: Bensebaa, F.; Voicu, R.; Huron, L.; Ellis, T.H. *Langmuir* **1997**, 13, 5335.

[3-4]: Debono, R.F.; Loucks, G.D.; Manna, D.D.; Krull, U.L. *Can. J. Chem.* **1996**, 74, 677.

[3-5]: Peterlinz, K.A.; Georgiadis, R. *Langmuir* **1996**, 12, 4731.

[3-6]: Dannenberger, O.; Buck, M.; Grunze, M. *J. Phys. Chem. B* **1999**, 103, 2202.

[3-7]: Xu, S.; Laibinis, P.E.; Liu, G-Y. *J. Am. Chem. Soc.* **1998**, 120, 9356.

[3-8]: Xu, S.; Cruchon-Dupeyret, S.J.N.; Garno, J.C.; Liu, G-Y.; Jennings, G.K.; Yong, T-H.; Laibinis, P.E. *J. Chem. Phys.* **1998**, 108(12), 5002.

[3-9] : Hu, K.; Bard, A.J. *Langmuir* **1998**, 14, 4790.

[3-10]: Forouzan, F.; Bard, A.J.; Mirkin, M.V. *Israel Journal of Chemistry* **1997**, 37, 155.

[3-11]: Bandyopadhyay, K.; Vijayamohanan, K.; Shekhawat, G. S.; Gupta, V. *J. Electroanal. Chem.* **1998**, 447, 11.

[3-12]: Subramanian, R.; Lakshminarayanan, V. *Electrochimica Acta* **2000**, 45, 4501.

[3-13]: Yang, D-F.; Morin, M. *J. Electroanal. Chem.* **1997**, 429, 1.

[3-14]: Yang, D-F.; Morin, M. *J. Electroanal.Chem.* **1998**, 441, 173.

[3-15]: Ishida, T.; Nishida, N.; Tsuneda, S.; Hara, M.; Sasabe, H.; Knoll, W. *Jpn. J. Appl. Phys.* **1996**, 35(pt.2, No.12B), L1710.

[3-16]: Shimazu, K.; Yagi, I.; Sato, Y.; Uosaki, K. *Langmuir* **1992**, 8, 1385.

[3-17]: Kawaguchi, T.; Yasuda, H.; Shimazu, K.; Porter, M. D. *Langmuir* **2000**, 16, 9830.

[3-18]: Schneider, T.W.; Buttry, D.A. *J. Am. Chem. Soc.* **1993**, 115, 12391.

[3-19]: Frubose, C.; Doblhofer, K. *J. Chem. Soc. Farad. Trans.* **1995**, 91(13), 1949.

[3-20]: Karpovich, D.S.; Blanchard, G.J. *Langmuir* **1994**, 10, 3315.

[3-21]: Schessler, H.M.; Karpovich, D.S.; Blanchard, G.J. *J. Am. Chem. Soc.* **1996**, 118, 9645.

[3-22]: Karpovich, D.S.; Schessler, H.M.; Blanchard, G.J. *Thin Films* **1998**, 24, 43.

[3-23]: Pan, W.; Durning, C.J.; Turro, N.J. *Langmuir* **1996**, 12, 4469.

[3-24]: Kim, Y.-T.; McCarley, R. L.; Bard, A. J. *Langmuir* **1993**, 9, 1941.

[3-25]: Kunitake, M.; Narikiyo, Y.; Manabe, O.; Nakashima. N. *J. Materials Sci.* **1995**, 30, 2338.

[3-26]: Kim, H.J.; Kwak, S.; Kim, Y.S.; Seo, B.I.; Kim, E.R.; Lee, H. *Thin Solid Films* **1998**, 327-329, 191.

[3-27]: Thomas, R.C.; Sun, L.; Crooks, R.M. *Langmuir* **1991**, 7, 620.

[3-28]: Sun, L.; Thomas, R.C.; Crooks, R.M. *J. Am. Chem. Soc.* **1991**, 113, 8550.

[3-29]: Rocha, T.A.P.; Gomes, M.T.S.R.; Duarte, A.C.; Oliveira, J.A.B.P. *Anal. Commun.* **1998**, 35, 415.

[3-30]: Burgess, J.D.; Howkridge, F.M. *Langmuir* **1997**, 13, 3781.

[3-31]: Schreiber, F.; Eberhardt, A.; Leung, T.Y.B.; Schwartz, P.; Wetterer, S.M.; Lavrich, D.J.; Berman, L.; Fenter, P.; Eisenberger, P.; Scoles, G. *Phys. Review B* **1998**, 57, 12476.

[3-32]: Shon, Y-S.; Lee, T.R. *J. Phys. Chem. B* **2000**, 104, 8182.

[3-33]: Poirier, G.E.; Pylant, E.D. *Science* **1996**, 272, 1145.

[3-34]: Ma, F.; Lennox, R. B. *Langmuir* **2000**, 16, 6188.

[3-35]: Qu, D.; Morin, M. *J. Electroanal. Chem.* In press.

[3-36]: McDermott, C.A.; McDermott, M.T.; Green, J.B.; Porter, M.D. *J. Phys. Chem.* **1995**, 99, 13257.

[3-37]: Strong, L.; Whitesides, G.M. *Langmuir* **1988**, 4, 546.

[3-38]: Widrig, C.A.; Chung, C.; Porter, M.D. *J. Electroanal. Chem.* **1991**, 310, 335.

[3-39]: Sauerbrey, G. *Z. Phys.* **1959**, 155, 206.

[3-40]: Yang, D.-F.; Wilde, C.P.; Morin, M. *Langmuir* **1997**, 13, 243.

[3-41]: Yang, D.-F.; Wilde, C.P.; Morin, M. *Langmuir* **1996**, 12, 6570.

[3-42]: Walczak, M.M.; Deinhammer, R.S.; Lamp, B.D.; Chung, C.; Porter, M.D. *Langmuir* **1991**, 7, 2687.

[3-43]: Tsionsky, V.; Daikhin, L.; Zilberman, G.; Gileadi, E. *Faraday Discuss.* **1997**, 107, 337.

[3-44]: Daikhin, L.; Gileadi, E.; Tsionsky, V.; Urbakh, M.; Zilberman, G. *Electrochimica Acta* **2000**, 45, 3615.

[3-45]: Harrison J. A.; Thirsk H. R. in A.J.Bard(Ed.) *Electroanalytical Chemistry*, Vol.5 **1971**, 67.

[3-46]: S. Xu ; P.E. Laibinis ; G-Y. Liu *J. Am. Chem. Soc.* **1998**, 120, 9356.

[3-47] : Bare, S.; Buess-Herman, C. *Colloids and Surfaces A* **1998**, 134, 181.

[3-48] : Buess-Herman, C.; Bare, S; Poelman, M.; Van krieken, M. *Interfacial Electrochemistry- Theory, Experiment and Applications* P599, A Wieckowski (Eds) Marcel Dekker, New York, Basel **1999.**

[3-49]: Cramer, C.J.; Truhlar, D.G. *Journal of Computational Chemistry* **1992**, 13, 1089.

[3-50]: Cabani, S.; Gianni, P.; Mollica, V.; Lepori, L. *Journal of Solution Chemistry* **1981**, 10, 563.

[3-51]: Pearson, R.G. *J. Am. Chem. Soc.* **1986**, 108, 6109.

[3-52]: Yang, D-F; Al-Maznai, H.; Morin, M. *J. Phys. Chem. B* **1997**, 101, 1158.

[3-53]: Byloos, M.; Al-Maznai, H.; Morin, M. *J. Phys. Chem. B* **1999**, 103, 6554.

[3-54]: Hobara, D.; Miyake, K.; Imabayashi, S.; Niki, K.; Kakiuchi, T. *Langmuir* **1998**, 14, 3590.

Chapter 4

The effects of temperature and concentration on the oxidative adsorption of alkanethiols and alkanethiolates on gold

4.1. Introduction

In the previous section, we studied the oxidative deposition of alkanethiolates and alkanethiols on gold. The deposition were described by a two-step process: A fast, potential dependent step followed by a slow, potential independent step. The fast step occurs by a nucleation and growth mechanism and the slow step occurs via a slower potential independent Langmuir process. We also presented the RSH and RS^- adsorption mechanisms. The dissociation of the S-H bond and the solvation energy were suggested to be the main energy barriers in the first step of the oxidative deposition of the alkanethiols and alkanethiolates on gold, respectively. These results were obtained at room temperature and at one RSH or RS^- concentration. In order to better understand this process, we carried out kinetic measurements at different temperatures and concentrations.

4.2. Oxidative deposition of alkanethiols on gold at different temperatures

Temperature affects the kinetics of chemical reactions. Measurements of the rates of chemical reactions at different temperatures yield the activation energy of a reaction.

We oxidatively deposited alkanethiols and alkanethiolates on gold from alkaline and neutral solutions at different temperatures. The methodology described in chapter 3 was used to follow this process.

4.2.1. The oxidative deposition of alkanethiol.

Figure 4-1 shows the EQCM signals and cyclic voltammograms of 1 mM butanethiol in 0.1 M $KClO_4$ at different temperatures. The EQCM signals are similar to those measured at room temperature. On the voltammograms, we see that on the initial negative going potential scan, the mass begins to increase at –0.80 V when the reductive current increases. The mass continuously increases until the potential reaches –0.95 V, even though there are two reductive current peaks between –0.80 V and –0.95 V. These two current peaks may due to the different crystallographic domains on the gold quartz crystal surface [4-1, 4-2]. On the following positive going potential scan, the peak potential of the butanethiol oxidative deposition moves to more negative potentials at higher temperatures. The oxidative current peak became broader with decreasing temperature. The EQCM shows a corresponding slower deposition at decreasing temperature.

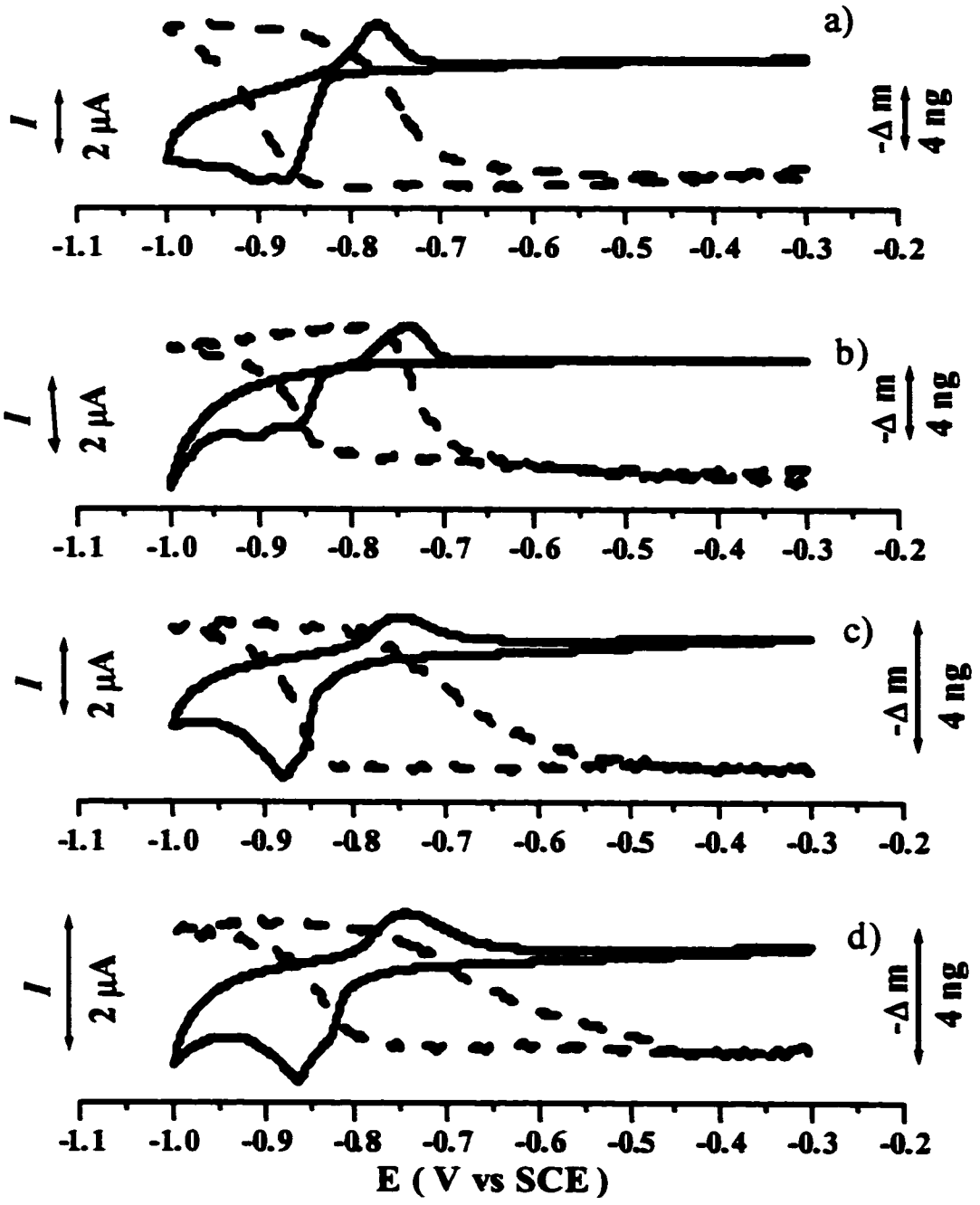

Figure 4-1: Cyclic voltammograms and mass change for the oxidative adsorption/reductive desorption of butanethiols on gold recorded in 0.1 M $KClO_4$ at (a) 35^0C, (b) 25^0C, (c) 15^0C, (d) 5^0C. Potential scan rate: 10 mV s^{-1}.

The mass change and the integrated charge (obtained from the oxidative charge corrected for the capacitive current from cyclic voltammograms in the figure 4-1) of the oxidative deposition of butanethiols in 0.1 M $KClO_4$ for different temperatures are shown in Table 4-1. We see that, the integrated charge is constant. The mass changes decrease when the temperature decreases.

Table 4-1: Mass change and integrated charge of the oxidative deposition of butanethiol in 0.1 M $KClO_4$ at different temperatures.

Temperature (^0C)	Oxidative deposited butanethiol in 0.1 M $KClO_4$ solution	
	Mass change (ng)	Charge (μC)
5	4.0 ± 2%	8.7 ± 10%
15	4.2 ± 8%	7.5 ± 6%
25	7.6 ± 3%	8.4 ± 8%
35	8.3 ± 5%	9.8 ± 2%

Figure 4-2 shows the moles of butanethiol deposited and the moles of electron transferred at different temperature. At 35 ^0C the moles of butanethiol deposited (obtained from the mass change) and the mole of electron transferred (obtained from the integrated charge) are equal. The mole of electron transferred is 8 X 10^{-10} mol cm^{-2} (around 70% of the full monolayer) at 5°C. There is a large difference between the charge and mass change at low temperature. The mass change is smaller. This deviation may come from the quartz crystal itself and the electrolyte solution. f_0, the resonant frequency of the uncoated quartz crystal, changes with temperature. So the

proportionality factor in the Saubery equation will be affected by the temperature. In our case, the Δm between the 5 ^{0}C and 35 ^{0}C changed by almost a factor of 2. (4.0 ng at 5^{0}C vs. 8.3 ng at 35^{0}C) The variation of f_0 with temperature cannot cause this big change. Between 5^{0}C and 35^{0}C, f_0 does not change significantly (see chapter 2 for details). Another possibility is a visco-elastic change, but in this temperature range, the viscosity of the aqueous solution does not change very much. So we can also rule out this possibility. We suggest that this deviation is related to the solubility of the butanethiol in aqueous solution and the time elapsed between the reductive desorption and oxidative deposition in the cyclic voltammetry. At low temperature, the solubility of butanethiol in aqueous solutions is low. In the cyclic voltammogram, the time between the butanethiol reductive desorption and oxidative redeposition is about 3 to 4 seconds. At low temperature and in a short time scale, most of the butanethiols remain close to the electrode surface. EQCM will only detect the molecules leaving the surface. The detected mass change will thus be smaller than the one estimated from the charge at low temperatures.

We minimize this effect in the kinetics studies, by holding the potential at –1.10 V for about 20 sec. This is long enough to let the butanethiols diffuse away from the surface prior to the deposition. We found that under these conditions, the total mass deposited is constant at different temperatures and almost equal to a full monolayer (see below).

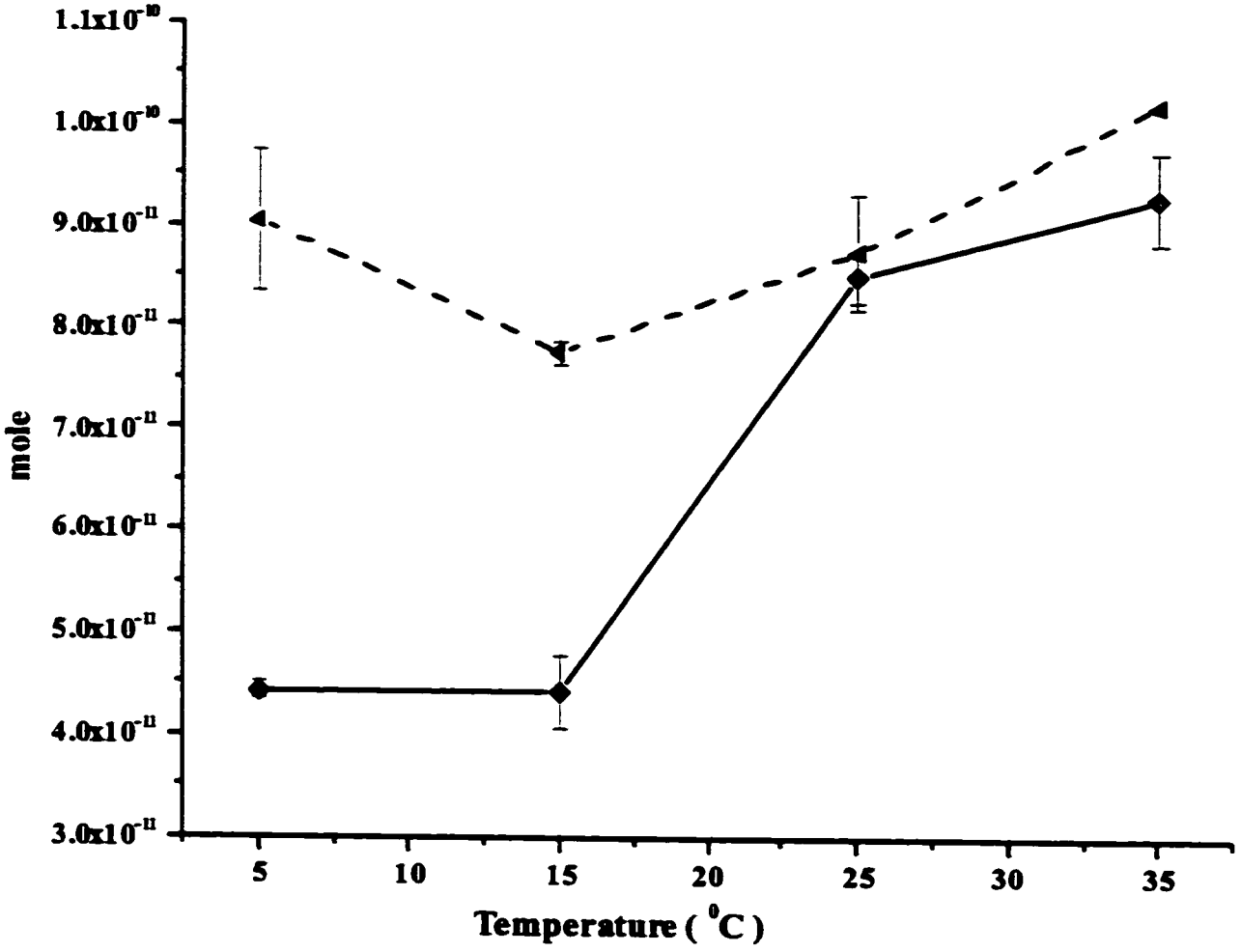

Figure 4-2: Mole of electron (calculated from 5 cyclic voltammograms such as in Figure 4-1, dashed line) and the mole of butanethiol deposited (calculated from 5 EQCM signals such as in Figure 4-1, solid line) at different temperatures.

The oxidative depositions of butanethiol on gold from a 0.1 M $KClO_4$ at different temperatures are shown in Figure 4-3 and Figure 4-4. Figure 4-3 shows the EQCM response to a potential step at each temperature. For each temperature, the potential is stepped from –1.10 V to the potentials shown on Figure 4.3. We see that the adsorption profile of butanethiol is almost independent of the final potential for all temperatures. This agrees with the results obtained at room temperature.

Figure 4-4 shows the EQCM responses at different temperatures for a potential step to the oxidative peak potential. In this case the adsorption of butanethiol is almost independent of the temperature. This temperature independent adsorption agrees with the mechanism we suggested in the previous section. In that mechanism, the main barrier to chemisorption in the pH-neutral solution is the surface dissociation of S-H bond. This process is not strongly dependent on the temperature.

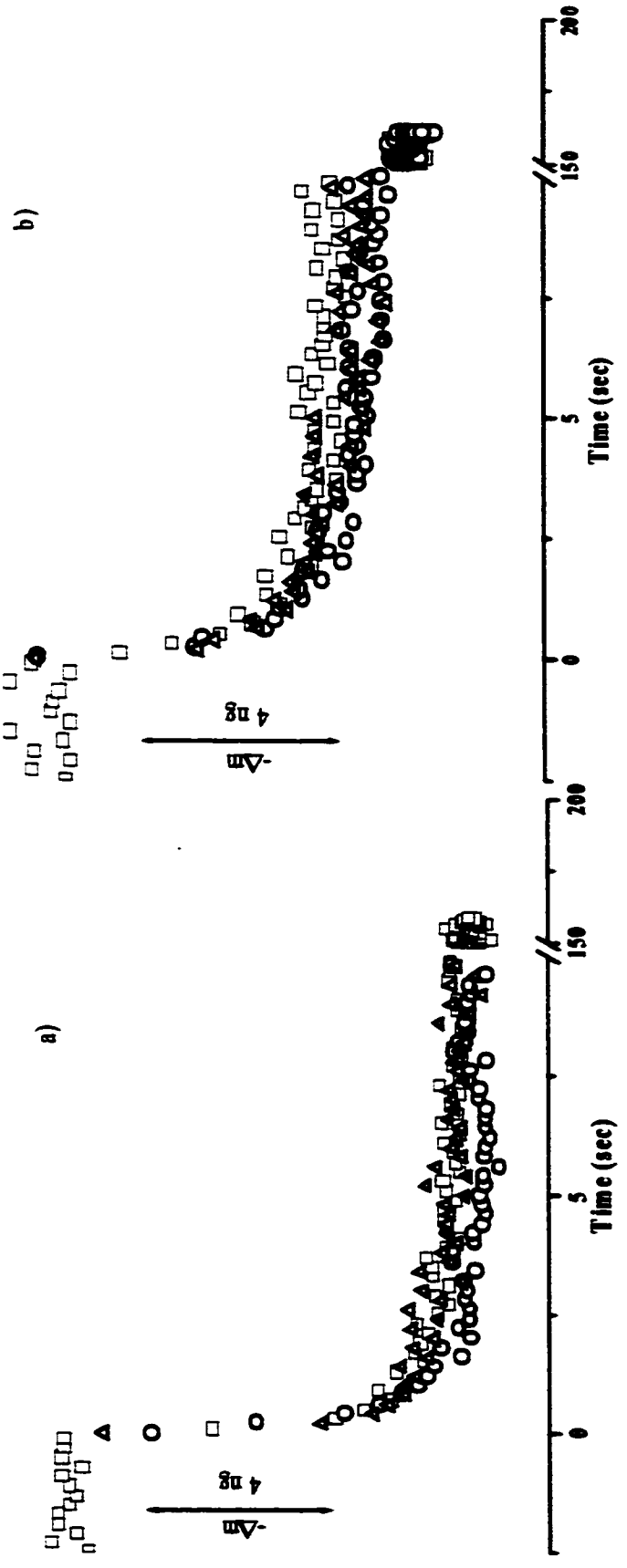
a)
b)
-Δm
4 mg
Time (sec)
0
5
150
200

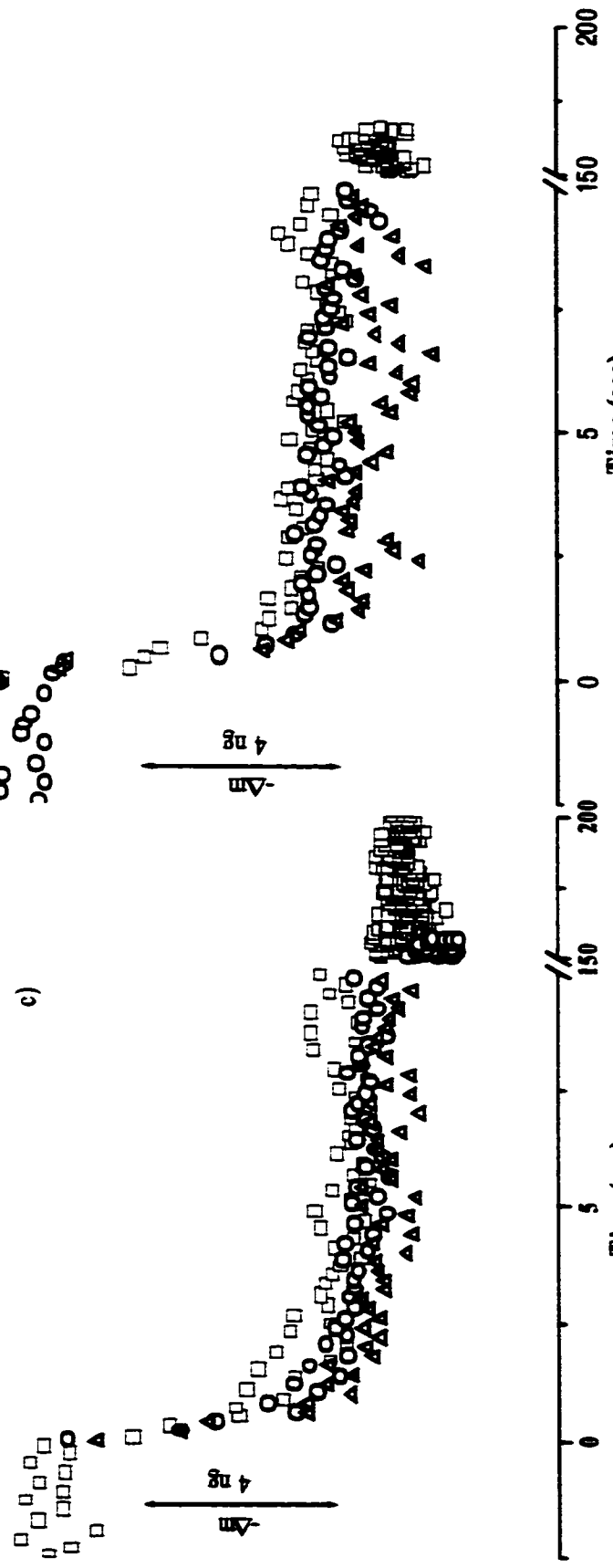

Figure 4-3: Mass change for potential steps causing the oxidative deposition of butanethiol on gold in 0.1 M $KClO_4$ at (a) 5^0C, (b) 15^0C, (c) 25^0C, (d) 35^0C. The potential is stepped from –1.10 V to □: 0.04 V vs the Peak potential (Ep); O: Ep; Δ: -0.04 V vs Ep. For clarity only every 20^{th} data points are shown.

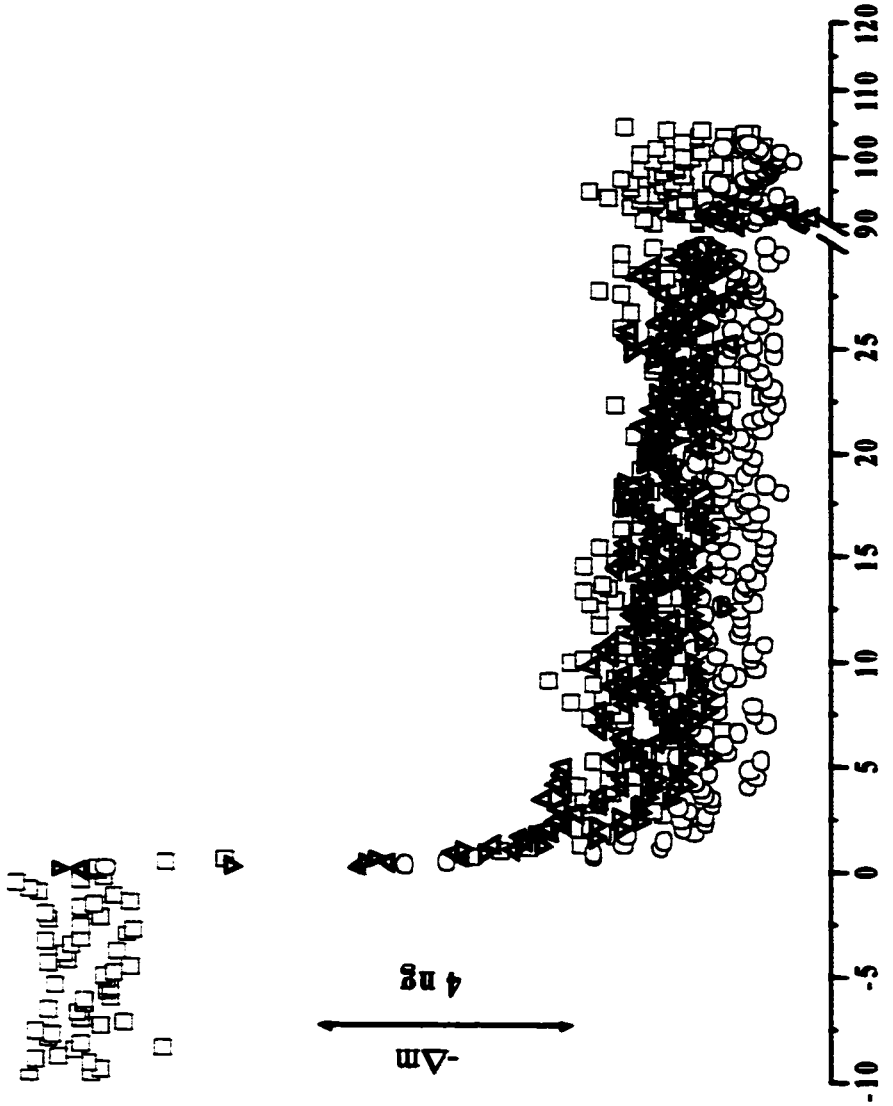

Figure 4-4: Mass change for potential steps causing the oxidative deposition of butanethiol on gold in 0.1 M $KClO_4$ at O: 5 ^{0}C , Δ: 15 ^{0}C , ∇: 25 ^{0}C , □: 35 ^{0}C. The potential is stepped from –1.10 V to the peak potential of the cyclic voltammograms at each temperature. For clarity only every 20th data points are shown.

The same model, used in the previous section, is used to analyze the electro-deposition of alkanethiols on gold at different temperatures. This model is a combination of a nucleation and growth process and a Langmuir process. The observed rate constants for these two steps are calculated from a fitting of the plot of mass change against time with the following bi-exponential equation:

$$m(t) = m_{max} A \exp(-k_1 t^2) + m_{max}(1-A) \exp(-k_2 t) \qquad (4\text{-}1)$$

The symbols have been described in Chapter 3. The rate constant of the first step, k_1, in 0.1 M $KClO_4$ at different deposition potentials and temperatures are shown in Table 4-2. The rate constant, k_1, increases slightly as the deposition potential becomes more positive. It is almost constant at different temperatures. The rate constant of the second step, k_2 is around 0.02 s^{-1} and is independent of the applied potential and temperature. These rates are similar to what we obtained at room temperature in a $KClO_4$ solution.

Table 4-2: The rate constant of first step, k_1, for the oxidative deposition of butanethiol in 0.1 M $KClO_4$ at different final potentials and temperatures.

Temperature	k_1 (0.2 V vs. Ep)	k_1 (0.04 V vs. Ep)	k_1 (Ep)	k_1 (-0.04 V vs. Ep)
5	3.7 ± 0.5	2.18 ± 0.04	1.24 ± 0.06	0.5 ± 0.1
15	2.85 ± 0.13	1.4 ± 0.1	1.51 ± 0.06	1.10 ± 0.03
25	3.71 ± 0.02	2.06 ± 0.07	1.48 ± 0.08	1.03 ± 0.02
35	9.67 ± 0.06	5.38 ± 0.04	3.36 ± 0.07	1.67 ± 0.03

- Ep is peak potential, k_1 (s^{-2}) see the text.

The activation energy of the first-step process was estimated using the Arrhenius equation. For a simple activated process, the relationship between the rate constant (k), the temperature (T) and the activation energy (E_a) can be described by the Arrhenius equation:

$$k_1 = A \exp(-E_a / RT) \qquad (4\text{-}2)$$

To use the Arrhenius equation, we must assume that the reaction mechanism does not change in the range of temperatures under study. The EQCM responses in the potential-step experiments are similar at all temperatures. On the short-time scale (shown in Figure 4-5), the first step processes are similar at all temperatures. The slope of ln k vs. 1/T (Arrhenius plot) allows the estimation of the activation energy.

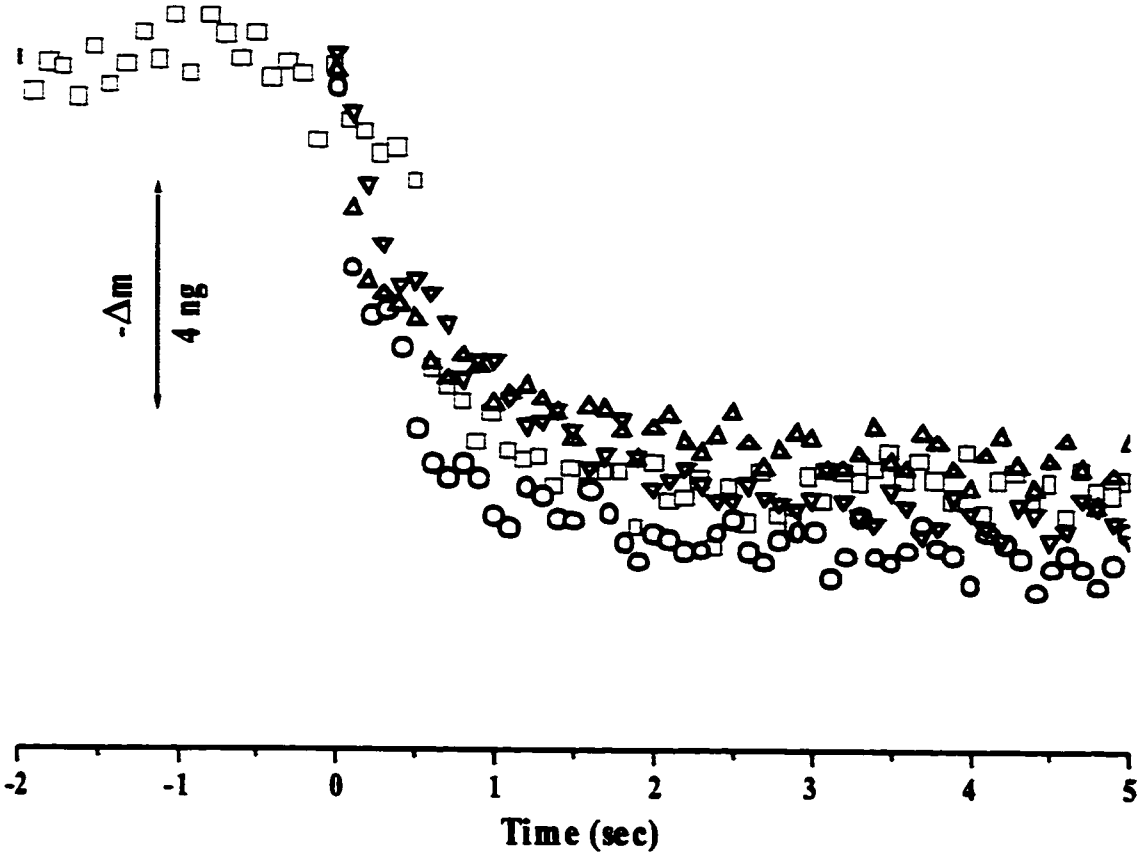

Figure 4-5: Mass change for potential steps causing the oxidative deposition of butanethiol on gold in 0.1 M $KClO_4$ for the first 5 sec of deposition at O: 5^0C , Δ: 15^0C , ∇: 25^0C , □: 35^0C. The potential is stepped from −1.10V to the peak potential of the cyclic voltammograms of each temperature. For clarity only every 20^{th} data point is shown.

Arrhenius plots for different deposition potentials in 0.1 M $KClO_4$ are shown in Figure 4-6. The activation energies at different deposition potentials are listed in Table 4-3. We note that in the small range of temperatures that we used, the activation energies for the adsorption of alkanethiols in 0.1 M $KClO_4$ are around 23 ± 10 kJ mol^{-1}, and are potential-independent. These results agree with previous studies [4-3 to 4-6]. D. S. Karpovich, H. M. Schessler and G. J. Blanchard [4-3, 4-4, 4-5], gave an activation energy for the adsorption of alkanethiols of 23 KJ mol^{-1} in an organic solvent. Another study [4-6] carried out under

UHV conditions, shows that the activation energy to chemisorption is 28.8 kJ mol^{-1} and is independent of the chain-length. These results give further support to the mechanism presented in chapter 3, which suggested that the main barrier to chemisorption is the S-H dissociation. If the solvation energy played an important role in this adsorption process, the activation energy would be different in different solvents and in UHV. Since the estimated activation energies are very close in aqueous solution, in organic solvent and under UHV, the rate-limiting step in the formation of a self-assembled monolayer from alkanethiols is likely to be the surface S-H dissociation.

Table 4-3: Activation energies for the oxidative adsorption of butanethiol at different deposition potentials.

	0.2 V vs. Ep	0.04 V vs. Ep	Ep	-0.04 V vs. Ep
Slope in Arrhenius Plot (K^{-1})	2.8±1	2.8±1	2.6±1	3.0±1
$E_{activation}$ (kJ mol^{-1})	23	23	22	25
Average $E_{activation}$ (kJ mol^{-1})	23 ± 40%			

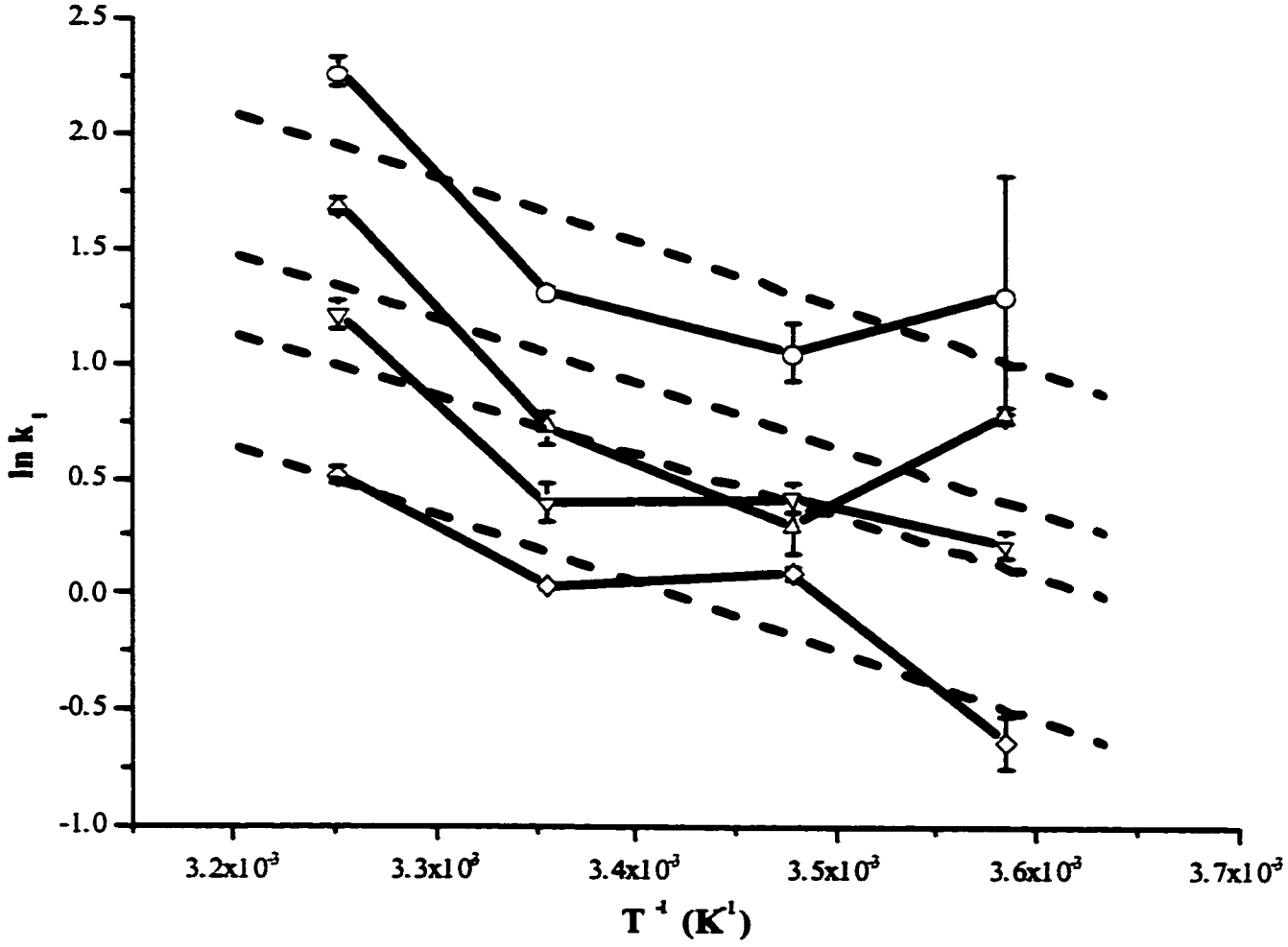

Figure 4-6: Arrhenius plots of the rate of oxidative deposition of butanethiol on gold in 0.1 M $KClO_4$ at different overpotential O: 0.2 V vs. Ep; Δ: 0.04 V vs. Ep; ∇: Ep; □: -0.04 V vs. Ep. Ep is the peak potential in the cyclic voltammogram recorded at each temperature. The dashed lines are linear fits.

4.2.2. The oxidative deposition of alkanethiolate on gold at different temperatures

The EQCM signals and cyclic voltammograms from octanethiolates in 0.1 M KOH at different temperatures are shown in Figure 4-7. The EQCM signals and cyclic voltammograms are all similar to those at room temperature (see Chapter 3). In these cyclic voltammograms, the reductive/oxidative current peak potentials are all at more negative potentials than those of butanethiol in 0.1 M $KClO_4$ (Figure 4-1). On the initial negative-going potential scan, the frequency is almost constant from –0.20 V to –1.02 V. It increases over the range of potentials corresponding to the reductive current peak. On the subsequent positive-going potential scan, the frequency decreases slowly up to -1.00V, which corresponds to the onset of the oxidative current peak. The frequency decreases sharply over the narrow potential range of the oxidative current peak. Then from –0.91 V to –0.20 V it has a constant value close to the initial one. The reductive/oxidative current peak potentials are relatively constant between 5 ^{0}C and 35 ^{0}C. In contrast to what was observed in the neutral solution, only one reductive current peak appeared in each cyclic voltammogram. However, narrow and symmetric oxidative current peaks were observed at different temperatures.

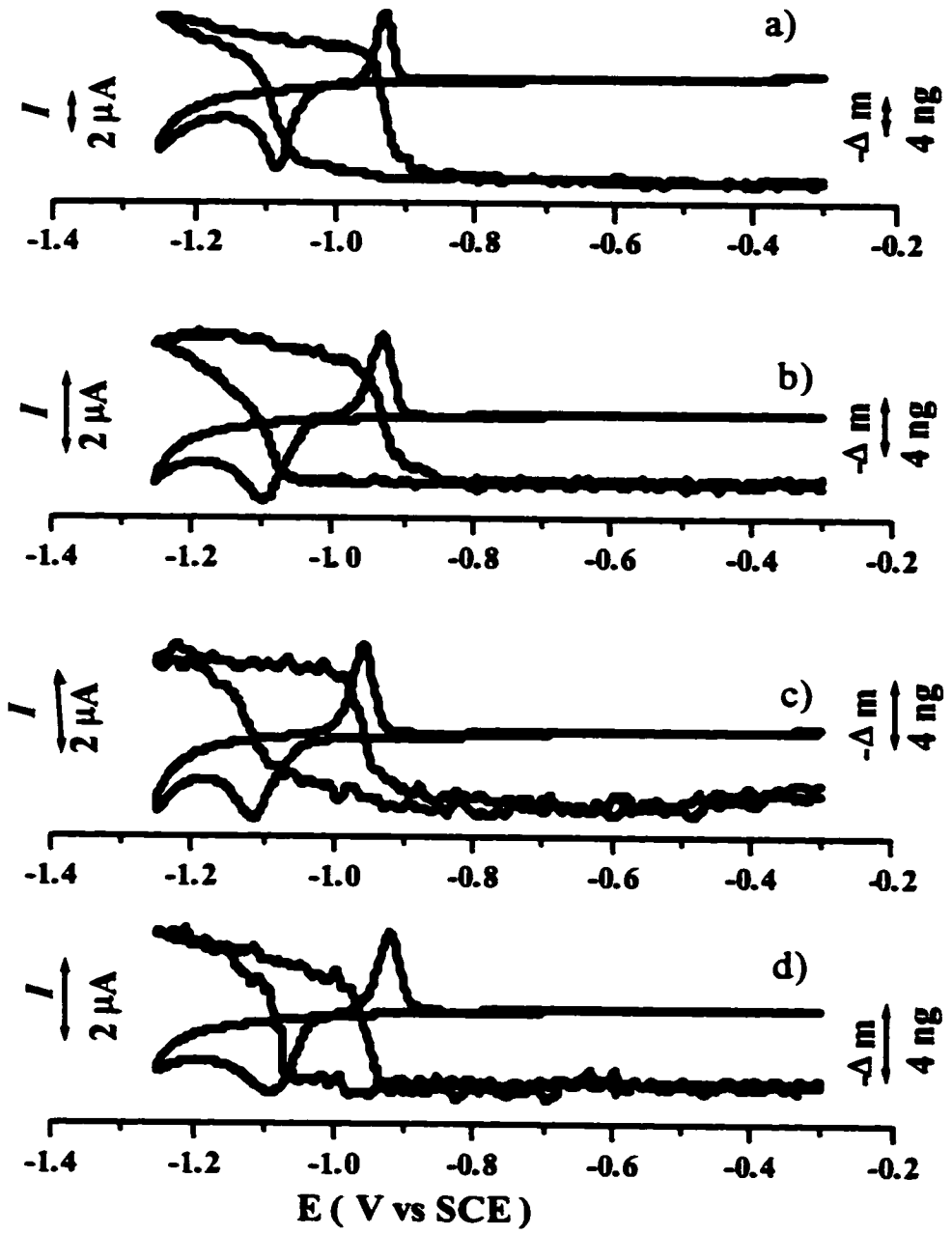

Figure 4-7: Cyclic voltammograms and mass change for the oxidative adsorption/reductive desorption of octanethiol on gold recorded in 0.1 M KOH at (a) 35^{0}C, (b) 25^{0}C, (c) 15^{0}C, (d) 5^{0}C. Potential scan rate: 10 mV s^{-1}.

In alkaline solution, the EQCM response also changes with temperature. At 5^0C (Figure 4-7d), the mass change takes place prior to the beginning of the oxidative current. The mass change (obtained from EQCM traces in Figure 4-7) and the integrated charge (obtained from the oxidative charge corrected for the capacitive current from cyclic voltammograms in Figure 4-7.) in 0.1 M KOH at different temperatures are shown in Figure 4-8 and Table 4-4. The integrated charge for octanethiolate remains constant at different temperatures. However, the mass changes decreased with temperature. Above 25^0C there is a good correspondence between mass change and integrated charge. Some of the reduced thiolates remain physisorbed on the surface below 25^0C, thus decreasing the EQCM signal.

Table 4-4: Mass changes and integrated charges for the oxidative deposition of octanethiolate on gold in 0.1 M KOH at different temperatures.

Temperature (^{0}C)	Oxidative deposited Octanethiolate in 0.1 M KOH solution	
	Mass change (ng)	Charge (μC)
5	6.1 ± 15%	7.1 ± 10%
15	9.7 ± 7%	8.0 ± 5%
25	10.3 ± 4%	8.0 ± 6%
35	13.5 ± 4%	8.4 ± 2%

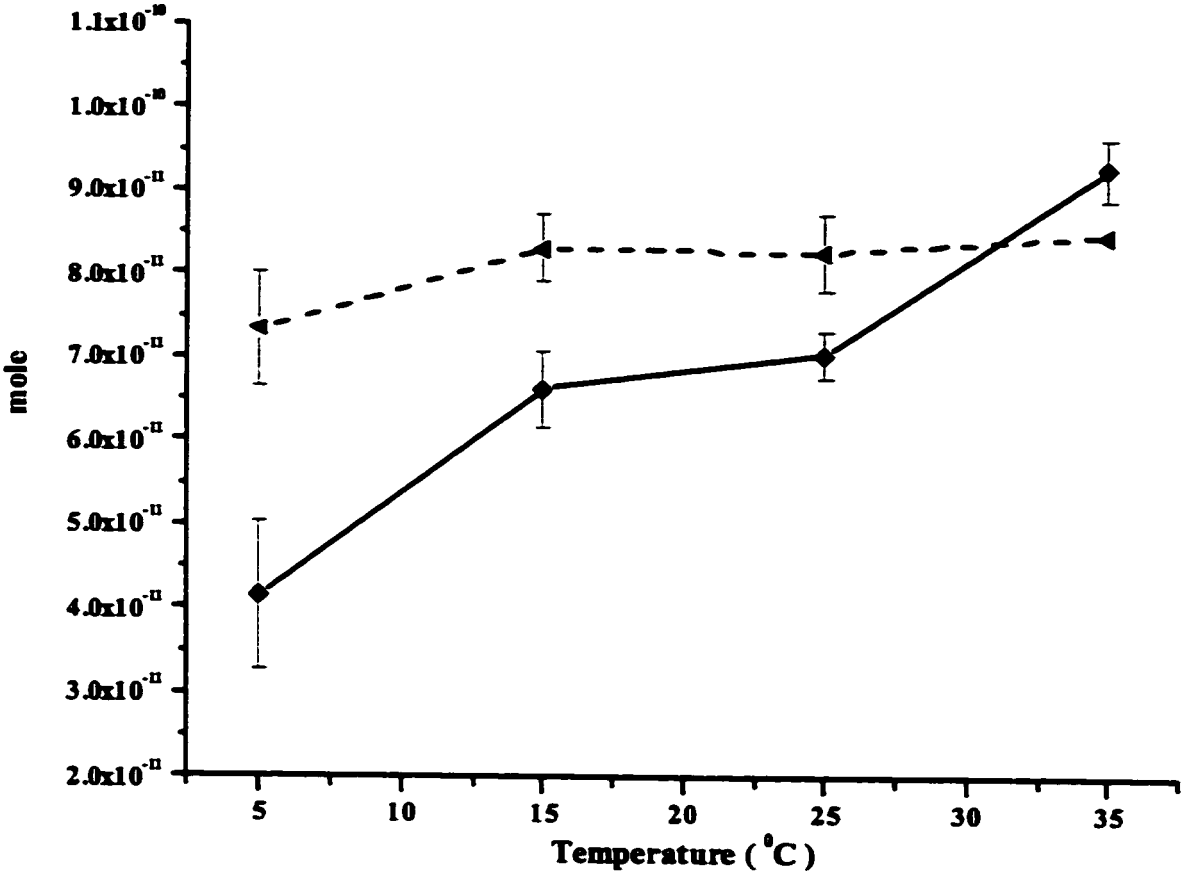

Figure 4-8: Mole of electron (calculated from 5 cyclic voltammograms such as those in Figure 4-7, dashed line) and the mole of octanethiol deposited (calculated from 5 EQCM measurements such as those in Figure 4-7, solid line) at different temperatures.

Typical Δm vs t curves for the oxidative deposition of octanethiolate on gold from aqueous alkaline solution at different temperatures are shown in Figure 4-9 and Figure 4-10. Figure 4-9 shows Δm's for different deposition potentials at various temperatures. The oxidative deposition of octanethiolates shows a slight dependence on the deposition potential at all temperatures. This agrees with the results we obtained at the room temperature.

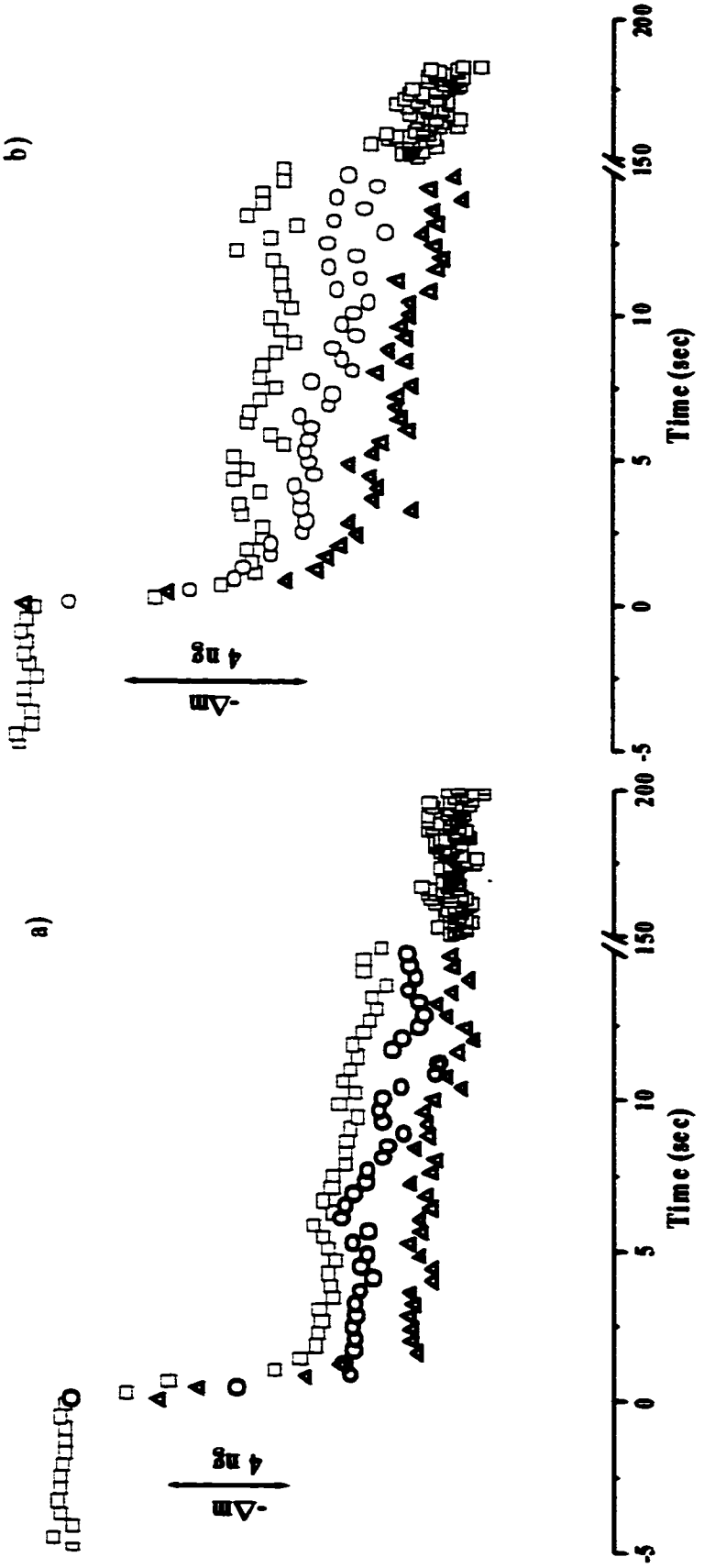
a)
b)
-ΔB
4 mg
Time (sec)
-5
0
5
10
150
200

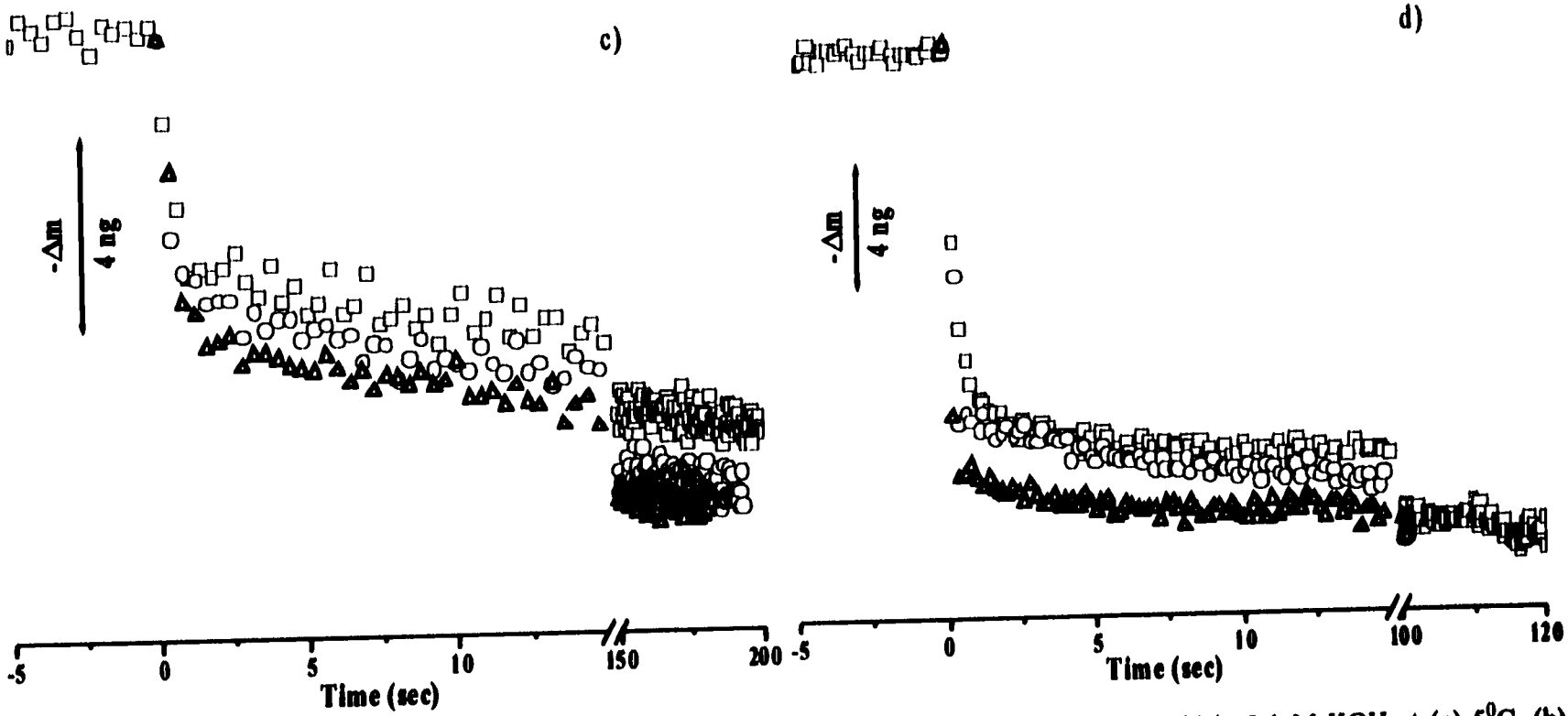

Figure 4-9: Mass change for potential steps causing the oxidative deposition of octanethiol on gold in 0.1 M KOH at (a) 5^0C, (b) 15^0C, (c) 25^0C, (d) 35^0C. The potential is stepped from –1.10 V to □: 0.04 V vs Peak potential (Ep); O: Ep; Δ: -0.04 V vs Ep. For clarity only every 20^{th} data point is shown.

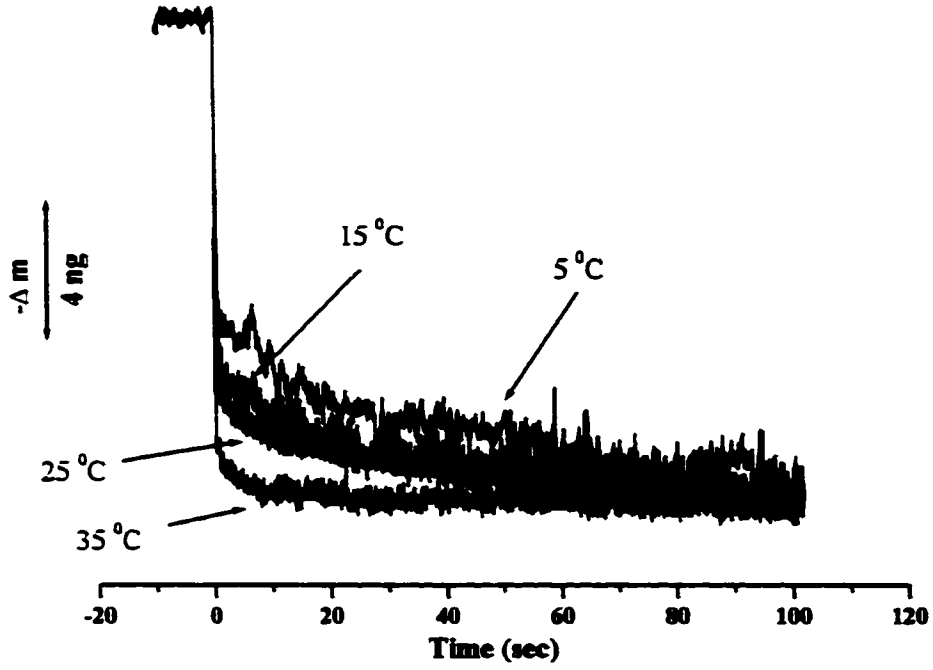

Figure 4-10: Mass change for potential steps causing the oxidative deposition of octanethiolate on gold in 0.1 M KOH at the temperatures shown on the figure. The potential is stepped from –1.10 V to –0.95 V at each temperature. For clarity only every 20th data point is shown.

Figure 4-10 shows Δm's for different temperatures but for one deposition potential (-0.95 V). The oxidative deposition of octanethiolates is slower at lower temperature. When the temperature increased, the first step become faster. At 35^{0}C, the second step almost disappears. This indicates that the adsorption process undergoes significant changes in the range of temperatures studied.

We suggest that this temperature dependent adsorption process is due to a reorganization of thiolate aggregates in the solution and at the surface. Insoluble molecules are known to form aggregates in the solution that can be physisorbed at surfaces. At higher temperature, such as 35^0C, the thiolate aggregates are in disordered state and of small size. They can thus be easily reoriented and thiolates can chemisorb to the gold surface. Also surface diffusion facilitates the self-assembly process at higher temperatures. When the temperature becomes low enough (i. e. 5^0C), the aggregates are more stable. We also expect a larger fraction of the thiolates to remain physisorbed after their reduction, thereby leading to a smaller mass change. Thus, the time required to destroy the aggregates so that the thiolates can chemisorb onto the surface is longer, and the rate of adsorption becomes slower at lower temperature. This temperature dependence of the electrospreading (i.e. dissolution) of thiolate aggregates was observed in a previous study [4-7]. This phenomenon could explain why the mass change occurs before the oxidative current in Figure 4-7d. There would be a stable physisorbed monolayer formed prior to the oxidative process. Finally, since the oxidative adsorption changes with temperature, we cannot use the Arrhenius plot to obtain the activation energy in alkaline solutions.

In this section, the temperature effect on the oxidative deposition of alkanethiols and alkanethiolates from aqueous solution was studied. The oxidative deposition of alkanethiols on gold is weakly temperature dependent. The activation energy of this process is found to be 23 kJ mol^{-1}. The oxidative deposition of alkanethiolates on gold is more temperature dependent. As temperature increases, the first step in the adsorption

process becomes faster and the second step (i.e. reorganization) becomes easier. These results agree with the mechanism suggested in Chapter 3.

4.3. The oxidative adsorption of alkanethiolate on gold at different concentrations

Monolayers of different coverages and structures are obtained after incubation in thiol solutions of different concentrations [4-9, 4-11 to 4-15]. In this section, we measured the rate of oxidative deposition for various concentrations of alkanethiolates. The solubility of long alkane-chain thiols in aqueous neutral solution is low, thus the range of concentrations is too limited. Therefore, only butanethiolates solutions were used in this study. The preparation of the solutions was described in chapter 2. Four different concentrations were used: $4x10^{-3}$ M, $7x10^{-4}$ M, $7x10^{-5}$ M and $7x10^{-6}$ M.

Figure 4-11 shows four cyclic voltammograms for the oxidative deposition/ reductive desorption of butanethiolates on the gold surface at four different concentrations. In two cyclic voltammograms, corresponding to $4x10^{-3}$ M and $7x10^{-4}$ M butanethiol in 0.1 M KOH, narrow and symmetric oxidative and reductive current peaks are observed. They are similar to the cyclic voltammogram recorded in 1 mM butanethio / 0.1 M KOH solution (Figure 3-1b in Chapter 3). The reductive peak potentials are –0.96 V and –0.95 V for $4x10^{-3}$ M and $7x10^{-4}$ M, respectively. The oxidative peak potentials are –0.86 V (for $4x10^{-3}$ M) and –0.88 V (for $7x10^{-4}$ M).

The cyclic voltammograms corresponding to the $7x10^{-5}$ M and $7x10^{-6}$ M butanethiolate solutions are shown in Figure 4-11. Broader and asymmetric oxidative and reductive current peaks are observed. These broad peaks are similar to those in the cyclic voltammograms of butanethiol recorded in 0.1 M $KClO_4$ solution (Figure 3-13). The cause of the peak current broadening at low concentrations is however different (see below). The reductive peak potentials are –0.82 V and –0.79 V for $7x10^{-5}$ M and $7x10^{-6}$ M, respectively. The oxidative peak potentials are –0.72 V (for $7x10^{-5}$ M) and –0.73 V (for $7x10^{-6}$ M). These peak potentials are more positive than those recorded in solutions with higher concentrations of thiolates.

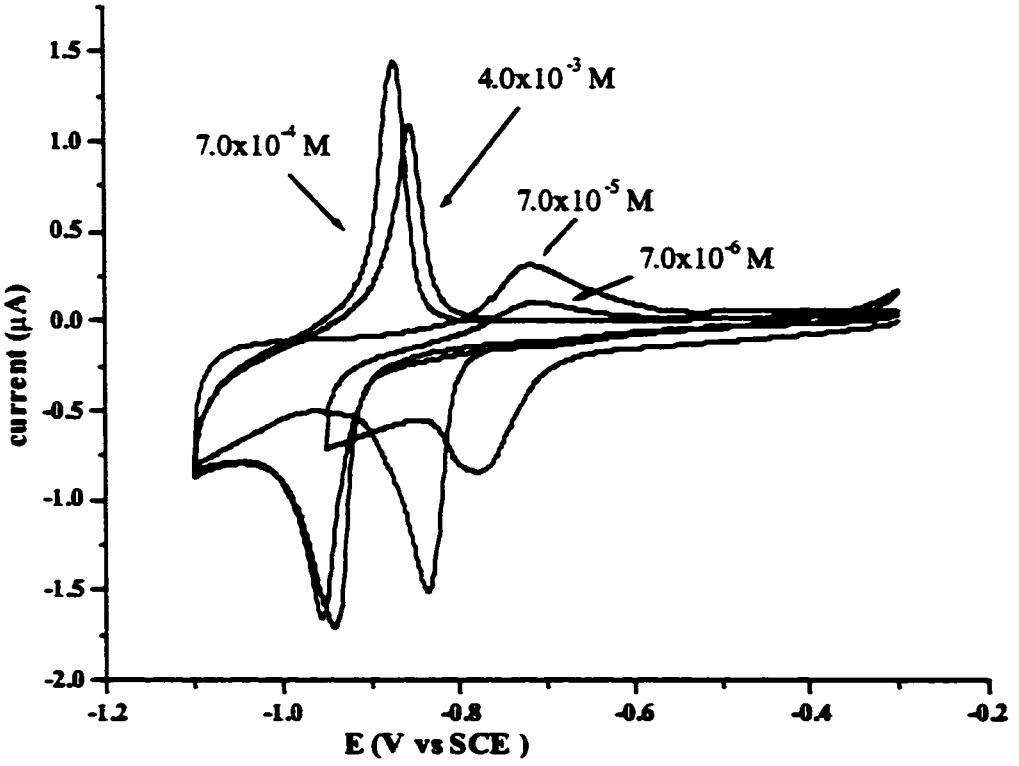

Figure 4-11: Cyclic voltammograms for the oxidative adsorption/reductive desorption of butanethiolate on gold in 0.1 M KOH solutions containing the different concentrations of butanethiol indicated on the figure.

Even though, the concentration of the butanethiolates only changes by one order of magnitude, the current peak potentials change suddenly from low concentrations ($7x10^{-5}$ M and $7x10^{-6}$ M) to high concentrations ($4x10^{-3}$ M and $7x10^{-4}$ M). This phenomenon suggests that the monolayers generated from the solutions of low thiolate concentrations ($7x10^{-5}$ M and $7x10^{-6}$ M) differ from those generated from the more concentrated ones ($4x10^{-3}$ M, $7x10^{-4}$ M). The narrow and more negative oxidative current peak observed at high concentrations ($4x10^{-3}$ M and $7x10^{-4}$ M) indicates that there are attractive interactions between the adsorbates [4-8]. At these concentrations, the adsorption is via an instantaneous nucleation and growth process. The more positive oxidative current peak potentials observed at lower concentrations ($7x10^{-5}$ M and $7x10^{-6}$ M) that the adsorption at low concentrations is slow and difficult.

The integrated oxidative charges at different concentrations are given in Table 4-5. We see that, at low concentrations, the coverage is only 15% of the full monolayer.

Table 4-5: The integrated charges at different concentrations of butanethiolate.

	4×10^{-3} M	7×10^{-4} M	7×10^{-5} M	7×10^{-6} M
Integrate charge (μC)	7.4 ± 2%	6.9 ± 5%	3.2 ± 7%	2.4 ± 10%

A concentration dependent layer was suggested by Rowntree and co-workers [4-9]. They found that, at high concentration, the IR spectrum is compatible with the formation of a monolayer of butanethiol in a crystalline state [4-10]. At lower concentration, the widths and wavenumbers of the C-H stretching modes suggested that the monolayers is disordered.

A phase transition in the adsorption process of the alkanethiols on the gold surface was observed in some studies [4-11 to 4-15]. A schematic diagram of the suggested mechanism for the phase transition is shown in Figure 4-12. In the early stage of the adsorption, the alkanethiols are lying-down. This phase has a low coverage. As the coverage increases there is a phase transition to a standing-up configuration. This yields the usual SAM structure.

This "lying-down" phase agrees with the lower charge observed at low concentrations. It is likely that the disordered monolayer is not in its final state in a cyclic voltammogram. At a scan rate of 10 mV s^{-1}, the time between deposition and reduction is only 3-4 seconds. Therefore, a full monolayer cannot be formed at these low concentrations in a few seconds. Notwithstanding whether this low coverage monolayer is in its final state or not, the kinetics of the adsorption process are different when different thiolate concentrations are used.

The oxidative adsorption at the different concentrations of butanethiolate was studied with EQCM combined with potential-step. Typical Δm vs time curves are shown in Figure 4-13. For the two highest concentrations ($4x10^{-3}$ M, $7x10^{-4}$ M) (Figure 3-13a and b), the increase of Δm occurs on a similar time scale to that measured in a 1 mM butanethiolate / 0.1 M KOH solution (Figure 3-7b). At these two concentrations, a two-step increase of the mass was observed. A bi-exponential equation (equation 4-1) was used to fit the Δm vs time curves of $4x10^{-3}$ M and $7x10^{-4}$ M butanethiolates. The fits in Figure

4-14 show that this two-step model, which consists of a nucleation and growth and a Langmuir process will describe the adsorption process at these concentrations.

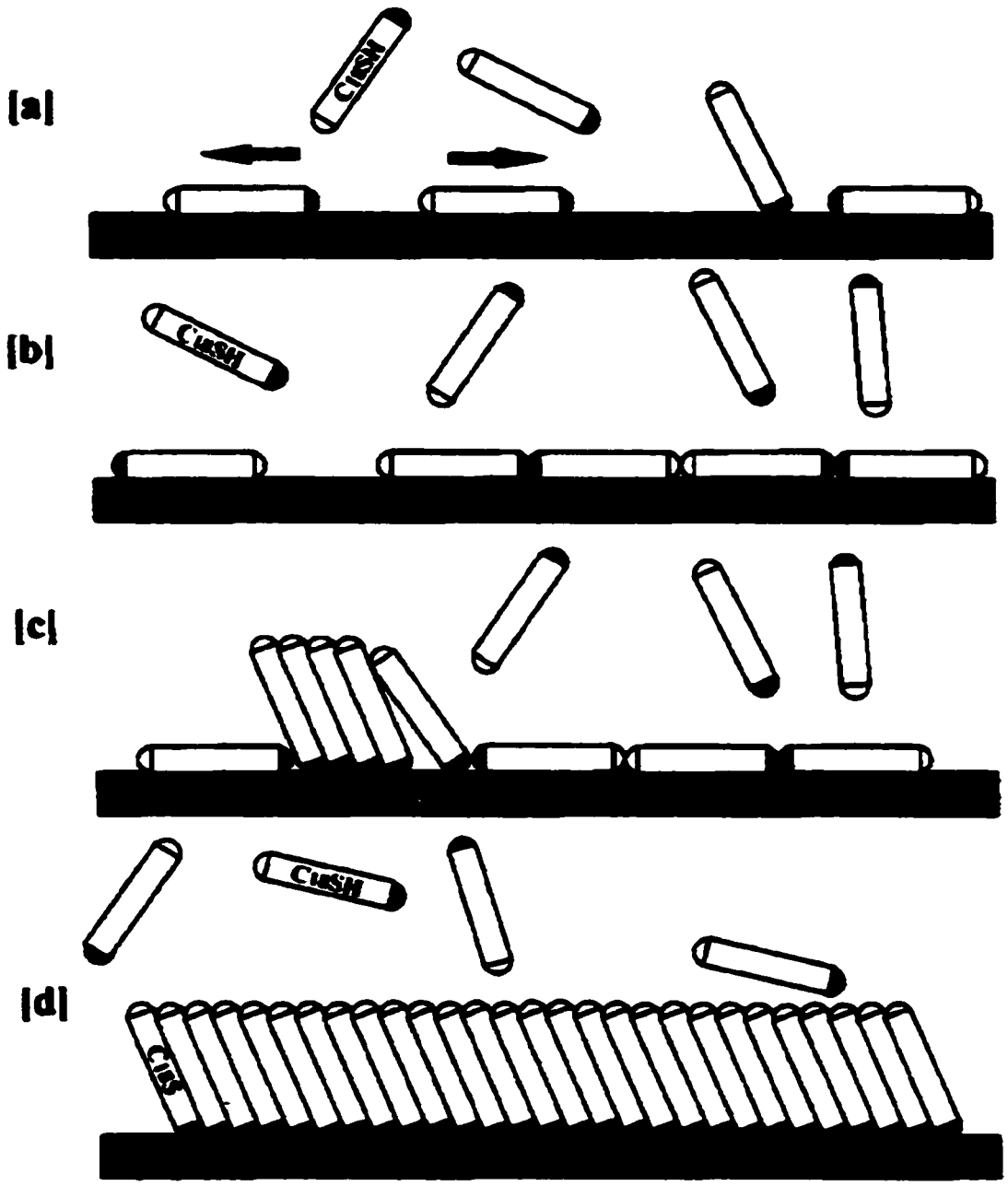

Figure 4-12: Scheme of an adsorption process of alkanethiol on gold, which goes through a phase transition from a lying-down (a,b) to a standing-up orientation (c, d). Copy from ref. 4-13.

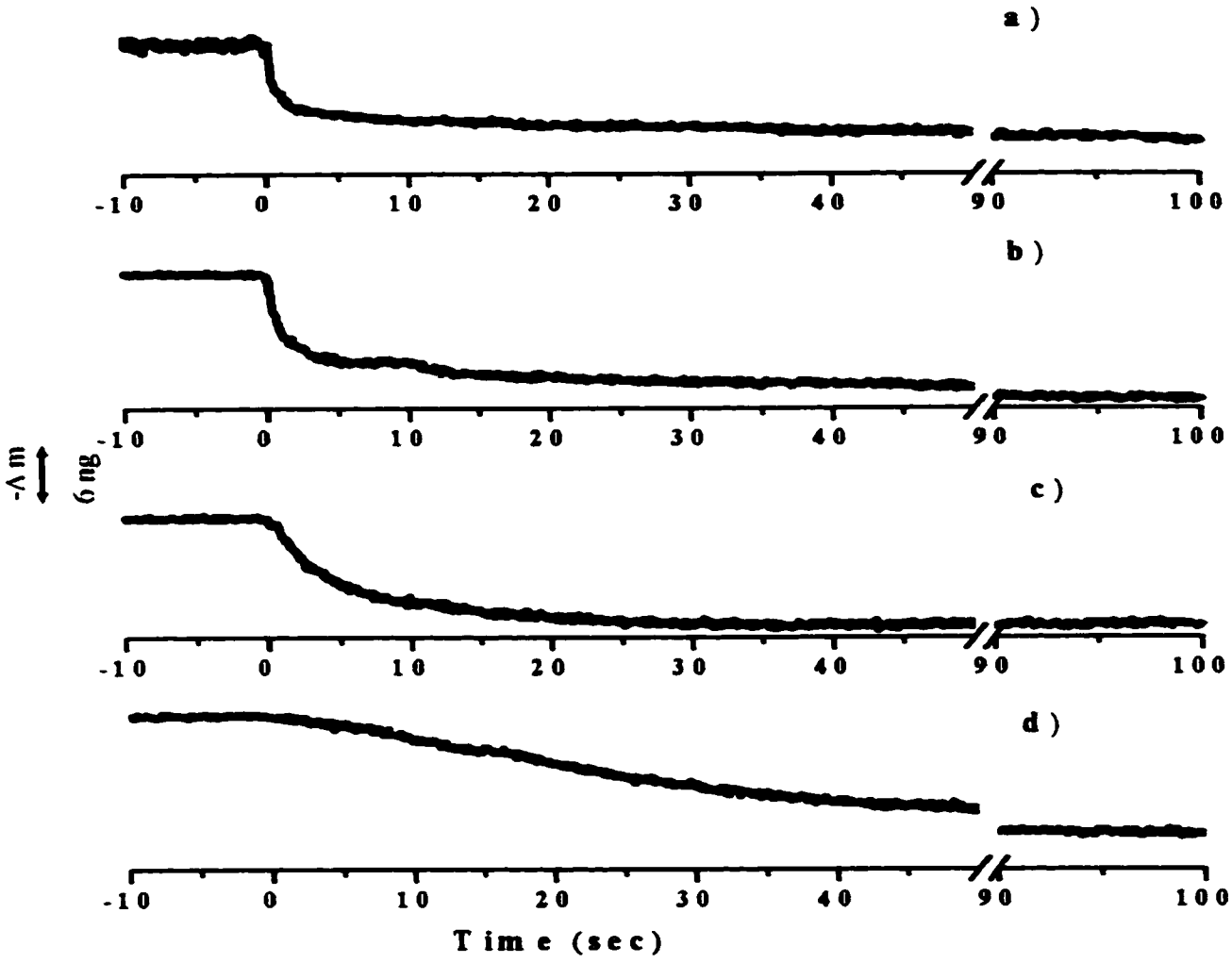

Figure 4-13: Mass change after potential steps causing the oxidative deposition of butanethioltae on gold at a) $4x10^{-3}$ M; b) $7x10^{-4}$ M; c) $7x10^{-5}$ M; d) $7x10^{-6}$ M butanethiolate in 0.1 M KOH. The potential is stepped from -1.10 V to –0.4 V.

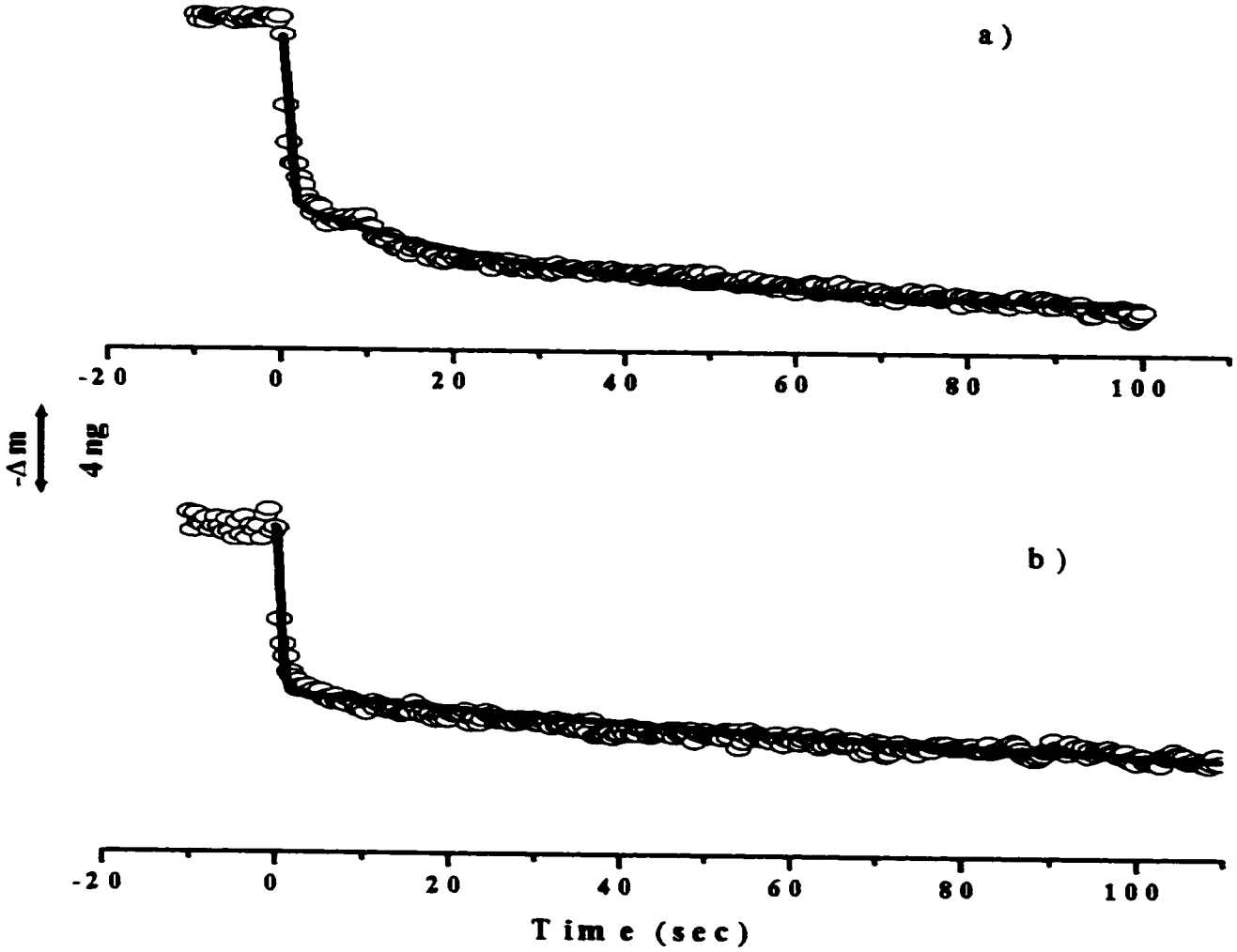

Figure 4-14: Mass change (dotted line) fitted with a two–step model (eq. 4-1, solid line); for the oxidative adsorption of a) $4x10^{-3}$ M butanethiolate and b) $7x10^{-4}$ M butanethiolate on gold in 0.1 M KOH. For clarity only every 20th data point is shown.

For the low concentrations ($7x10^{-5}$ M, $7x10^{-6}$ M), the Δm vs time curves (Figure 4-13c and d) show a more homogeneous increase of the mass. At low concentrations, the oxidative adsorption is slower. This is supported by previous studies [4-11, 4-16]. The two-

step model, which is a combination of a instantaneous nucleation and growth process and a Langmuir process, cannot describe the adsorption process of the alkanethiolates at low concentrations. Fits of the Δm vs time curves of $7x10^{-5}$ M and $7x10^{-6}$ M butanethiolates in Figure 4-15 using eq. 4-1 clearly show that at low concentrations, the oxidative adsorption does not follow this two-step model.

For the kinetics of the oxidative adsorption of alkanethiols from solutions of low concentration, a two-step Langmuir process [4-14, 4-16 to 4-24] and one-step Langmuir process [4-3, 4-4, 4-5, 4-25] were suggested. We thus used these two equations:

$$m(t) = m_{max} A \exp(-k_1 t) + m_{max}(1-A) \exp(-k_2 t) \qquad (4-3)$$

$$m(t) = m_{max} \exp(-kt) \qquad (4-4)$$

which represent the two-step Langmuir process (equation 4-3) and one-step Langmuir process (equation 4-1), respectively to fit the mass change vs time recorded at the low concentrations of butanethiolate. In equations 4-3 and 4-4, m (t) is the mass of alkylthiols oxidatively adsorbed at a time t after the potential step, m_{max} is the total mass change for a full coverage, A is the percentage of the total mass change occurring via the first Langmuir process, and k_1 and k_2 are the rate constants for the two Langmuir processes.

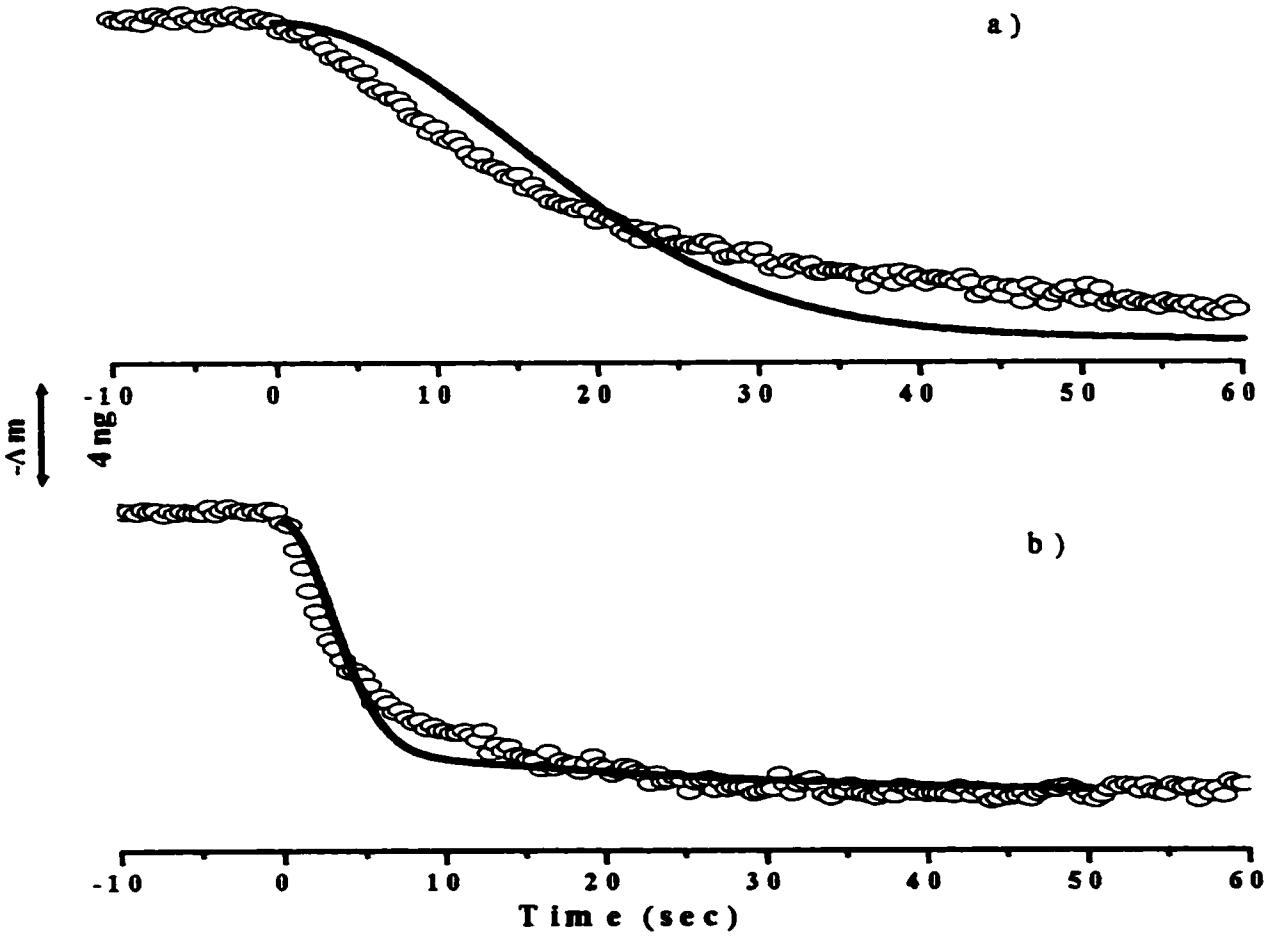

Figure 4-15: Mass change (dotted line) fitted with a two–step model (eq. 4-1, solid line); for the oxidative adsorption of a) $7x10^{-5}$ M butanethiolate and b) $7x10^{-6}$ M butanethiolate on gold in 0.1 M KOH. For clarity only every 20th data point is shown.

The fits are shown in Figures 4-16 and 4-17. From the graph, we see that the two-step Langmuir model describes the oxidative adsorption at low concentrations better than the one-step Langmuir model. The observed rate constants k_1 and k_2, and A obtained from the fits with equation 4-3 are shown in Table 4-6. We noticed that the rate constants vary significantly with the concentration. In $7x10^{-6}$ M, they are small. Only 50 ~ 60% of a monolayer is depositied via the first-step instead of 80 ~ 90% measured at higher concentrations of thiolates. This agrees with the suggested phase transition. We assign the first Langmuir process to the formation of a lying-down phase and the second Langmuir process to the formation of the standing-up phase (reorganization).

Table 4-6: Rate constants k_1 and k_2 obtained from a fit with a two-step Langmuir model for solutions of low concentration of butanethiolate.

	7×10^{-5} M	7×10^{-6} M
A	0.53 ± 0.01	0.63 ± 0.01
k_1 (s^{-1})	0.32 ± 0.006	0.05 ± 0.001
k_2 (s^{-1})	0.08 ± 0.001	0.006 ± 0.001

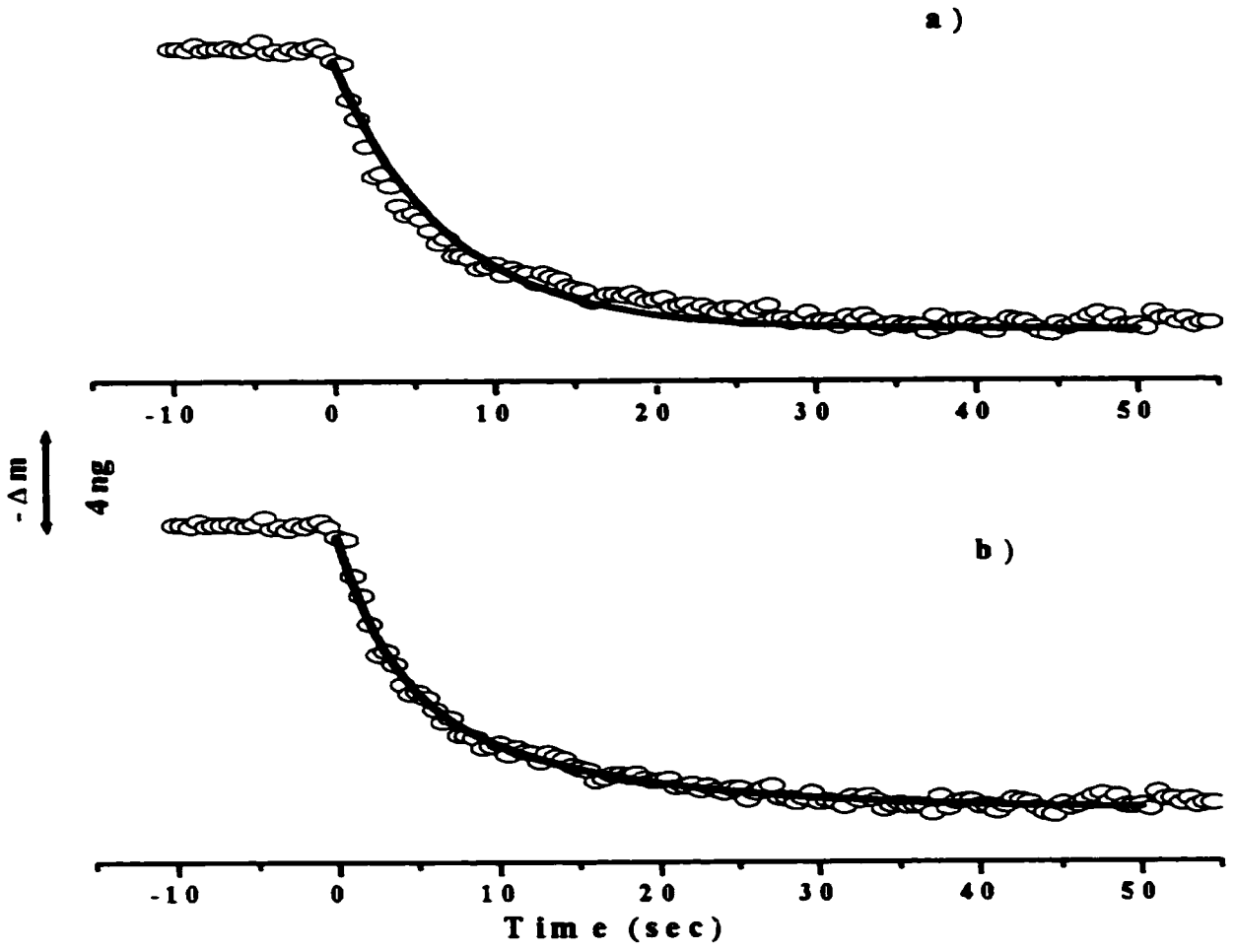

Figure 4-16: Mass change (dotted line) fitted with a) one–step Langmuir model (eq. 4-4, solid line); b) two-step Langmuir model (eq. 4-3, solid line) for the oxidative adsorption of $7x10^{-5}$ M butanethiolate on gold in 0.1 M KOH. For clarity only every 25^{th} data point is shown.

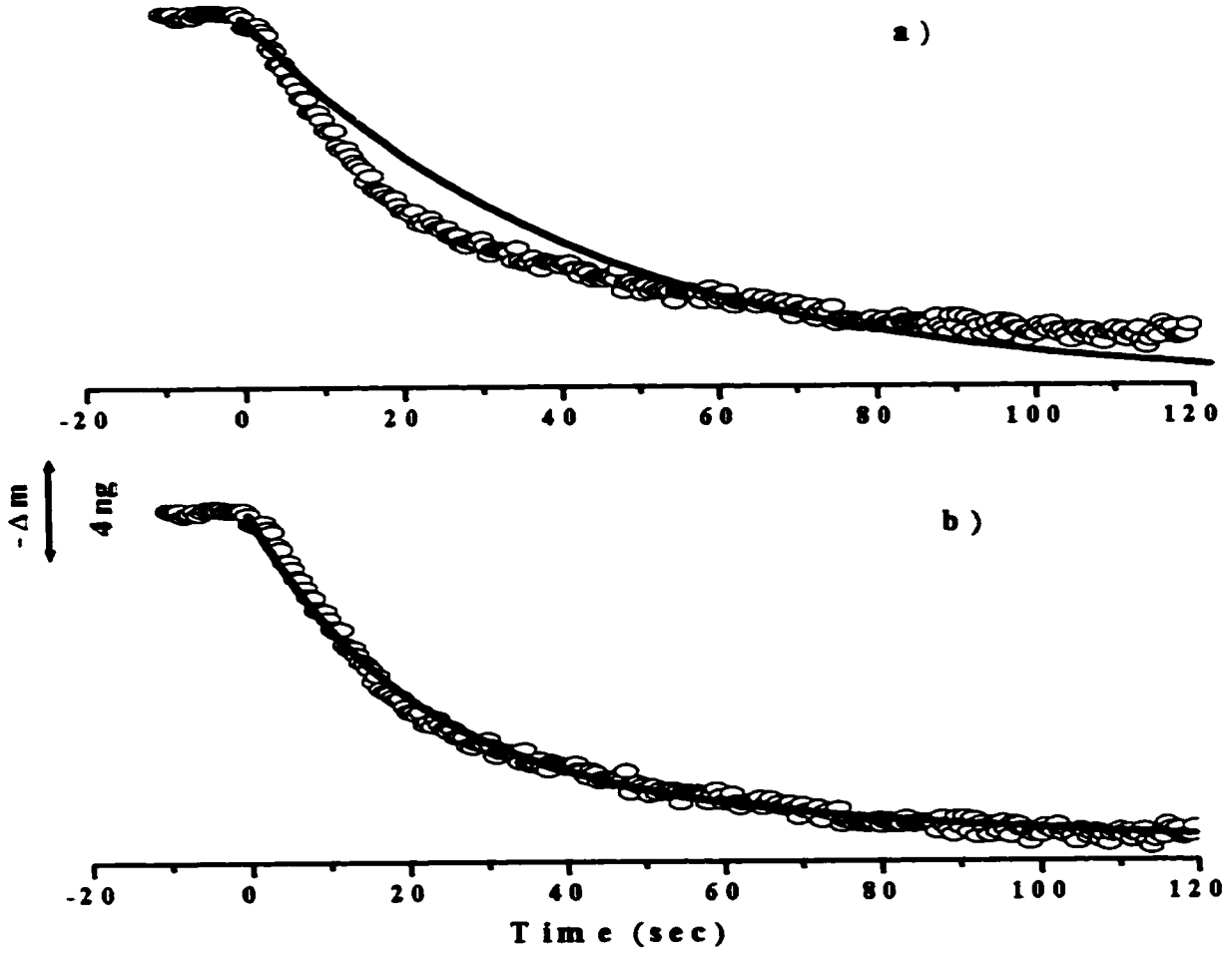

Figure 4-17: Mass change (dotted line) fitted with a) one–step Langmuir model (eq. 4-4, solid line); b) two-step Langmuir model (eq. 4-3, solid line) for the oxidative adsorption of $7x10^{-6}$ M butanethiolate on gold in 0.1 M KOH solution. For clarity only every 25th data point is shown.

In summary, a two-step model, which consists of a nucleation and growth and a Langmuir processes, was used to describe the adsorption process of the alkanethiolate on the gold surface at concentrations above $7x10^{-4}$ M. At concentrations below $7x10^{-5}$ M, the oxidative adsorption was described by a two-step Langmuir model. The first Langmuir step can be described as a random (independent) adsorption of alkanethiolates, and the second Langmuir step is assigned to a transition to an ordered phase.

References :

[4-1]: Hamelin, A.; Sottomayor, M.J.; Silva, F.; Chang, S-C; Weaver, M.J. *J. Electroanal. Chem.* **1990**, 295, 291.

[4-2]: Hamelin, A. *J. Electroanal. Chem.* **1996**, 407, 1.

[4-3]: Karpovich, D.S; Blanchard, G.J. *Langmuir* **1994**, 10, 3315.

[4-4]: Schessler, H.M; Karpovich, D.S; Blanchard, G.J, *J. Am. Chem. Soc.* **1996**, 118, 9645.

[4-5]: Karpovich, D.S; Schessler, H.M; Blanchard, G.J. *Thin Films* **1998**, 24, 43.

[4-6]: Lavrich, D.J; Wetterer, S.M; Bernasek, S.L; Scoles, G. *J. Phys. Chem. B* **1998**, 102, 3456.

[4-7]: Byloos, M.; Al-Maznai, H.; Morin, M. *J. Phys. Chem. B* **2001**, 105, 5900.

[4-8]: Bockris, J.; Khan, S.U.M. (eds) *Surface Electrochemistry,* Plenum press, New York and London, **1993**.

[4-9]: Truong, K.D.; Rowntree, P.A. *J. Phys. Chem.B* **1996**, 100, 19917.

[4-10]: Snyder, R.G. *J. Chem. Phys.* **1967**, 47, 1316.

[4-11]: Peterlinz, K.A.; Georgiadis, R. *Langmuir* **1996**, 12, 4731.

[4-12]: Xu, S.; Laibinis, P.E.; Liu, G-Y. *J. Am. Chem. Soc.* **1998**, 120, 9356.

[4-13]: Xu, S.; Cruchon-Dupeyret, S.J.N.; Garno, J.C.; Liu, G-Y.; Jennings, G.K.; Yong, T-H.; Laibinis, P.E. *J. Chem. Phys.* **1998**, 108(12), 5002.

[4-14]: Schreiber, F.; Eberhardt, A.; Leung, T.Y.B.; Schwartz, P.; Wetterer, S.M.; Lavrich, D.J.; Berman, L.; Fenter, P.; Eisenberger, P.; Scoles, G. *Phys. Review B* **1998**, 57, 12476.

[4-15]: Poirier, G.E.; Pylant, E.D. *Science* **1996**, 272, 1145.

[4-16]: Bain, C.D; Troughton, E. B; Tao, Y.-T; Evall, J; Whitesides, G. M; Nuzzo, R. G. *J. Am. Chem. Soc.* **1989**, 111, 321.

[4-17]: Hannoch, R. ; Rubinstein, I. *J. Am. Chem. Soc.* **1998**, 120, 13444.

[4-18]: Bensebaa, F.; Voicu, R.; Huron, L.; Ellis, T.H. *Langmuir* **1997**, 13, 5335.

[4-19]: Debono, R.F.; Loucks, G.D.; Manna, D.D.; Krull, U.L. *Can. J. Chem.* **1996**, 74, 677.

[4-20] : Hu, K.; Bard, A.J. *Langmuir* **1998**, 14, 4790.

[4-21]: Forouzan, F.; Bard, A.J.; Mirkin, M.V. *Israel Journal of Chemistry* **1997**, 37, 155.

[4-22]: Subramanian, R.; Lakshminarayanan, V. *Electrochimica Acta* **2000**, 45, 4501.

[4-23]: Shimazu, K.; Yagi, I.; Sato, Y.; Uosaki, K. *Langmuir* **1992**, 8, 1385.

[4-24]: Frubose, C.; Doblhofer, K. *J. Chem. Soc. Farad. Trans.* **1995**, 91(13), 1949.

[4-25]: Pan, W.; Durning, C.J.; Turro, N.J. *Langmuir* **1996**, 12, 4469.

Chapter 5

The electro-adsorption of dialkyl sulfides on gold

5.1. Introduction

It is widely accepted that self-assembled monolayers (SAMs) prepared from alkanethiols and dialkyl disulfides are structurally identical [5-1 - 5-7]. Both species are adsorbed as alkanethiolates on the gold surface [5-6]. As mentioned in the chapter 1, the structure and the properties of the equilibrated monolayers of alkanethiolates on gold were extensively studied [5-1 - 5-3]. On the other hand, the structure of the SAMs formed from dialkyl sulfides has not been elucidated. Contradictory conclusions have been reached [5-8 - 5-21]. A controversy concerning carbon - sulfur bond cleavage stems from a series of papers reported by Porter et al [5-8 - 5-10]. They studied the adsorption of sulfide on gold from ethanol solution with cyclic voltammetry, Infrared Spectroscopy (IR) and X-ray Photoelectron Spectroscopy (XPS). Initially, they claimed that the dialkyl sulfide adsorbed dissociatively on gold. In their proposed mechanism, one of the carbon - sulfur bonds is broken and the surface bonded species is an alkanethiolate. Other studies [5-11, 5-12] concluded that sulfides adsorb molecularly on the gold surface. This conclusion was drawn from the frequencies of the C-H stretching modes of the chemisorbed sulfides that showed that they formed disordered monolayers. Time-of flight secondary ion mass spectrometry (TOF-SIMS) [5-13, 5-14] suggested that the sulfides adsorbed molecularly. Jung. et al [5-15] used cyclic voltammetry, XPS and Second-Harmonic Generation (SHG)

to study the SAMs prepared from the adsorption of alkanethiols, dialkyl disulfides and dialkyl sulfides. They found that the films made from sulfides were significantly different from those produced by thiols and disulfides. They also pointed out that impurities significantly affect these studies. Other research groups have also noted the problem of thiol impurities. Trevor et al [5-16] found that there were alkanethiol and dialkyl disulfide impurities in commercially available sulfides. In a recent paper [5-17], Porter and co-workers concluded that these impurities are the source of the variability of the properties of sulfide monolayers. The presence of trace quantities (less than 0.1%) of thiols or disulfides in sulfide solutions can prevent the adsorption of sulfides. This results in adlayers whose composition and structure are dominated by the trace components (thiol and disulfide). After purification of the sulfide sample, no evidence of the carbon - sulfur bond dissociation was found [5-17].

Another controversy concerns the properties of the monolayers formed by sulfides. Troughton et al [5-11], in their first publication on sulfide SAMs, reported that monolayers resulting from the adsorption of sulfides on gold are less densely packed and less ordered than films originating from the adsorption of alkanethiols and disulfides. Most of the later studies [5-12, 5-15 - 5-19] supported these observations. Reinhoudt et al [5-13, 5-20, 5-21] observed that large receptors (β-cyclodextrin) with long dialkyl sulfides form more regular layers on gold than layers formed by thiols. They suggest that the multiple attachment points of the sulfides was responsible for this effect. It is clear from these results that the adsorption of sulfides depends on the experimental conditions and that utmost purity of the sulfides is essential.

In a previous study [5-22], we found that monolayers formed by dialkyl sulfides are similar to those originating from thiols and disulfides. Physisorbed sulfides go through a surface S_{N2} reaction and dissociate to form a thiolate as is shown in Figure 5-1. Reactions with various nucleophiles suggest that an adsorbed reactive sulfide is a precursor to the formation of a monolayer of thiolates. In order to clarify this process and to examine if an electric field can promote this S_{N2} surface reaction, we applied a potential to the gold electrode to control the kinetics of the sulfide adsorption. The following is our study of the electro-deposition of sulfides on gold.

5.2. Experimental

We purified all sulfide compounds to eliminate or significantly reduce the thiol/disulfide contaminations. Liquid chromatography (LC) and High Pressure Liquid Chromatography (HPLC) were used to purify the liquid sulfide compounds. Re-crystallization was used to purify the solid sulfide compounds. Gas Chromatography/Mass Spectrometry (GC/MS) was used to determine the purity level (see Chapter 2 for the details). The GC/MS results of pentamethylene sulfide before and after the purification are shown in Figure 5-2. We see that after the purification, there is only the sulfide compound. The detection limit is estimated to be 0.1% of the concentration of sulfide.

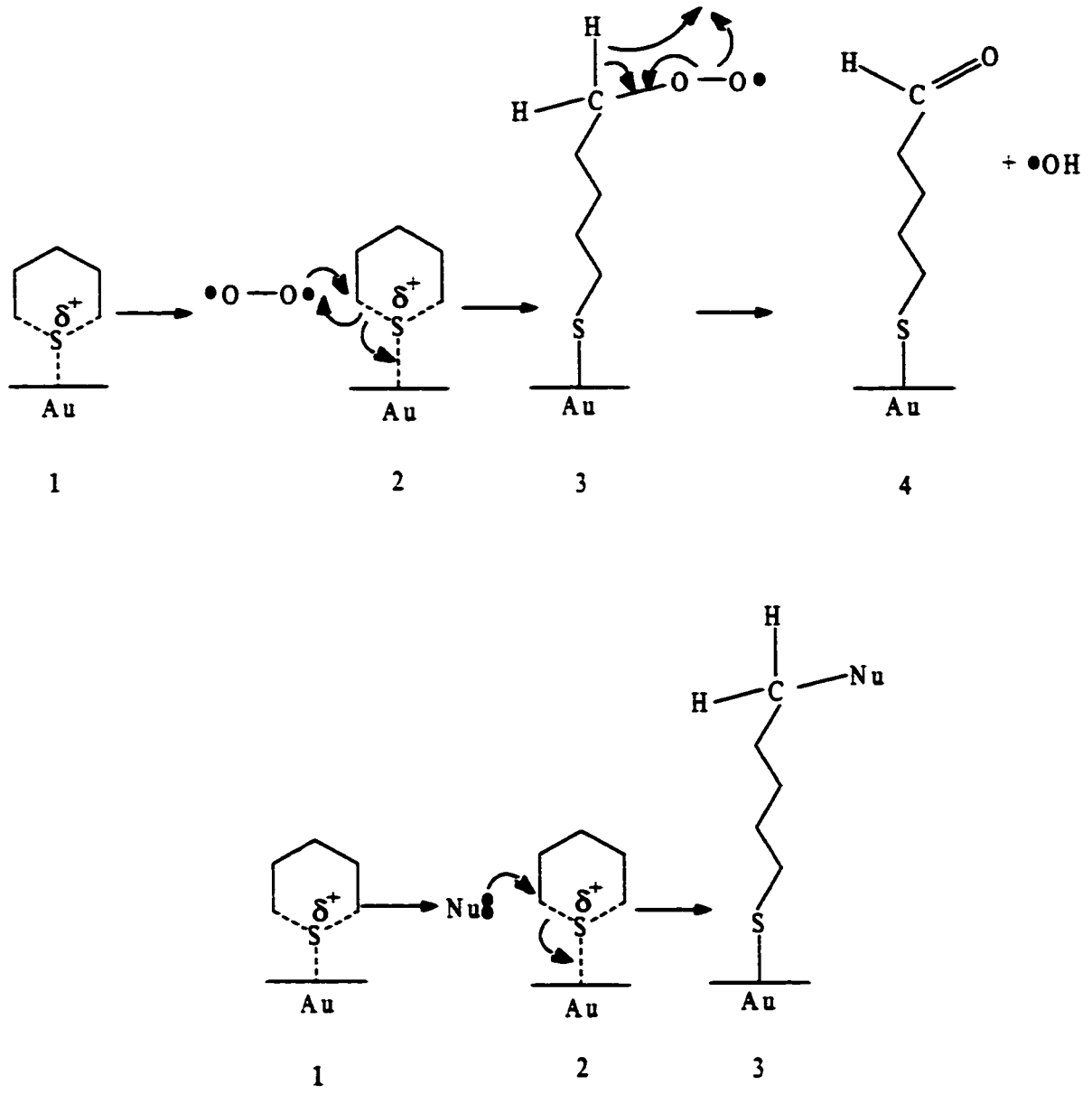

Figure 5-1: S_{N2} reactions between adsorbed pentamethylene sulfide, and oxygen, or a nucleophile, Nu.

a)

b)

c)

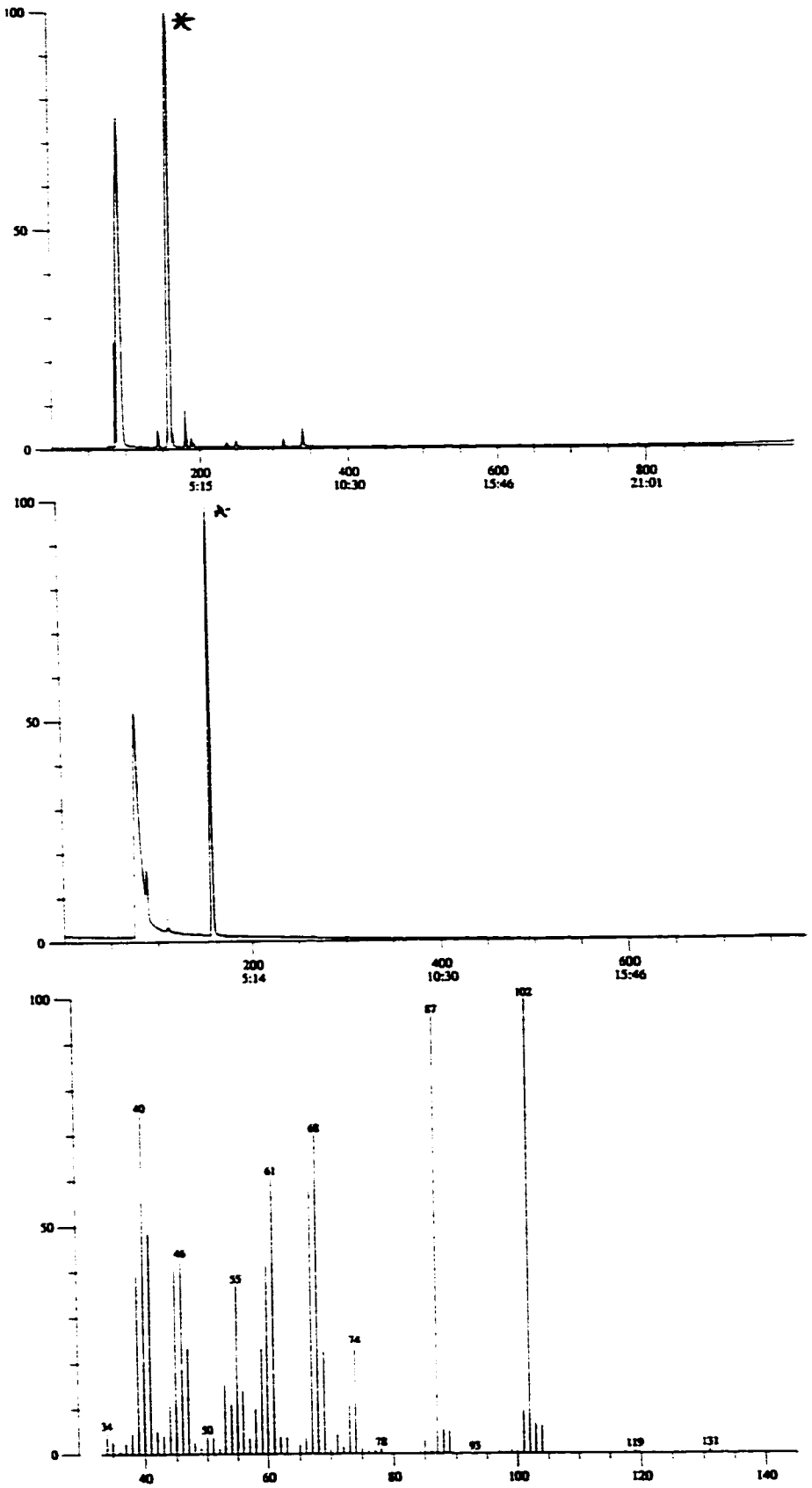

Figure 5-2: GC of pentamethylene sulfide. a) before the purification. b) after the purification. c) Mass spectrum of the purified pentamethylene sulfide.

5.3. Results and discussion

5.3.1. Sulfide adsorption with and without potential control

Chemical (open circuit) adsorption was used to prepare the sulfide SAMs on gold. The resulting SAMs were obtained after long enough time so that they were at equilibrium. A typical IR spectrum of a SAMs made from pentamethylene sulfide is shown in Figure 5-3. This spectrum shows that an aldehyde has been formed [5-23]. There are four bands in this spectrum. There is a CO stretching mode at 1730 cm^{-1} and two C-H stretching modes at 2820 cm^{-1} and 2725 cm^{-1} (assigned to a Fermi resonance of the C-H stretching mode of the aldehyde C-H band with the overtone of its C-H bending mode). The other broad C-H stretching band at 2929 cm^{-1} is assigned to the methylene groups. This suggests that the dialkyl sulfide goes through a reaction with molecular oxygen.

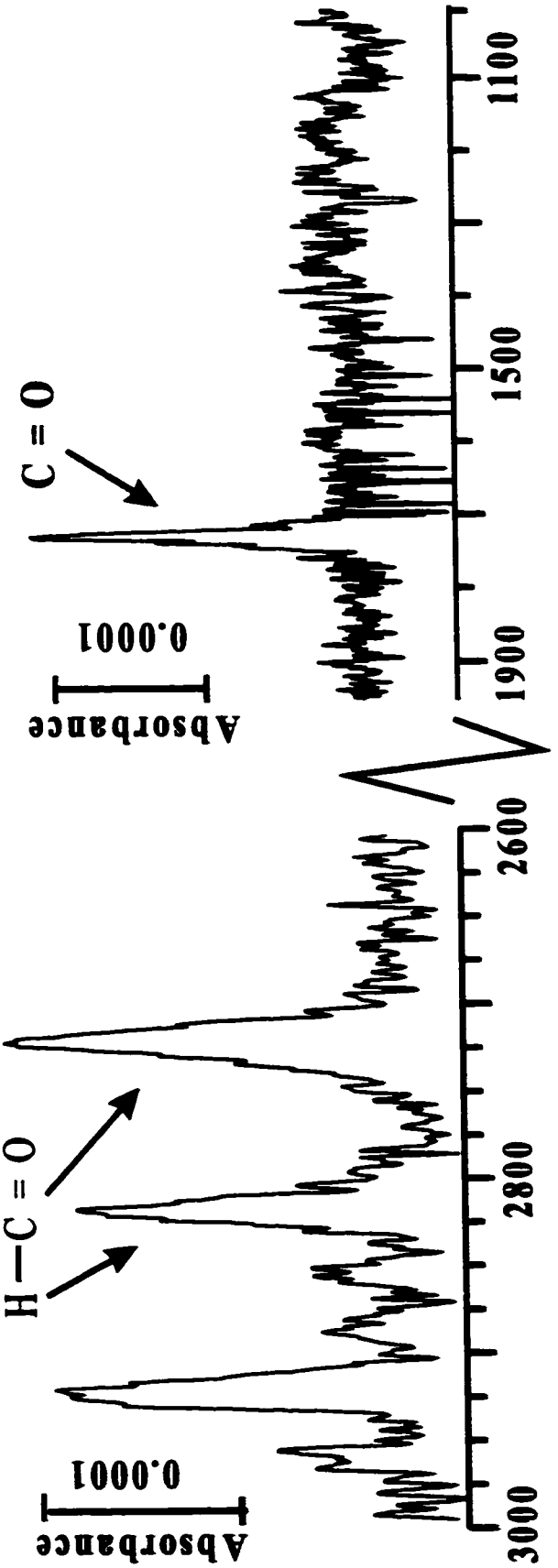

Figure 5-3; Infrared spectrum of a monolayer formed by incubating a Au(111) single crystal in a 0.01M pentamethylene sulfide ethanolic solution. Copy from ref. 5-22.

5.3.2. Oxidative deposition of sulfides on gold from 0.1 M $KClO_4$

The scheme for the electro-deposition of dialkyl sulfide is as follows. First, we set the potential at –1.10 V, where the gold surface is uncoated. Then we step the potential to 0.00 V, where it is positive enough to form a sulfide monolayer. We hold the potential at 0.00 V for different times. We estimate the amount of deposition by scanning the potential back to –1.10 V. The corresponding reductive current peaks provide information (coverage and peak potential) on the monolayer formed at different electro-deposition time scales.

Figure 5-4 shows the cyclic voltammograms for the reduction of pentamethylene sulfide in 0.1 M $KClO_4$ solutions on gold, obtained by the electro-deposition method described in the previous paragraph. After a short holding time (1 min of electro-deposition), there is a single reductive current peak at –0.58 V. When the deposition time increases to 15 min of electro-deposition, there are two reductive current peaks at –0.65 V and –0.75 V. When the electro-deposition time increases to one hour, a third reductive current peak appears at –0.86 V. The first reductive current peak has almost disappeared at this time. When the electro-deposition time reaches two hours, only the reductive peak at -0.86 V remains.

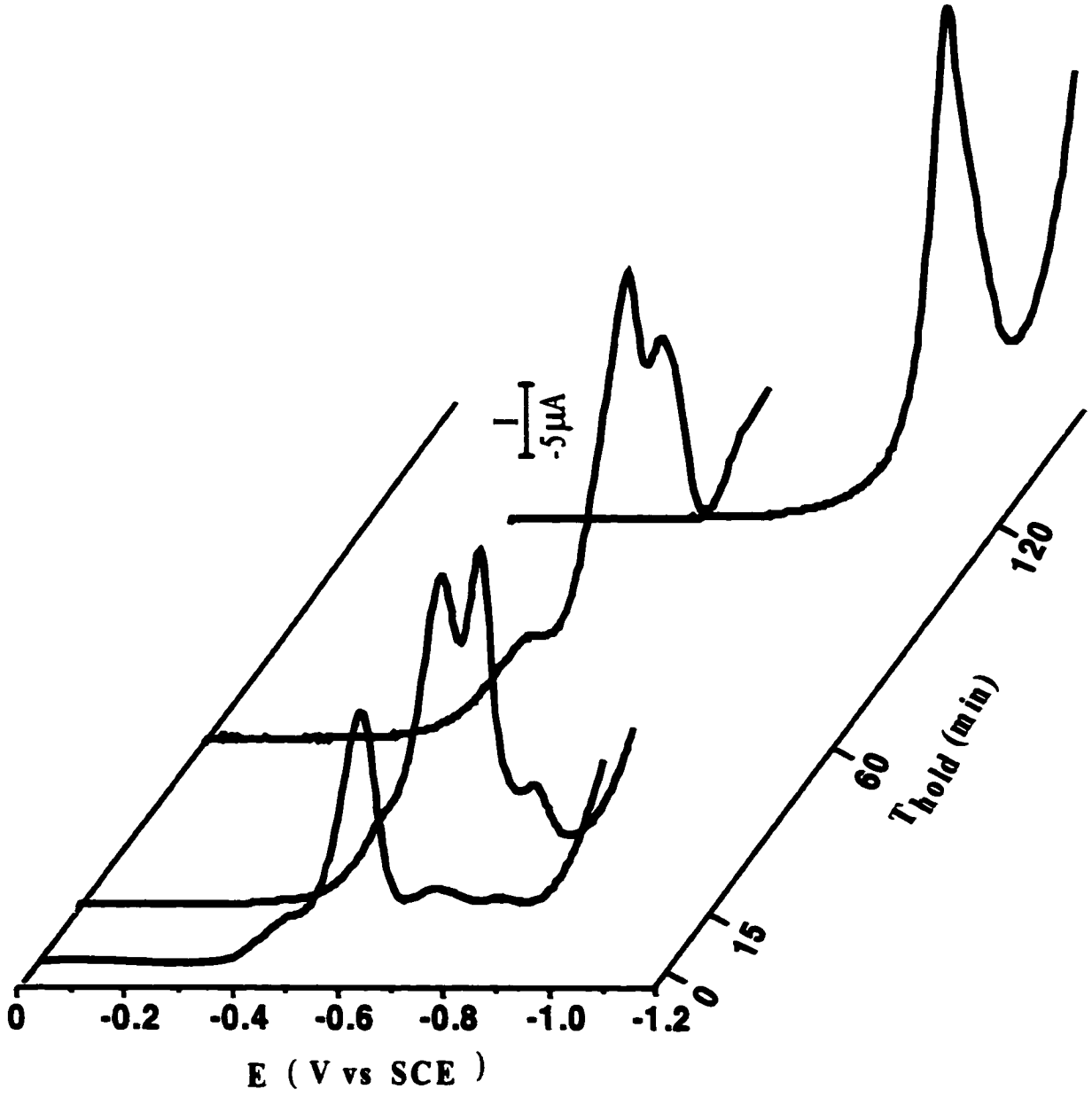

Figure 5-4: The cyclic voltammograms for the reduction pentamethylene sulfide on Au (111) in 0.1 M $KClO_4$ following different electro-deposition times.

The peak potential in the cyclic voltammograms and the integrated reductive charge (integrated from cyclic voltammograms after correction for the capacitive charge) for the different electro-deposition times are listed in Table 5-1.

Table 5-1: Peak potentials and integrated reductive charges (integrated from reductive voltammograms after capacitance charge correction) of pentamethylene sulfide in 0.1M $KClO_4$ for the different electro-deposition times.

Holding time (min)	Peak potential (V vs SCE)	Charge ($\mu C\ cm^{-2}$)
1	-0.60	-42 ± 3%
15	-0.65 (1^{st}) ; -0.75 (2^{nd})	-54 ± 5%
60	-0.75 (2^{nd}); -0.86 (3^{rd})	-70 ± 6%
120	-0.85 (3^{rd})	-73 ± 2%

From Table 5-1, we see that the reductive peak potential shifts to negative values when the electro-deposition time increases and that the total reductive charge increases with the holding time. This reductive peak potential shift cannot simply be explained by an increase of the coverage of a single adsorbed species on gold. It is true that, when the coverage of the adsorbed species (such as thiolates) increases, the reductive peak potential of this adsorbed species will shift to negative values. We described this phenomena in Chapter 4 for low concentrations of thiols. However, this is not the origin of the potential shift observed here. In the previous chapter, when the value of the integrated charge doubled, the reductive peak potential only shifted by -0.09 V (from -0.86 V to -0.95 V). For the sulfide, for a change in the integrated charge from 41 $\mu C\ cm^{-2}$

to 73 μC cm^{-2}, the reductive peak potential shifts by -0.28 V (from -0.58 V to -0.86 V). If we assume 73 μC cm^{-2} corresponds to the formation of a full monolayer, the coverage only changes from 56% of monolayer to a complete monolayer. Another piece of evidence which suggests that this observation is not due to a simple variation in the coverage of a single adsorbed species, is the appearance of the multiple reductive peaks. If the coverage change was only due to the adsorption of thiolates, we would see a single peak that would shift to more negative values as the reductive charge (i.e. coverage) increases. The large potential shift and the appearance of multiple reductive peaks indicate that there are different adsorbed species involved in the electro-formation SAMs from dialkyl sulfides.

Even though, we carefully purified the sulfide, it is possible that there are up to 0.1% of thiols or other impurities in the compound. This could affect the sulfide adsorption. However, as presented in Chapter 3, the adsorption of thiol is slow in 0.1 M $KClO_4$. The adsorption of alkanethiols from aqueous pH-neutral solutions requires the dissociation of the S-H bond. This is the main energy barrier in the thiol adsorption process. Based on the estimation [5-24, 5-25, 5-26] of the bond dissociation energy (BDE) made in a previous study [5-22], the BDE of S-H bond is 370 kJ mol^{-1} [5-24, 5-25] and the BDE of C-S bond is around 306 kJ mol^{-1} [5-22]. This suggests that the dissociation of a S-H bond could be harder than that of a C-S bond on gold. We thus believe that in aqueous pH-neutral solutions we observe the adsorption of sulfide. We interpret the cyclic voltammograms as an indication that the adsorption of sulfide on gold in neutral solution goes through a slow dissociation as shown in Figure 5-5. First the sulfide adsorbs on the

surface and forms a reactive intermediate, then one of the C-S bond dissociates (possibly via an S_{N2} reaction) and a thiolate monolayer is formed.

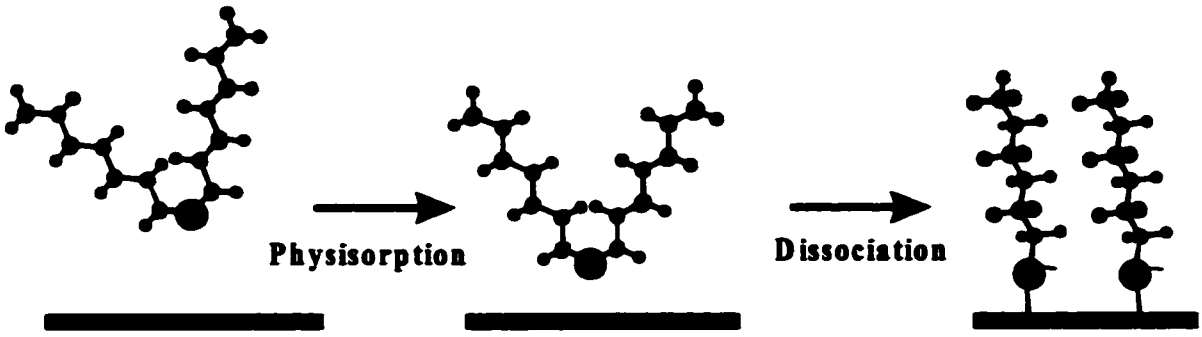

Figure 5-5: Electro-adsorption of dialkyl sulfide on gold in 0.1 M $KClO_4$.

5.3.3. Oxidative deposition of sulfide in alkaline solution

5.3.3.1 EQCM

As mentioned before, a S_{N2} mechanism is proposed to describe the dissociative adsorption of sulfide on gold. The presence of a nucleophile should promote sulfide dissociation. Hence we use OH^- as a nucleophile to study the electro-deposition process of the sulfide on gold in 0.1 M KOH. The mass change in the electro-deposition process can give information about a possible S_{N2} mechanism for sulfide dissociation on gold as well as the effect of the electric field on this process.

The EQCM signal and cyclic voltammogram of butyl sulfide in 0.1 M KOH are shown in Figure 5-6. The potential is scanned between –0.10 V and –1.10 V vs. SCE. On the initial negative going potential scan, the current and frequency are almost constant

until –0.80 V. Then as the current due to the reductive desorption of the adsorbate appears, the frequency increases. On the following positive going potential scan, the onset of frequency decrease corresponds to the one of the oxidative current peaks. After the oxidative current peak, the frequency continuously decreases. At -0.55 V the frequency is almost the same as the initial one.

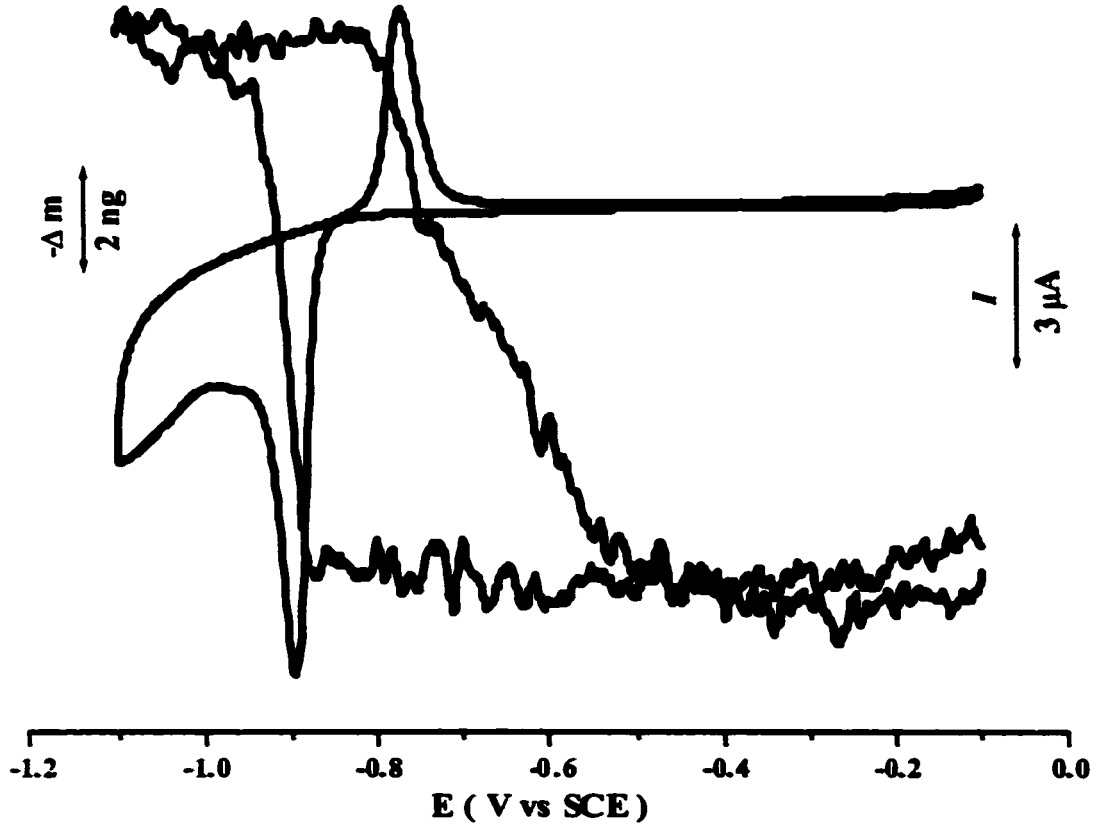

Figure 5-6: Cyclic voltammogram and mass change for the oxidative adsorption /reductive desorption of butyl sulfide on gold recorded in 0.1M KOH. Potential scan rate: 10 mV s^{-1}.

The mass change and cyclic voltammogram shown in Figure 5-6 are very similar to those obtained for butanethiolate in 0.1 M KOH (see Chapter 3). We found that the thiolates oxidatively adsorb more rapidly than their protonated form. It is likely that their rate of adsorption (thiolate) will be faster than that of sulfides, which involves a surface dissociation step. Thus, instead of recording the behavior of butyl sulfide reductive desorption/oxidative deposition, we could be measuring in a KOH solution the adsorption of traces of thiolates.

Thiolate impurities may come from two sources. The original sample could still contain traces of thiols. Another possibility is that the thiolate could be formed by the dissociative adsorption of alkyl sulfides. We could generate a significant amount of thiolates since we record cyclic voltammograms for up to one hour prior to the EQCM measurement.

This former effect does not occur in 0.1 M $KClO_4$ solution, since the thiolates generated from reductive desorption will be protonated and form thiols again. This was also shown in various studies [5-27 - 5-31]. However, in an alkaline solution, the presence of a nucleophile (OH^-) could make sulfide dissociation faster and increase the rate of production of thiolates.

We carried out EQCM potential holding experiments as described in section 5.3.2. Figure 5-7 shows the EQCM signals and cyclic voltammograms of butyl sulfide in 0.1 M KOH for the different electro-deposition times. We noticed that, in the initial

negative going potential scan, the reductive current peak potentials changed with the electro-deposition time. With no holding (Figure 5-7a), the reductive current peak potential is -0.89 V. When the electro-deposition time increases, the reductive peak potential becomes more negative (-0.93 V after 5 min and -0.95 V after 15 min). For 30 min of electro-deposition (Figure 5-7d), the reductive peak potential shifts to -0.96 V, which is identical to that of butanethiolates. These reductive potential shifts with the different holding times are smaller than those observed in 0.1 M $KClO_4$.

The mass change and the reductive charge (the integrated oxidative charge obtained from cyclic voltammograms in Figure 5-7 after correction for the capacitive charge) corresponding to different electro-deposition times are plotted in Figure 5-8. The integrated charges remain constant, but the mass change increases as the holding time increases.

We see on Figure 5-7 that on the following positive-going potential scan, the oxidative peak potential shifts negatively as the electro-deposition time increases. The mass change also increases with the electro-deposition time.

The EQCM results and the cyclic voltammograms for butyl sulfide in alkaline solution obtained after different electro-deposition times are similar to those measured in the low concentrations experiments described in Chapter 4. This suggests the presence of thiolates in the solution.

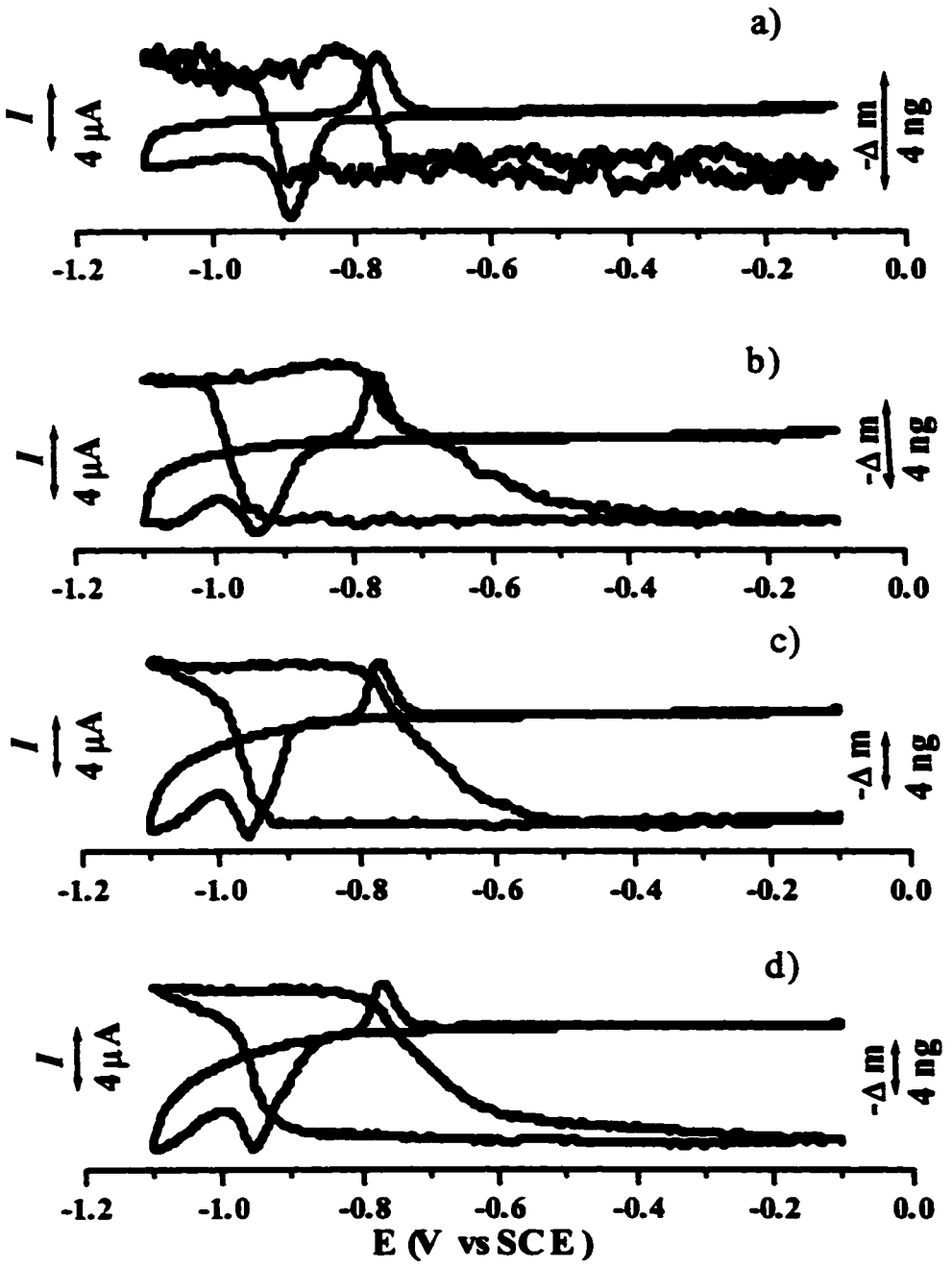

Figure 5-7: Cyclic voltammograms and mass change for the oxidative adsorption /reductive desorption of dibutyl sulfide on gold recorded in 0.1M KOH after different holding times: a) 0 min; b) 5 min; c) 15 min; d) 30 min. Potential scan rate: 10 mV s^{-1}. Potential hold at –0.2 V

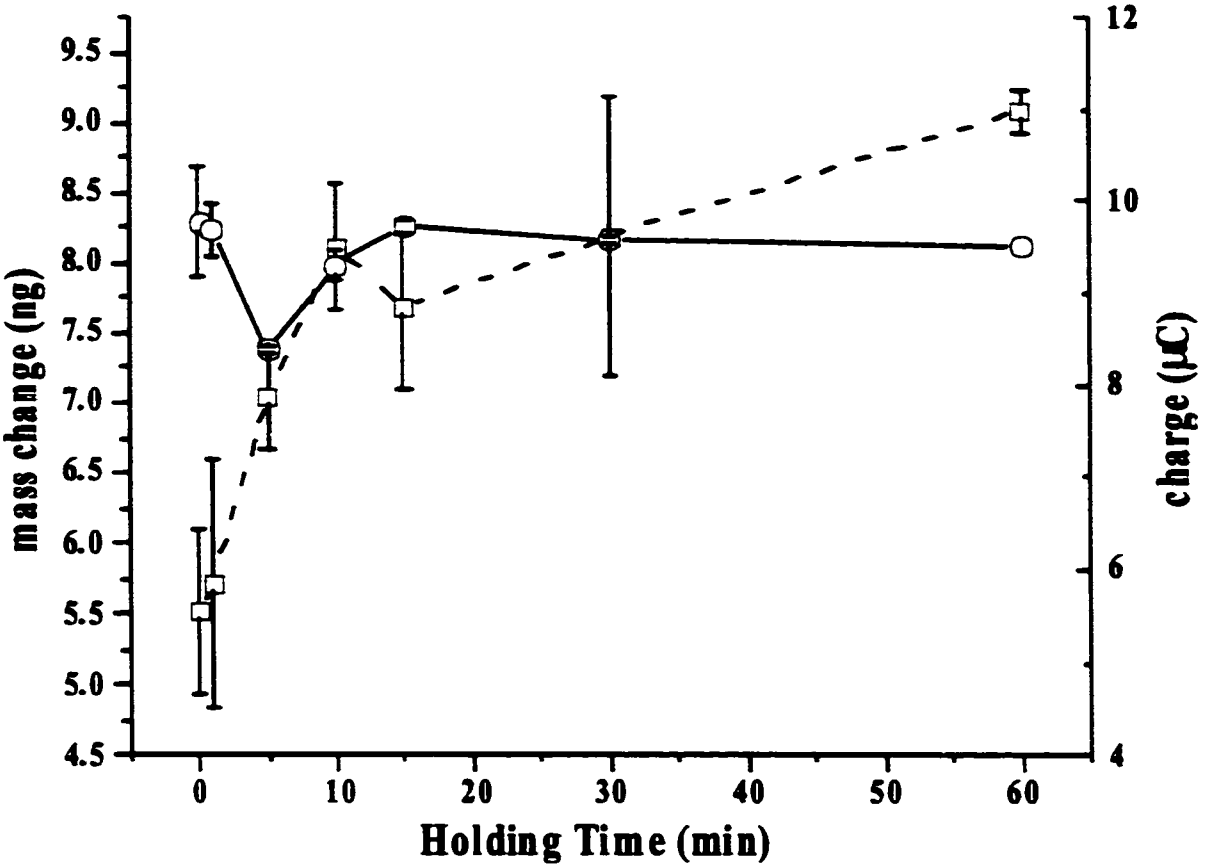

Figure 5-8: Plot of the mass change obtained from the EQCM signal (dashed line) and the reductive charge (corrected for the capacitive charge, solid line), obtained from the integration of cyclic voltammograms, vs the electro-deposition time.

5.3.3.2. In-situ IR study

We used in-situ IR spectroscopy to monitor the orientation of the species formed on gold during the electro-formation of a monolayer from dialkyl sulfide.

We used dodecyl sulfide since it has a longer alkyl-chain, and it is thus easier to detect the C-H stretching band in the IR spectra. The experiment is done in 0.1 M KOH and we control the potential as we did in the previous cyclic voltammetry experiments.

We hold the potential at –1.20 V for 5 min to remove the adsorbed species. We then step the potential to –0.20 V, and hold at this value for different times. Then we record the spectrum in the region of the C-H stretching modes (between 3000 cm^{-1} and 2800 cm^{-1}). We save this spectrum as R_{sample}. Then we step the potential back to –1.20 V to desorb the species from the gold surface and record this spectrum as $R_{background}$. We expressed the spectra as:

$$\Delta R / R = R_{sample} - R_{background} / R_{background}$$

The in-situ IR spectra of the electro-deposition of dodecyl sulfide at different holding times are shown in Figure 5-9. The wavenumbers of each peak and its intensity are listed in the Table 5-2.

Table 5-2: Intensity (differential reflectance in %) and wavenumbers of the C-H stretching bands of the IR spectra in Fig 5.9. $-CH_3(\nu_a,ip)$ is the asymmetric in-plane C-H stretching mode of the CH_3 group, $-CH_2(\nu_a)$ and $-CH_2(\nu_s)$ are the asymmetric and symmetric C-H stretching modes, respectively.

Holding time (min)	$-CH_3$ (ν_a , ip)	$-CH_2$ (ν_a)	$-CH_2$ (ν_s)
15	-----	-----	-----
30	2958/0.18%	2925/0.22%	2851/0.20%
60	2958/.006%	2930/0.11%	2860/0.08%
90	-----	2925/-0.08%	2856/-0.09%

*wavenumber(cm^{-1}) / ΔR/R%

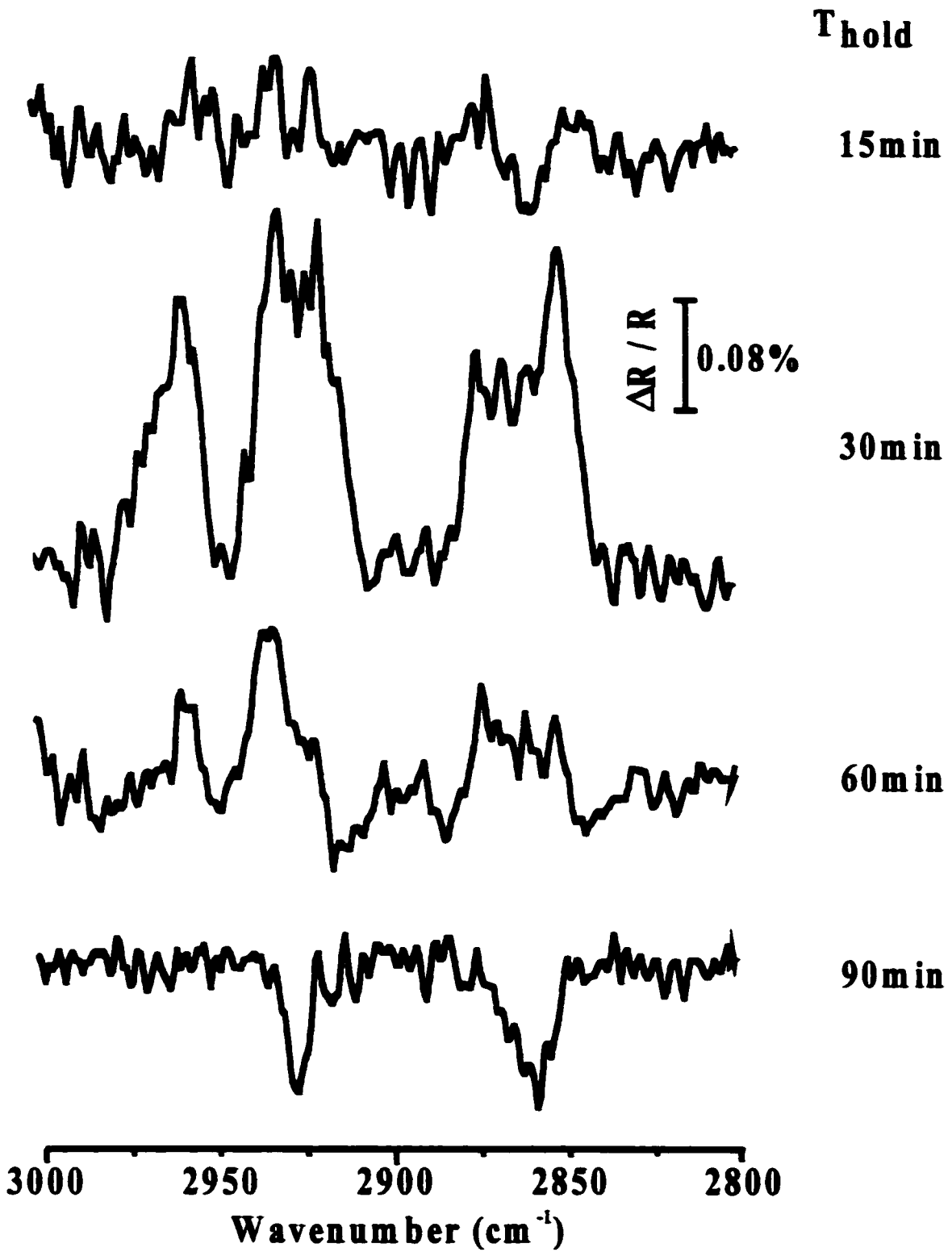

Figure 5-9: In-situ IR spectra of the electro-deposition of dodecyl sulfide in 0.1M KOH after different electro-deposition time (see text for details).

As is shown in Figure 5-9, after 15 min, there are no peaks in the spectrum. This shows the dipole moments of the methylene stretching modes of the species adsorbed on the surface are as randomly oriented as in the solution. When the holding time is 30 min, positive reflectance peaks are observed. In this case, the dipole moments of the methylene stretching modes are on average more parallel to the surface compared to those in the solution. When the holding time is 60 min, smaller positive reflectance peaks are observed. This shows that the dipole moments of the methylene stretching modes of the adsorbed species near the surface are still in a preferential orientation parallel to the surface. When the holding time is 90 min, sharper negative reflectance peaks appear. In this case, the dipole moments of the methylene stretching modes of the adsorbed species are more perpendicular to the surface compared to those in the solution.

These in-situ IR spectra suggest a phase transition similar to the one described in section 4.3 in Chapter 4. This phase transition is illustrated in Figure 4.12. For a holding time of up to 30 min, the adsorbed species are randomly adsorbed and are mostly lying-down on the surface. Broad positive reflectance bands appear in the C-H stretching region of the IR spectrum. After around 30 min, the intensity of the positive reflectance bands decreases and the bands become sharper and shift to lower wavenumbers. This shows that the adsorbed species on the surface are ordering themselves. Finally, when the electro-deposition time is 90 min, a monolayer of thiolate is formed and the alkanechains are in the standing-up state. This gives rise to sharp negative reflectance peaks. This suggests that the dipole moments of the methylene stretching modes have

become more perpendicular to the surface. This differs from the oxidative deposition of alkylthiolates, which show positive reflectance peaks upon desorption [5-30].

We thus believe that in alkaline solution, the adsorption process may due to the adsorption of (low concentration) thiolates possibly involving a phase transition from a lying-down to a standing-up arrangement.

5.4. Conclusion

In summary, the adsorption of dialkyl sulfides is complex. There is a competitive adsorption between the sulfide and, thiol or thiolate impurities in the solution. We suggest that in the 0.1 M $KClO_4$ solution sulfides adsorb molecularly. Then they slowly dissociate on the gold surface. The thiol impurities do not significantly affect this adsorption process. In alkaline solution, the sulfide adsorption process is still not clear. Thiolate impurities are found to adsorb more readily than the sulfide. However, OH^-, a nucleophile, could increase the dissociation rate of the sulfides via an S_{N2} reaction and also produce thiolates.

References:

[5-1]: Ulman, A. *An introduction to ultra-thin organic films* Academic press, San Diego, 1991.

[5-2]: Ulman A. *Chem. Rev* **1996**, 96, 1533.

[5-3]: Finklea, H.O. *Electroanalytical chemistry* Vol.19, p.109 Bard, A.J; Rubinstein, I Eds; Marcel Dekker, New York, 1990.

[5-4]: Bain, C.D.; Biebuyck, H.A.; Whitesides, G.M. *Langmuir* **1989**, 5, 723.

[5-5]: Biebuyck, H.A.; Whitesides, G.M. *Langmuir* **1993**, 9, 1766.

[5-6]: Biebuyck, H.A.; Bain, C.D.; Whitesides, G.M. *Langmuir* **1994**, 10, 1825.

[5-7]: He, Z.; Bhattacharyya, S.; Cleland, W.E., Jr.; Hussey, C.L. *J. Electroanal. Chem.* **1995**, 397, 305.

[5-8]: Zhong, C.J.; Porter, M.D. *J.Am.Chem.Soc.* **1994**, 116, 11616.

[5-9]: Zhong, C.J.; Porter, M.D. *Anal.Chem.* **1995**, 67, 709A.

[5-10]: Weisshaar, D.E.; Walczak, M.M.; Porter, M.D. *Langmuir* **1993**, 9, 323.

[5-11]: Troughton, E.B.; Bain, C.D.; Whitesides, G.M.; Nuzzo, R.G.; Allara, D.L.; Porter, M.D. *Langmuir* **1988**, 4, 365.

[5-12]: Zhang, M.; Anderson, M.R. *Langmuir* **1994**, 10, 2807.

[5-13]: Beulen, M.W.; Huisman, B.H.; van der Heijden, P.A.; van Veggel F.C.J.M.; Simons, M.G.; Biemond, E.M.E.F.; de Lange, P.J.; Reinhoudt, D.N. *Langmuir* **1996**, 12, 6170.

[5-14]: Hagenhoff, B.; Benninghoven, A.; Spinke, J.; Liley, L.; Knoll, W. *Langmuir* **1993**, 9, 1622.

[5-15]: Jung, Ch.; Dannenberger, O.; Xu, Y.; Buck, M.; Grunze, M. *Langmuir* **1998**, 14, 1103.

[5-16]: Trevor, J.L.; Lykke, R.L.; Pellin, M.J.; Hanley, L. *Langmuir* **1998**, 14, 1664.

[5-17]: Zhong, C.J.; Brush, R.C.; Anderegg, J.; Porter, M.D. *Langmuir* **1999**, 15, 518.

[5-18]: Leavy, M.C.; Bhattacharyya, S.; Cleland, W.E., Jr.; Hussey, C.L. *Langmuir* **1999**, 15, 6582.

[5-19]: Takiguchi, H.; Sato, K.; Ishida, T.; Abe, K.; Yase, K; Tamada, K. *Langmuir* **2000**, 16, 1703.

[5-20]: Beulen, M.W.; Bugler, J.; Lammerink, B.; Geurts, F.A.J.; Biemond, E.M.E.F.; van Leerdam, K.G.C.; Veggel F.C.J.M.; Engbersen, J.F.J.; Reinhoudt, D.N. *Langmuir* **1998**, 14, 6424.

[5-21]: Schonherr, H.; Vancso, J.; Huisman, B-H; Veggel F.C.J.M.; Reinhoudt, D.N. *Langmuir* **1999**, 15, 5541.

[5-22]: Qu, D. M. Sc. Thesis, University of Ottawa 1998.

[5-23]: Colthup, N.B.; Daly, L.H.; Widerley, S.E. *Introduction to infrared and Raman spectroscopy*, 3rd edition, Academic Press inc., SanDiego, **1990**.

[5-24]: Lias, S.G.; Bartmess, J.E.; Leibman, J.F.; Holmes,J.L.; Levin, R.D.; Mallard, W.G. *J. of Physical and Chemical Reference Data* **1988**, 17, supplement No.1.

[5-25]: Moran, S.; Ellison, G.B. *J. Phys. Chem.* **1988**, 92, 1794.

[5-26]: Benson, S.W. *Thermochemical Kinetics, methods for the estimation of thermochemical data and rate parameters, 2nd Editon.* A Wiley-Interscience Publication, John Wiley & Sons, New York, **1976.**

[5-27]: Yang, D.-F.; Wilde, C.P.; Morin, M. *Langmuir* **1997**, 13, 243.

[5-28]: Yang, D.-F.; Wilde, C.P.; Morin, M. *Langmuir* **1996**, 12, 6570.

[5-29]: Yang, D-F; Al-Maznai, H.; Morin, M. *J. Phys. Chem. B* **1997**, 101, 1158.

[5-30]: Byloos, M.; Al-Maznai, H.; Morin, M. *J. Phys. Chem. B* **1999**, 103, 6554.

[5-31]: Hobara, D.; Miyake, K.; Imabayashi, S.; Niki, K.; Kakiuchi, T. *Langmuir* **1998**, 14, 3590.

Chapter 6

Conclusion and Claims to original work

6.1. Conclusion

We developed an electrochemical method of depositing monolayers of organo-sulfur compounds. The effects of the potential, temperature and adsorbate concentration were examined. These studies provided detailed insights into the electroformation of SAMs.

We demonstrated that electro-deposition allows a good control of the deposition rate and the coverage of these adsorbates. These are not easily achieved in the absence of an applied electric field.

In summary, the process of oxidative electro-deposition of alkanethiolates on gold consists of two steps: a fast, potential dependent step followed by a slow, potential independent step. The fast deposition follows an instantaneous nucleation and growth mechanism. The slow deposition occurs via a Langmuir process. At slow deposition rates, the Langmuir mechanism is assigned to the reorganization of the monolayer (adsorption between islands). At higher deposition rates, for the octanethiolate, the Langmuir mechanism is related to a diffusion limited adsorption process. For the butanethiolate, the Langmuir mechanism is due to diffusion limitation and/or a reorganization of the monolayer. At concentrations lower than $7x10^{-5}$ M, the electro-

formation process is described by a two-step Langmuir model. This result is compatible with a phase transition from a lying down to a standing-up orientation of the alkyl chains.

The oxidative adsorption of alkanethiols on gold is also a two-step process that is weakly dependant on the deposition potential. The weak effect of the electric field is due to the fact that the rate-limiting step in the adsorption of alkanethiols is the surface dissociation of the S-H bond. The mechanism of oxidative deposition of alkanethiols contrasts with the one of alkanethiolates where desolvation was found to be the rate-limiting step. Therefore, control of the deposition rate by an applied potential is not possible for thiols but is the case for thiolates.

The oxidative deposition of alkanethiols on gold is weakly temperature dependent. The activation energy of this process is found to be 23 kJ mol^{-1}. The oxidative deposition of alkanethiolates on gold is more temperature dependent. At high temperature, the first step in the adsorption process (i.e. desolvation of thiolates) is easier as well as the reorganization of the monolayer (second step).

The adsorption of dialkyl sulfides is complex. There is a competitive adsorption between the sulfide and thiol or thiolate impurities in the solution. In a 0.1 M $KClO_4$ solution, sulfides adsorb molecularly. Then they slowly dissociate on the gold surface. The thiol impurities do not significantly affect this adsorption process. In alkaline solution, the sulfide adsorption process is still not clear. The data is compatible with the presence of thiolates. However, the origin of the thiolate remains unclear. The presence

of OH^- can increase the rate of the sulfide dissociative adsorption to produce thiolates. Thiolate impurities can also be present in the sulfide samples.

6.2. Claims to original work

1. We found that the electro-deposition of alkanethiol/kanethiolate from pH-neutral/alkaline aqueous solutions occurs via a two-step process. The first step is a nucleation and growth process and the second step is a Langmuir process.

2. For electro-deposition of alkanethiolate in the alkaline solution, the main barrier to adsorption is the desolvation. For electro-deposition of alkanethiol in the pH-neutral solution, it is the surface dissociation of the S-H bond.

3. The electro-deposition of thiols is a reliable, fast and selective method. Compare to the open circuit adsorption method.

4. From electro-deposition at different temperatures, we found that the activation energy for deposition of alkanethiol on gold in the pH-neutral solution is 23 ± 10 KJ mol^{-1}.

5. Electro-deposition of alkanethiolates from concentration below around 1×10^{-4} M leads to the formation of a lying down phase, where at higher concentration a standing phase is observed.

6. The electro-deposition of sulfide from neutral solution is a slow dissociative process yielding a monolayer of thiolates.